FLUTe FACT™ Laboratory Studies on Uptake and Extraction Method Variability and Implications for Field Performance

by

Brent A. Redmond

A Thesis

presented to

The University of Guelph

In partial fulfilment of requirements
for the degree of

Master of Applied Science

in

Engineering

Guelph, Ontario, Canada

ABSTRACT

FLUTe FACT™ LABORATORY STUDIES ON UPTAKE AND EXTRACTION METHOD VARIABILITY AND IMPLICATIONS FOR FIELD PERFORMANCE

Brent A. Redmond
University of Guelph, 2022

Advisor:
Dr. Beth Parker

The FLUTE FACT™ (FLUTe Activated Carbon Technique) is a borehole technology used for mapping contaminant distribution in the subsurface. Batch experiments were performed to determine the equilibrium partitioning behaviour of VOCs with respect to the FACT, and to assess how effectively VOC mass is desorbed from the FACT for analysis. Multiple extraction techniques were tested for effectiveness at desorbing mass from the FACT. The partitioning behaviour of the VOCs was reasonably well described by the Langmuir isotherm, with $C_{s\ max}$ values for different VOCs ranging from $8x10^3$ to $2x10^4$ µmol/kg. The methanol shake flask method was the best performing extraction technique, which displayed average mass percent recovery of 96%±6%. The experiment showed that the FACT and the procedures involved in sampling the FACT display great variability in data output between replicate samples, suggesting, while still useful for delineating contaminant distribution, should not be used in a quantitative manner.

ACKNOWLEDGEMENTS

I would firstly like to thank my advisor Dr. Beth Parker for her continued support and guidance throughout my thesis work. This project would not have been possible without Dr. Parker and her decades of hard work advancing the science of fractured rock hydrogeology. Being a member of Beth's research group has led to many fascinating and educational experiences over the years. I would also like to thank my advisory committee members Dr. Jana Levison for her extensive knowledge and insight, and Erica Pensini for her unwavering support and invaluable perspectives throughout my degree. My appreciation is also extended to Dr. Tadeusz Gorecki, whose expertise in analytical organic chemistry and excellent feedback proved to be invaluable while interpretating lab results and specific methods related to sorption behaviour and isotherm modelling.

The success of this project is owed in large part to Maria Gorecka, who was heavily involved within the planning, execution, and closing stages to the laboratory experiments performed – I could not have done this without your knowledge and support. Thanks also to Rashmi Jajaeda, Bruna Sousa and Brandyn Leteirt for the various supports in the lab.

Thank you to Steve Chapman, who played a major role with respect to the project management and field components of this study. I greatly appreciate the guidance in the field, and enjoyed our time spent travelling from site to site. My gratitude is also extended to Carlos Maldaner, Jessica Bulova, Jessi Meyers, Marina Nunes, Ryan Kroeker and many others for the different aspects of data collection related to this project.

I would like to acknowledge Carl Keller, the principal scientist and owner of FLUTe^{TM} – Flexible Liner Underground Technologies. The multitude of products available under the FLUTe^{TM} name has advanced the science of contaminant hydrogeology drastically. Thank you for your participation in this study, and the ongoing communications with respect to the FACT^{TM}.

To the community of friends that have supported me throughout this journey- I will always be grateful. To the students of G^{360}, you helped keep grad. life light and enjoyable. We shared many good times, hopefully we can sit down over a plate of cross-trax and scientific beers soon.

To my parents, Glenn and Kim Redmond – you have both been extremely loving and supportive over the years and encouraged me from day one to pursue my interests – I could not have done it without you. Thank you to my sister Laura, who paved the way as a scientist in our family and made grad. school seem a little less daunting.

TABLE OF CONTENTS

LIST OF TABLES

LIST OF FIGURES

LIST OF ABBREVIATIONS

c-DCE: cis-Dichloroethylene

DCM: Dichloromethane

DFN: Discrete Fracture Network

EPM: Equivalent Porous Media

FACT: FLUTe Activated Carbon Technique™

FLUTe: Flexible Liner Underground Technologies™

MAE: Microwave Assisted Extraction

MLS: Multilevel System (multilevel monitoring well)

NAPL: Non-Aqueous Phase Liquid

PCE: Tetrachloroethylene

TCE: Trichloroethylene

VOA: Volatile Organic Analysis

VOC: Volatile Organic Compound

1 Introduction

Contaminant delineation in fractured bedrock boreholes to understand contaminant transport and/or remediation feasibility is a difficult and data intensive process, due to the fracture networks introducing high levels of discontinuity, anisotropy, and heterogeneity to the hydrogeologic system (e.g. Berkowitz 2002; Golder, 2010; Parker et al. 2012). The FLUTe FACT™ (FACT), FLUTe Activated Carbon Technique is a commercially available technology, used for mapping contaminant distributions in high spatial resolution in subsurface environments. A comprehensive evaluation of the FACT was completed to assess the consistency at which the technology provides quantitative and representative VOC contaminant mass distributions in fractured rock boreholes, with goals of determining its effectiveness at improving contaminated site characterizations to inform hydrogeologic conceptual site models for risk-assessment and remediation performance.

1.1 Contaminant Hydrogeology in Fractured Rock

Fractured rock aquifers are used for water supply around the world, as much of the Earth's surface and/or near surface deposits consist of bedrock. Groundwater flow in fractured rock environments is a complex process in which the bulk of the system is made up of low permeability matrix rock, with discrete and discontinuous intervals of high hydraulic conductivity fractures, where most of groundwater flow occurs. In contaminated groundwater environments, these preferential flow paths have the potential of transporting contaminates at high flux rates, leading to rapid pollution of downgradient receptors. Distribution of the contaminants within the system are also controlled by the physical and chemical characteristics of the rock matrix, allowing contaminants in the fractures to transfer into the rock matrix by such processes as diffusion and sorption, leading to higher dispersion of the contaminant in the system (Parker et al, 1994). The highly irregular distribution of the contaminant phase due to complex transport mechanisms over decades creates a challenging environment to characterize, requiring time-intensive and expensive methodologies to build conceptual site models.

Standard equivalent porous medium (EPM) models are rarely sufficient to characterize fractured rock environments, and therefore more comprehensive discrete fracture network (DFN) models are necessary (Parker et al, 2012). These types of models are built from obtaining complementary datasets from one to several core holes, with hopes of defining the physical, chemical, and biological controls of the fractured rock transport. In DFN models, the characterization of the flow systems is extremely important in terms of modelling the transport of groundwater contaminants, but delineation of the contaminants spatially across the site and with depth are significant for determining remediation techniques necessary. Many different characterization techniques are commonly used in the industry for delineating contaminates, including the simplest technique, a single screened well or piezometer. Standard, single screen wells are often ineffective at characterizing fractured rock environments, as the screens stretch over intervals too large to delineate discrete fractures, and average out hydraulic properties

and contaminant concentrations that can be strongly variable over the length of the screen.

Nested piezometers/wells can be used to increase the resolution of contaminant datasets, with screens at numerous depths, but nested systems have major drawbacks as well. Multiple wells are often installed in a single hole, but the integrity of the seal is often questionable, leading to cross contamination between depths. Drilling wells in different hole can counter these problems, but this leads to high drilling costs for multiple core holes. Another technology that solves a lot of the issues related to nested piezometers are multilevel monitoring systems (MLS), in which multiple monitoring ports are found in a single well casing. These systems can be designed to target specific hydraulic zones and depths, with multiple types of systems commercially available from different companies, each which have their strengths and weakness depending on project specifics such as depth of the investigation, number of ports needed, whether or not the well will be permanent and budget. While these systems are extremely useful for characterizing hydraulic parameters with depth, the weakness to delineating contaminates with these systems is that when sampling these ports, only the free, advective-phase water within high conductivity features is characterized. A high proportion of the bulk water and contaminant mass are found within the secondary matrix porosity of the rock, which is left completely uncharacterized. To characterize the rock matrix, rock core contaminant analyses, based on DFN-M methods can be used (Sterling et al. 2005; Parker et al., 2012; Pierce et al. 2018; Parker et al. 2018), which involves drilling a continuous cored hole, in which closely spaced rock samples are analyzed for contaminant mass concentrations in lab, and physical/chemical characteristics of rock are also logged. This technique is extremely useful for understanding fracture network and mass distribution in rock matrix, but does not characterize primary fracture mass, except when used alongside MLS install. The entire process can be time intensive, expensive, and not all drilling techniques are supported for this methodology (Parker et al. 2012).

The characterization methods discussed so far have not considered the flux of the contaminates within the rock formation, and only describe “snapshots” of the contaminant distribution at the given sampling time. Mass flow is difficult to characterize due to spatial variations in both contaminant distribution and groundwater flow velocities, leading to an even wider range in mass fluxes. Hydrogeologists will estimate mass flux or discharge to inform numerical models that are used to forecast risk to downgradient receptors, and therefore accurate estimates are vital to produce reliable models. The passive flux meter (Hatfield et al, 2004; Klammler et al, 2016) is a monitoring technology that provides direct, *in situ* point measurements of time averaged mass flux and water flux (Hatfield et al., 2004). The system is, but the technology is non-continuous and therefore intervals of the borehole are left unstudied. The FACT is a continuous, non-permanent, inexpensive technology that provides flux-based concentration profiles with depth, accounting for mass within the matrix and in advective fracture features. This study seeks to produce a comprehensive evaluation of the FACT technology, to gain a better understanding as to the precision and accuracy of the datasets produced by the technique, as well as

determining the best methods of practice for analyzing the activated carbon material through intensive laboratory testing.

1.2 FLUTe FACT™

The FACT™ is a commercially available product (www.flut.com/fact) consisting of a continuous strip of activated carbon felt on the exterior of a sealing flexible liner, along with a reactive cover for NAPL detection, with a diffusion barrier placed between the liner and the carbon felt to isolate the carbon from contact with the liner (Fig. 1.1). The liner is everted into a borehole by adding water to the top of the liner, which creates a pressure differential between the water added and the potentiometric surface in the borehole. The liner presses the reactive NAPL cover directly against the borehole wall and wicks contaminants from the primary and secondary porosity of the formation onto the carbon felt located behind the liner where it is sorbed. The strong seal of the borehole liner due to the applied pressure differential prevents any hydraulic cross contamination (i.e. vertical flow) from one depth of the borehole to another, resulting in a representative contaminant profile of the rock formation. The liners are left everted in the boreholes for a pre-determined time-period deemed suitable for contaminants to flow through fractures or diffuse from the rock formation and not exceed the maximum sorption capacity of the FACT (typically a few days to a couple weeks), chosen based on the estimated contaminant concentrations and groundwater flow rates. The liner is removed by inversion (after sufficient exposure time), which prevents the carbon strip or the NAPL liner from touching any other section of the borehole wall.

Figure 1-1: Cross section of FLUTe FACT™ technology everted into borehole (Left). FACT strip found within diffusion barrier, which is attached to inside of reactive NAPL cover (right) (Mosthaf et al, 2014).

Vials are pre-prepared volumes of solvent, in which they are weighed empty and with the solvent to allow for precise calculation of solvent volume. It is recommended that the FACT is sampled immeditaly after removal from the borehole, as the exposure to the atmosphere can result in a change in the stability of the contaminants sorbed to the material.When working with sorbed VOC masses, open vials of MeOH solvent (relatively non-volatile) can be laid out beside the FACT liner at various depths when sampling to assess any volatilization of the VOCs during sampling, and potentially cross contamination between samples. Eversion point markings on the FLUTe are compared to a tape measure to quantify any liner stretch. The NAPL cover and carbon strip are photgraphed with the depths recorded and then wrapped in foil, put in a zip top bag and placed in a cooler with ice as quickly as possible. The sections are then transferred to the sampling station

At the sampling station (fig. 1.2), the tools for sampling are laid out before opening up the diffusion barrier exposing the FACT^{TM} strips. For each interval of strip sampled, a different set of tools are used to prevent cross-contamination. A rotary blade cutter is used to cut the activated carbon strips into smaller lengths, tweezers are used to pick up each sub-section and place it in a VOA vial pre-preprepared with a known volume of high purity solvent for preservation and extraction. Once the diffusion barrier is cut open, the FACT strips are cut lengthwise. One side of the strip is sectioned and placed into the prepared solution VOA vials, and the other side of the strip is used to take field duplicates at a rate of 1 duplicate per 20 samples. The samples are put on ice in a cooler immediatley after sampling. Once the sampling of each section is completed, all sampling equipment (rotary cutting tool, tweezers) are decontaminated using a five part process. After the FACT^{TM} sampling is complete, the NAPL cover is cut lengthwise to expose the side of the fabric pressed against the borehole wall. The staining is noted and scaled photographs are taken. The process is repeated for each five-foot section of FACT^{TM} strip. Once all intervals are completed, the FACT^{TM} samples in their respective VOA containers are re-weighed and sent for laboratory analysis.

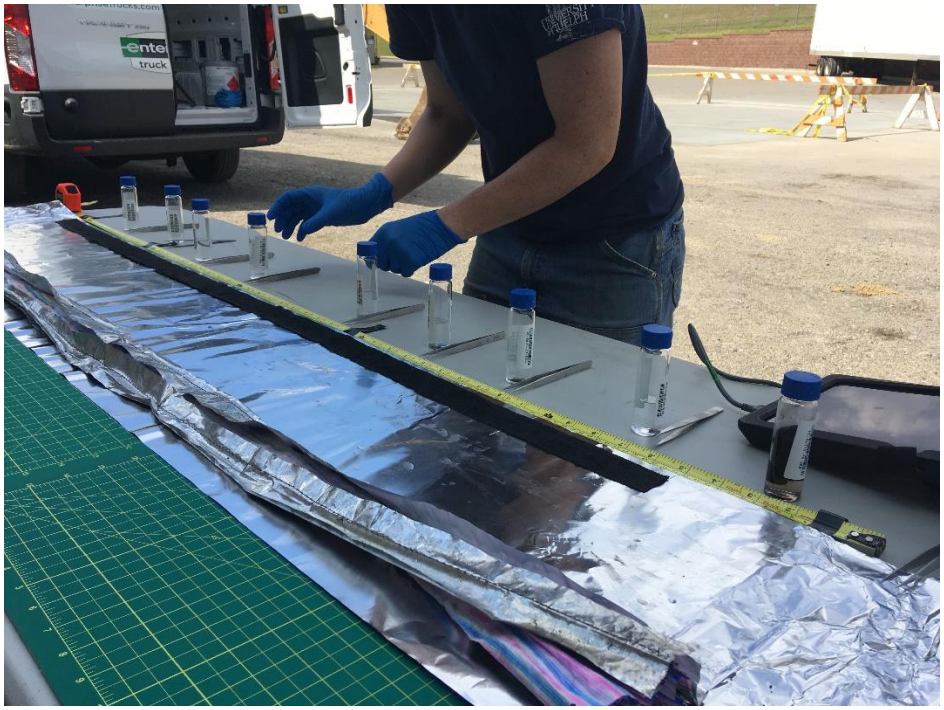

Figure 1-2: Sampling set-up for the field preparation of each individual FACT sample.

In the laboratory, each sample is shaken until sufficient time allows for complete extraction (equilibration in the solvent) and weighed again before an aliquot of the solvent is taken from each vial with the activated carbon strips inside. The samples are analyzed using EPA method 8260 (EPA, 2006). The system contains a purge and trap unit and a gas chromatograph equipped with a mass spectrometric detector (GC-MS). This method is used for the identification and measurement of purgeable volatile organic compounds in groundwater samples. The solvent aliquots obtained by the extraction from FACT samples is analyzed with the same method. The sample for the analysis is prepared by adding 1mL (or less if the sample was highly contaminated) of methanol aliquot into 40mL VOA vial filled with nano-water. An appropriate dilution factor is applied to the sample concentration calculations.

1.3 Motivation and Research Questions

The FACT laboratory test was designed and performed to determine how representative the contaminant profiles produced by the FACT are of the true distribution of contaminant concentrations and varying flux conditions due to groundwater flow and diffusion. The use of the technology is a multi-step process involving the sorption of contaminates to the FACT during deployment, desorption of the contaminant mass from the FACT using a solvent extract and analysis of the desorbed mass using a Gas Chromatograph- Mass Spectrometer (GC-MS). Without understanding the mechanics and the uncertainties that

are found in the procedures used to generate the contaminant profiles, the accuracy of these datasets remains unknown.

The two main goals of the FACT uptake and extraction experiment was to determine the equilibrium partitioning behaviour of multiple VOCs with respect to the FACT to gain a better understanding of the sorption mechanics during FACT deployment, and to assess how effectively VOC mass can be desorbed from the FACT. Three extraction techniques were tested for their effectiveness at desorbing mass from the FACT, and the greatest performing technique was determined.

To build off of the laboratory experiments, the FACT was observed under an optical microscope and scanning electron microscope (SEM) to gain a better understanding of the composition of the activated carbon material, and BET surface area measurements were conducted on replicate FACT samples to assess the degree of variability in the sorption properties of the material below the scale of the sampling method

2 Methods

2.1 Uptake and Extraction Experiments

Batch water solutions containing a) TCE only and b) a VOC mixture of PCE, TCE, c-DCE and DCM were prepared for the experiment to simulate different groundwater contaminant conditions. Five different concentration levels were used: 0.1 mg/L. 1 mg/L, 5 mg/L, 10 mg/L, 50mg/L, for both the TCE and VOC solution to assess any changes in the behaviour of the FACT with varying levels of contamination. For the water solution containing TCE only, the concentration level represented the total concentration of the water solution, whereas in the VOC mixture, each individual VOC constituent had a concentration of the indicated concentration level, leading to a higher total concentration for the VOC solution. For example, for the VOC mixture indicated by 10 mg/L, each compound had a concentration of 10 mg/L, representing a total concentration level of 50 mg/L for the solution.

FACT strips were cut into 1.9 cm (half the width of the standard material) x 15 cm in a clean lab to avoid contamination and placed in individual, pre-weighed 40 mL VOA vials and re-weighed to determine the mass of the FACT strip. The dry FACT was removed and soaked in nano-water and pressed against a hard surface while submerged to remove air from the material. The wet FACT was placed back in the vial and re-weighed to determine the wet FACT mass, then the vial was filled with the water solution without headspace to ensure there was minimal losses of the VOCs to the gaseous phase and weighed again. Five replicates of each water solution type and concentration were produced to ensure the results were representative, for a total of 130 FACT samples (table 2.1).The samples were stored in a cold room at 4℃ for three weeks (approximate deployment time of the FACT in the field) to allow for the contaminants from the water solution to diffuse out of solution and sorb to the clean FACT, with transport being driven by the concentration gradient. The samples were shaken at 350 RPM using an orbital

shaker approximately three times a week. After the three-week period, the FACT samples were removed from the water solution vials and the water solutions were analyzed using a GC-MS to determine the mass of contaminants that were not sorbed to the FACT strip during the uptake experiment.

Table 2.1 ***Number of samples prepared for each individual extraction method, and totals. A total of 125 samples were prepared for each extraction. The samples at 10 and 50 mg/L were mot extracted using the MAE method due to potential for the high concentrations contaminating the microwave vessel.***

Concentration (mg/L)	Number of Sample					
	Methanol Extraction		Pentane/Water Extraction		MAE	
	TCE	VOC	TCE	VOC	TCE	VOC
0.1	5	5	5	5	5	5
1.0	5	5	5	5	5	5
5.0	5	5	5	5	5	5
10	5	5	5	5	N/A	N/A
50	5	5	5	5	N/A	N/A
SUM	25	25	25	25	15	15

The mass sorbed to the FACT was calculated using the difference between the initial quantity of mass found in the water solution before the 3-week equilibration period, and the residual mass left in the water solution after equilibration. Water solution controls were created using identical vials and water solutions as used to submerge the FACT strips in, but with the absence of the FACT strip. The controls were analyzed after the equilibration period and mass losses were estimated using the residual concentrations. The equilibrium distribution of the VOC mass sorbed to the FACT strip (C_s) and the mass remaining in the water solution (C_w) of the different initial water solution concentrations were plotted. The relationship between C_s and C_w over the range in concentrations were described by sorption isotherm models.

Two isotherm model types were fit to the experimental data: the Freundlich Isotherm and the Langmuir Isotherm. The Freundlich solution describes a system in which the sorbate has sorption sites of limited sorbate capacities, which are either filled, or the sorbate is less drawn to sorption sites at higher concentration levels (Freundlich, 1909). The Freundlich isotherm model (Eq. 2.2) is an analytical solution that is fit to the equilibrium distribution of the sorbate between the sorbent and the water solution that describes this relationship.

Equation 2.1: Freundlich Isotherm

$$C_S = K_F \times C_w^n$$

C_S = Equilibrium Sorbate Concentration

C_W = Equilibrium Water Solution Concentration

n = Freundlich Exponent

K_F = Freundlich Constant

When the Freundlich coefficient (n) is equal to 1, the isotherm is a linear relationship in which the partitioning behaviour of the sorbent is not affected by concentration level. When n is less than 1, the model curves downward with an increase in concentration, indicating a lower affinity of the sorbent to the sorbate at higher concentrations. When n is greater than 1, the model curves upward with an increase in concentration, indicating the sorbate has a higher affinity for the sorbent at higher concentrations.

In situations where there are a limited number of sorption sites that reach saturation at higher concentration levels, the Freundlich model cannot be considered a suitable model as it does not have constraints against Cs continually increasing. The Langmuir Isotherm model (Langmuir, 1916) is more appropriate in these situations, as the Γ_{max} parameter represents a maximum achievable surface concentration for the sorbent. K_L, the Langmuir constant, represents the equilibrium constant of sorption affinity, which assumes a constant sorbate affinity for all surface sites. The Langmuir isotherm assumes that the sorbent is sorbed to a single, homogeneous, monolayer surface, in which the maximum achievable surface concentration is reached when this surface is completely covered (Eq. 2.2).

Equation 2.2: Langmuir Isotherm

$$C_S = \frac{\Gamma_{max} \cdot K_L \cdot C_W}{1 + K_L \cdot C_W}$$

C_S = Equilibrium Sorbate Concentration

C_W = Equilibrium Water Solution Concentration

Γ_{max} = Maximum Sorbate Concentration

K_L = Langmuir Coefficient

To avoid an iterative parameter-estimation procedure for fitting isotherm models to experimental datasets, a common practice involves manipulating the adsorption isotherm

equation to obtain linear relationships of the parameters, allowing for use of traditional least-squares procedures (Osmari et al, 2013). For the Freundlich Isotherm, this process involved plotting the Log transform of the experimental dataset, and extracting the slope and intercept of the linear regression (Eq. 2.3) to determine the isotherm parameters K_F and n for the fitted isotherm curve.

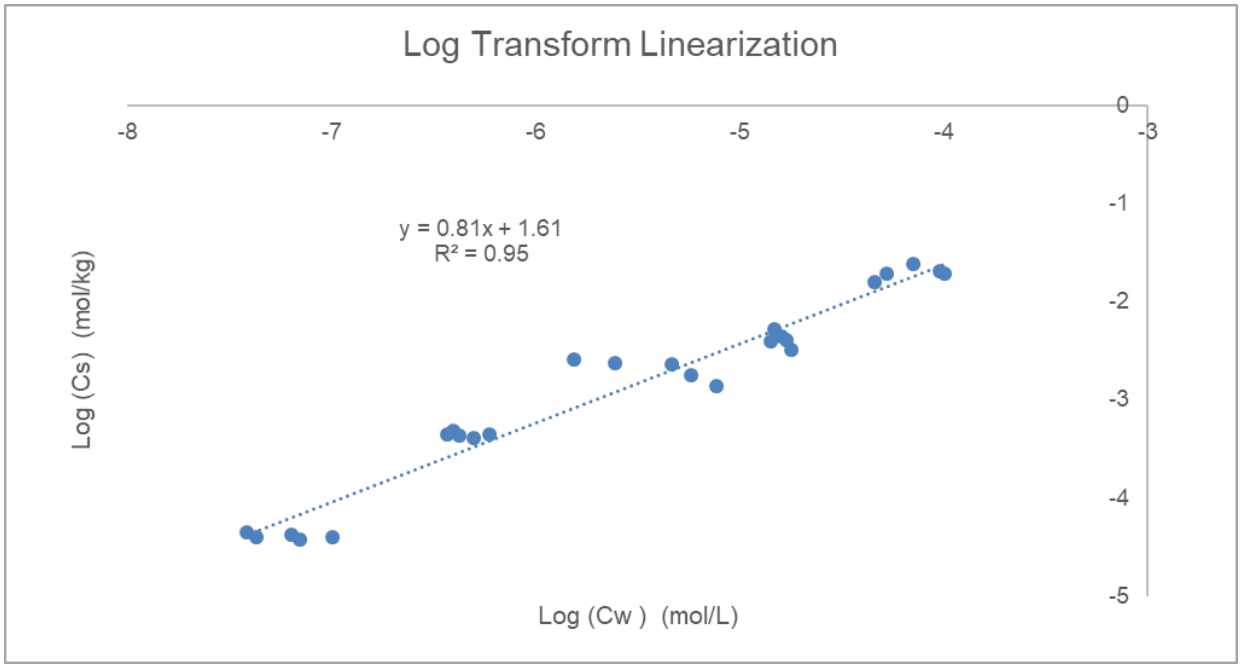

Figure 2-1: Example of a Log transform to experimental sorption data to extract the Freundlich Isotherm Parameters.

For the Freundlich Isotherm, this process involved plotting the Log transform of the experimental dataset, and extracting the slope and intercept of the linear regression (Eq. 2.3) to determine the isotherm parameters K_F and n for the fitted isotherm curve.

Equation 2.3: Freundlich Isotherm Log Transform

$$logC_s = nlogC_w + K_F$$

C_S = Equilibrium Sorbate Concentration

C_W = Equilibrium Water Solution Concentration

n = Freundlich Exponent

K_F = Freundlich Constant

For the Langmuir Isotherm fitting process, the reciprocal values of the experimental datasets were plotted (Fig. 2.2), and the isotherm parameters were extracted from equation to calculate the fitted Langmuir curve.

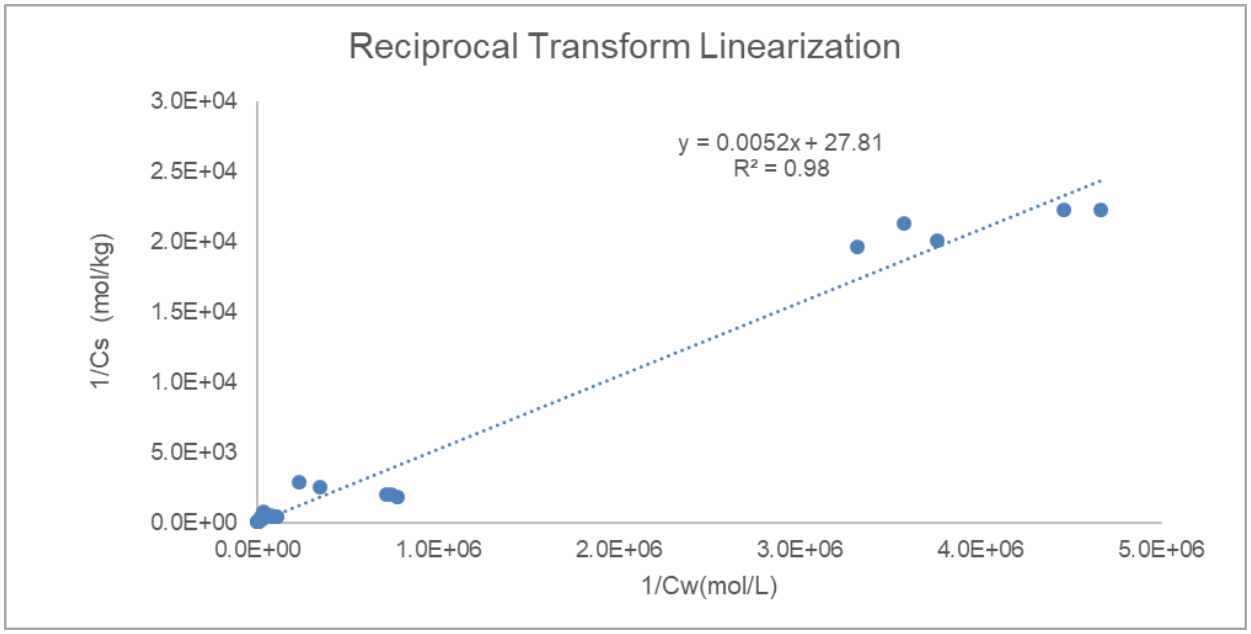

Figure 2-2: Example of a Recipricol transform to experimental sorption data to extract the Langmuir Isotherm Parameters.

The linearization of the model equations for fitting to experimental datasets is a standard method of practice, and was based off methods from Swarzenbach et al, 2003. However the linearization of isotherm model equations can modify the statistical interpretation of experimental error distributions (Osmari et al, 2013), creating models that are not representative of equilibrium partitioning behavior. For example, the linearization of the experimental datsets (which is completed for the Langmuir Model) leads to regression problems dominated by low concentration values, where the model focusses on lower concentration values and neglects higher concentrations. To compensate for issues resulting from the linearization of the models, the estimated parameters were adjusted manually using the least squares method of the model fitting to the non-linearized experimental data, which greatly improved the predictiveness of the models.

Equation 2.4: Langmuir Isotherm Reciprocal Transform

$$\frac{1}{C_S} = \left(\frac{1}{C_{S,max} \cdot K_L}\right)\frac{1}{C_W} + \frac{1}{C_{s,\,max}}$$

C_S = Equilibrium Sorbate Concentration

C_W = Equilibrium Water Solution Concentration

Γ_{max} = Maximum Sorbate Concentration

K_L = Langmuir Coefficient

In parallel to analyzing the water phase, the FACT samples from the batch experiments were transferred to new 40 mL VOA vial, where the FACT was extracted with a solvent to desorb the contaminants from the material. Three different solvent extraction techniques were assessed for effectiveness at desorbing VOC mass from the FACT strips: methanol shake flask method, microwave assisted extraction (MAE) and a pentane/water mixture shake flask method.The objective was to directly measure the total mass of sorbate onto the sorbent, and provides a basis for evaluating uncertainty by comparing the mass adsorbed by calculating the difference in mass measured initially and in the water phase after equilibration.

For the methanol shake flask method, the FACT was removed from the water solutions and placed in pre-weighed 40mL VOA vials using tweezers to avoid cross contamination and re-weighed. 15mL of Purge-and-Trap (P&T) grade methanol was placed in the vial using a bottle top dispenser and re-weighed to determine the mass of methanol added. The samples were shaken using an orbital shaker for 1 hour at 350 RPM daily and stored in a cold room at 4°C when not being shaken. Select samples at different concentrations were chosen for time-series analysis, where an aliquot of the methanol that the FACT was immersed in was taken and analyzed using the GC-MS periodically. Aliquots were taken daily during the beginning of the extraction when the concentration gradient between the FACT and the extractant were greatest, and less often as the concentration gradient decreased and the desorption rates began to slow. Once the concentration of contaminants reached equilibrium in the methanol solvent extractant, the FACT strip was removed and transferred to a new vial and the procedure was repeated to perform three replicate extractions on each FACT sample. This repeat extraction was done to enhance the concentration gradient between the FACT and the fresh methanol and allow for any residual contaminant remaining on the FACT strip to be desorbed, increasing the yield

(recovery) of the extraction technique. Three replicate extractions were completed on each individual FACT sample during the sequential extraction steps.

The MAE extractions were only performed on the lower three concentrations: 0.1, 1.0 and 5.0 mg/L of the batch experiment, because the higher concentrations posed a greater risk of permanently contaminating the microwave vessel used, leaving future work with the vessel vulnerable to cross contamination. The FACT samples were removed from the water solutions and placed in pre-weighed vials with 15 mL of P&T grade methanol following the same procedure as was used during the methanol extractions. After preparation, the extractions were conducted in microwave system model: Ethos Sel Labistation, built by Milestone Srl, Italy. The microwave procedure used was originally developed for the extraction of contaminates from rock and clayey soils where desorption dominates extraction times, and follows the methods used in the paper by Dincutoiu et al., 2006. The FACT samples were microwaved for three 20-minute intervals at 120°C for a total of 60 minutes. An aliquot was taken from selected samples at each 20-minute interval to be used for time series analyses.

The pentane/water method was established at the Technical University of Denmark and is described in Beyer et al, 2012 for a FACT study and purposefully used as a published method for benchmarking the other methods. The method involves the use of a water/pentane mixture to extract the sorbents from the FACT. The FACT was cut into 2-10 cm sections and inserted into 20 mL VOA vials. 10 mL of tap water was added in the field and finally 3 mL of pentane were added in the lab. The idea behind this method is that the chlorinated solvents sorbed to the FACT in the DTU study (similar to the contaminants used in this study) are hydrophobic, and by adding the water in the field the contaminants are conserved in the FACT and will not be lost to volatilization during shipment/storage of the samples. Once the pentane is added to the vial in the lab, the chlorinated solvents will begin to desorb into the solvent that they have a high affinity towards. The samples were shaken continuously for 3-4 days after the pentane was added and kept in a cold room at 4 ^{o}C. A single 1 mL aliquot of pentane was taken from the sample and analyzed. Longer samples of the FACT were also tested (30 cm strips) and inserted into larger 40 mL vials with 30 mL of water and 9 mL of pentane. In this experiment, 1.9 x 15 cm long FACT strips consistent with the rest of the extraction methods tested in the experiment were placed in 40 mL VOA vials and 15 mL of water was added with 4.5 mL of pentane. The samples were shaken daily for 1 hr and stored in a cold room between shaking intervals. Aliquots of the pentane were taken from each sample after 24 and 48hrs, and approximately a week later to be sure the samples had reached equilibrium concentrations. Similar to the methanol extractions, once the FACT and the pentane:water mixture reached equilibrium, the FACT strip was removed and placed in a new vial with a clean pentane:water mixture to reintroduce a concentration gradient and remove residual contaminants from the FACT. Three replicate aliquot samples were completed for each extraction sequence.

Multiple blank samples were analyzed throughout the experiment to ensure that the samples were not contaminated by outside sources of the VOCs used as analytes in the

experiment. FACT blanks were prepared for each type of solution that the material was submerged in, which consisted of a clean FACT strip submerged in: DI water, methanol, and pentane:water. A blank was also prepared by submerging the FACT in methanol and was microwaved to determine background VOC levels during the MAE extraction method. Storage blanks were placed alongside the FACT samples when stored in the cold room to determine if there was any VOC present in the cold room that may have contaminated the samples. Solvent blanks were also taken from the top and bottom of all methanol and pentane bottles used in the experiment to desorb mass from the FACT samples (i.e. extraction step), to identify any background contamination found in the solvents. A total of 45 blanks were analyzed in the experiment. For samples in the experiment for quality to pass quality assurance/quality control (QA/QC), the concentration level of the sample had to be five times higher than it's associated blank samples (within the range used in EPA procedures for determining Limits of Quantitation).

2.2 Gas Chromatography/Mass Spectrometry Analysis

All water solutions and extractant concentrations were analyzed using a gas chromatograph connected to a mass spectrometer. The method used was based on EPA method 8260B (EPA, 1996) which is used for identification and measurement of purgeable volatile organic compounds in water samples. 5 mL of water sample containing VOCs is introduced into a purge-and-trap system (Teledyne Tekmar, model AtomX), separated using a gas chromatographic capillary column and detected by a mass spectrometric detector (Agilent, chromatograph model 7890A, MSD model 5975C). The target VOCs are identified in the sample by analyzing the standards under the same conditions and comparing the mass spectra and GC retention times. The target compounds are quantitated using the internal standard procedure. The instrument settings used for each instrument during sample analysis can be observed in table 2.2.

Table 2.2: Instruments used and system configurations for the FACT sample analysis. Table a) represents the purge and trap systems in use, table b) the GC configurations, and table c) the MS configurations.

a) Purge-and- trap system configurations (Teledyne Tekmar, Model Atomx)

Sample Volume	5 mL
Purge Time	11 min
Purge Flow	Helium, 40 mL/min flow at 20°C
Dry Purge Time	0.5 min

Dry Purge Flow	100 mL/min at 20°C
Desorb Preheat Temperature	245°C
Desorb Temperature	250°C
Desorb Time	2 min
Trap	Purge Trap “9”

b) Gas Chromatograph Configuration (Agilent, Model 7890A)

Column	20 m x 0.18 mm x 1 µm, DB-VRX
Carrier Gas	Helium, 1 mL/min, split 1:50
Oven Program	Initial temperature 36°C, hold 4 min, 16°C/min to 85°C, 30°C/min to 210°C, hold for 3 min

c) Spectrometer Configurations (Agilent, Model 5975C)

Ionization Mode	EI
Acquisition Mode	Scan and SIM
Scanning Range	35 to 300 m/z
Scanning Rate	5 scan/s
Environmental analysis software	Agilent ChemStation software

2.3 Micro-Analysis of FACT

The FLUTe FACT^{TM} is a strip of felt material that has been impregnated with AC, but the actual composition of the felt backing material, and the type and/or size of AC pore structure that has been embedded is unknown. Depending on the surface characteristics of the AC in the FACT, the technology could display very different sorptive properties (Chiang et al., 2001). The uniformity that the AC is distributed throughout a strip of FACT is also vital for the technology to provide representative contaminant datasets between analyzed samples. If the carbon is not distributed consistently throughout the backing material with length, the amount of sorbate that will sorb to FACT will be largely attributed to the quantity of AC found in the strip at a given interval, leading to contaminant profiles that are skewed and not representative of the actual distribution of mass in the subsurface.

To better understand the composition of the FLUTe FACT^{TM} material and the distribution of AC embedded, the FACT material was cut into 6-inch samples (sampling size for FACT strip used for field scale characterization, Fig. 2.4), and each sample was visually observed at multiple smaller-scale intervals (µm and nm scale). A VHX-5000 Keyence digital microscope was used to observe the FACT at several positions within the 15-cm long strip at the µm scale and a FEI Quanta GEG 250 SEM was used to observe the material at nm scale. The FACT samples were sputter coated with platinum-iridium for the SEM observations. Visual observations were recorded for each sample, and a qualitative assessment of the structure of the backing material and the distribution of visually observed AC was performed. Five different replicate samples from different locations on the FACT roll, in which multiple field of views (approximately 3) from each sample were visually observed for variability based on the characteristics of the FACT. Extending on this study, the methodology was repeated on two other FACT versions with noticeably different properties that were provided by different manufacturers and suppliers to FLUTe (Carl Keller, FLUTe personal communications). Five replicate samples from 3 different manufacturing years (identified as 2017, 2019, 2020) were observed, for a total of 15 samples to determine if the characteristics of the FACT material has changed throughout production years.

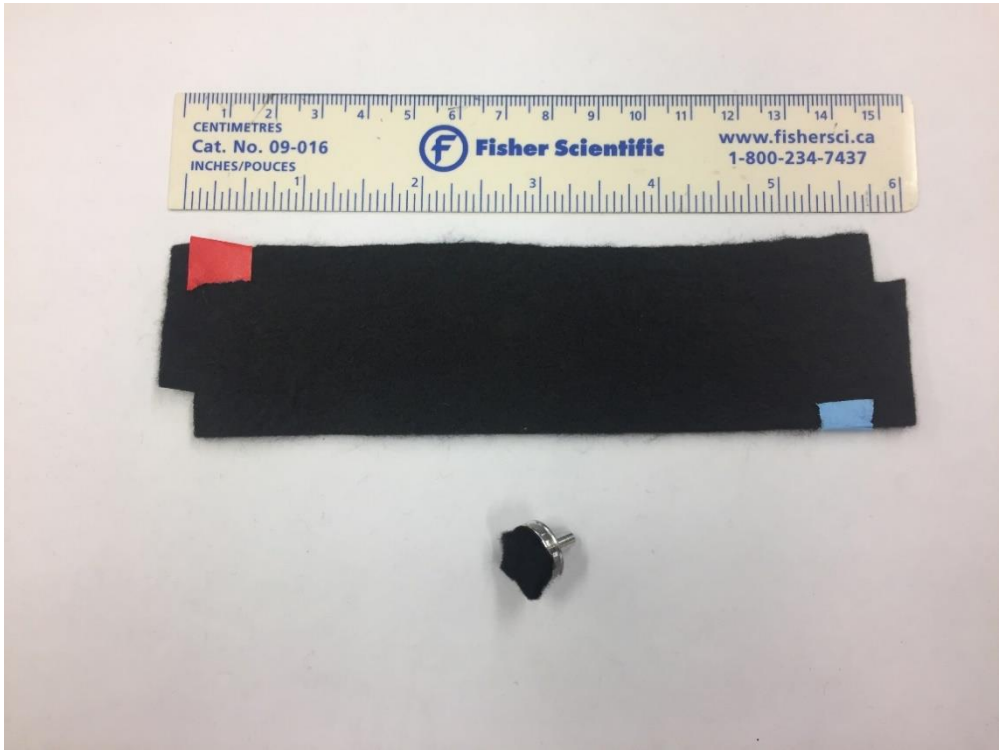

Figure 2-3: Six-inch FACT sample displayed, which is representative of the size of strip that was observed under the optical microscope. Smaller sections of the sample were sectioned of, sputter coated and placed on a stage to be observed under the SEM.

A Brunauer-Emmett-Teller (BET) surface area analysis was also performed on three replicate samples from each manufacturing year, for a total of nine measurements, to observe how the surface area of the FACT varies between replicate samples and between manufacturing years. The replicate sample measurements were used to compare the consistency of the FACT material from the same production roll, and the sorption capacity from different FACT manufacturing years were used to determine sorption variance over time. The analysis performed was based on the methods developed in Brunauer et al., 1938, which measures inert gas adsorption to the adsorbent as a function of relative pressure to determine surface area. A 3-point determination was performed to determine the amount of nitrogen that adsorbed to the FACT samples at three different relative pressures. A Tristar II 3020 version 3.02 Surface Area and Porosity System was used to complete these tests. The BET equation (Eq. 2.5) was used to calculate surface area from these experimental measurements.

Equation 2.5: BET Surface Area

$$\frac{1}{V_a\left(\left(\frac{P}{P_0}-1\right)\right)} = \frac{C-1}{V_m C}\ X\ \frac{P}{P_0} + \frac{1}{V_m C}$$

$\frac{P}{P_0}$ = Relative pressure

V_a = Volume of gas adsorbed

V_m = Volume of gas adsorbed to produce an apparent monolayer on the surface

C = BET Constant

For the BET transform, $\frac{1}{V_a\left(\left(\frac{P}{P_0}-1\right)\right)}$ is plotted against the relative pressures corresponding to the values at these pressures. V_m, the volume of gas necessary to produce a monolayer on the surface and C, the BET constant, are derived from the slope and y-intercept from the linear regression of the plot. The total surface area of the sample is then calculated using equation 2.4:

Equation 2.4: Total Surface Area

$$S_t = \frac{V_m N s}{V}$$

S_t= Total Surface Area of Sample Material

V_m= Monolayer Absorbed Gas Volume

N = Avogadro's Number = 6.02 x 10^{23} molecules/mol

s = cross- sectional area of adsorbed gas molecule

V = molar volume of adsorbed gas

The mass of the sample can then be used to normalize the total surface area of the sample to specific surface area. The specific surface area calculations of each sample are an indirect measurement of the sorption capacity for each sample. The replicate sample measurements were used to compare the consistency of the FACT material from the same production roll, and the sorption capacity from different FACT manufacturing years were used to determine sorption variance over time.

3 Results and Discussion

3.1 Water Solution Controls

The water solution controls, with identical water solution with matching concentrations used during the experiment to submerge the FACT samples were placed in 40 mL VOA vials without the FACT strips and were analyzed after the 3-week equilibration period to assess analyte losses. The main sources of mass loss to be expected in this section of the experiment were losses to volatilization as well as sorption and diffusion of the analytes to the silicon in the silicon-teflon lined septum helping to create a gas-tight seal with the plastic screw-top vial cap. For volatilization to occur, it must be assumed the vial cap does not create a perfect seal, allowing the gaseous phase of the VOCs to escape to the atmosphere, and/or if there is any unintended headspace in the vial, allowing the VOCs to partition out of the water solution and into the headspace into the gaseous phase. Diffusion and sorption of the VOCs to the silicon backing of the septum is expected because the less polar analytes used in this experiment are all generally hydrophobic, and will have affinity for non-polar surfaces (Stumm, 1992), such as the silicon.

For each solution type (VOC mixture and TCE alone) and concentration level, three water solution controls were analyzed. The average loss of mass from the control solutions and confidence intervals for each of these control types is provided in Table 3.1.

Table 3.1: Average mass losses for the water solution controls, sorted by compound type and solution are displayed, along with relevant compound parameters.

Solution	Compound	Average Percent Loss of Mass (%) (n = 3)	Confidence Interval, 90 %	Vapor Pressure (torr)	Aqueous Solubility (mg/L)
VOC	PCE	13	12	19	200
VOC	TCE	21	7	75	1 100
VOC	c-DCE	23	9	205	3 500
VOC	DCM	11	9	415	20 000
TCE	TCE	20	9	75	1 100

The average percent loss of mass for the different VOCs ranged from 11% to 23 %, with an average percent loss of mass for all compounds of 18 %. At a 90% confidence interval for the average loss of mass, the concentration values of the different contaminants overlapped, or were very close to overlapping, suggesting that the difference in mass loss values for the VOC constituents were statistically insignificant. Hence, there was no apparent trend in mass loss with respect to the volatility of the compound (vapor pressure) or polarity of the compound (aqueous solubility), which results in difficulty determining the source of mass losses from controls.

To further assess mass losses from the water solution controls for each compound and initial concentration, boxplots were created (Fig.1). In general, a high amount of variability was observed for the mass recovered from the initial water solution controls for all VOC compound constituents, at all concentration levels. The mid-concentration level (C3, 5 mg/L) water solution controls displayed the highest mass recovery, whereas the lowest and highest concentration levels showed the lowest recovery values. The mid-concentration levels also displayed the highest variability in mass recovery between replicate samples, which can be observed by the larger box heights in Figure 3.1.

The PCE analyte in the VOC solution control showed mean mass percent recoveries ranging from 57% to 117% for the different concentration groups, with standard deviation values ranging from 1% to 13%. PCE followed the general trend mentioned earlier, in which the mid-concentration levels displayed the highest mass recoveries, where the lowest and highest concentrations displayed the lowest mass recovery values. The highest mass recovery value out of the solution controls for PCE was 127% of the mass recovered from the original mass found in the control solution before the 3-week equilibration time. Multiple analytes displayed mass recovery values over 100%.

TCE in the VOC solution controls displayed mean mass percent recoveries ranging from 61% to 98%, for the different concentration levels, with standard deviation values ranging from 1% to 13%. The trends in mass recoveries with respect to the concentration levels agreed well with PCE, but the total mass recovery for TCE appeared to be slightly less for the mid-range concentrations, with the highest mass recovery value for TCE being 108%.

c-DCE in the VOC solution control had mean mass recovery values ranging from 47% to 102% between concentration groups, with standard deviation values ranging from 1% to 22%. c-DCE displayed slightly different mass recovery trends between groups, where the mid-concentration controls showed the highest percent recoveries (as did the PCE and TCE controls), with the exception of concentration group four (C4, 10 mg/L), which displayed the lowest mass recovery value, with a mean percent recovery of 47% and a standard deviation of 1%, indicating this group also showed the least variation between replicate samples. With the exception of the C4 group, c-DCE generally displayed higher mass recovery values than the less polar PCE and TCE compounds in solution.

DCM in the VOC solution control displayed mean mass percent recoveries ranging from 61% to 116%, with standard deviation values ranging from 0% to 16%. DCM showed similar mass recovery trends between concentration groups as c-DCE, with higher mass recovery values for the mid-concentration levels, with the exception of concentration group four, which displayed the lowest recovery values (61% ± 2%). DCM also showed higher mass recovery values than the less polar molecules PCE and TCE, with the exception of contaminant group four. This implies that the mass losses to volatilization is minimal relative to losses due to sorption and diffusion into the silicon vial cap, because the less polar molecules, with lower vapour pressures (refer to table 3.1.), showed the highest mass losses in the water solution controls. For concentration group four, where the trend in mass losses was opposite (more volatile compounds showed higher losses), it is possible that these control solutions may have been compromised, and an analytical error occurred in these samples, which would have led to more potential for losses to the gaseous phase.

The TCE alone in solution control displayed mean mass percent recoveries ranging from 66% to 110%, with standard deviation values ranging from 1% to 24%. TCE in solution alone displayed similar mass recovery percentages as TCE in the mixed VOC solution, but there appeared to be more variation in mass recoveries between replicate samples, though the differences may be statistically insignificant.

a)

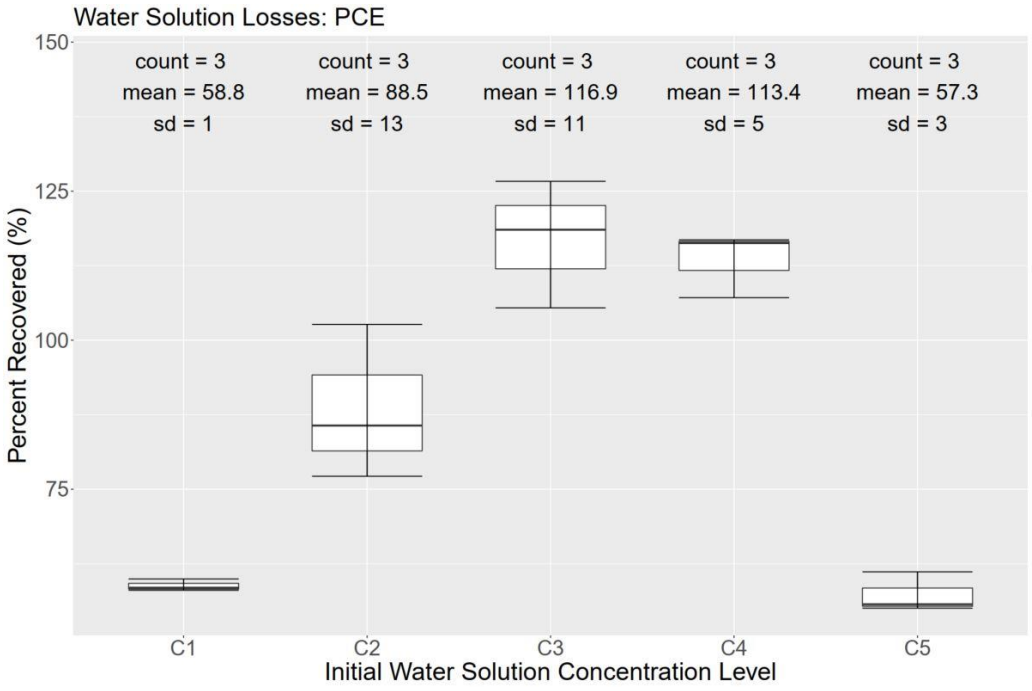
Water Solution Losses: PCE
count = 3
mean = 58.8
sd = 1
count = 3
mean = 88.5
sd = 13
count = 3
mean = 116.9
sd = 11
count = 3
mean = 113.4
sd = 5
count = 3
mean = 57.3
sd = 3
150
125
100
75
Percent Recovered (%)
C1
C2
C3
C4
C5
Initial Water Solution Concentration Level

b)

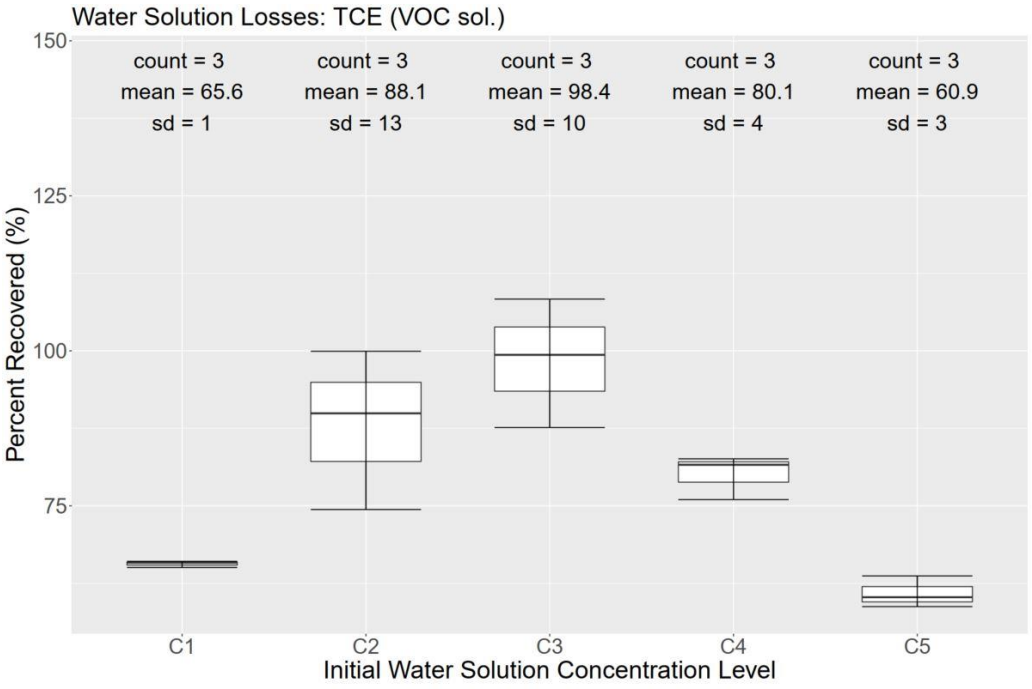
Water Solution Losses: TCE (VOC sol.)
count = 3
mean = 65.6
sd = 1
count = 3
mean = 88.1
sd = 13
count = 3
mean = 98.4
sd = 10
count = 3
mean = 80.1
sd = 4
count = 3
mean = 60.9
sd = 3
150
125
100
75
Percent Recovered (%)
C1
C2
C3
C4
C5
Initial Water Solution Concentration Level

c)

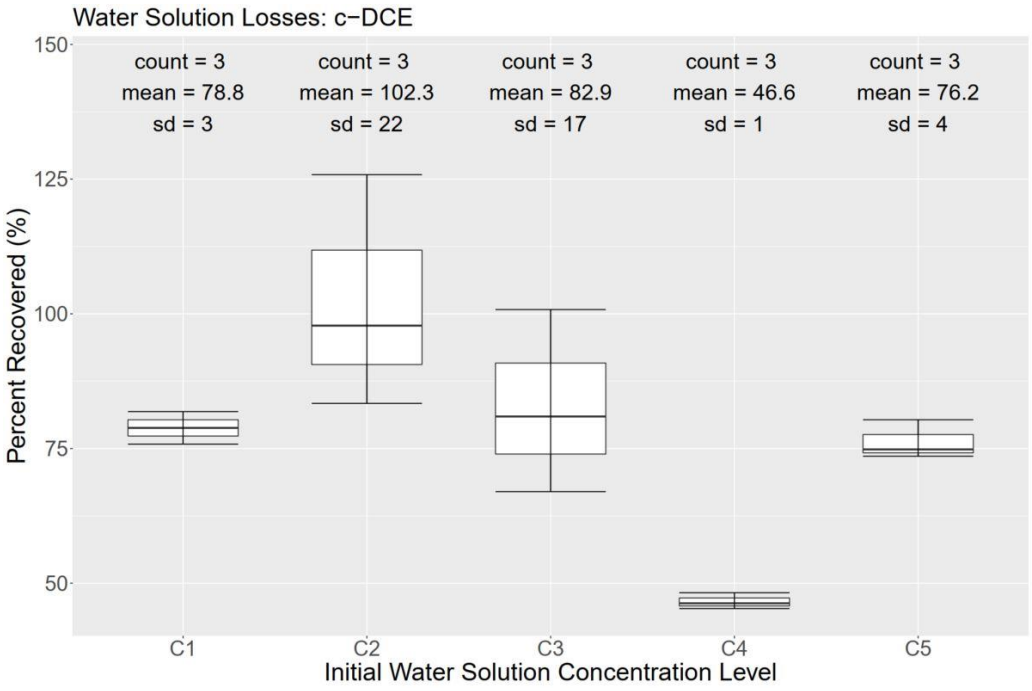
Water Solution Losses: c−DCE
count = 3
mean = 78.8
sd = 3
count = 3
mean = 102.3
sd = 22
count = 3
mean = 82.9
sd = 17
count = 3
mean = 46.6
sd = 1
count = 3
mean = 76.2
sd = 4
150
125
100
75
50
Percent Recovered (%)
C1
C2
C3
C4
C5
Initial Water Solution Concentration Level

d)

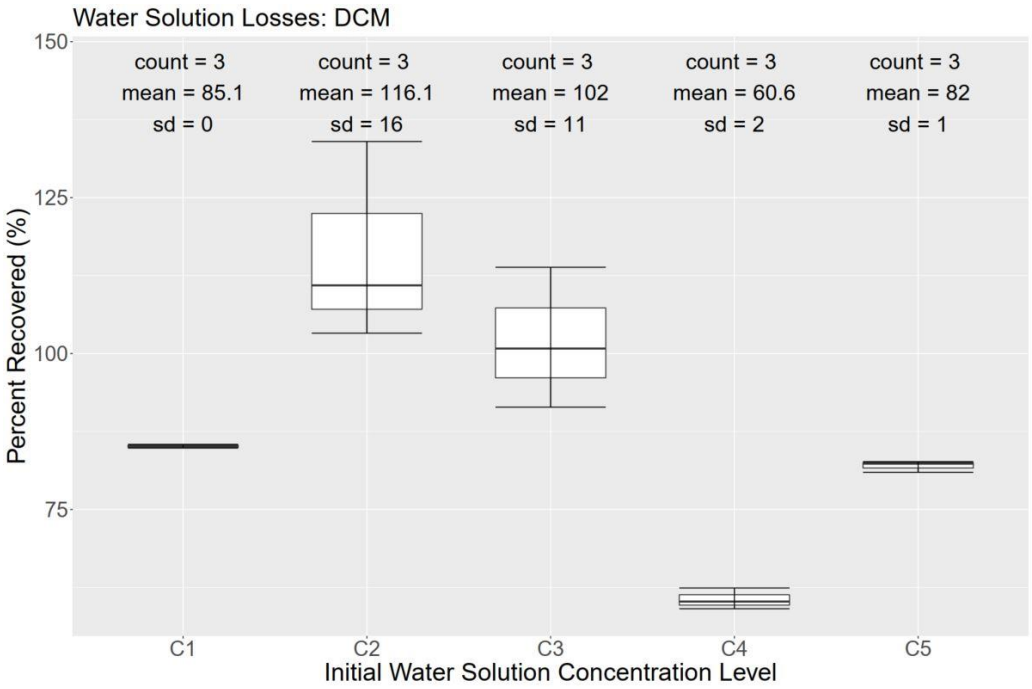
Water Solution Losses: DCM
count = 3
mean = 85.1
sd = 0
count = 3
mean = 116.1
sd = 16
count = 3
mean = 102
sd = 11
count = 3
mean = 60.6
sd = 2
count = 3
mean = 82
sd = 1
150
125
100
75
Percent Recovered (%)
C1
C2
C3
C4
C5
Initial Water Solution Concentration Level

e)

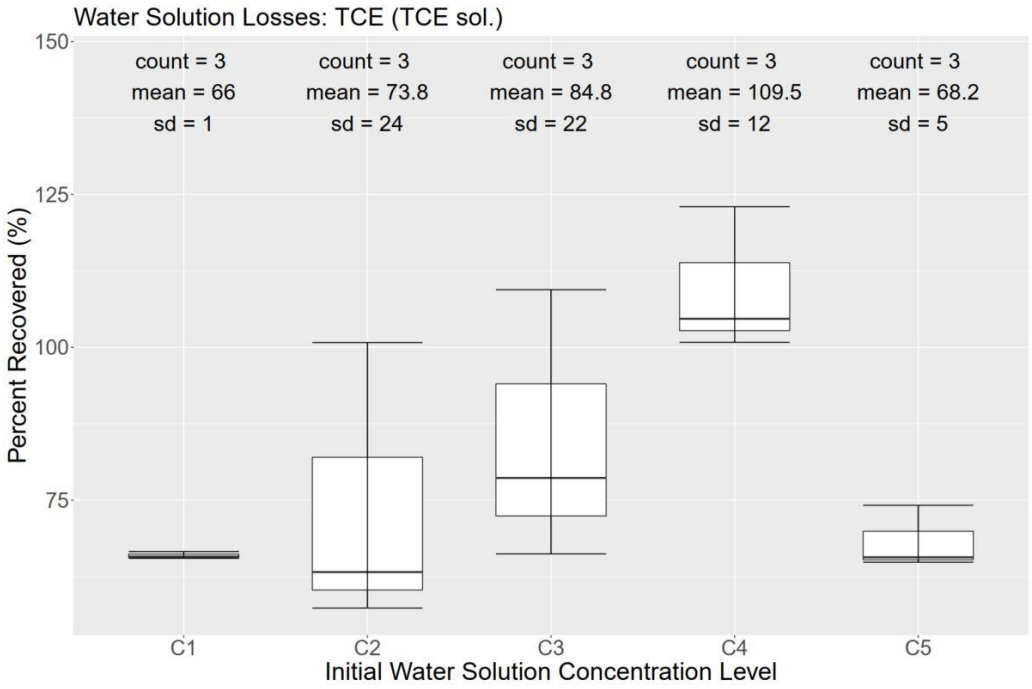

Figure 3-1: Boxplots of the percent of mass recovered from the initial water solution controls after the 3-week equilibration period, binned by the different water solution concentration levels. The VOC water solution control boxplots are displayed in in figure 3.1 a), b), c), and d) and TCE alone in solution is displayed in figure 3.1e).

The average loss of mass for all solution control types and concentrations was calculated to be 18%, which is a higher percent mass loss than what was estimated in the experimental samples. The major difference between the water solution control samples and the experimental samples is that the controls did not have a FACT strip sample submerged in the water solution. Without the FACT sample in the controls, there was the absence of a solute sink for the compounds to sorb to. With the FACT strip present in the water solution, a large proportion of the hydrophobic VOC compounds will sorb to non-polar surfaces, resulting in a more thermodynamically stable system. Without the presence of the FACT, the only other sources for the compounds to partition out of solution would be through sorption to the silicon in the septum and volatilizing into the gaseous phase (i.e. headspace). As a result, a higher percentage of the VOC mass would be lost in the control samples. Therefore, the mass loss values obtained from the water

solution controls were used only as a reference for maximum mass loss (worst case scenario) and were not used as a correction factor for the experimental samples.

Without a direct measurement of the amount of mass lost during the equilibration period, there is inherent uncertainty with respect to the amount of mass sorbed to the FACT strip. The equilibrium sorbed mass quantity was calculated by subtracting the amount of mass left in the water solution after the three-week equilibration time, from the mass concentration measured in the initial water solution with the assumption being that any mass not found in the water solution after equilibration was sorbed to the FACT. It is acknowledged that this is an invalid assumption, however it is assumed the average mass loss for the water controls of 18% is a conservative, overestimation of mass losses. Due to the unaccountable losses of mass in this experiment, the exact parameters and values calculated from the isotherm fittings (ex. distribution coefficients), and desorption efficiencies cannot be stated. However, it is still valid to observe the trends of the equilibrium mass distributions between the FACT and the water solutions with changing concentration levels and VOC types using the statistics derived from the five replicates as part of the experiment design.

3.2 Equilibrium Partitioning Behaviour of VOCs with Respect to FACT

3.2.1 Statistical Analysis of Mass Remaining in Water solution

The equilibrium distribution of compounds from the batch water solutions sorbed to the FACT (Cs, mol/kg dry FACT) and remaining in the water solution (Cw, mol/L) after the three-week immersion of the FACT were determined. The mass losses of the water solution during the equilibrium period was assumed to be zero, because the control solutions were not deemed to be accurate representations of losses during uptake experiment. All mass not remaining in the water solution after the three weeks was assumed to be sorbed to the FACT. A statistical analysis of the equilibrium distribution of the VOC mass was conducted to determine the consistency at which VOC mass sorbed to the surface of the FACT, and the quantity of mass sorbed to the FACT between the different VOCs.

a)

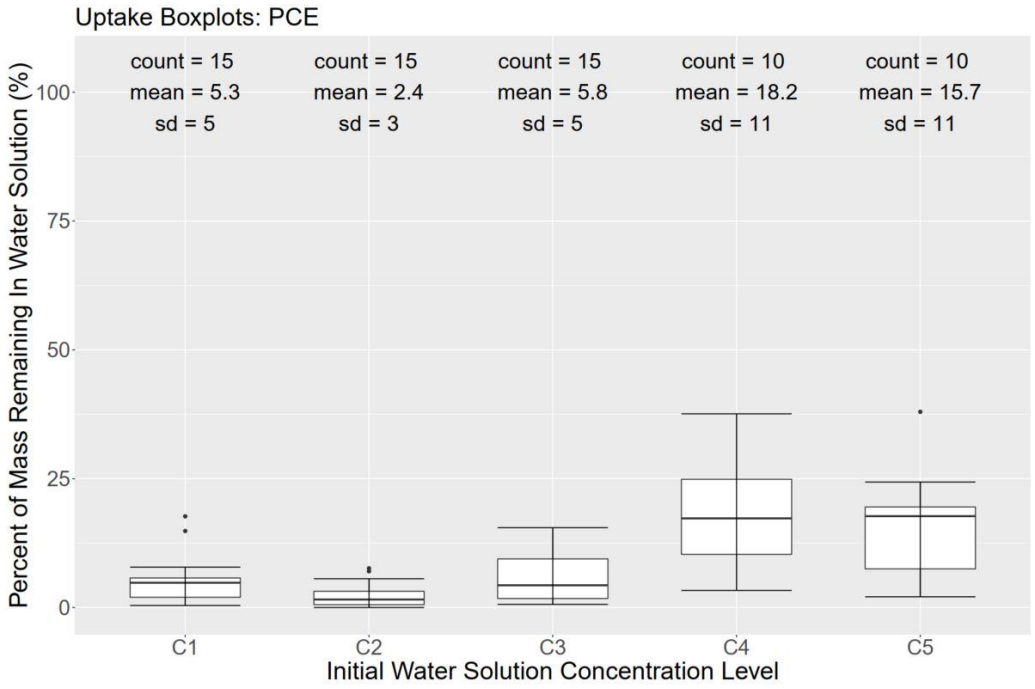
Uptake Boxplots: PCE
count = 15
mean = 5.3
sd = 5
count = 15
mean = 2.4
sd = 3
count = 15
mean = 5.8
sd = 5
count = 10
mean = 18.2
sd = 11
count = 10
mean = 15.7
sd = 11
Percent of Mass Remaining In Water Solution (%)
100
75
50
25
0
C1
C2
C3
C4
C5
Initial Water Solution Concentration Level

b)

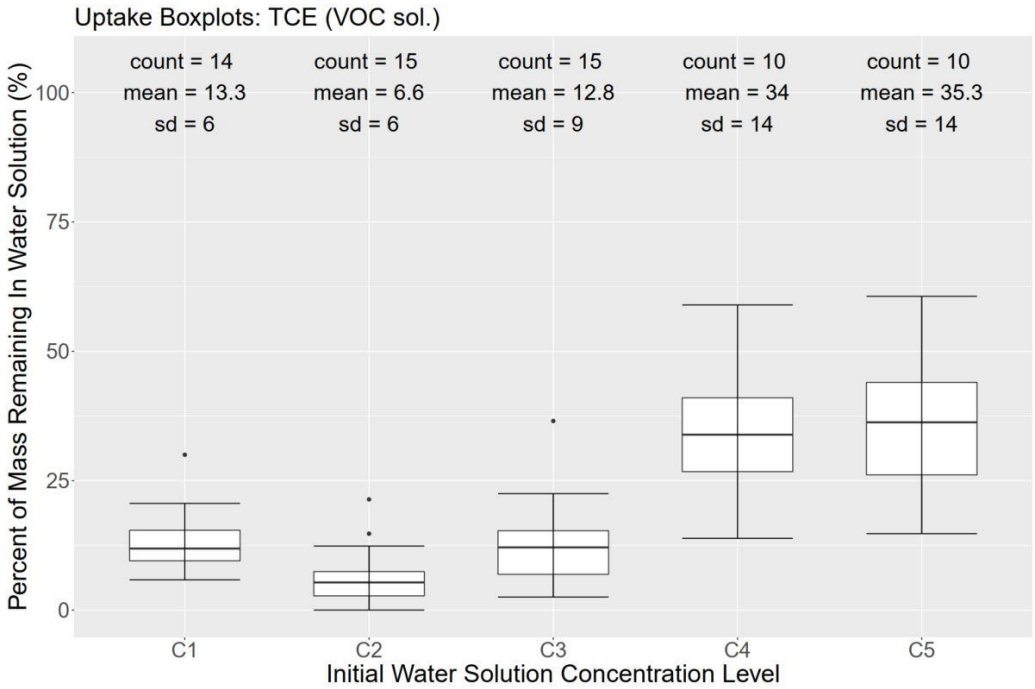
Uptake Boxplots: TCE (VOC sol.)
count = 14
mean = 13.3
sd = 6
count = 15
mean = 6.6
sd = 6
count = 15
mean = 12.8
sd = 9
count = 10
mean = 34
sd = 14
count = 10
mean = 35.3
sd = 14
Percent of Mass Remaining In Water Solution (%)
100
75
50
25
0
C1
C2
C3
C4
C5
Initial Water Solution Concentration Level

c)

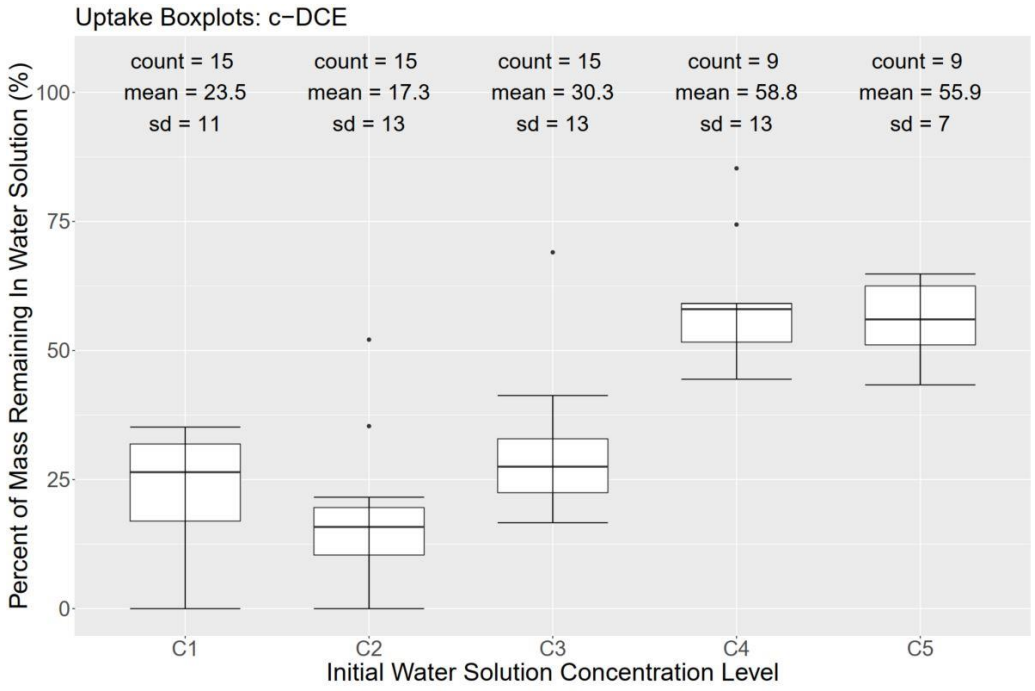
Uptake Boxplots: c−DCE
count = 15
mean = 23.5
sd = 11
count = 15
mean = 17.3
sd = 13
count = 15
mean = 30.3
sd = 13
count = 9
mean = 58.8
sd = 13
count = 9
mean = 55.9
sd = 7
Percent of Mass Remaining In Water Solution (%)
100
75
50
25
0
C1
C2
C3
C4
C5
Initial Water Solution Concentration Level

d)

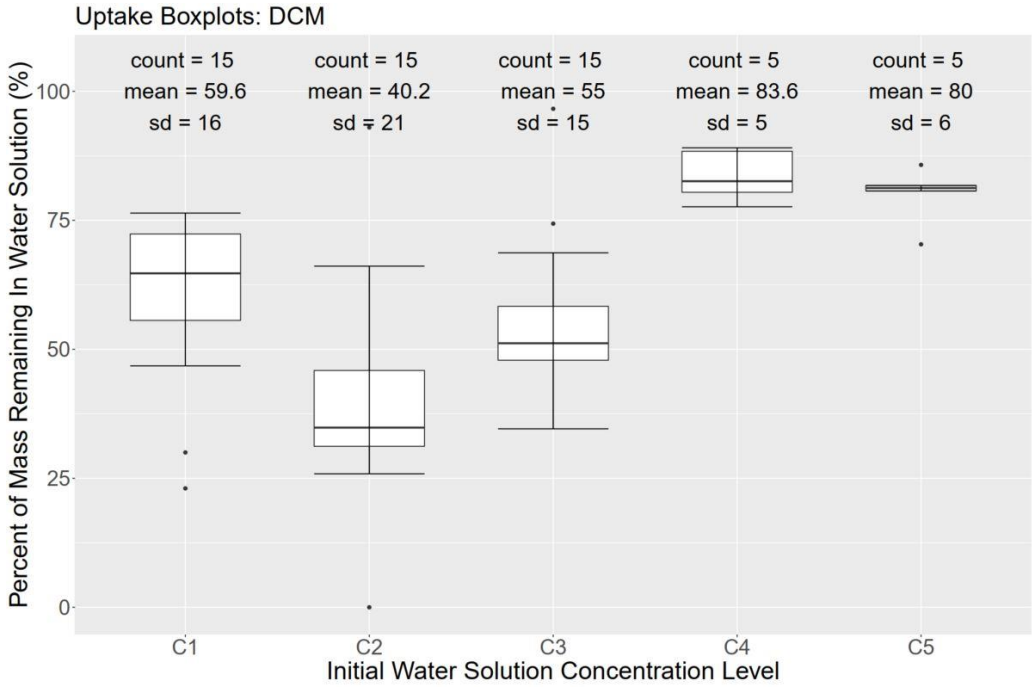
Uptake Boxplots: DCM
count = 15
mean = 59.6
sd = 16
count = 15
mean = 40.2
sd = 21
count = 15
mean = 55
sd = 15
count = 5
mean = 83.6
sd = 5
count = 5
mean = 80
sd = 6
Percent of Mass Remaining In Water Solution (%)
100
75
50
25
0
C1
C2
C3
C4
C5
Initial Water Solution Concentration Level

e)

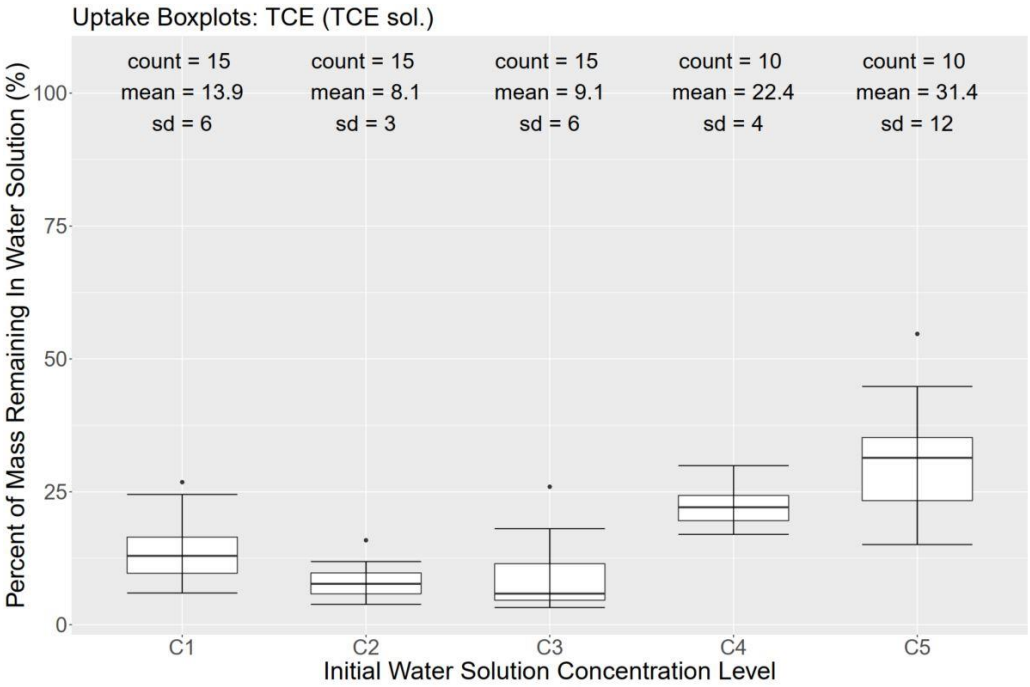

Figure 3-2: Boxplots illustrating the percent of mass remaining in the water solution after the three-week equilibration period to assess for mass uptake efficiencies between contaminant concentration and VOC type. The VOC water solution control boxplots are displayed in in Figure 3.2a), b), c), and d) and TCE alone in solution in figure 3.2e).

The percent of mass remaining in the water solution (C_W) after the three-week equilibration period (any mass not found in solution assumed to be sorbed to the FACT, C_S) was plotted on a box and whisker diagram (fig. 3.2), where the boxes are binned by the different initial water solution concentration levels, ranging from 0.1 to 50 mg/L. Each box represents approximately 15 identical samples, with the exception of concentration levels 4 and 5, in which the experiments were not conducted for the samples used for the MAE extraction, as the higher concentration levels were high enough to contaminate the microwave vessels. Additional samples were removed from the experimental dataset due to analytical errors and/or lack of data results. Figures 3.2a to 3.2d represent a different contaminant constituent in the VOC solution, and TCE alone in solution is plotted in Figure 3.2e.

PCE showed mean percent of mass remaining in the VOC water solution between concentration levels ranging from 2% to 18%, and standard deviation values from 3% to 11% with 4 outlier values identified. PCE displayed more consistent sorption characteristics at the lower two concentration groups (0.1 and 1 mg/L), with less variability with respect to mass left in solution between replicate samples. As the water solution

concentrations increased, more variability was observed, which is displayed by the larger box heights (1.5 interquartile ranges) and higher standard deviation at concentration levels C3-C5 (5, 10 and 50 mg/L respectively). It is also evident that a higher percentage of PCE mass remained in the water solution with an increase in solution concentration, with the mean mass percentage left in water solution of 18% for the highest concentration level.

TCE in the VOC water solution displayed mean mass percentage remaining in water solutions ranging from 7% to 35% and standard deviation values from 6% to 14%, with 4 outliers identified. The compound also displayed more consistent sorption characteristics at the lower two water solution concentrations, displaying less variation in mass sorbed to the FACT between replicate samples at these levels. A higher percentage of the TCE mass remained in solution at the higher concentration levels, with a mean mass percentage left in solution of 35%. While TCE appears to show similar sorption characteristics with respect to the water solution concentration levels as PCE, a greater percent of TCE remained in solution.

c-DCE did not display a clear difference in sorption characteristics between lower and higher water solution concentrations and instead showed less consistent tendencies at all concentration levels tested. The analyte had resulting mean mass percentages remaining in solution ranging from 17% to 56% and standard deviations of 7% to 13%, with 5 outliers identified. While c-DCE did not show the same trends as PCE and TCE with respect to sorption consistency, it did display a decrease in mass sorbed to the FACT at the higher concentration levels, with an average of over half the c-DCE mass remaining in water solution (56%) at the highest water solution concentration level. Overall, c-DCE displayed much lower affinity to the surface of the FACT than the less polar molecules PCE and TCE.

DCM showed similar sorption tendencies to c-DCE, where a high level of variability was displayed in sorbed mass percentages across all concentration levels, with mean mass percentages remaining in solution from 40% to 84% and standard deviations of 5% to 21% and 6 identified outliers. DCM had the least consistent sorption characteristics and the highest mass was left in the water solution after the three-week equilibrium period overall. The compound did display a higher percentage of mass left in solution at the upper concentration level, with a mean mass percentage of 84% remaining in solution.

TCE in solution alone (Fig. 3.2e) displayed less variance in its sorption tendencies overall than the individual constituents in the VOC solution. It had mean mass percentages remaining in solution ranging from 8% to 31%, with standard deviations of 3% to 12% and 4 identified outliers; similar results to the TCE in VOC solution. While the standard deviations of TCE alone were similar to those of PCE and TCE in the VOC solution, the boxplots clearly showed that the box heights of TCE alone (1.5 interquartile range) were consistently smaller than those of the VOC solution constituents, including TCE in the VOC solution. A trend in which a higher percentage of mass was left in water solution at

the highest water solution concentration was observed for TCE alone, consistent with each analyte in the VOC solution (mean value of 31%).

The boxplots illustrate that a lower percentage of mass was sorbed to the FACT for the more polar molecules, DCM and c-DCE, compared to the less polar TCE and PCE. The less polar molecules have a higher affinity to the non-polar surface of the FACT due to their hydrophobic properties. It is also clear that there was a high level of variability in terms of the amount of mass sorbed to the FACT between replicate samples, for all VOC types. The variability was higher for c-DCE and DCM, which are not only more polar, but also have higher vapour pressures (Table 3.1), suggesting uncertainty in values due to losses to volatility. An apparent increase in mass left in solution with an increase in the VOC water solution concentration was observed, suggesting a maximum number of sorption sites being filled by other molecules in solution. Nearly the same mean and range values were obtained, however, with less variability in the amount of mass sorbed to the FACT between TCE alone in solution and TCE in the VOC solution, although the differences may be statistically insignificant. TCE alone in solution displayed standard deviations ranging from 3% to 12%, and the TCE in VOC solution displayed levels of 6% to 14%. This can be related to intermolecular forces leading to more uncertain sorption capacities and more thermodynamically unstable environments.

Outliers can be identified as the points outside the whiskers of the box (outside 1.5 IQR). A total of 26 outliers were found, differing significantly from the remaining population of observations. These outliers were removed before the extraction section of the experiment, to remove bias from the first half of the experiment with respect to the performance of different extraction techniques.

3.2.2 Isotherm Modelling

The partitioning behaviour of the VOCs with respect to the FACT was analyzed using isotherm models, in which the equilibrium mass distributions of the compounds sorbed to the FACT and remaining in the water solutions after the three-week time-period were plotted; the trends observed were then fitted with different models and the performance of the models was statistically measured. The two models fitted to the experimental datasets were Freundlich and Langmuir Isotherms. Both models have been proven to be suitable for fitting the equilibrium distribution of VOCs in solution and sorbed to activated carbon surfaces (Kim et al., 2006; Ramos et al., 2010; Yu et al., 2002)). Although the specific type of activated carbon used in the FACT material is unknown, the isotherms have been fit to datasets involving multiple activated carbon types including: powdered, granular and pelleted. Figure 3.3 displays the Freundlich and Langmuir isotherms fitted to the experimental data, separated by contaminant constituent and sample group. The three sample groups: A, B, and C are identical experiments run parallel to each other, and during the second part of the experiment where the contaminant mass will be desorbed from the FACT, each group will have a different extraction technique applied to them.

The partitioning behaviour of the VOCs follow a linear trend at lower concentration levels, where the sorption sites of the FACT have not begun to be filled with the sorbate. The lower concentration levels appear to described well by the Freundlich Isotherm, which is an empirical relationship that is described by a power equation, and therefore has the ability to describe linear relationships when the exponent is approximately 1. As the concentration levels increase, and the available sorption sites on the FACT begin to saturate, the data points approach a horizontal asymptote, where the capacity of the FACT for sorption begins to be reached. The Langmuir isotherm describes the datasets more appropriately when the FACT saturation occurs at higher concentration levels, as the Freundlich isotherm does not describe a maximum sorption value. These maximum concentration values are described by the Cs max parameter in the Langmuir Isotherm equation. The Cs max values for each isotherm model fitting can be found in Table 3.2 and range from 1.04×10^4 to 4.29×10^4 µmol/kg.

While the Langmuir Isotherm was a better fit for the data as a whole, there are many cases (Ex. Figure 3.3a, Group C) in which the isotherm overcompensates for the sorption saturation assumption, and the model line curves below the actual data points on the plot and the Freundlich model describes the higher concentration levels more appropriately. However, in most cases the Freundlich isotherm underestimates the experimental sorption capacity, and the model continues to rise at higher concentrations, well above the experimental data points (ex. fig. 3.3a, Group A). In situations where the FACT is exposed to higher concentrations than tested in this experiment (maximum water solution concentration tested was 50 mg/L), the Freundlich isotherm would continue to model sorption values well above the sorption capacity of the FACT, resulting in poorer simulations as the water solution concentration increases.

Overall, the Langmuir Isotherm was the superior fit, which can be observed visually, and by the sum of square values between the isotherm and experimental datasets presented in Table 3.2. However, neither of the tested models are necessarily predictive of the equilibrium partitioning behaviour of the VOCs tested with respect to the FACT, due to the inconsistent nature of the VOC sorption behavior to the FACT. The observed data scatter was likely attributed to the inhomogeneities of the FACT material itself, rather than indicating that the model did not describe the experimental dataset well. While there is room for experimental and observational errors in the experiment, it is likely that a large percentage of the error is coming from the variability of the FACT material itself, which is discussed in greater detail in section 3.5.

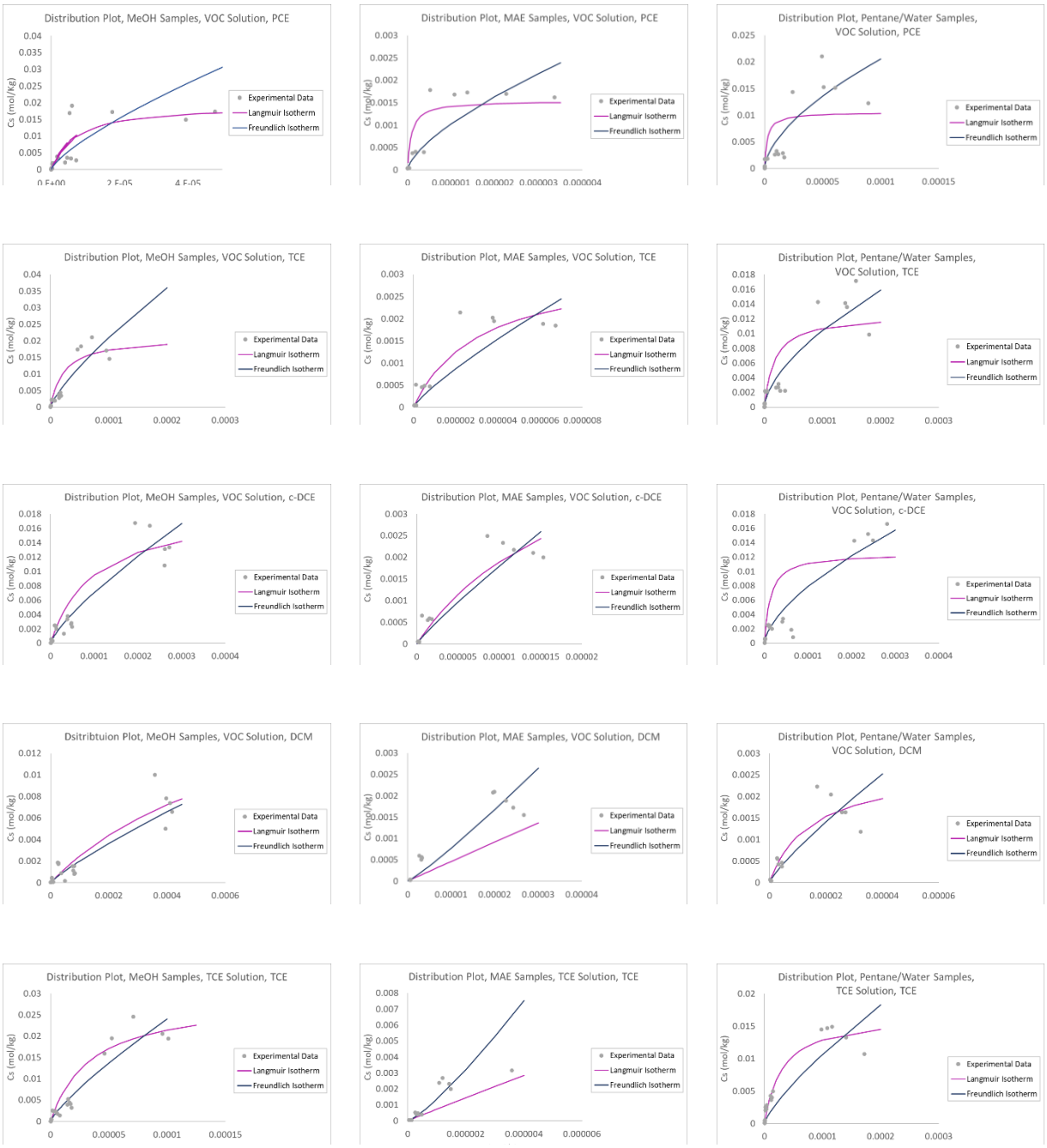

Figure 3-3: All isotherm model fits performed in the labratory experiment are described in this figure. The experimental data, along with the Freundlich (blue line) and Langmuir (magenta line) are found on each individual plot. The plots are separated by experimental group (A, B,C), of which each group were used to test a different extraction/desorption method in the second half of the experiment, and VOC type: PCE, TCE in the VOC solution, c-DCE, DCM and TCE alone in solution are marked by a), b), c), d) and e), respectively.

Table 3.2: Isotherm Parameters for all fittings performed in the laboratory experiment. The Freundlich Isotherm Parameters: K_f and n, along with the Sum of Square values defining the wellness of fit of the models for each experimental group and VOC type are described in table 3.2a). In table 3.2b), the Langmuir parameters K_L, and Cs max and wellness of fit values were described.

a)

Freundlich Isotherm									
	Group A			Group B			Group C		
Contaminant	K_f (mol/kg)	n	Sum of Square	K_f (mol/kg)	n	Sum of Square	K_f (mol/kg)	n	Sum of Square
PCE	5.2E+01	7.5E-01	6.1E-04	1.1E+01	6.7E-01	2.4E-06	5.0E+00	6.0E-01	2.0E-04
TCE (VOC sol.)	2.7E+01	7.8E-01	1.6E-04	4.5E+01	8.3E-01	2.6E-06	2.9E+00	6.1E-01	8.7E-05
c-DCE	9.1E+00	7.8E-01	7.2E-05	5.6E+01	9.0E-01	2.0E-06	2.5E+00	6.3E-01	5.7E-05
DCM	5.3E+00	8.6E-01	2.8E-05	3.2E+02	1.1E+00	1.6E-06	1.3E+01	8.4E-01	2.4E-06
TCE (TCE sol.)	4.1E+01	8.1E-01	1.3E-04	3.8E+04	1.2E+00	1.4E-05	1.4E+01	7.8E-01	1.1E-04

b)

Langmuir Isotherm									
	Group A			Group B			Group C		
Contaminant	K_L (L/umol)	Cs max (umol/kg)	Sum of Square	K_L (L/umol)	Cs max (umol/kg)	Sum of Square	K_L (L/umol)	Cs max (umol/kg)	Sum of Square
PCE	1.5E-01	1.9E+04	3.1E-04	1.2E+01	1.5E+03	2.2E-06	4.6E-01	1.1E+04	4.3E-04
TCE (VOC sol.)	4.4E-02	2.1E+04	2.1E-04	3.2E-01	3.2E+03	1.1E-06	5.8E-02	1.3E+04	1.9E-04
c-DCE	1.0E-02	1.9E+04	9.4E-05	5.1E-02	5.6E+03	1.4E-06	7.8E-02	1.3E+04	3.5E-04
DCM	1.4E-03	2.0E+04	2.6E-05	5.6E-04	8.3E+04	4.7E-06	6.8E-02	2.7E+03	1.4E-06
TCE (TCE sol.)	3.0E-02	2.9E+04	1.9E-04	8.8E-03	8.3E+04	8.8E-06	3.3E-02	1.7E+04	3.1E-05

Another limitation of this experiment was the inability to quantitatively assess losses of the VOCs during the three-week equilibration time. While water solution controls were built into the experimental setup, the absence of the FACT strip in the controls changed the nature of these experiments such that there could be elevated losses; the lack of FACT strip in the controls removed a major sink for the analyte from these vials leading to these hydrophobic molecules of interest to have higher affinity to the silicon cap and the gaseous phases not measured in the experiment.

Isotherm modelling was also performed on the VOCs with all 3 sample groups A, B and C combined together, to assess how the experimental results change with a higher number of data points used, and to test the scalability of the experimental design. The Freundlich model and Langmuir model plots with all contaminant groups, and contaminant constituents plotted together can be observed in Figure 3.4.

A trend can be observed that displayed higher sorption rates for compounds with lower polarity. This trend was consistent with what was observed in the boxplots earlier in the section (section 1.2.1), where the less polar, hydrophobic molecules had a higher affinity for the non-polar surface of the FACT. With the increase in experimental data points used to build these models (by combining all three experimental groups into a single dataset), both the Freundlich and the Langmuir isotherms visually appeared to be more predictive of the sorption tendencies with respect to the FACT. The Freundlich isotherm does not appear to under predict the saturated FACT surface curve as poorly, and the Langmuir does not over predict the saturation curve as drastically. Visually inspecting the plots does indicate that the models appear to be as predictive as they possibly can be, as the experimental data showed high levels of spread at the different concentration levels, which was especially apparent at the higher concentration levels. Overall, the model lines from both the Freundlich and Langmuir isotherms predict the general trends of the VOC partitioning behaviour, and the spread of data points indicate that the statistical inconsistencies displayed by the models are representative of the variation in sorption properties of the FACT.

a)

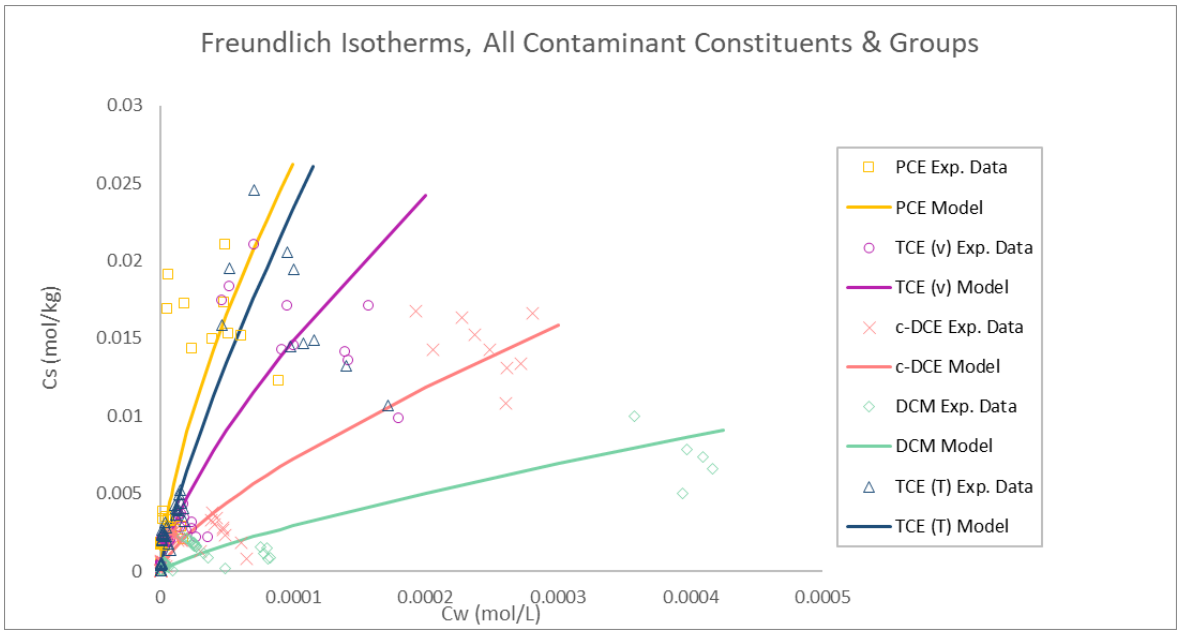

b)

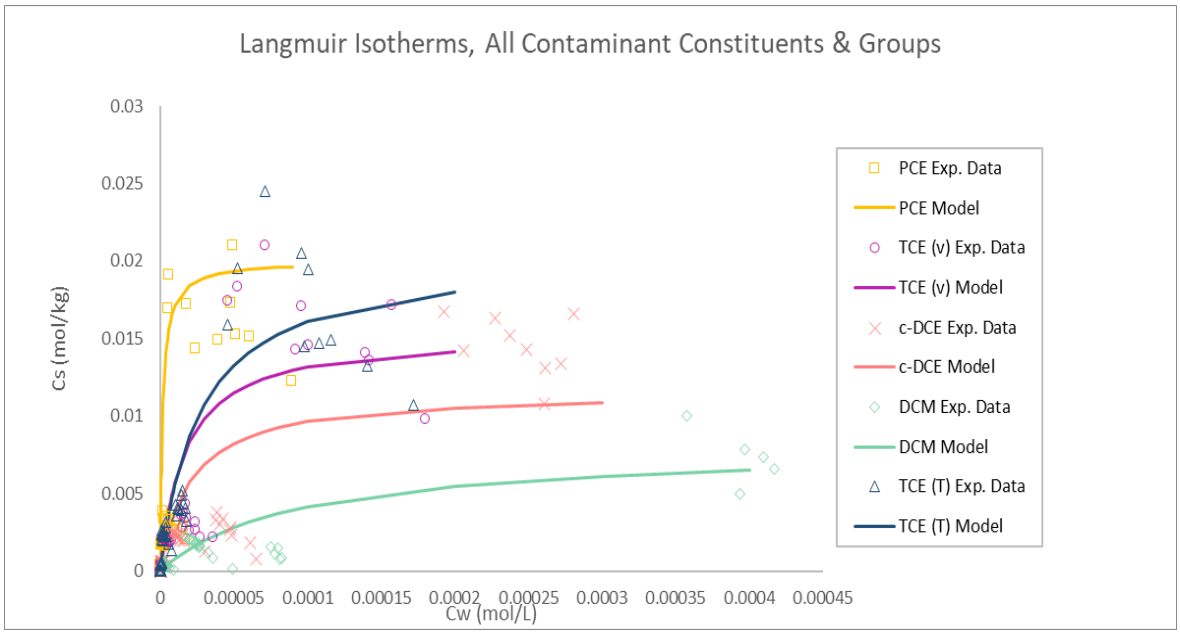

Figure 3-4: Freundlich (3.4a) and Langmuir (3.4b) Isotherm models are displayed with all three experimental datasets combined. A trend can be observed for both model types, in which the less polar molecules (PCE being the least polar, DCM being the most polar) partition a higher amount of mass sorbed to the surface of the FACT than the polar molecules. Both model types seem relatively predictive of the experimental sorption behaviours.

The model parameters for the modelling performed on the combined datasets are presented in table 3.3. The Cs Max parameter from the Langmuir Isotherm model fits were displayed in Table 3.3b), and are an indication of the FACT's sorption capacity. The different contaminant constituents showed Cs max values ranging from 8.0 x 10^3 µmol/kg to 2.04 x 10^4 µmol/kg, indicating a relatively consistent sorption capacity value for the surface of the FACT. The higher polarity molecules- c-DCE and DCM showed lower sorption capacities than the less polar molecules PCE and TCE, but this may be more indicative of the fact that the initial water solution concentrations were not high enough to sorb substantial mass to the surface of the FACT to saturate the surface.

Table 3.3: Corresponding model parameters to isotherm fittings for combined datasets of all three experimental groups. Table 3a) contains the parameters related to the Freundlich Isotherm and 3b) contains the model parameters related to the Langmuir.

a)

Contaminant	Kf (mol/kg)	n	Sum of Square
PCE	12.059	6.66E-01	7.87E-04
TCE (VOC solution)	9.896	7.06E-01	5.43E-04
c-DCE	5.180	7.14E-01	1.20E-04
DCM	3.935	7.82E-01	4.89E-05
TCE (TCE solution)	35.194	7.95E-01	1.39E-03

b)

Contaminant	KL (L/umol)	Cs max (umol/kg)	Sum of Square
PCE	5.95E-01	2.00E+04	2.60E-03
TCE (VOC solution)	5.90E-02	1.54E+04	5.41E-04
c-DCE	4.85E-02	1.16E+04	5.31E-04
DCM	1.08E-02	8.00E+03	6.36E-05
TCE (TCE solution)	3.71E-02	2.04E+04	3.59E-04

The trend in which TCE alone and TCE in VOC solution displayed that a higher level of the TCE is sorbed to the FACT when alone in water solution than when found in solution with other compounds. This can be observed in further detail in figure 3.5, where only the TCE constituent in the VOC solution and TCE alone in solution are displayed on the same isotherm plot.

a)

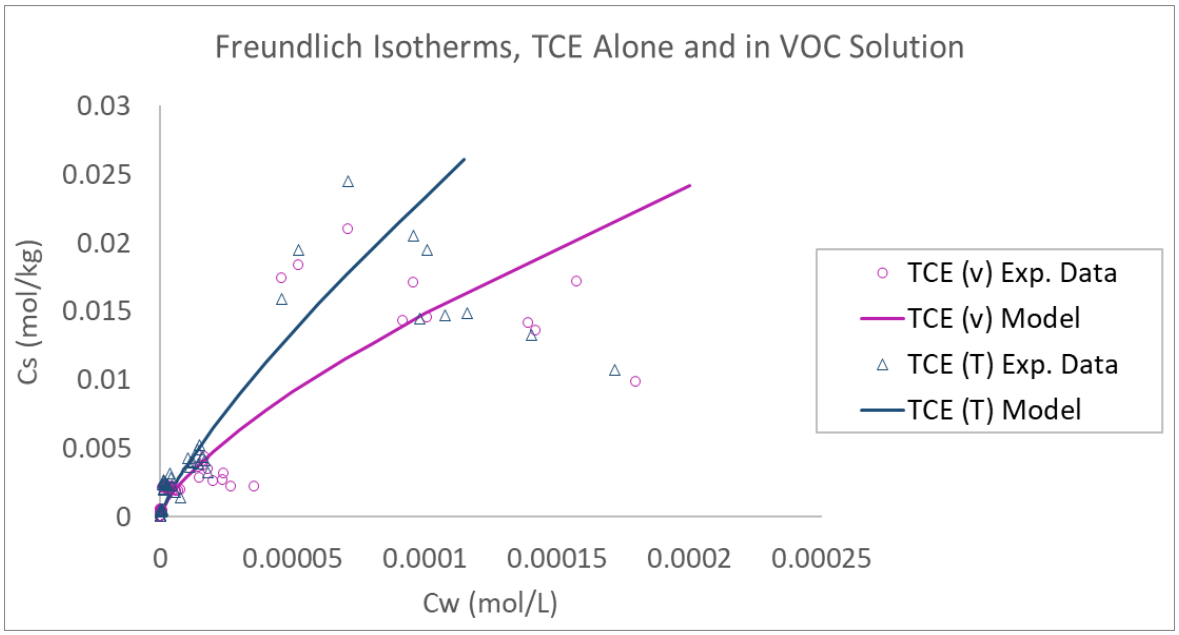

b)

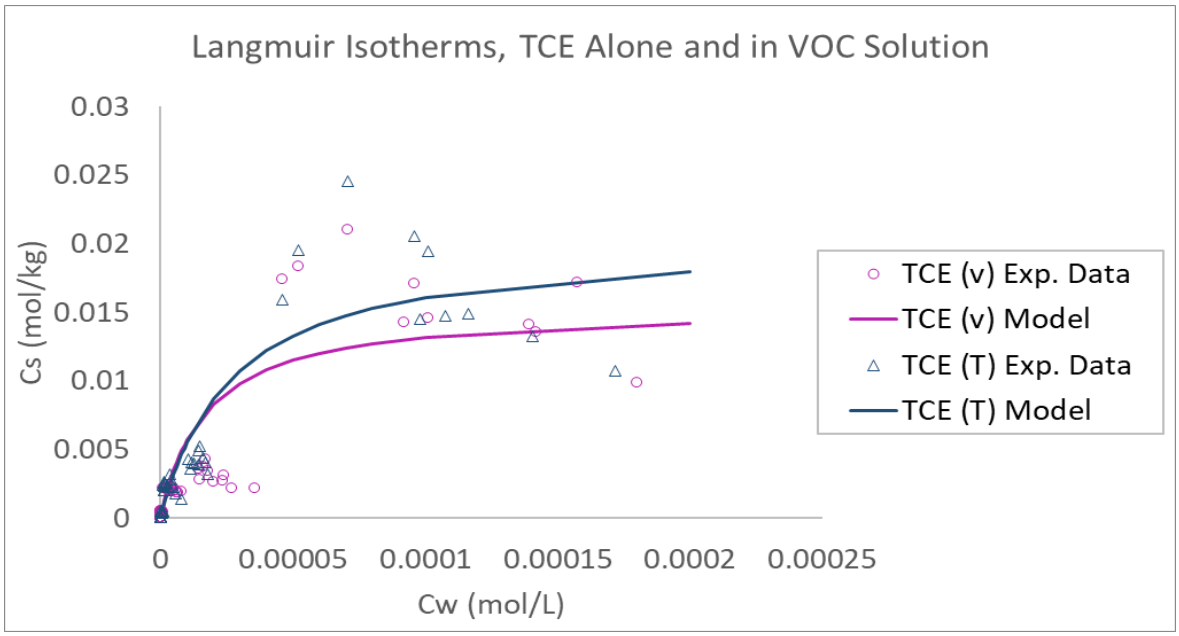

Figure 3-5 : Images of the combined datasets for TCE in VOC solution vs TCE alone in solution. TCE in solution alone appeared to sorb a higher portion of mass to the surface of the FACT compared to TCE in the VOC solution, strongly indicating competitive sorption in the VOC solution. Figure 3.5a) showed the Freundlich Isotherm fit to the datasets and 3.5b) displayed Langmuir modelling.

Figure 3.5 displayed that a higher portion of TCE mass from the solution containing only TCE sorbed to the FACT than in the VOC mixture solution, indicating a competitive sorption affect. While the difference in the model fits between the equilibrium partitioning of TCE in the solution may be within the uncertainties of the experiment for both the Freundlich and the Langmuir model, the TCE molecules alone in solution had more mass sorbed to the FACT at all concentration levels tested.

3.3 Time Period Necessary for Extractant Techniques to Desorb Mass From FACT

Time series data were collected to determine the times necessary for each extraction technique to desorb the maximum amount of solute mass from the FACT (i.e. equilibration times). The results showed these equilibration times to be 3-5 days for the methanol shake flask method, 20 minutes for the MAE method and 24-48 hours for the pentane/water shake flask method. The time series analyses of each extraction, for all techniques tested can be observed in Appendix B.

3.4 Effectiveness of VOC Mass Desorption from FACT Material

The effectiveness of mass extraction from the surface of the FACT is a vital step in analyzing the representativeness of the FACT datasets of in-situ contaminant conditions, i.e. FACT concentrations along the length of the borehole for determining the time-integrated mass uptake onto the FACT during deployment. Before determining the most complete extraction technique, the effectiveness at which each individual VOC can be desorbed from the FACT was studied.

The percent of mass desorbed from the calculated sorbed mass to the FACT (sorbed mass estimated by calculation in the uptake section of experiment (Sorbed Mass = Initial Water Solution Mass - Residual Water Solution Mass After Equilibration) was determined for each VOC and concentration level. Boxplots were completed (Fig. 3.6), where the percent of mass recovered from calculated sorbed mass to FACT is plotted on the y-axis and the boxes are binned by the five different initial concentration levels ranging from 0.1 to 50 mg/L. These boxplots were built using data from all three extraction techniques, first to determine the behavior of the different VOCs during extraction, prior to evaluating the extraction techniques themselves. Each box represents approximately 15 samples (5 replicate samples for the three different extraction types), and plots in Figure 3.6 a) through e) represent the different VOC constituents. The outliers that were defined by the statistical analysis of the uptake section of the experiment have been removed from this analysis to remove bias carrying over to the extraction methods, showing a unique count (number of samples) for each box plot. The extraction boxplots were used to calculate new outliers, which were not used in determining the most effective extraction technique.

PCE displayed a mean percentage recovery of the calculated mass sorbed to the FACT ranging from 47% to 119% and standard deviations from 15% to 60%. The C4 and C5 samples with greater masses sorbed to the FACT displayed greater mass recovery

values, and the masses was also desorbed more consistently between replicate samples at the higher concentration levels. However, in general, the reproducibility of mass desorbed from the FACT between replicate samples was poor, which is displayed by the large box heights representative of the large range in mass desorption values.

TCE displayed a mean percentage recovery of the calculated mass sorbed to the FACT ranging from 43.6 % to 106.4 % and standard deviations from 11% to 62 %. The sorbed TCE mass behaved similarly to PCE, in which the samples with higher concentrations of sorbed mass showed greater mass recovery values and less variability between identical samples, however, for both PCE and TCE there were one and three outliers for this category of samples. In general, the reproducibility of TCE mass desorption values was also very poor.

c-DCE displayed mean percentage recoveries of the calculated mass sorbed to the FACT ranging from 49 % to 159 % and standard deviations from 20% to 64%. A higher percentage of the compound was desorbed for the samples with higher initial mass concentrations (i.e. C4 and C5). Overall, c-DCE showed similar variation in mass recovery values between replicate samples to PCE and TCE showing great variability at all concentration levels. At the two highest concentration levels, c-DCE displayed mass recovery values well over 100% (average values of 131.1% and 159.2%).

DCM displayed mean percentage recoveries of the calculated mass sorbed to the FACT ranging from 59 % to 225.9 % and standard deviations from 31% to 94%. Greater mass recovery yields were observed at the higher concentration levels for the compound, but DCM showed the least reproducibility (i.e. greatest variability) in mass yields between identical samples. Extremely high mass recovery values were observed for DCM at all concentration levels, with mass recovery results well over 200% for individual samples in C1, C3, C4 and C5 groups.

For TCE alone in solution, the compound showed mean mass recovery values ranging from 53.7% to 115.7% and standard deviations ranging from 18% to 34% between concentration levels. TCE-alone showed the same trend as the compounds in the VOC solution. With all analytes, a higher percentage of mass was recovered from the FACT when higher quantities of mass were sorbed to the FACT (i.e. C4 and C5) and also the lowest initial concentration (C1). In terms of consistency at which mass was desorbed from the FACT, TCE alone showed much less variability than TCE and any of the compounds within the VOC solutions, with smaller ranges in mass recovery values at all concentration levels. TCE alone in solution did not demonstrate noticeably different total mass recovery values than TCE in the VOC solution.

Overall, it can be stated that the consistency at which mass was desorbed from the FACT is very poor, regardless of compound type or concentration levels of the initial water solutions that the FACT samples were submerged in. It is noteworthy that C2 (1 mg/L) was the poorest recovery for all analytes in the VOC solution and C3 (5 mg/L) for the TCE alone solution. In terms of which VOC behaved most consistently, PCE, TCE and c-DCE

showed similar variation between mass recovery values, while DCM showed the highest variation in recovery values between replicate samples. TCE alone in solution displayed the most consistent desorption tendencies, compared to the compounds within the VOC solution. It is difficult to assess which compound was desorbed from the FACT at the highest mass recovery percentages overall, because the percentages ranged greatly within each and between all the different concentration levels. Some mass percentage values, particularly the results from the more polar molecules c-DCE and DCM, have unreasonably large mean recovery percentages upwards of 150%, considered further below.

The unusually large recovery values are attributed to the uncertainties involved with the calculated sorbed mass values from the first section of the experiment. The equilibrium distribution of compounds from the batch water solutions sorbed to the FACT (Cs, mol/kg dry FACT) and remaining in the water solution (Cw, mol/L) after the three-week immersion of the FACT were determined by subtracting the quantity of mass left in the water solution after the equilibrium period from the initial mass in the water solutions, confirmed by analysis. Any mass not remaining in the water solution after the three weeks was assumed to be sorbed to the FACT, which introduces an unknown amount of uncertainty in the experiment, that is carried over to the desorption section of the experiment. For c-DCE and DCM, which display the most erroneously high recovery values, it is expected to be due to an underestimation of the mass sorbed to the FACT, leading to a higher amount of mass desorbed from the FACT than expected during the second part of the experiment. This would indicate a cross contamination event occurring during the laboratory experiment as the root cause for these overly high recovery values, although we do not see evidence of this from our controls/blanks.

a)

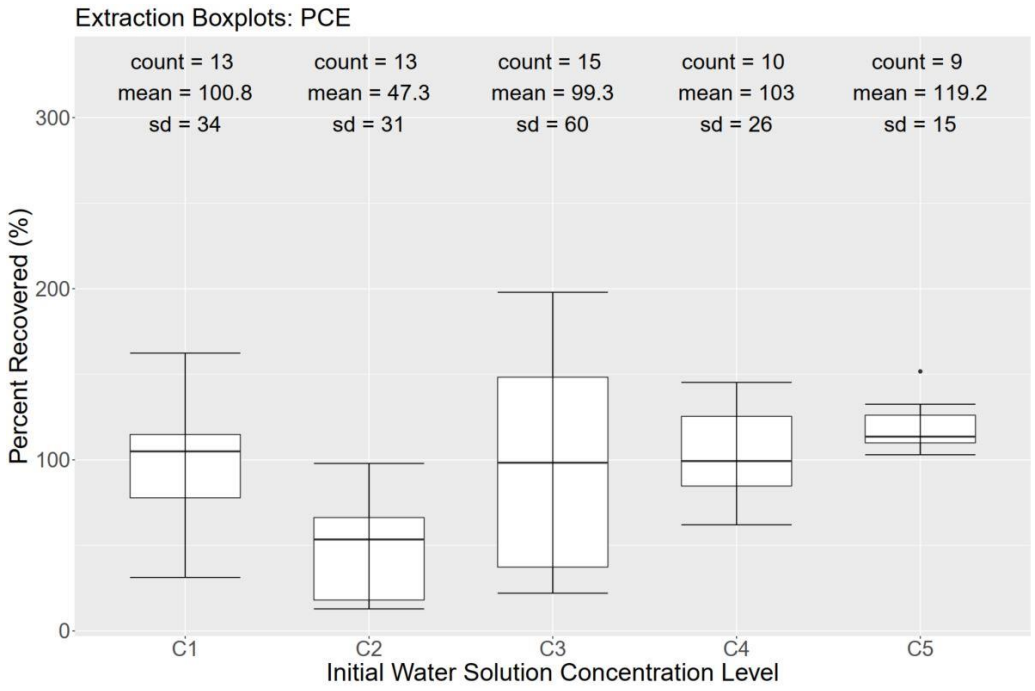
Extraction Boxplots: PCE
count = 13
mean = 100.8
sd = 34
count = 13
mean = 47.3
sd = 31
count = 15
mean = 99.3
sd = 60
count = 10
mean = 103
sd = 26
count = 9
mean = 119.2
sd = 15
300
200
100
0
Percent Recovered (%)
C1
C2
C3
C4
C5
Initial Water Solution Concentration Level

b)

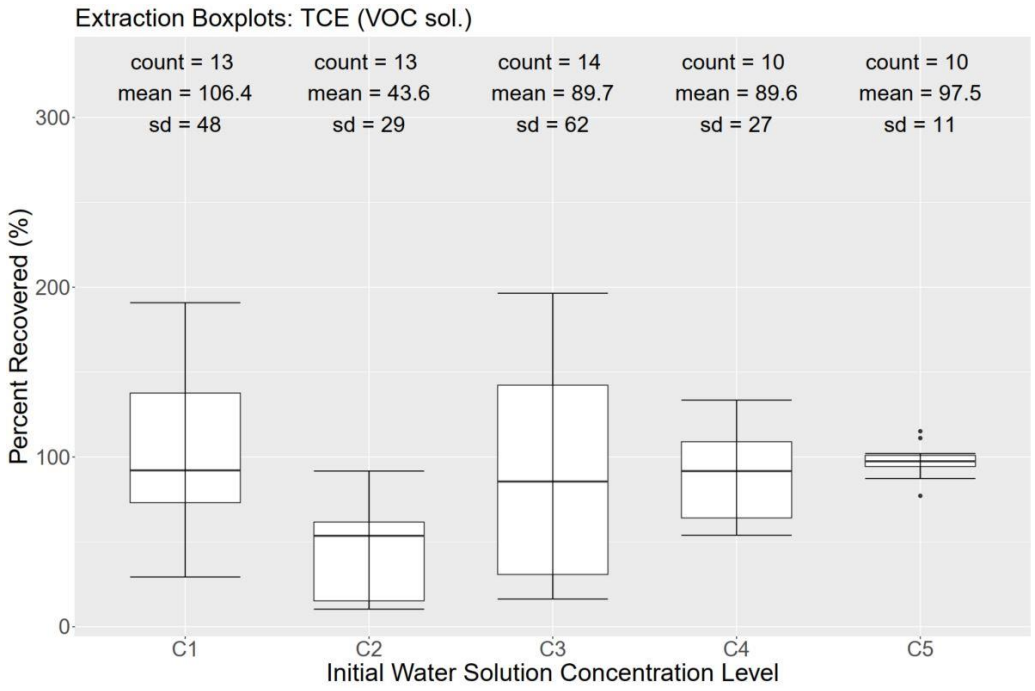
Extraction Boxplots: TCE (VOC sol.)
count = 13
mean = 106.4
sd = 48
count = 13
mean = 43.6
sd = 29
count = 14
mean = 89.7
sd = 62
count = 10
mean = 89.6
sd = 27
count = 10
mean = 97.5
sd = 11
300
200
100
0
Percent Recovered (%)
C1
C2
C3
C4
C5
Initial Water Solution Concentration Level

c)

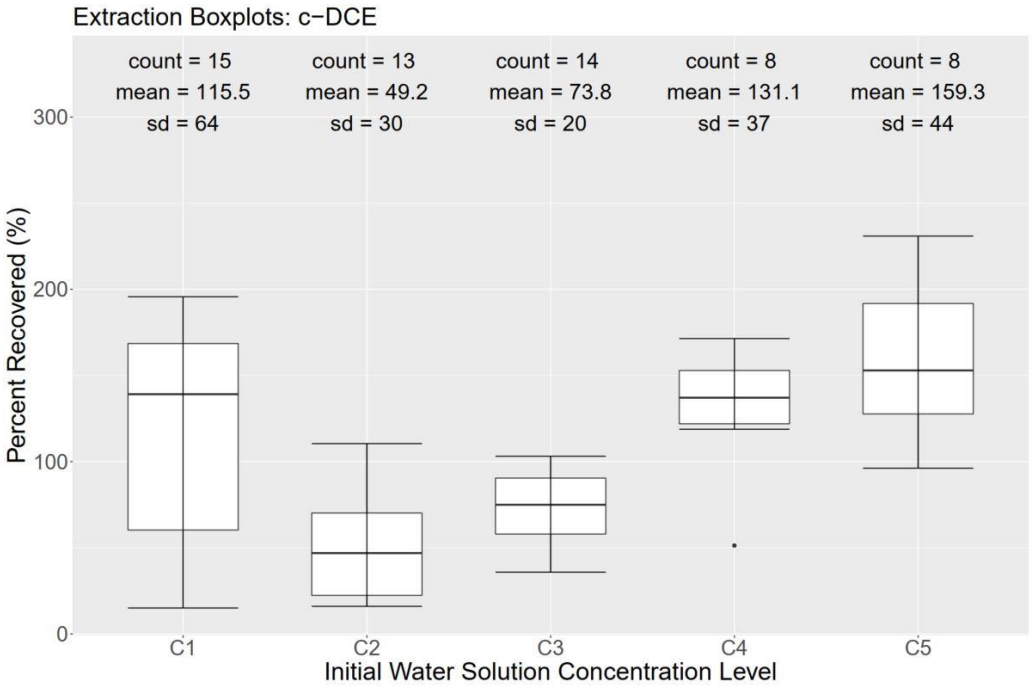
Extraction Boxplots: c−DCE
count = 15
mean = 115.5
sd = 64
count = 13
mean = 49.2
sd = 30
count = 14
mean = 73.8
sd = 20
count = 8
mean = 131.1
sd = 37
count = 8
mean = 159.3
sd = 44
300
200
100
0
Percent Recovered (%)
C1
C2
C3
C4
C5
Initial Water Solution Concentration Level

d)

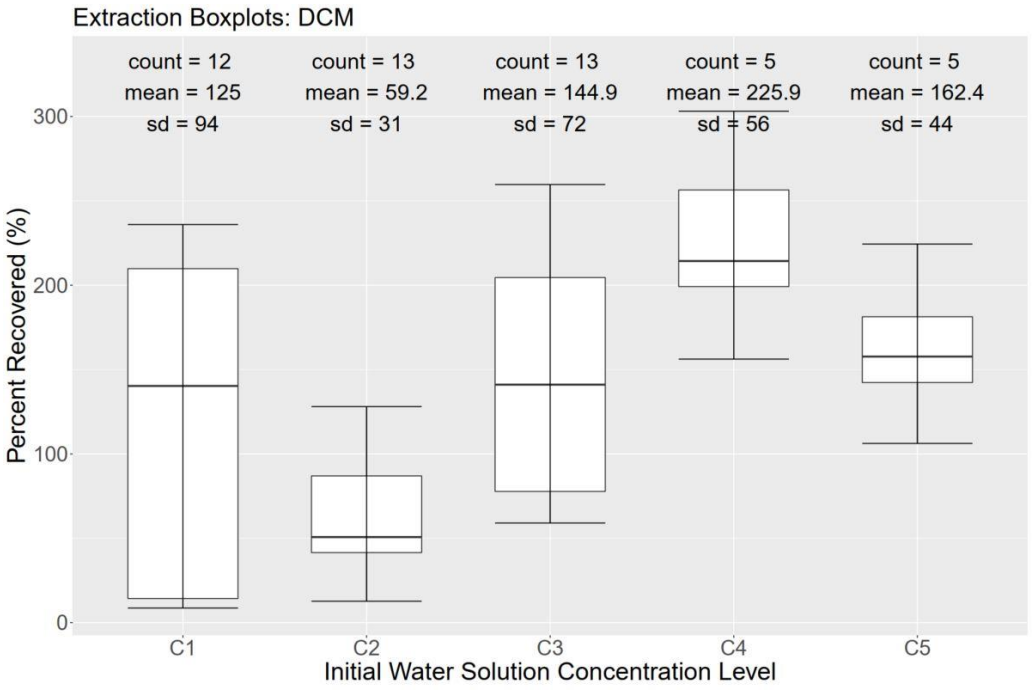
Extraction Boxplots: DCM
count = 12
mean = 125
sd = 94
count = 13
mean = 59.2
sd = 31
count = 13
mean = 144.9
sd = 72
count = 5
mean = 225.9
sd = 56
count = 5
mean = 162.4
sd = 44
300
200
100
0
Percent Recovered (%)
C1
C2
C3
C4
C5
Initial Water Solution Concentration Level

e)

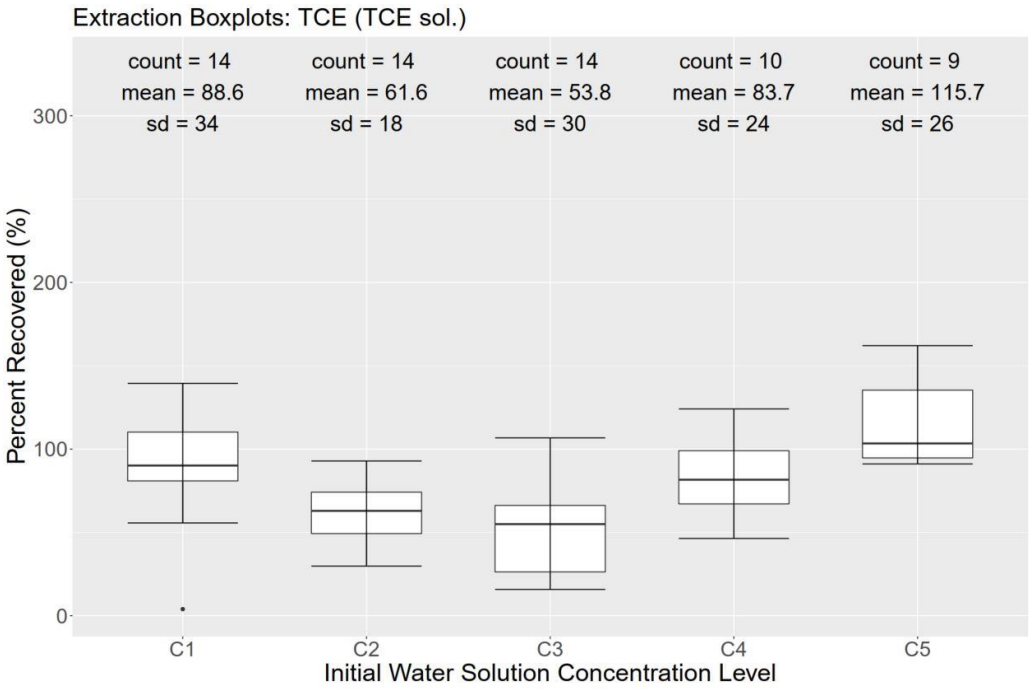

Figure 3-6: Boxplots displaying the percent of theoretical mass sorbed to the FACT desorbed, binned by the different initial water solution concentration levels. The desorption data for PCE, TCE, c-DCE and DCM in the VOC solution are displayed in plots a), b), c) and d) respectively. TCE alone in solution is shown in figure e).

To assess the effectiveness of the different extraction techniques, a statistical analysis was completed on the percent recovered for all samples involved, for all concentration levels and contaminant types, which can be observed in Table 4. The average percent recovered for the methanol shake flask method and microwave assisted extraction methods displayed high average percent recovery values of 96% ± 6% and 113% ± 12 respectively, while the pentane/water mixture method resulted in an average percent recovery of only 70% ± 7 at a 90% confidence interval. It was evident at all concentration levels and for all VOC analytes, the pentane/water mixture was the least effective method at desorbing contaminant mass from the surface of the FACT. Due to the variable nature of the dataset, the geometric mean for the mass percent recovery values was also used, which is often a better representation of datasets that have a large range in values/many outliers, as it puts less emphasis on outliers than the arithmetic mean (Seybold et al, 1992). The geometric mean recovery percentages for the MeOH, MAE and Pentane/Water extraction techniques were 83%, 91% and 54% respectively. Again, it is clear that MeOH and MAE methods were clearly more effective for analyte desorption from the surface of the FACT, but the geometric mean displayed slightly lower recovery

values for the dataset as a whole. The geometric mean may display a better representation of the recovery values, suggesting that the recovery efficiencies are lower than calculated using a standard average.

Table 3.4: Average percent recovered from the theoretical sorbed mass to the FACT for each extraction techniques tested in the experiment, along with complementary parameters.

	MeOH	MAE	Pentane/Water
Avg. Percent Recovered	96	113	70
CI 90%	6	12	7
Sample Size	144	73	116
Geometric Mean Percent Recovered	83	91	54

To further assess the performance of the methanol shake flask and the methanol with microwave assisted extraction methods, both determined to be the most useful desorption techniques, the effectiveness of the methods were compared based on VOC type and concentration level and the results presented in Tables 3.5 & 3.6. In Table 3.5, the extraction technique efficiency based on the different VOC constituents were displayed, where the average percent recovered by each compound is shown, along with the confidence interval, sample size and geometric mean percent recovery. It is important to note that the MAE method was not used for samples that were at the two highest concentration levels, and therefore a direct comparison between the two methods is not attainable due to the different sample sizes. For all VOC samples tested, the MAE method desorbed a higher average percent of mass from the surface of the FACT regardless of compound type. That being said, the 90% confidence intervals for the average results were consistently greater for the MAE extraction, and were close to or are overlapping with the average values from the methanol shake flask method. This suggests that the higher recovery averages obtained by the microwave method were not statistically significant, and that the effectiveness at removing mass from the FACT are comparable between the two methods. However, the methanol shake flask method displayed more consistent desorption results than the microwave method (lower standard deviations for the chlorinated ethenes and shake flask technique, but nearly equal for DCM), demonstrating that it is a superior extraction technique for removing VOC mass from the FACT.

Table 3.5: Percent of mass recovered from theoretical mass sorbed to the FACT by VOC type, for a) - methanol shake flask method and b)- methanol with microwave assisted extraction.

a)

MeOH					
Compound	**PCE**	**TCE (V sol.)**	**c-DCE**	**DCM**	**TCE (T sol.)**
Avg. Percent Recovered (%)	109	94	118	115	92
CI 90%	7	6	14	33	7
Standard Deviation	22	17	40	88	20
Sample Size	24	22	22	19	24
Geometric Mean Percent Recovered (%)	107	92	111	74	89

b)

MAE					
Compound	**PCE**	**TCE (V sol.)**	**c-DCE**	**DCM**	**TCE (T sol.)**
Avg. Percent Recovered (%)	118	123	97	159	72
CI 90%	23	25	22	38	13
Standard Deviation	53	58	52	87	31
Sample Size	14	15	15	14	15
Geometric Mean Percent Recovered (%)	102	105	82	119	60

In table 3.6, the extraction efficiencies of the methods are assessed based on the initial mass concentration levels of the VOCs in the water solution that the FACT was submerged in for 3 weeks. Again, it should be noted that the two highest concentration levels: 10 mg/L and 50 mg/L were not tested with the MAE method due to danger of contaminating the microwave vessel. Similar trends can be observed in table 6 as in table 3.5, where higher mass percent recoveries were produced by the MAE technique than the methanol shake flask method, but were still well within the uncertainties of the experiment. The methanol shake flask method displayed mass recovery percentages over 100% for the higher two concentration levels, suggesting greater uncertainty in the experimental design at these concentration levels.

Table 3.6: Percent of mass recovered from theoretical mass sorbed to the FACT by initial water solution concentrations, for a) - methanol shake flask method and b)- methanol with microwave assisted extraction.

a)

MeOH					
Water Solution Concentration	**0.1 mg/L**	**1.0 mg/L**	**5.0 mg/L**	**10 mg/L**	**50mg/L**
Avg. Percent Recovered	100	79	83	138	113
CI 90%	16	8	8	17	9
SD	46	22	22	53	28
Sample Size	23	19	20	26	23
Geometric Mean Percent Recovered	82	76	81	131	109

b)

MAE					
Water Solution Concentration	**0.1 mg/L**	**1.0 mg/L**	**5.0 mg/L**	**10 mg/L**	**50mg/L**
Avg. Percent Recovered	146	52	136	N/A	N/A
CI 90%	19	7	19	N/A	N/A
SD	57	22	58	N/A	N/A
Sample Size	25	23	25	N/A	N/A
Geometric Mean Percent Recovered	124	46	124	N/A	N/A

Overall, the methanol shake flask method was the best performing extraction technique in this experiment for desorbing mass from the FACT by providing high mass-recovery percentages and displayed the most consistent recovery values between replicate samples. The methanol with microwave assisted extraction did extract, on average a higher percentage of VOC mass from the FACT, but the methanol shake flask method showed a much lower variance in the amount of mass desorbed between replicate samples. In terms of the consistency at which VOCs are extracted from the FACT, regardless of the extraction method, the procedure shows a high level of uncertainty. The FACT material appears to be the greatest source of variability in the experiment, which further emphasizes the importance of determining the composition of the FACT and the distribution of AC to determine the origination of the inherent variability.

3.5 FACT Micro-Analysis

Three different versions of the FACT strip were observed under a digital microscope and a scanning electron microscope, which were taken from FACT versions that were in circulation in 2017, 2019 and 2020. The different versions of the FACT are variable in nature, as the activated carbon impregnated material used in the technology were received from different distributors throughout the years. The 2020 FACT strip was the technology that was assessed during the uptake and extraction laboratory experiment.

a) b)

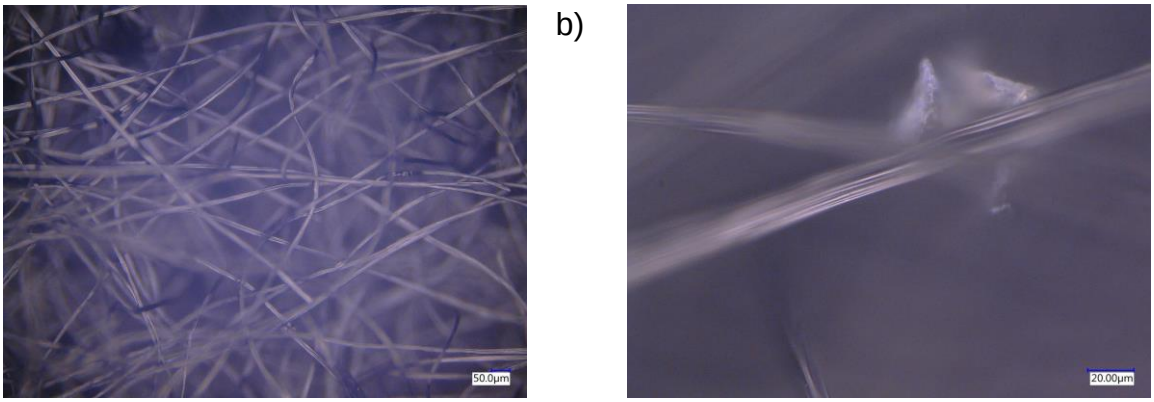

Figure 3-7: Digital microscope images of the FACT, manufactured in the 2017. Figure 3.7a) displays the general matrix structure of the FACT backing, and figure 3.7b) shows a zoomed image of a single backing strand, where striations parallel to the strand's length can be observed, along with a particle fastened to the side of the strand.

Observing the 2017 FACT with a digital microscope (Fig.3.7) revealed a complex, three-dimensional matrix of interwoven fabric strands, which represented the backing material in which the activated carbon was impregnated into. The density of the backing material varied slightly within a single microscopic field of view (FOV, approximately 1000 x 1000 um) and varied greatly when observing different sections of a 6-inch FACT sample. Minimal to no particulate matter was observed on the surface of the backing fibers in most FOVs. When particulate matter was observed, very small granules were seen, distributed sparsely within the backing material matrix. The resolution of the digital microscope was fairly poor while observing the samples at this scale, and therefore, it is possible that there were smaller particles that could not be detected by the digital microscope.

a) b)

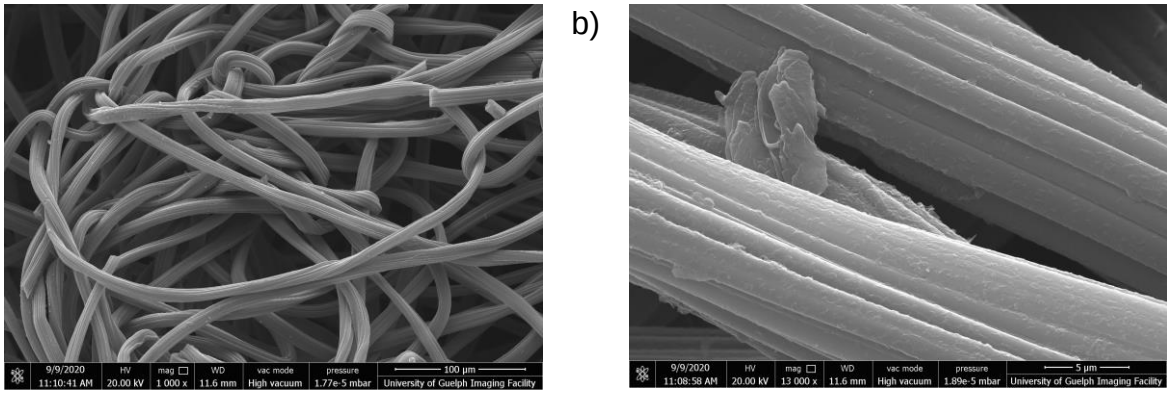

Figure 3-8: Scanning electron microscope images of the 2017 FACT. Figure 8a) displays the general structural characteristic of the material, in more detail than the digital microscope image, and figure 8b) displays a zoomed image, with higher resolution details of the striations and particle structure.

The SEM assessment of the 2017 FACT revealed similar conclusions, where the backing material was observed as a complex matrix of interwoven fabric strands with varying density and little to no evidence of particulate matter impregnated into the matrix (Fig. 3.8). The particles can be observed in greater detail using the SEMs greater resolution and higher magnifications than the digital microscope. The particles appear to be combined in a collection of thin sheets connected horizontally together. When the backing material was observed at a finer scale (nanometer scale), extremely small particles were observed on the surface of the material strands. While it is possible that these particles are impregnated AC material it is unlikely that the technology uses an AC type with such fine particles. The higher resolution images also displayed parallel striations on the backing strands, which was only observed on the 2017 FACT backing material.

a) b)

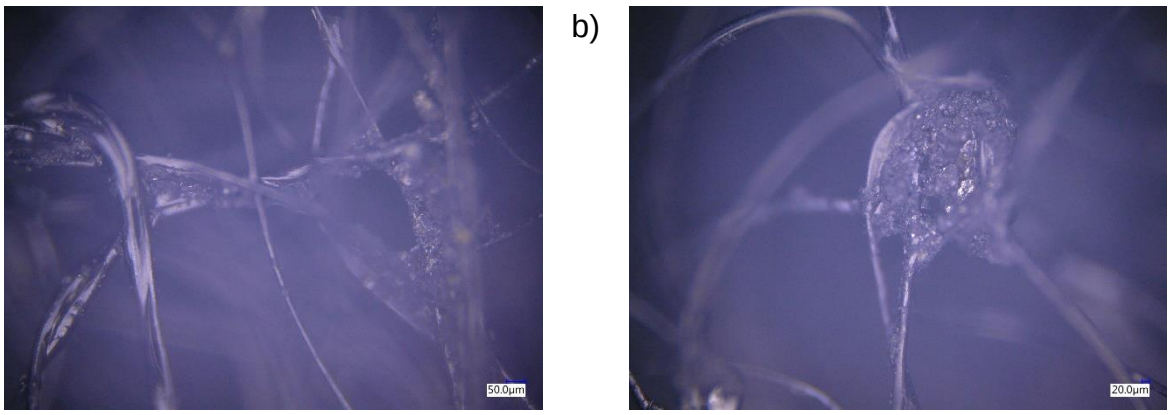

Figure 3-9: ***Digital Microscope images of FACT material manufactured in 2019. A less uniform thickness backing material can be observed, with higher concentrations of particulate found on the surface of the backing strands. Figure 3.9 a) displays the general structure of the backing material and Figure 3.9 b) shows a zoomed image of the particulate matter.***

The 2019 FACT displayed much different characteristics when observed under the digital microscope (Fig. 3.9). The backing material was interwoven into a complex matrix similar to the 2017 material, but the thickness of the individual strands was much less uniform, with bulging sections of varying thicknesses. The texture of the backing material was much smoother, with no observed striations/parallel grooves that were seen in the 2017 FACT. The thickness of the matrix was much greater than the 2017 version, with many different layers being possible to focus onto. The presence of particulate matter within the backing material was observed, with large chunks of dark material, with diameters as large as 500 µm distributed relatively consistently throughout the matrix in a single FOV. The particles were mainly present in areas where multiple backing strands terminated and also drooping down from the middle of strands. The distribution of particles varied significantly between different samples observed, but the consistency of particulate matter distribution was far greater than the 2017 FACT. The particles showed clear crystal-like structure, with high luster and multiple colourations of black, brown and orange. There appeared to be a coating in areas where the particles were found.

a) b)

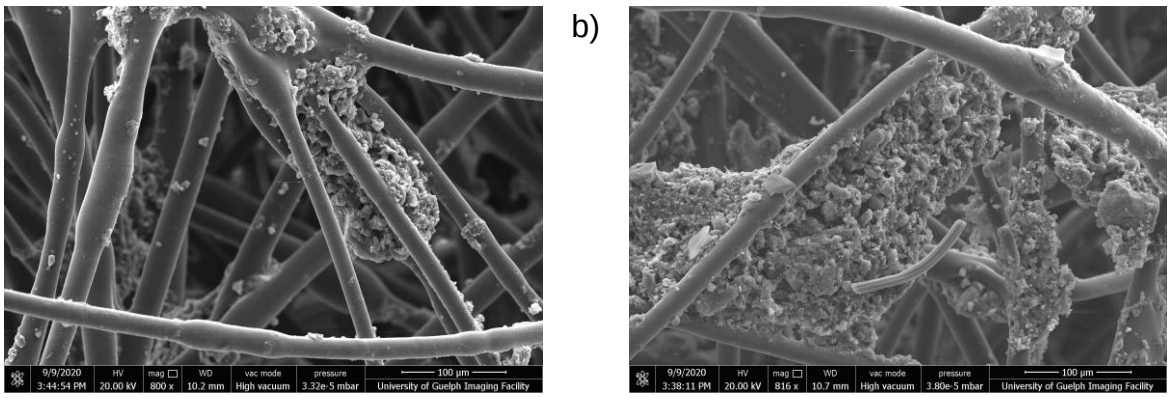

Figure 3-10: Scanning electron microscope images of FACT material manufactured in 2019. A less uniform thickness backing material can be observed than displayed in the 2017 manufacturing year, with higher concentrations of particulate matter found on the surface of the backing strands. Figure 9 a) displays the general structure of the backing material and Figure 9 b) shows a zoomed image of the particulate matter.

When observing the 2019 FACT with the SEM, the particle structure could be observed in much greater detail (Fig. 3.10), where a multitude of similar sized particles are aggregated together to form the particle chunks. With the higher resolution obtainable with the SEM, it could be observed that the backing material was packed more densely than in the 2017 FACT.

a) b)

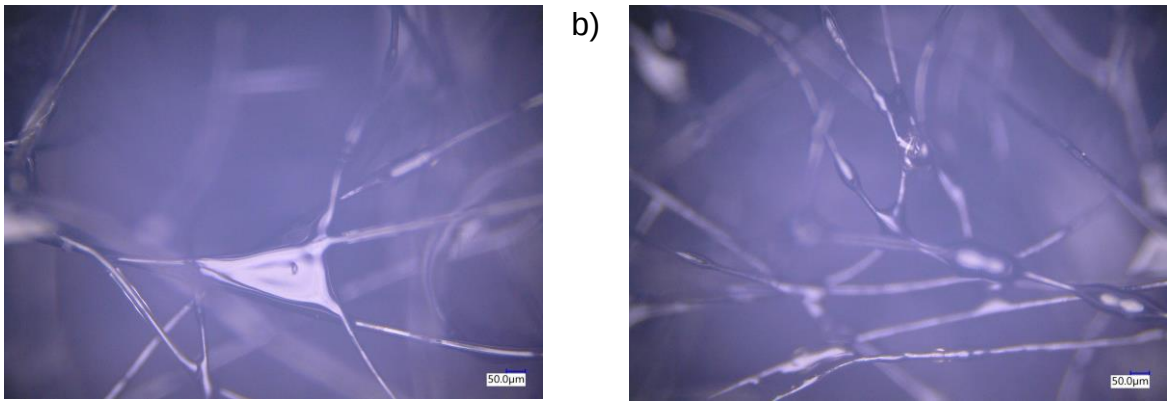

Figure 3-11: Digital Image of the FACT manufactured in 2020, the same FACT type that was used in the laboratory experiment. Figure a) and b) display the general structure of the FACT material, and apparent "coating" that appears to be located on the backing material and drooping down from strands and meeting points of strands.

The 2020 FACT, which is the FACT version that was used during the uptake and extraction experiment appeared to have a combination of the "coating" that was observed in the FACT 2019 when observing the material using the digital microscope and the

granular, crystal like particles (Fig. 3.11). There was a sparser distribution of the granular particles in this FACT material compared to the 2019 material. The backing matrix appeared to be the same material used in the 2019 FACT, with no evidence of ridging, and a non-uniform thickness for the individual strands. The thickness of the backing material as a whole also appeared to be similar to the 2019 FACT. While the distribution of particles appeared to not change significantly in a single FOV, the distribution did seem to change greatly from sample to sample. There was an inconsistent amount of particulate matter when looking at a different replicate 6-inch section, which would explain the high variation between replicate samples in the uptake/extraction experiments if these particles could be considered to be AC.

a) b)

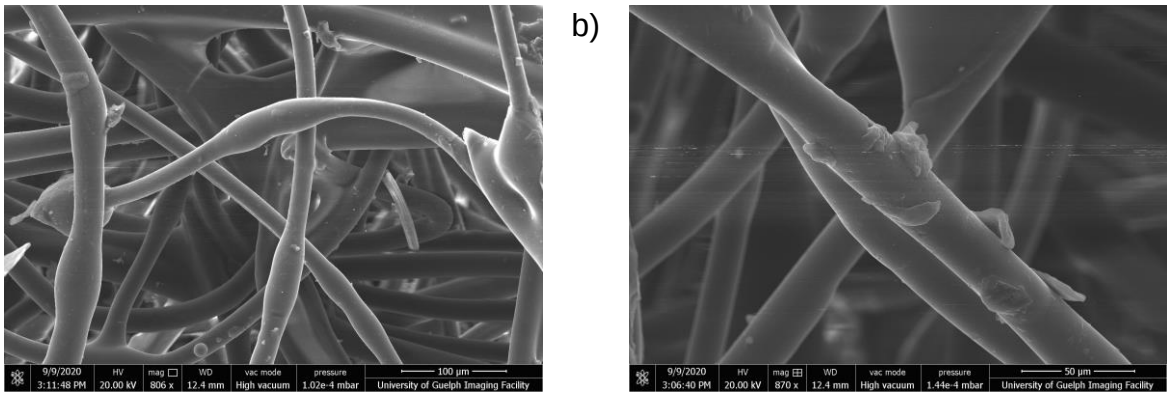

Figure 3-12: Scanning electron microscope image of the FACT manufactured in 2020. The backing material appears to show same characteristics as FACT 2019 version (displayed in figure 3.12 a), but contains different structured particulate matter on the surface of the strands than the 2019 version, displayed in figure 3.12 b).

Using the SEM with a higher resolution image, it again seemed apparent that the “coating” was not present in the FACT 2020 samples (fig. 3.12). The backing material appeared to be identical to the 2019 FACT backing material, but the number of granules was much lower than in the 2019 FACT. The distribution of the particulate matter also appears to be more variable, and the amount found in each replicate sample ranged significantly.

From the micro-scale analysis of the different FACT versions, it can be said that there were distinct and extensive differences in the characteristics of the FACTs from different years. The backing material density and texture varied from version to version, and the distribution of particles within the matrix material was extremely variable between FACT types. The type, and amount of particulate matter found between FACT materials was also extremely inconsistent, leading to materials with very different surface areas, and therefore far different sorption capacities. The FACT 2019 material appeared to have the most consistent properties in terms of backing density and particle distribution, and also displayed the highest particle content. The 2017 FACT material appeared to display the lowest particulate content, and the density of the backing material varied significantly.

The 2020 FACT material, which was the FACT that was focused on for the majority of the study showed an inconsistent distribution of particulate matter, with a much lower abundance than in the 2019 FACT. With the high inconsistency between the materials in the FACT versions, the use of this technology for comparative studies/long term studies in which FACT datasets would be compared over an extended time period using the different versions would become extremely imprecise. In a singular borehole, if a 2017 FACT was deployed and then later in time the 2019 or 2020 FACT was deployed, the concentration profiles reported would display different contaminant concentration levels year to year, regardless of the insitu conditions. Since the 2017 FACT appears to have a lower sorption capacity, the contaminant concentration would likely be reported as much lower than with the FACT 2019/2020 deployments, even if the groundwater conditions had not changed. Any past datasets that have used multiple FACT deployments over an extended time should not be directly compared to assess remediation/retardation of the contaminants. The number of different FACT materials used since the technology was made commercially available is unknown, and therefore any sites in which multiple FACT liners have been deployed over an extended time may have biased/imprecise datasets that are not directly comparable.

FACT 2017 **Zheng et al, 2014 – Commercial AC**

a) b)

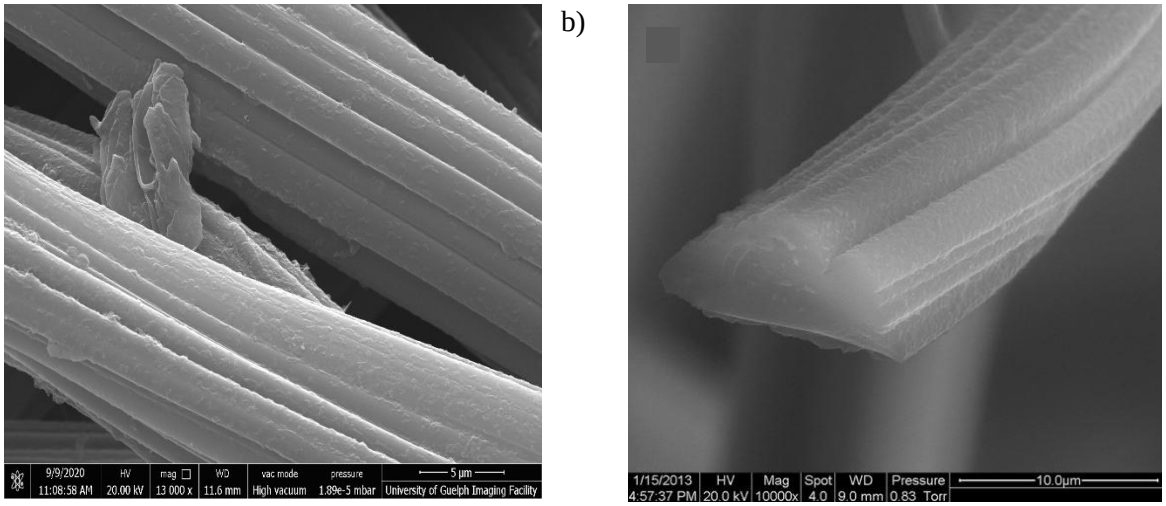

FACT 2020 **Zheng et al, 2014 – Cotton Fabric**

c) d)

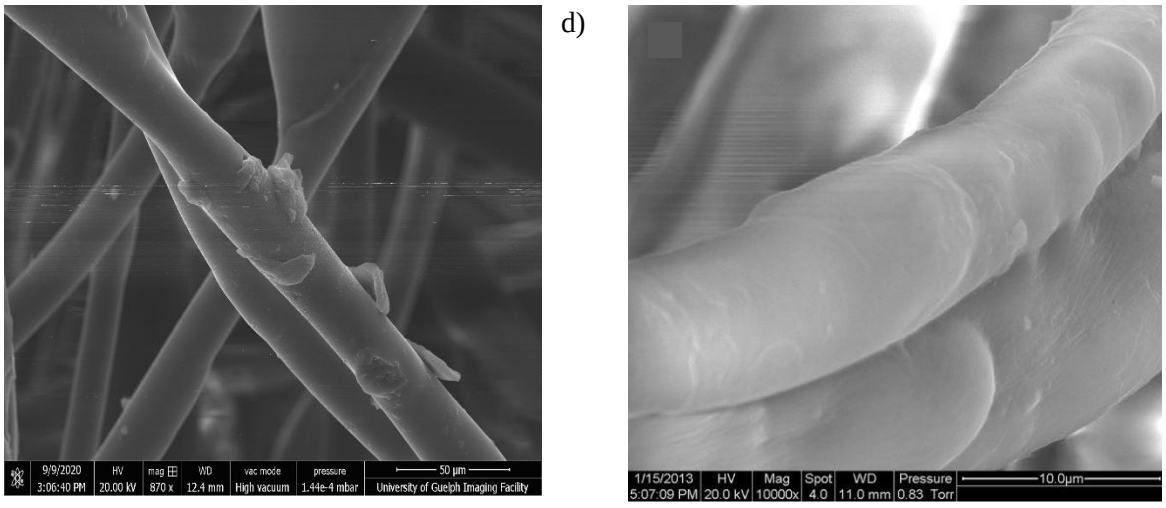

Figure 3-13: ***The FACT versions observed under an SEM in the laboratory experiment are displayed, along with different types of activated carbon materials observed under an SEM in the investigation conducted by Zheng et al in 2014. The 2017 FACT version, commercial activated carbon (Zheng et al, 2014), 2020 FACT version and prepared cotton fabric AC observed under an SEM are displayed in figures 13 a), b), c) and d), respectively.***

A literature review was conducted to determine the type of activated carbon used in the FACT material from manufacturing year to year, as it is clear that the same material was not used consistently. In a study coauthored by Zheng and coauthors titled “Preparation and Characterization of Activated Carbon Fiber From Cotton Woven Fiber” (Zheng et al, 2014), different types of activated carbon were observed under an SEM. In Figure 3.13, the types of FACT materials are compared to these SEM images from Zheng et al, 2014, in which striking similarities can be observed. The 2020 FACT used in this laboratory

study showed great similarities to the cotton fabric that had been heat treated to form activated carbon charcoal. This gives us greater understanding as to the material type we have studied in the uptake and extraction laboratory experiment. The 2017 FACT also showed very similar features to the commercial activated carbon material observed in Zheng et al, 2014, with the striations present running parallel to the length of the backing material.

The full laboratory report for the BET surface area analysis of the 15 FACT samples (5 replicate samples were measured for the 3 different FACT source materials identified in this study by year) is provided in Appendix F, and the individual results are summarized in Table 3.7.The 2017 FACT samples displayed an average specific surface area of 2067 ± 665 m^2/g, the 2019 FACT samples measured 4.35 ± 0.51 m^2/g and 2020 FACT measured 1.30 ± 0.51 m^2/g, each on a dry weight basis. Considerable variability in the specific surface area measurements was observed between the different FACT manufacturing versions (years), as the FACT 2017 samples displayed specific surface areas two orders of magnitude larger than the 2019 and 2020 samples. Additionally, the relative standard deviation of surface area for each manufacturing years were significantly high, ranging from 0.44-0.66, representing standard deviations that ranged from 44%-66% of the average surface area measurements.

Table 3.7: Summary of BET Surface Area Analysis of FACT Material.

Specific Surface Area (m^2/g)	FACT 2017	FACT 2019	FACT 2020
Average	2067	4.35	1.30
Geometric mean	1944	3.46	1.16
CI 90%	665	2.12	0.51
RSD%	0.44	0.66	0.53

The observed variability with respect to the small-scale structure of the FACT using the digital and scanning electron microscopes was confirmed with the BET analyses, and provides quantitative insights regarding the variable nature of the sorption capacity of the FACT within a 15 cm long strip. There were clear and distinctive visual differences between each FACT manufacturing version that also showed large inconsistencies in sorption properties.

The inherent variability between replicate FACT samples contributed substantially to the variability that was observed during the uptake and extraction laboratory tests of the FACT in this study. The FACT 2020 manufacturing year samples tested for surface area were taken from the same roll that was used in the laboratory experiments and showed large variation in surface area measurements. The variation in surface area is assumed to be an indirect representation for the variation in sorption capacity, which would lead to fluctuating VOC sorption values in the laboratory experiments, is expected to have contributed strongly to the large range in Cw and estimated Cs values for each of the initial concentrations.

Applying these findings to the field performance of the FACT, the variation of sorption capacity of a single FACT, activated carbon impregnated strip, would lead to inaccurate vertical concentration profiles of the subsurface environment. The FACT analyses reported in the literature or from other authors' individual experiences have been performed on samples as small as 4 cm and up to 75 cm in length. The variability of the FACT at these lengths has not yet been evaluated, but exclusively at the 15 cm length. Large concentrations of contaminant mass sorbed to a single section of the FACT strip could erroneously lead to interpretations of a major mass transporting fracture in the subsurface, but the actual rationale for the high concentration of contaminant mass may be due to the FACT having higher sorption capacities in this section of the strip relative to adjacent sections. However, in contaminated groundwater with low concentration levels in which the sorption capacities are not at risk of being exceeded, these variabilities may not have a large impact on the representativeness of vertical concentration profiles of the subsurface environment.

The inconsistency in the FACT manufacturing years sorption capacities would also have negative implications for field performances, as the FACT cannot be used effectively across timelines that would require multiple FACT liners. For example, in situations where monitoring of groundwater contamination in a single borehole is needed on a yearly basis, the FACT may display increasing or decreasing contaminate concentrations, even if the concentrations remain the same, due to the variability in sorption properties between FACT liners used. In cases where long term monitoring using the FACT is necessary, multiple FACT liners from the same manufacturing year should be purchased to be used in future monitoring boreholes.

To improve the application of the FACT technology for assessing contaminant mass concentrations and/or flux variability with depth in bedrock boreholes, a reliable distributor of activated carbon material should be established with well-constrained sorption properties. A distributor that can provide consistently made activated carbon material with high sorption capacities would generate quantitative vertical contaminant profiles, erasing most of the uncertainties that accompanies the current product design. The FACT deployment via FLUTe liners provides excellent versatility for mapping contaminant mass flux distributions in new and existing open rock boreholes, but at the moment is confounded by strong variability in properties. The future utility of this technology depends on improved product behavior at the desired sampling scale not provided in the 2017, 2019 and 2020 FACT manufacturers. Quantitative analysis requires determining the sorption behaviour and parameters to be conducted in a manner similar to this study, making it less practical and cost-effective. Additional complication in FACT interpretations at field sites due to site hydrogeologic and borehole hydraulic conditions also need to be considered and are beyond the scope of this study. However, the measured concentration uncertainty inherent in this technology supports the need for improved FACT specifications with known behaviour as well as use of complementary lines of evidence for interpretation of field site conditions being interpreted form this technology. This study supports the need for multiple data types to be used alongside the FACT. Borehole and

field site conditions have not been considered, which may also be a factor in terms of the representativeness of the profiles produced by the FACT.

4 Conclusion

The FLUTE FACT™ (FLUTe Activated Carbon Technique) is a borehole technology used for mapping organic contaminant distributions in the subsurface, typically in open bedrock boreholes and sometimes in well screens with sand packs. Batch experiments were performed to determine the equilibrium partitioning behaviour of VOCs with respect to the FACT, and to assess how effectively VOC mass is desorbed from the FACT for use as a reliable technique for mapping contaminant mass distributions in boreholes.

The equilibrium distribution of VOCs in water solution and sorbed to the FACT after a three-week equilibration period were determined to be best represented by the Langmuir Isotherm, for the compounds DCM, c-DCE, TCE and PCE, with maximum achievable surface concentration ($C_{s\ max}$) of the VOCs ranging from 8×10^3 to 2×10^5 µmol/kg. The parameters calculated from the isotherm fits (such as the distribution coefficient) cannot be assumed to be accurate because of the unaccountable loss of VOC mass during the equilibration period.

Equilibration times necessary for each extraction technique to desorb the maximum amount of mass from the FACT were determined to be approximately 3-5 days for the methanol shake flask method, 20 minutes for the MAE method and 24-48 hours for the pentane/water shake flask method.

Overall, the methanol shake flask method was the best performing extraction technique in this experiment for desorbing mass from the FACT in terms of efficiency at desorbing VOCs from the FACT (maximum mass recovered) and by providing the most consistent recovery values between replicate samples, with an arithmetic mean mass percent recovery of 96% ± 6%. The methanol with microwave assisted extraction did extract, on average a higher percentage of VOC mass from the FACT (113% ± 12%), but the methanol shake flask method showed less variance between replicate samples. The MAE method is a good alternative if a project is time sensitive and the use of a microwave is feasible. In terms of the consistency at which VOCs are extracted from the FACT, regardless of the extraction method, the procedure shows a high level of uncertainty.

It can be stated that the FACT provides generally inconsistent concentration datasets, with high variability in terms of the mass sorbed and desorbed between replicate samples. The microscopic analysis of the FACT showed there were distinct and extensive differences in the characteristics of the FACT material between different manufacturing years. A high level of inconsistency between replicate samples of the same FACT versions was also observed, suggesting that the material is variable in nature at the micro-scale. BET surface area measurements for the 2017, 2019 and 2020 FACT manufacturing versions were 2067 ± 665 m^2/g, 4.35 ± 0.51 m^2/g and 1.30 ± 0.51 m^2/g respectively, confirming the visually observed microscopic variability.

The FLUTe FACT™, while still useful for qualitative determination of vertical contaminant distributions, does not appear to be a characterization tool that can be used quantitatively, as the current FACT material used cannot provide reliable measures of contaminant concentrations without large uncertainty due to large variability in the FACT sorption properties. This suggests that the current technology should be used as a screening tool to determine the approximate distribution of contaminant mass, but it is not advised that the contaminant profiles obtained be used in numerical modelling to assess the transport and/or risk to receptors of the contamination.

REFERENCES

Berkowitz, B., 2002. Characterizing flow and transport in fractured geological media: A review. Advances in Water Resources, 25, 861-884.

Beyer, M., Janniche, G., Broholm, M., 2012. DNAPL characterization in clayey till & chalk by FACT (FLUTe Activated Carbon Technique). DTU Environment.

Brunauer, S., Emmett, P. H., Teller, E., 1938. "Adsorption of Gases in Multimolecular Layers". Journal of the American Chemical Society, 60(2), 309–319.

Chiang, Y., Chiang, P., Chang, E., 2001. Effects of Surface Characteristics of Activated Carbons on VOC Adsorption. J. Environ. Eng., 127(1), 54-62.

Dincutoiu, I., Gorecki, T., Parker, B., 2006. Microwave-assisted extraction of trichloroethylene from clay samples. International Journ. J. Environ. Anal. Chem., 86(15), 1113-1125.

EPA, 2006. Method 8260B – Volatile Organic Compounds by Gas Chromatography/Mass Spectrometry (GC/MS).

Freundlich, H., 1909. Eine darstellung der chemie der kolloide und verwanter gebiete". Kapillarchemie..

Hatfield, K., Annable, M., Cho, J., Rao, P., Klammler, H., 2004. A direct passive method for measuring water and contaminate fluxes in porous media. Journal of Contaminant Hydrology, 75, 155-181.

Kim, K., Kang, C., You, Y., Chung, M., Woo, M.-W., Jeong, W.-J., … Ahn, H.-G. 2006. Adsorption – desorption characteristics of VOCs over impregnated activated carbons. Catalysis Today, 111, 223–228. https://doi.org/10.1016/j.cattod.2005.10.030

Klammler, H., Hatfield, K., Newman, M., Cho, J., Annable, M., Parker, B., Cherry, J., Perminova, I., 2016. A new dvice for characterizing fracture networks and measuring groundwater and contaminant fluxes in fractured rock aquifers. Water Resources Research, 52(7), 5400-5420.

Kubicki, J. D., Brantley, S. L., & White, A. F., 2008. Kinetics of Water-Rock Interaction.Springer Science + Business Media.

Golder, 2010. Fractured Bedrock Field Methods and Analytical Tools, Volume I: Main Report.

Langmuir, I., 1916. The Evaporatioin, Condensation and Reflection of Molecules and the Mechanism of Adsorption.Physical Review, 8(4), 149-176.

Mosthaf, K., Broholm, M., Binning, J., 2014. The FACT-Flute technology. A modelling tool for interpreting field date. DTU Environment.

Osmari, T., Gallon, R., Schqaab, M., Barbosa-Cotinho, E., Severo Jr, J., Pinto, J., 2013. Statistical Analysis of Linear and Non-Linear Regression for the Estimation of Adsorption Isotherm Parameters. Adsorption Science & Technology, 31(5), 433-458.

Parker, B., Bairos, K., Maldaner, C., Chapman, S., Turner, C., Burns, L., Carter, R., Cherry, J., 2018. Metolachlor dense non-aqueous phase liquid source conditions and plume attenuation in a dolostone water supply aquifer. Geological Society London Specila Publications.

Parker, B., Cherry, J., Chapman, S., 2012. Discrete Fracture Network Approach for Studying Contamination in Fractured Rock. AQUA mundi, 101-116.

Parker, B., Gillham, R., Cherry, J., 1994. Diffusive Disappearance of Immiscible-Phase Organic Liquids in Fractured Gelogic Material. Ground Water, 32(5), 805-820.

Pierce, A., Chapman, S., Zimmerman, L., Hurley, J., Aravena, R., Cherry, J., Parker, B., 2018. Journal of Contaminant Hydrology, 212(2018), 96-114.

Ramos, M. E., Bonelli, P. R., Cukierman, A. L., Carrott, M. M. L. R., & Carrott, P. J. M. 2010. Adsorption of volatile organic compounds onto activated carbon cloths derived from a novel regenerated cellulosic precursor. Journal of Hazardous Materials, 177, 175–182. https://doi.org/10.1016/j.jhazmat.2009.12.014

Seybold,.J., Weeks, K., 1992. Arithmetic Versus Geometric Mean of Target Radar Cross Section. Microwave and Optical Technology Letters, 11(5), 263-265.

Schwarzenbch, R., Gschwend, P., Imboden, D., 2003. Environmental Organic Chemistry, 2nd Edition. John Wiley & Sons, Inc.

Sterling, S., Parker, B., Cherry, J., Williams, J., Lane Jr, J., Haeni, F., 2005. Vertical Cross Contamination of Trichloroethylene in a Borehole in Fractured Sandstone. Groundwater, 43(4), 557-573.

Stumm, W. (1992). Chemistry of the Solid-Water Interface. John Wiley & Sons, Inc.

Yu, F. D., Luo, L. A., & Grevillot, G., 2002. Adsorption Isotherms of VOCs onto an Activated Carbon Monolith : Experimental Measurement and Correlation with Different Models. J. Chem. Eng. Data, 47, 467–473. https://doi.org/10.1021/je010183k

Zheng, J., Zhao, Q., Ye, Z., 2014. Preparation ad characterization of activated carbon fiber (ACF) from cotton woven waste. Applied Surface Science, 299, 86-91.

Appendix A: Digital Microscope Image Descriptions

Image ID	Image	Image Description
OM-2017-1-1	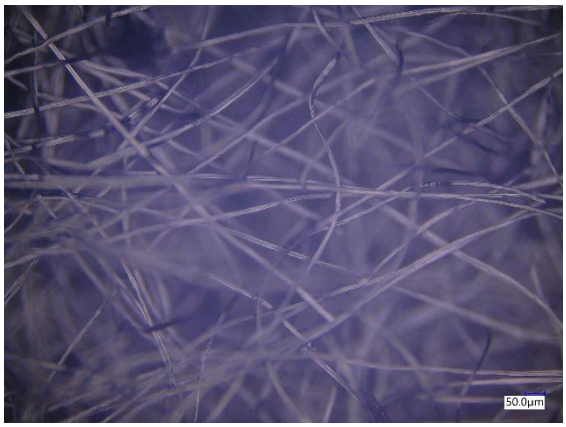	• “string like” features of backing material • No visible AC
OM-2017-1-2	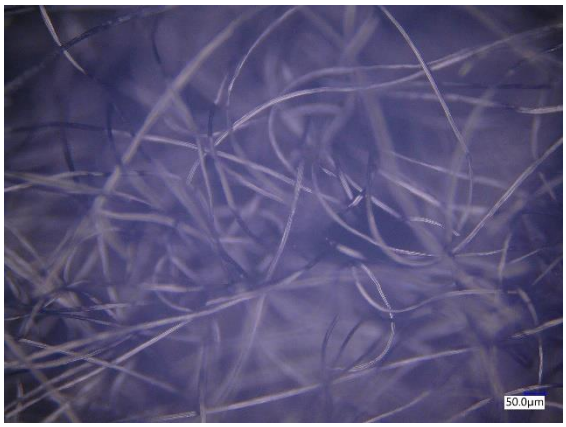	• Similar characteristics of 2017-1-1, no change in density of material or AC distribution
OM-2017-1-3	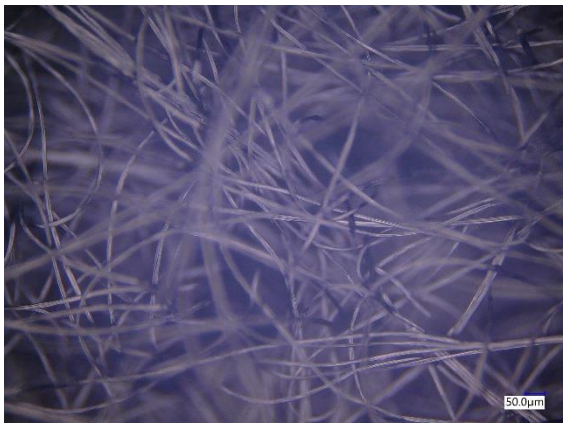	• Appears to be higher density of interwoven backing strings • No AC visible

Image ID	Image	Image Description
OM-2017-3-2	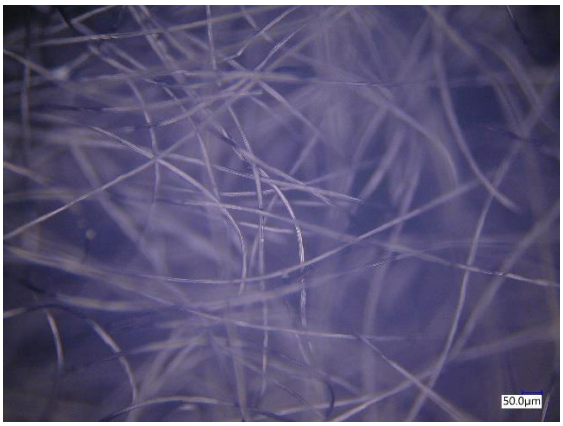	• No distinct features, similar backing density, no visible AC
OM-2017-3-3	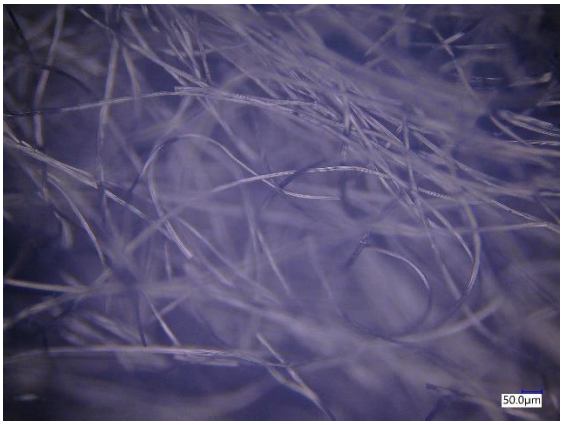	• Minor evidence of AC particles, standard backing structure
OM-2017-4-1	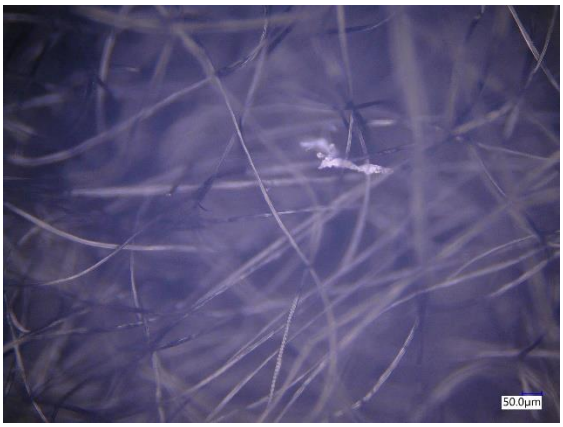	• Potential AC granule found in centre of image • No other evidence in FOV or surrounding area

Image ID	Image	Image Description
OM-2017-4-1-zoomed	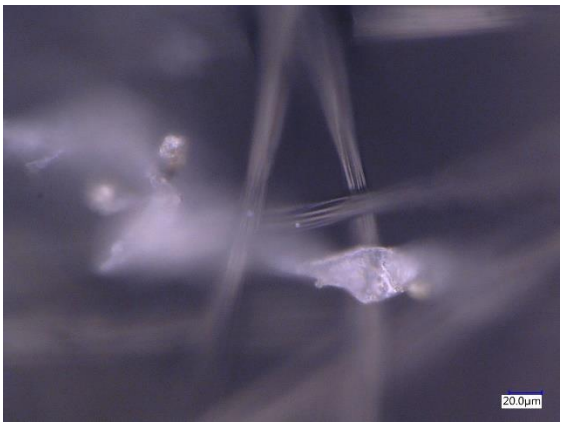	• Zoomed in shot of AC from 2017-4-1 shows shimmery lustre to other AC particles
OM-2017-4-2	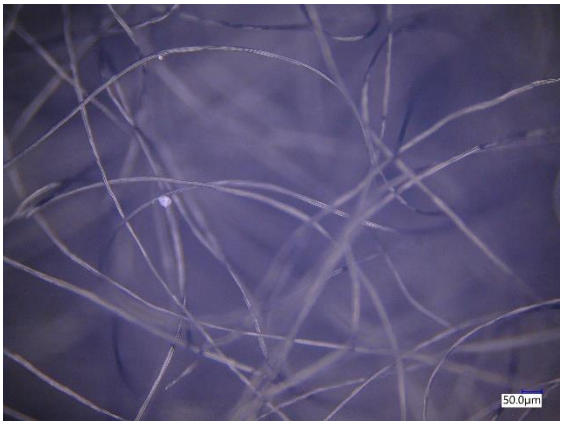	• Small particle of AC, only evidence found in FOV and surrounding area
OM-2017-4-3	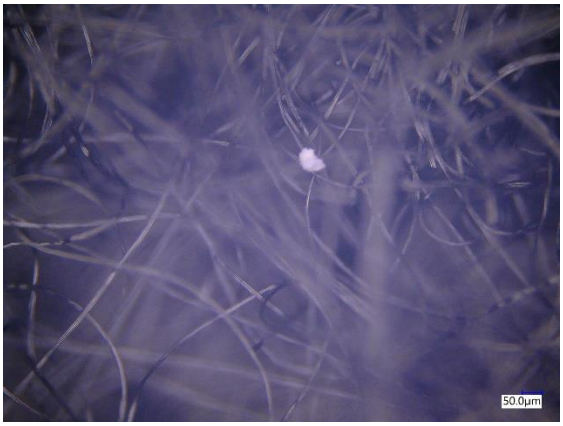	• Single AC particle in FOV, potentially more dense backing material in area

Image ID	Image	Image Description
OM-2017-5-1	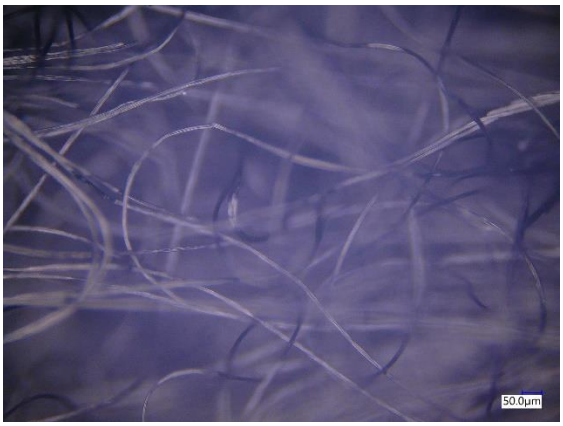	• No distinctive features • No evidence of AC, standard backing structure
OM-2017-5-2	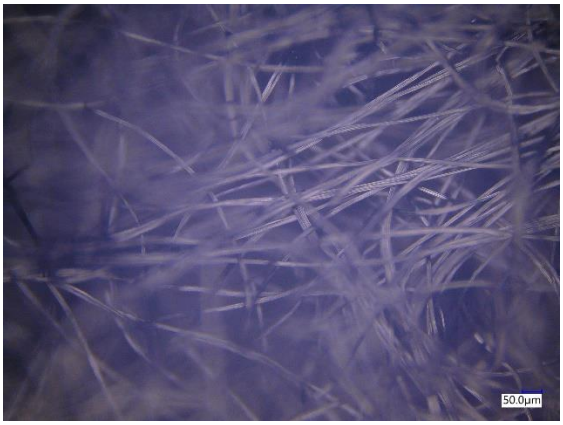	• Higher density of backing material, no evidence of AC
OM-2019-1-1	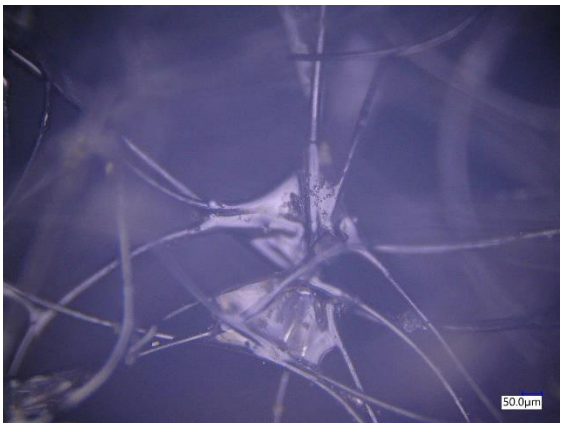	• Greater volumes of AC found than 2017 material, more evenly distributed, granules/chunks dominate, but potential evidence of AC coating on backing material • Backing material strands are less uniform in thickness, density similar to 2017 material

Image ID	Image	Image Description
OM-2019-1-1-zoomed	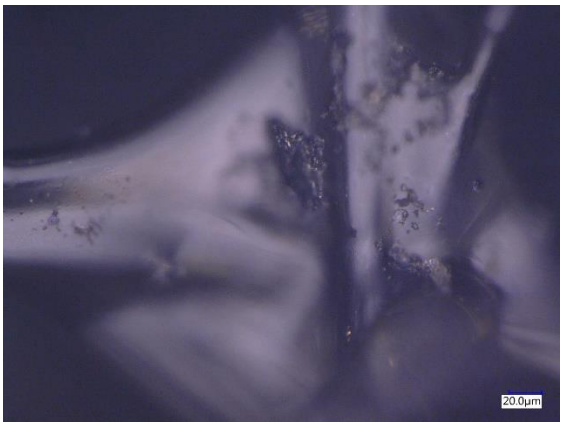	• Zoomed image of AC found in 2019-1-1 show potential for AC coating with solid granules of AC
OM-2019-1-2		• Backing material potentially less dense in FOV/surrounding area • Large mass of AC displayed in image at termination/intersection of multiple backing fibres
OM-2019-1-2-zoomed	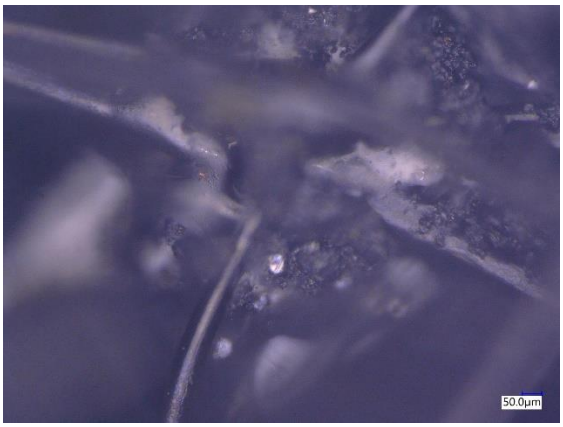	• Zoomed image of AC mass in 2019-1-2, crystal-like particles present within larger AC mass

Image ID	Image	Image Description
OM-2019-1-3	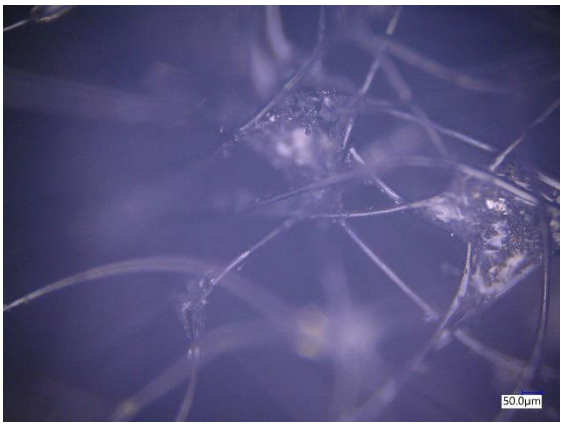	• Similar backing structure and AC network to past images
OM-2019-2-1	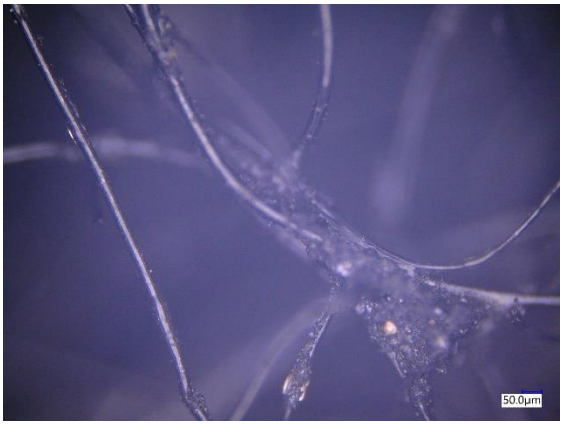	• AC distributed less frequently in area, but large particles still found
OM-2019-2-2	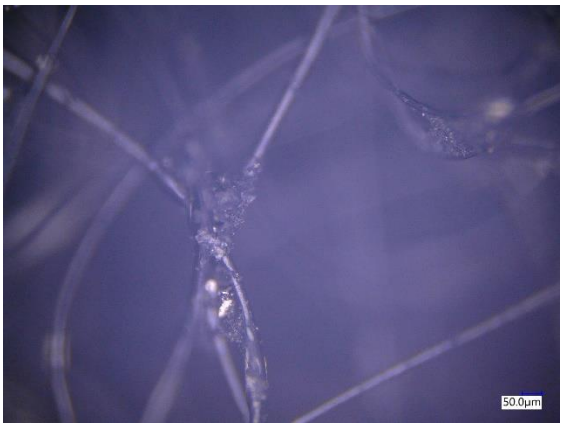	• Similar AC distribution to 2019-2-1, but chunks of AC are smaller

Image ID	Image	Image Description
OM-2019-2-3	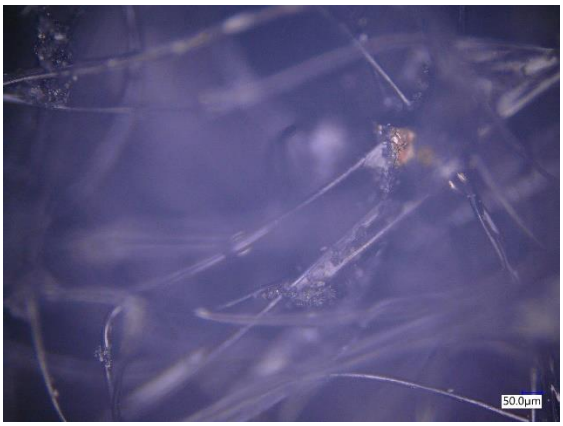	• Slightly higher distribution of AC in area • AC particle in FOV shows brownish tinge
OM-2019-2-3-zoomed	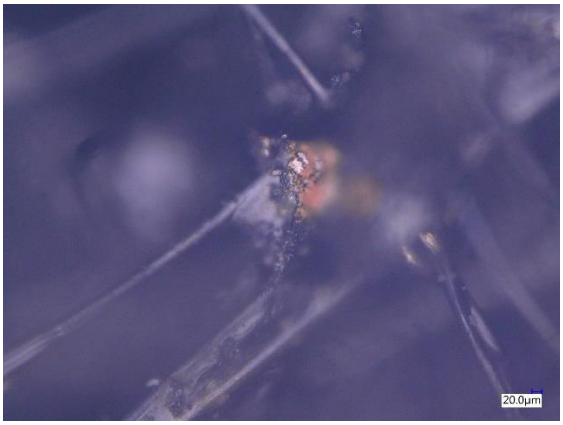	• Zoomed image of brown AC particle from, 2019-2-3 • Similar particle structure of other AC masses aside from colour/tinge
OM-2019-3-1		• Density of material appears to be higher in area of sample than 2019-2/2019-1 samples • Standard AC distribution

Image ID	Image	Image Description
OM-2019-3-2	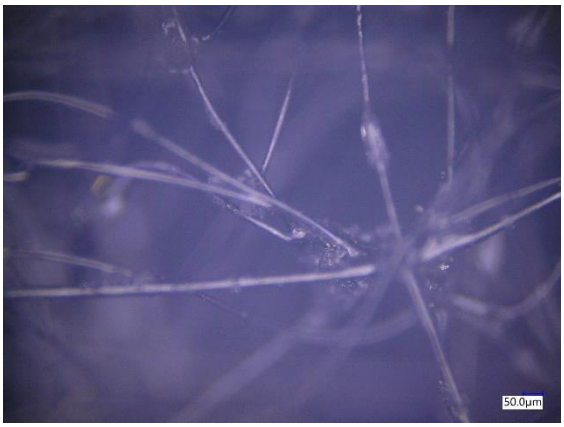	• Similar characteristics to 2019-3-1, but slightly less dense backing material
OM-2019-3-3		• Similar characteristics to past 2019 FACT samples • Interesting bulb-like AC mass in image
OM-2019-4-1	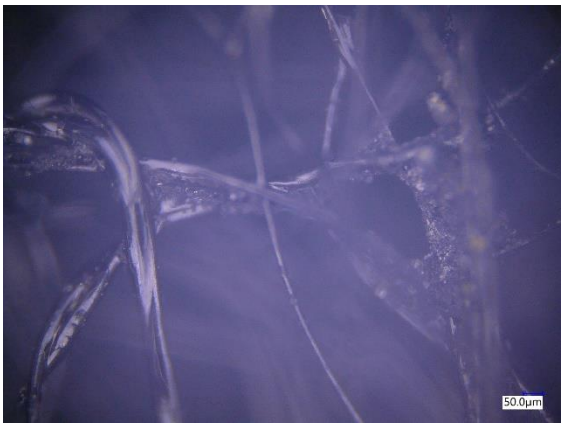	• More evenly distributed AC mass in FOV • Less large masses of AC

Image ID	Image	Image Description
OM-2019-4-2	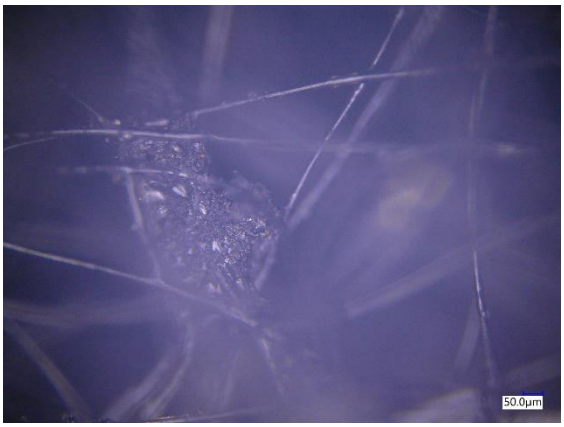	• Large mass found in FOV, standard AC distribution and backing material structure
OM-2019-4-3		• Evidence of coating-type AC in image, less nodular AC present
OM-2019-5-1	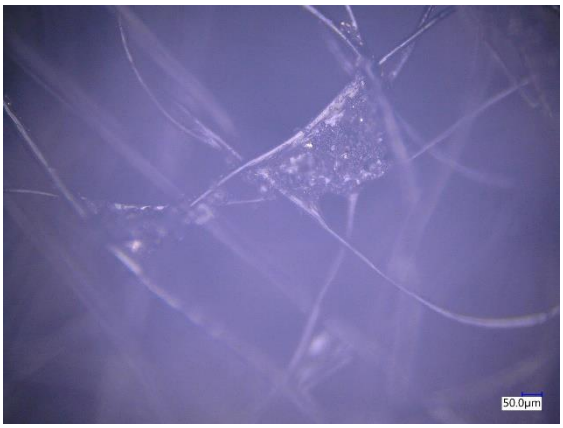	• Standard 2019 FACT characteristics, no distinctive features

Image ID	Image	Image Description
OM-2019-5-2	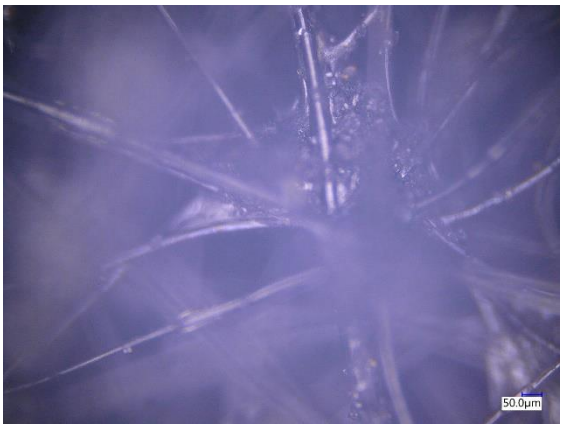	• Large mass found in image, but standard characteristics displayed in FOV and surrounding area
OM-2019-5-3	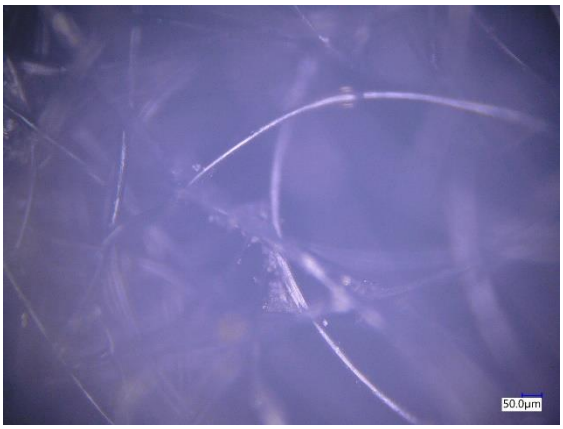	• Image taken in section of FACT strip that was visibly thinner to naked eye • Lower density of backing material observed under OM • Potentially less AC mass as well in area
OM-2020-1-1	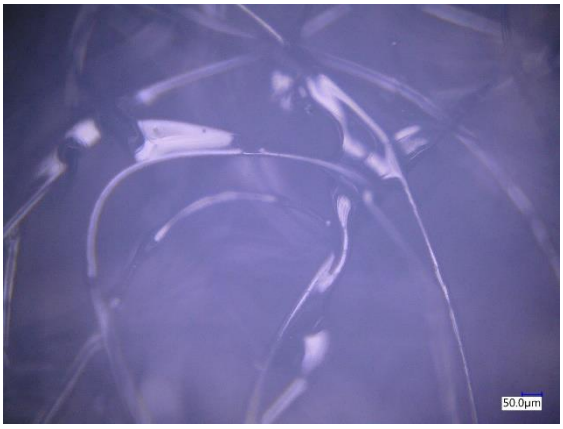	• Little evidence of granular type AC, mainly the coated AC type observed previously • AC builds up in same types of locations as 2019 (terminations, multiple strand crossings etc.) • Similar backing material density, relatively consistent AC distribution (if coating is AC)

Image ID	Image	Image Description
OM-2020-1-2	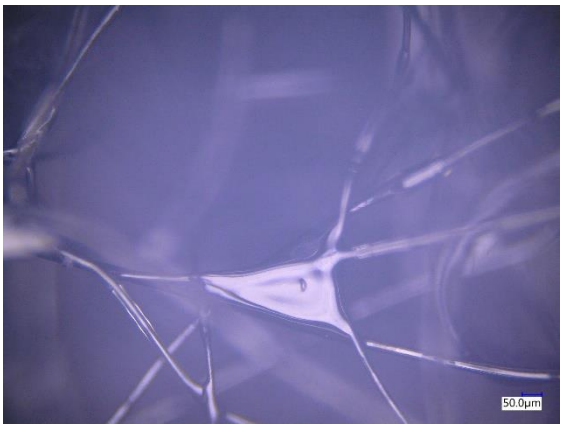	• Similar characteristics to 2020-1-2 • Coating present, similar backing structure and density
OM-2020-1-3	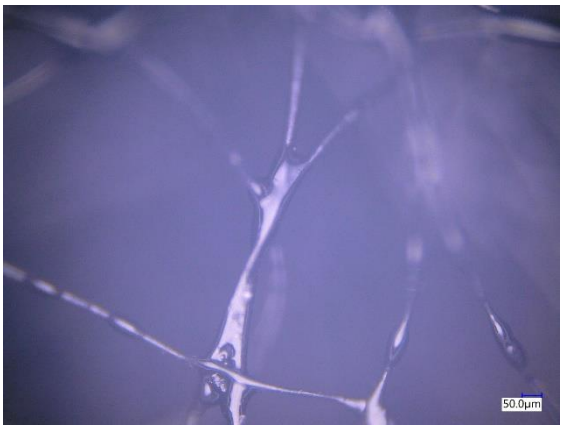	• Evidence of small granules of AC within coated matrix
OM-2020-2-1	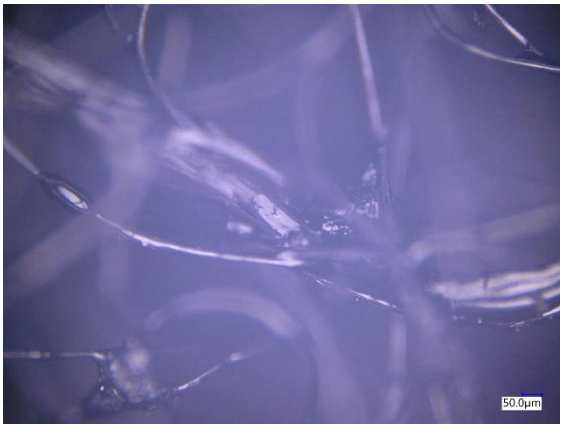	• Similar backing density and AC distribution • large coated “droop”

Image ID	Image	Image Description
OM-2020-2-2	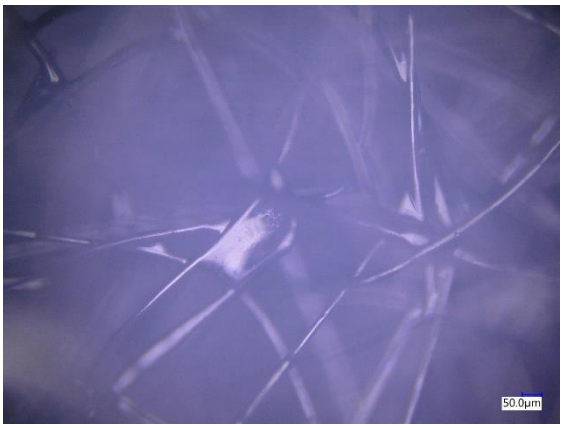	• Appears to display large variation in backing density and AC density in area • Not as evident in FOV displayed in image
OM-2020-2-3	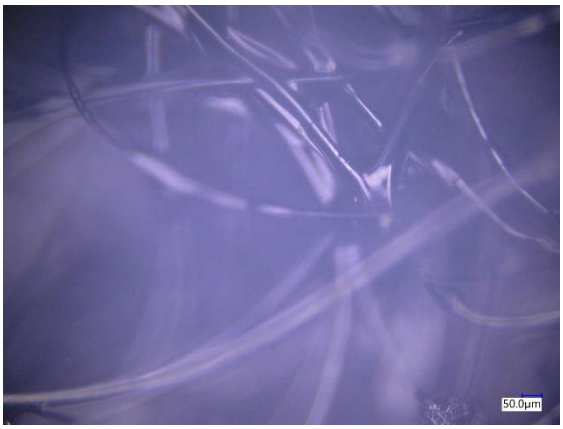	• Similar variation in characteristics as 2020-2-2
OM-2020-3-1	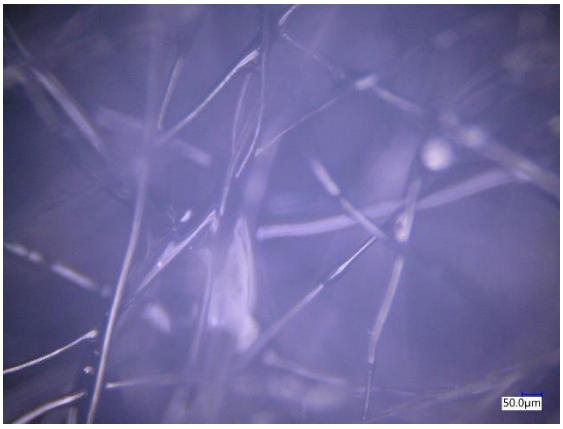	• FOV and area also shows variability in AC distribution and backing structure

Image ID	Image	Image Description
OM-2020-3-2		• Similar variability, AC coating remains present
OM-2020-3-3	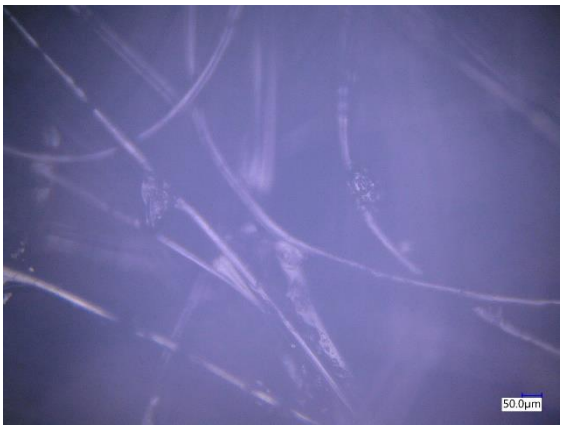	• Granular AC observed in FOV • Less variable in area
OM-2020-4-1	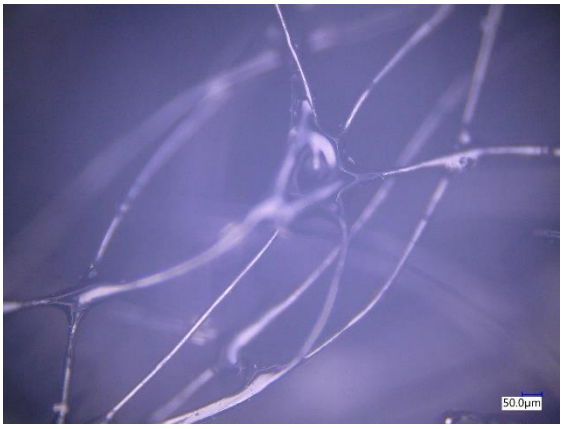	• Sample is less variable than past 2020 samples observed • Structure and AC distribution relatively consistent through all 2020-4 FOVs

Image ID	Image	Image Description
OM-2020-4-2		• Structure and AC distribution relatively consistent through all 2020-4 FOVs
OM-2020-4-3	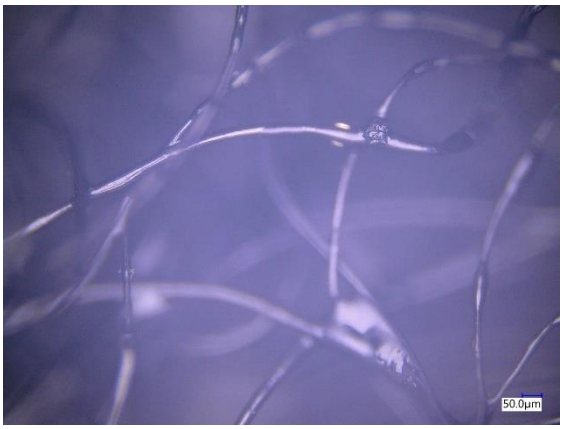	• Structure and AC distribution relatively consistent through all 2020-4 FOVs • Some granule-type AC observed
OM-2020-5-1	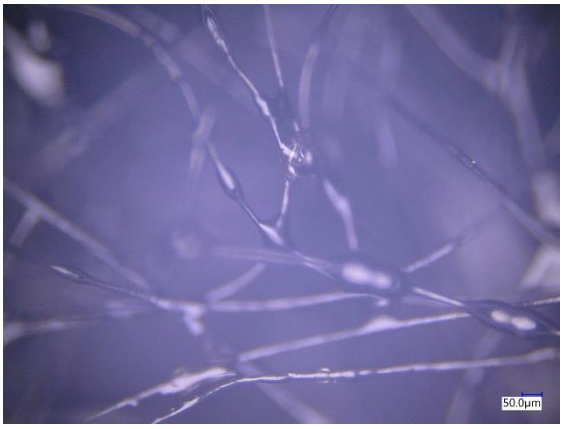	• Large globs of AC throughout • AC and backing structure characteristics relatively consistent

Image ID	Image	Image Description
OM-2020-5-2	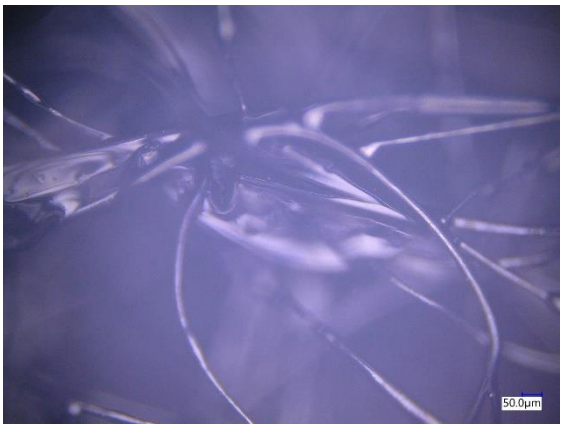	• Large masses of AC found in FOV and surrounding area • Inconsistent characteristics
OM-2020-5-3	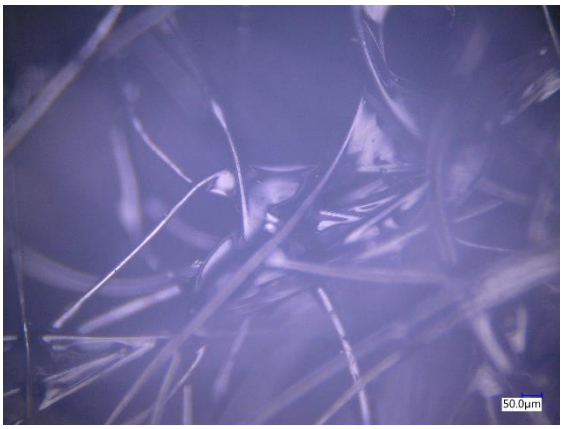	• Large granules, high density of AC

APPENDIX B: SEM IMAGE DESCRIPTIONS

Image ID	Image	Image Description
SEM-2017-1-1	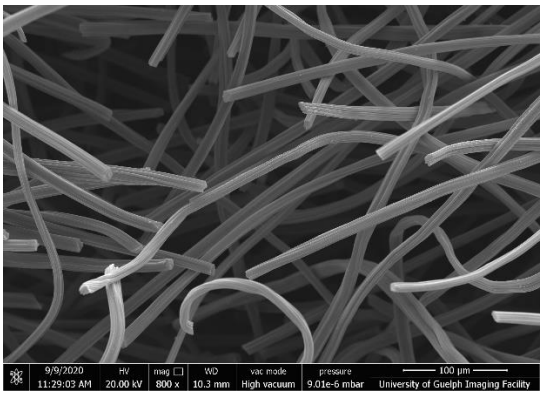	• 800 x mag • “string-like” material interwoven in complex 3-D matrix • No visible AC, but very small particles can be observed, likely resembling dust/debris. 1-2 µm in diameter
SEM-2017-1-2	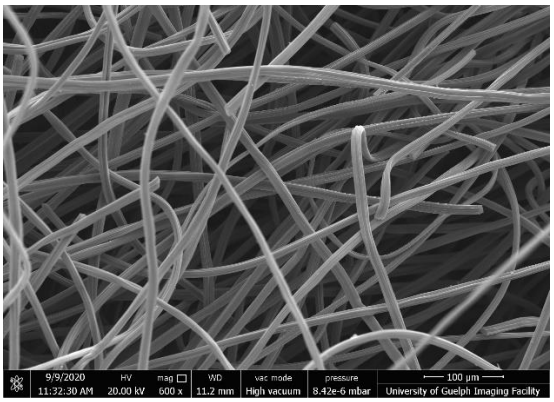	• 600 x mag • Similar to first sample: no change in backing density or AC distribution • Small particles observed
SEM-2017-2-1	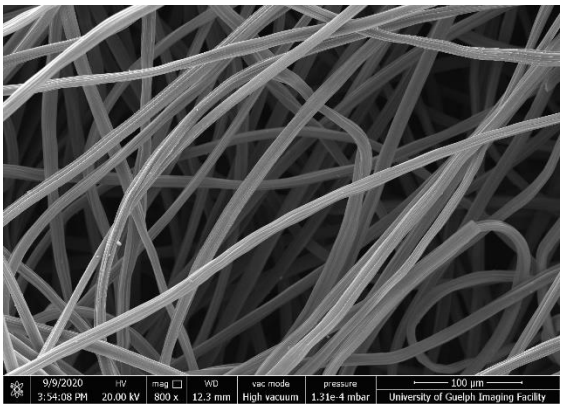	• 800 x mag • Few distinct features, more evidence of µm sized particles • Similar matrix density

Image ID	Image	Image Description
SEM-2017-2-2	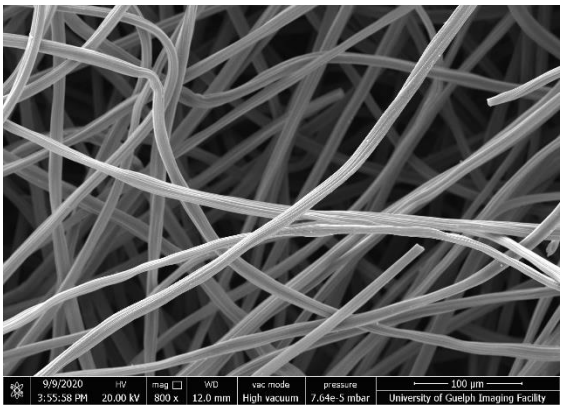	• 800 x mag • Slightly higher matrix density in FOV/section of sample • µm particles observed
SEM-2017-3-1	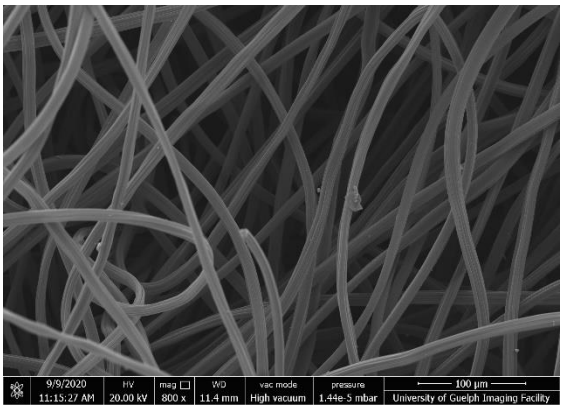	• 800 x mag • Larger granule type particle observed (5-10 µm diameter) in centre-right section of image, potentially AC • Smaller µm particles observed
SEM-2017-4-1	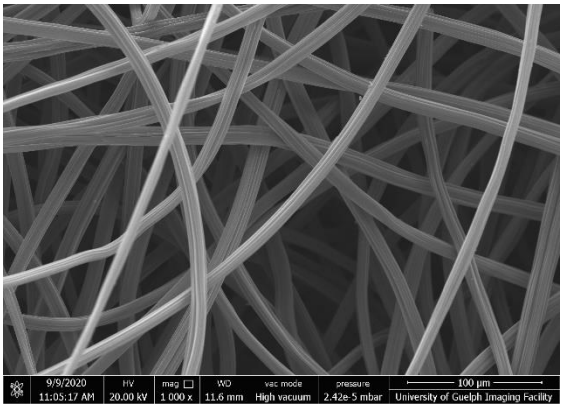	• 1 000 x mag • Similar matrix density, potentially higher in this FOV • Evidence of larger AC particles • Striations observed on backing fibre strands (lines parallel to fibre length)

Image ID	Image	Image Description
SEM-2017-4-2	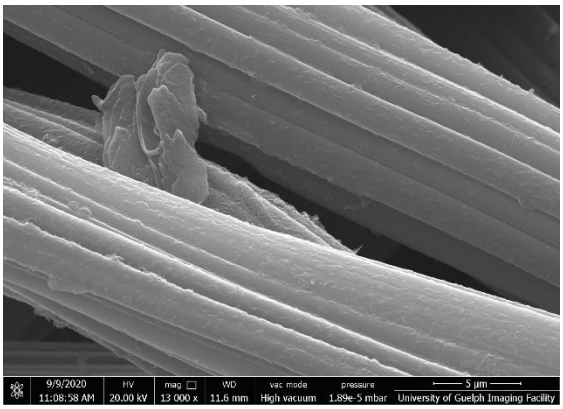	• 13 000 x mag • Zoomed image on larger AC particle • Particle has platy-like structure with thin sheets stacked horizontally on top of each other • Interpreted to be charcoal AC • Striations on backing fibres very apparent in image
SEM-2017-4-3	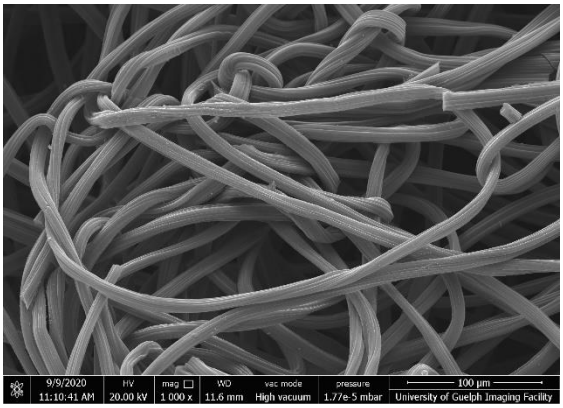	• 1 000 x mag • Much higher backing density in this FOV/area of sample • Little to no AC observed in FOV, smaller µm observed on surface of backing material
SEM-2017-5-1	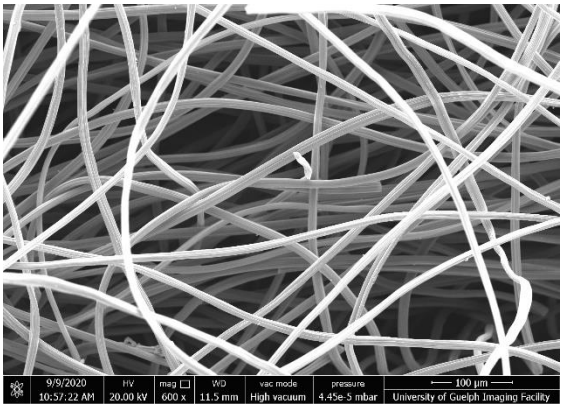	• 600 x mag • No distinct features, few AC particles observed, similar backing density to majority of samples observed

Image ID	Image	Image Description
SEM-2017-5-2	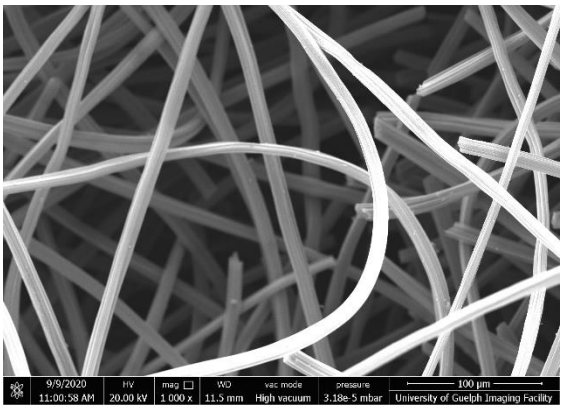	• 1 000 x mag • Similar backing density to other sample, µm dust particles observed
SEM-2019-1-1	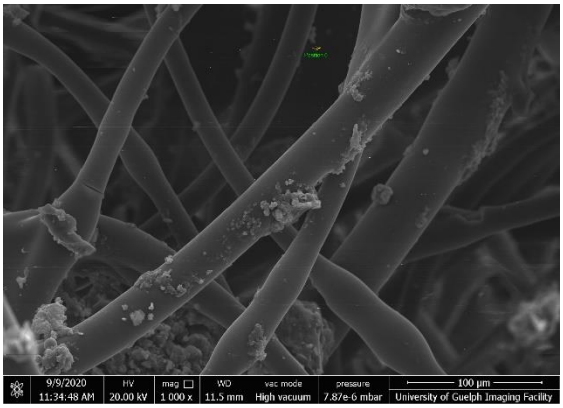	• 1 000 x mag • Large, distinct “chunks” of AC observed, distributed relatively evenly throughout matrix • AC particles have nodular, crystal-like structure
SEM-2019-1-2	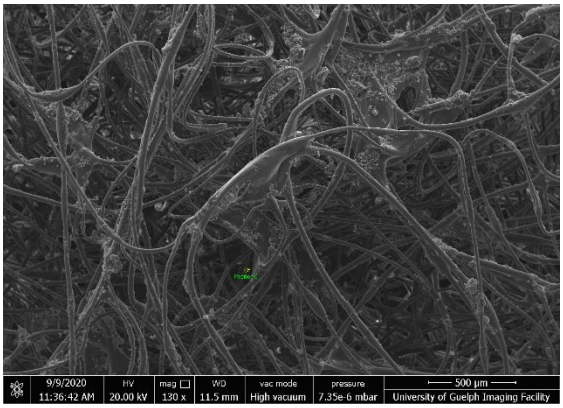	• 130 x mag • Zoomed out image displaying complex nature of 3-D matrix, and size of AC particles (up to 50-100 µm in diameter) • Matrix fibres drastically vary in thickness, compared to 2017 material in which thicknesses are uniform

Image ID	Image	Image Description
SEM-2019-1-3	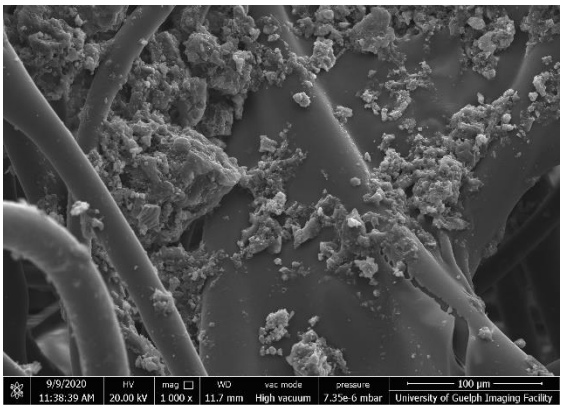	• 1 000 x mag • Large AC concentration at termination of multiple matrix fibres • Porosity of these AC particles can be observed • AC structure is much more nodular, with little platy structure that was observed in 2017 AC particles
SEM-2019-2-1	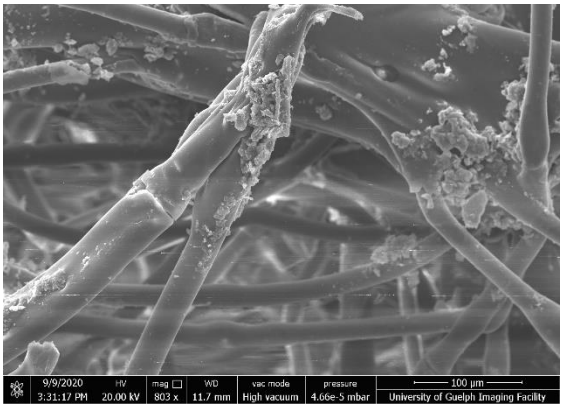	• 803 x mag • Similar matrix density and AC distribution found in first 2019 sample • Build up of AC at termination of multiple strands
SEM-2019-2-2	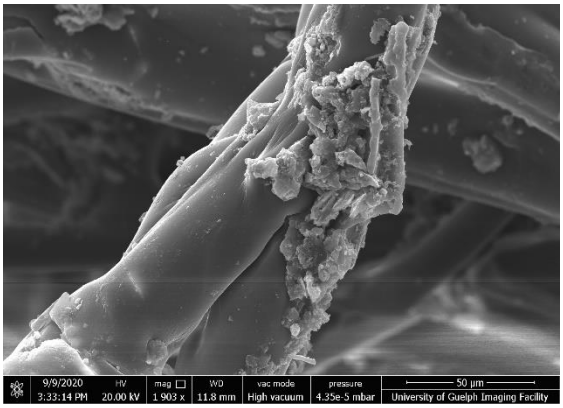	• 1 903 x mag • Zoomed image of AC concentration in 2019-2-1 • Porosity can be observed

Image ID	Image	Image Description
SEM-2019-2-3	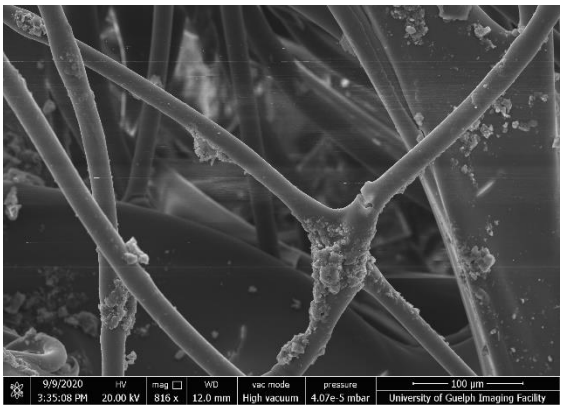	• 816 x mag • Similar backing density and AC distribution to other 2019 FOVs • Shows extent of differences of fibre thicknesses if backing material
SEM-2019-3-1	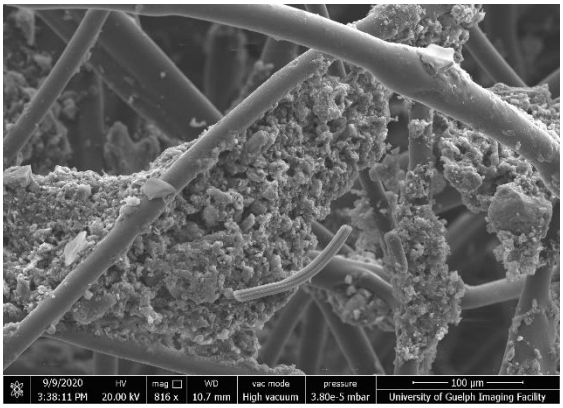	• 816 x mag • Large chunk of AC in image, easily observed porosity • In bottom middle section of image, a piece of the striated like matrix material from 2017 FACT can be observed stuck to AC chunk • Likely a strand from other 2017 sample that was transferred to 2019 sample
SEM-2019-3-2	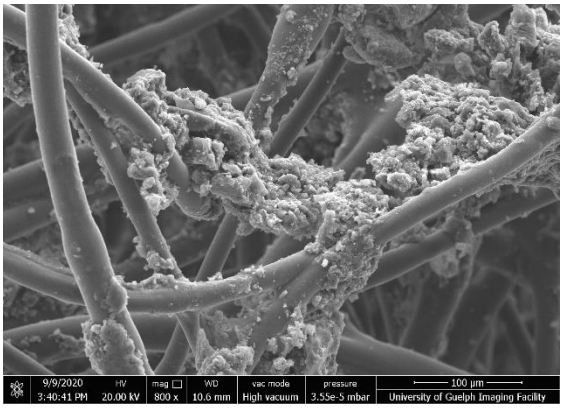	• 800 x mag • Similar characteristics to other 2019 FOVs, relatively large concentration of AC in this image

Image ID	Image	Image Description
SEM-2019-3-3	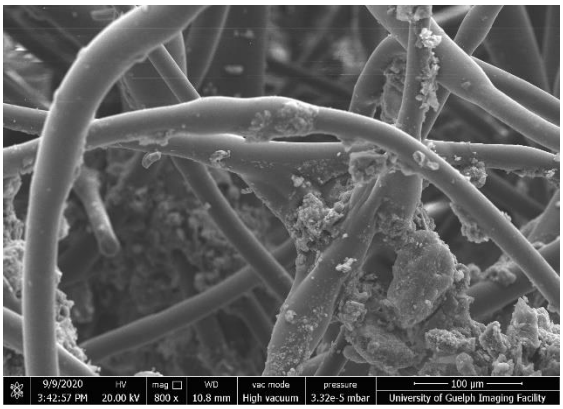	• 800 x mag • Similar matrix density and AC distribution
SEM-2019-4-1	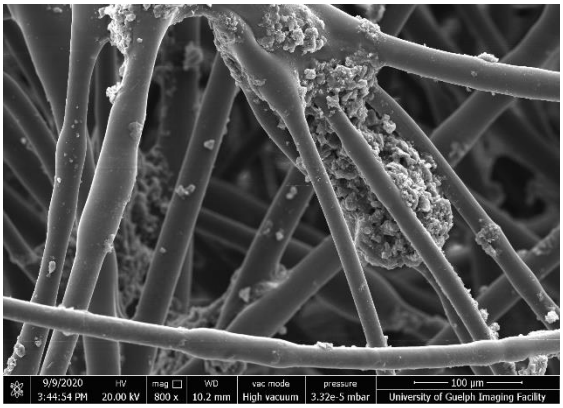	• 800 x mag • Chunk of AC built up at termination of multiple backing material strands • Similar characteristics of other 2019 samples
SEM-2019-4-2	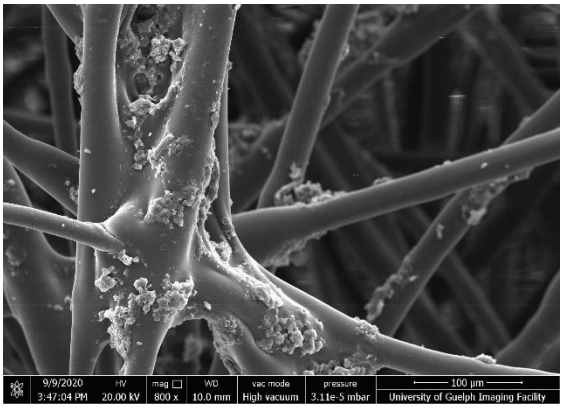	• 800 x mag • Different FOV than 2019-4-2, but very similar characteristics

Image ID	Image	Image Description
SEM-2019-5-1	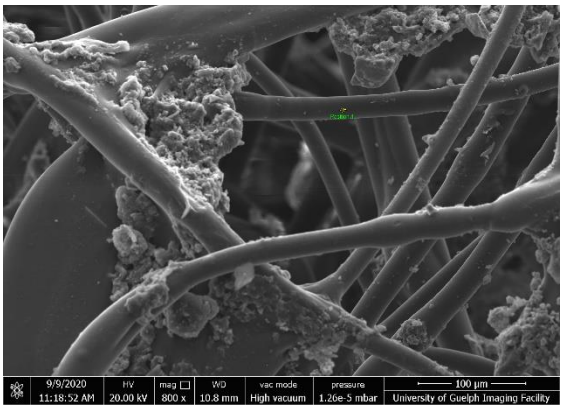	• 800 x mag • Backing density and AC distribution is very similar to 2019-4 samples
SEM-2019-5-2	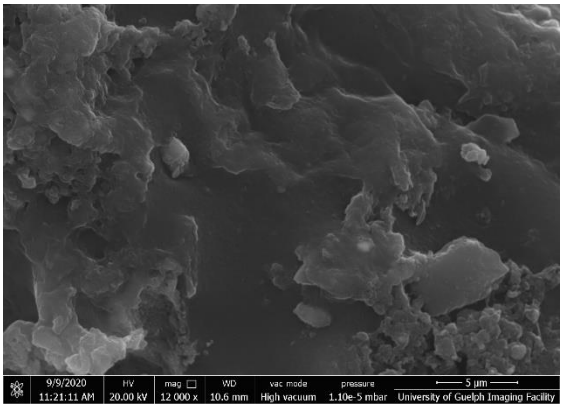	• 12 000 x mag • Zoomed image of AC particle • Porosity can clearly be observed, slight platy structure/layering
SEM-2019-5-3	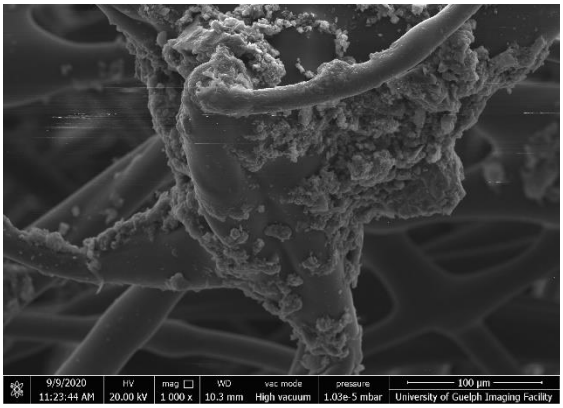	• 1 000 x mag • Standard characteristics observed of 2019 FACT

Image ID	Image	Image Description
SEM-2019-5-4	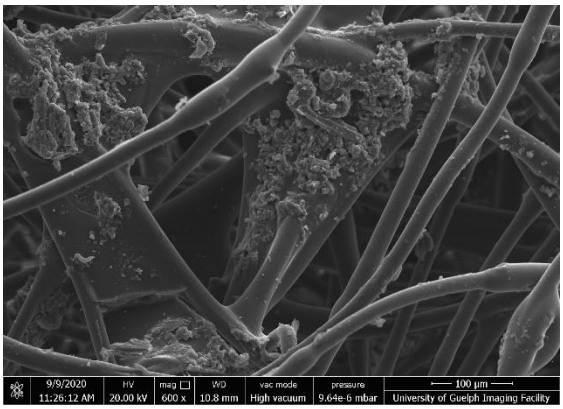	• 600 x mag • Slightly larger FOV to observe variations in matrix strand thicknesses, and complexity of 3-D matrix
SEM-2020-1-1	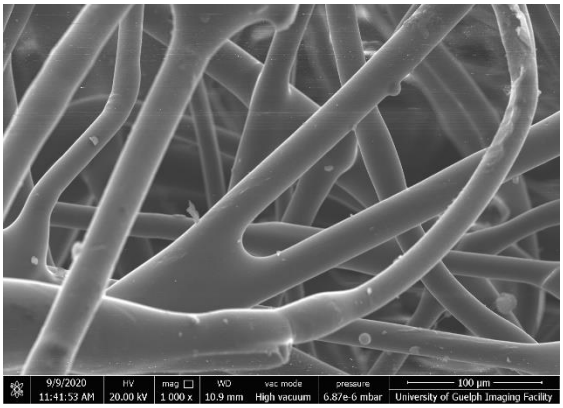	• 1 000 x mag • Very similar matrix characteristics and density as 2019 FACT, but appears to have far less AC present • AC can still be observed, but “chunks” are much smaller and distributed inconsistently
SEM-2020-1-2	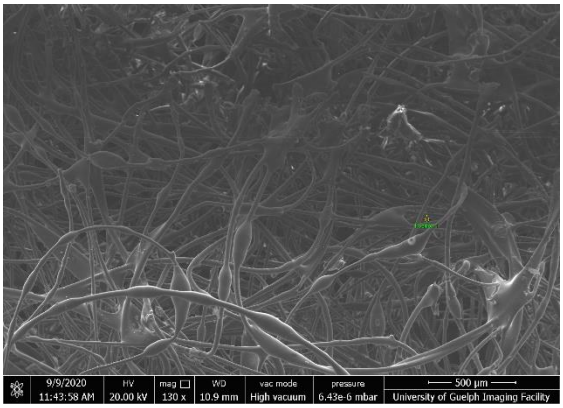	• 130 x mag • Zoomed out image, shows very similar characteristics to image 2019-1-2, but just with fewer AC particles • Matrix fibres show same inconsistent thickness as 2019 material

Image ID	Image	Image Description
SEM-2020-1-3	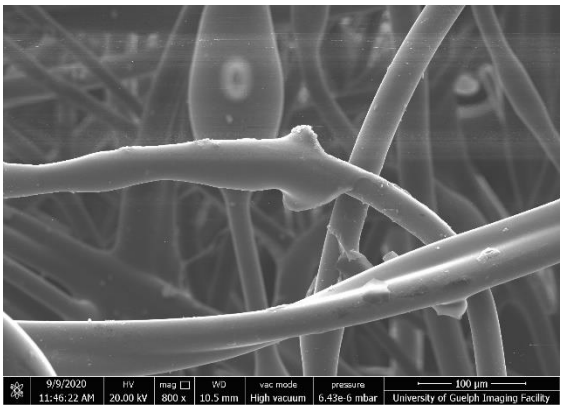	• 800 x mag • Appears to be less dense matrix than other FOV in 2020-1-1 image • Still sparse evidence of AC
SEM-2020-1-4	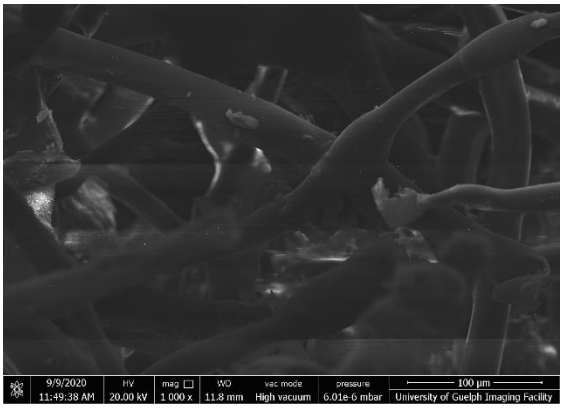	• 1 000 x mag • Poor image quality • Some slightly larger AC particles in image, backing density is variable again
SEM-2020-2-1	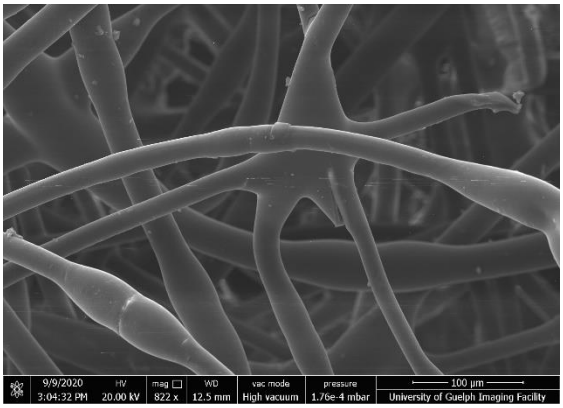	• 822 x mag • Relatively standard characteristics of 2020 material • Little AC observed

Image ID	Image	Image Description
SEM-2020-2-2	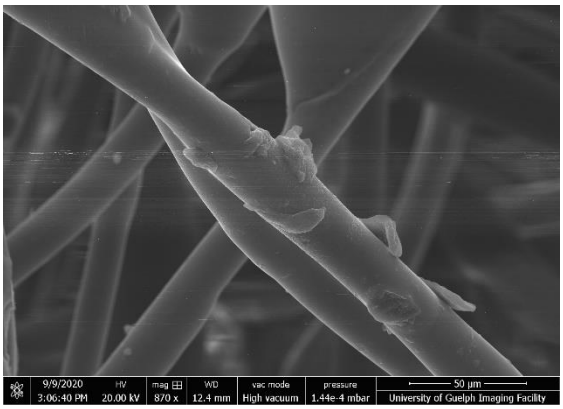	• 870 x mag • Slightly larger particles of AC observed in FOV, but still sparsely spaced in surrounding area
SEM-2020-2-3	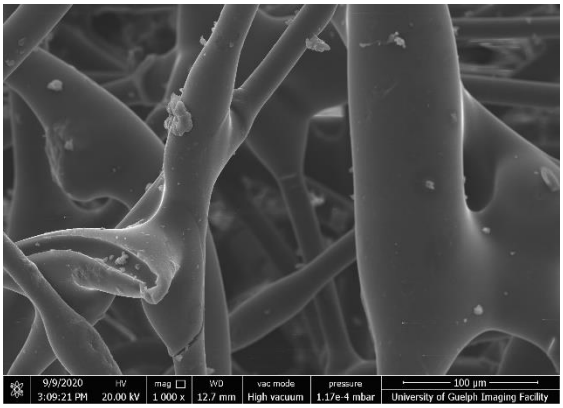	• 1 000 x mag • Large variation in backing fibre thicknesses, small amounts of AC observed • Backing material slightly denser in area
SEM-2020-3-1	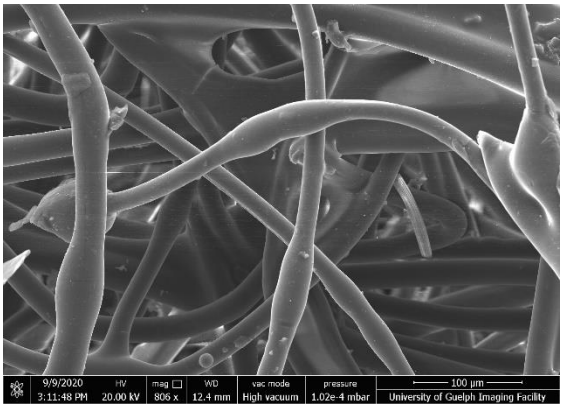	• 806 x mag • Standard 2020 FACT FOV, no distinctive characteristics

Image ID	Image	Image Description
SEM-2020-3-2	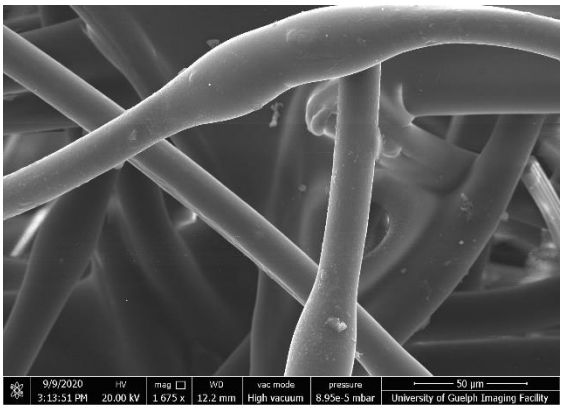	• 1 675 x mag • Zoomed image onto backing material fibre in attempts to observe more AC • Some evidence of smaller AC particles, but nothing substantial • AC distribution is still inconsistent
SEM-2020-3-3	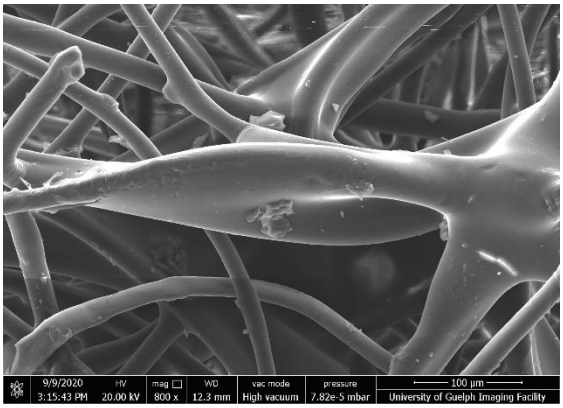	• 800 x mag • Higher density of backing material in FOV • Sparse AC distribution
SEM-2020-4-1	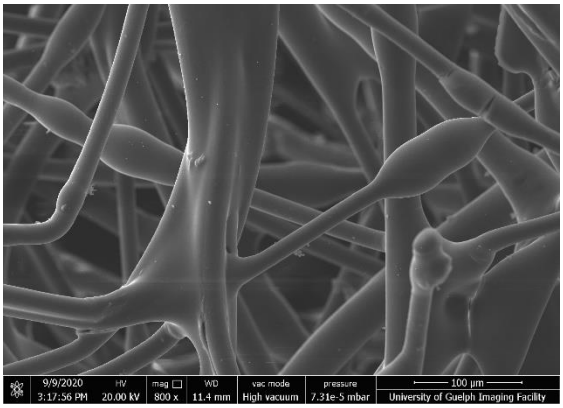	• 800 x mag • Extremely small volume of AC in FOV, very inconsistently distributed in area

Image ID	Image	Image Description
SEM-2020-4-2	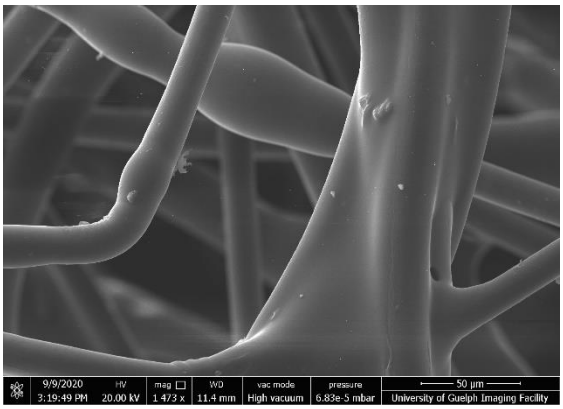	• 1 473 x mag • Zoomed image, very small volume of AC present
SEM-2020-4-3	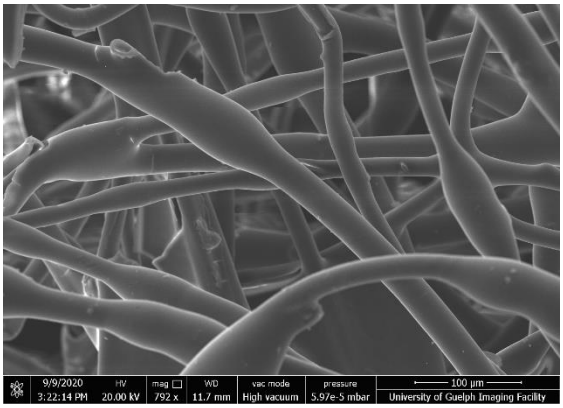	• 792 x mag • Slightly higher volume of AC present in FOV
SEM-2020-5-1	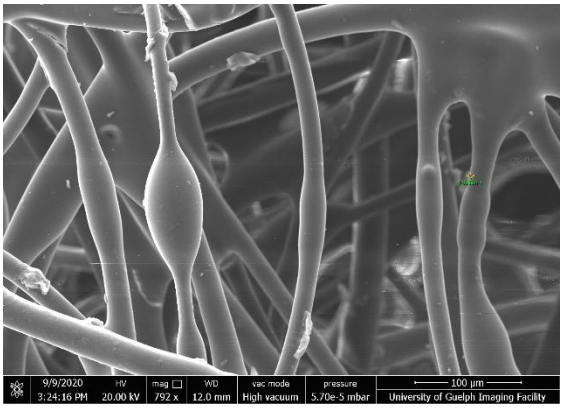	• 792 x mag • Higher volume of AC found in 2020-5-1 FOV than majority of 2020 FOVs observed

Image ID	Image	Image Description
SEM-2020-5-2	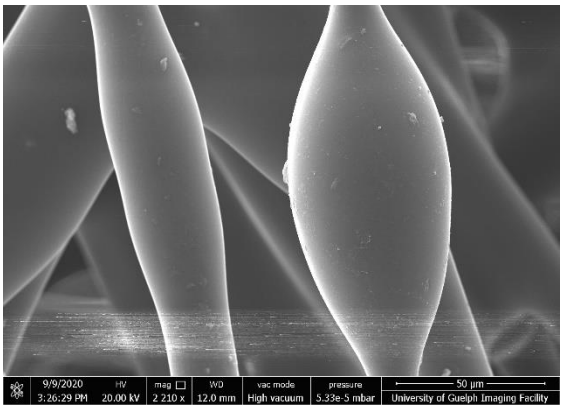	• 2 210 x mag • Zoomed image, similar amount of AC observed to other zoomed in images
SEM-2020-5-3	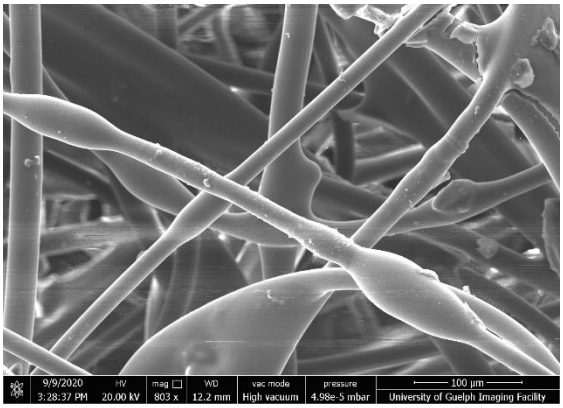	• 803 x mag • Standard AC distribution and matrix density for 2020 FACT samples

APPENDIX C: FACT MASS EXTRACTION TIME SERIES PLOTS-METHANOL SHAKE FLASK METHOD

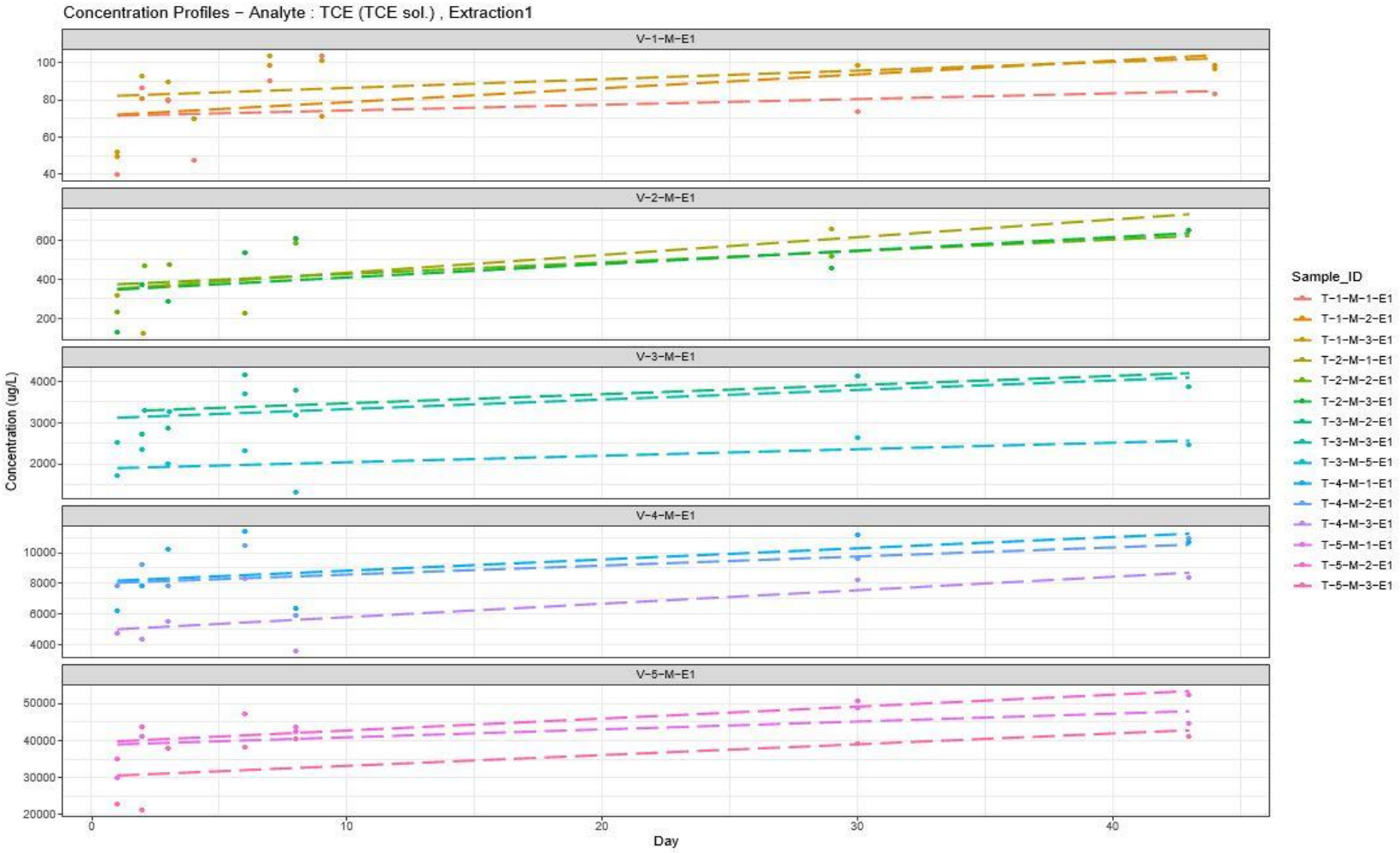
Concentration Profiles – Analyte : TCE (TCE sol.) , Extraction1
V-1-M-E1
V-2-M-E1
V-3-M-E1
V-4-M-E1
V-5-M-E1
Concentration (ug/L)
Day
Sample_ID
T-1-M-1-E1
T-1-M-2-E1
T-1-M-3-E1
T-2-M-1-E1
T-2-M-2-E1
T-2-M-3-E1
T-3-M-2-E1
T-3-M-3-E1
T-3-M-5-E1
T-4-M-1-E1
T-4-M-2-E1
T-4-M-3-E1
T-5-M-1-E1
T-5-M-2-E1
T-5-M-3-E1

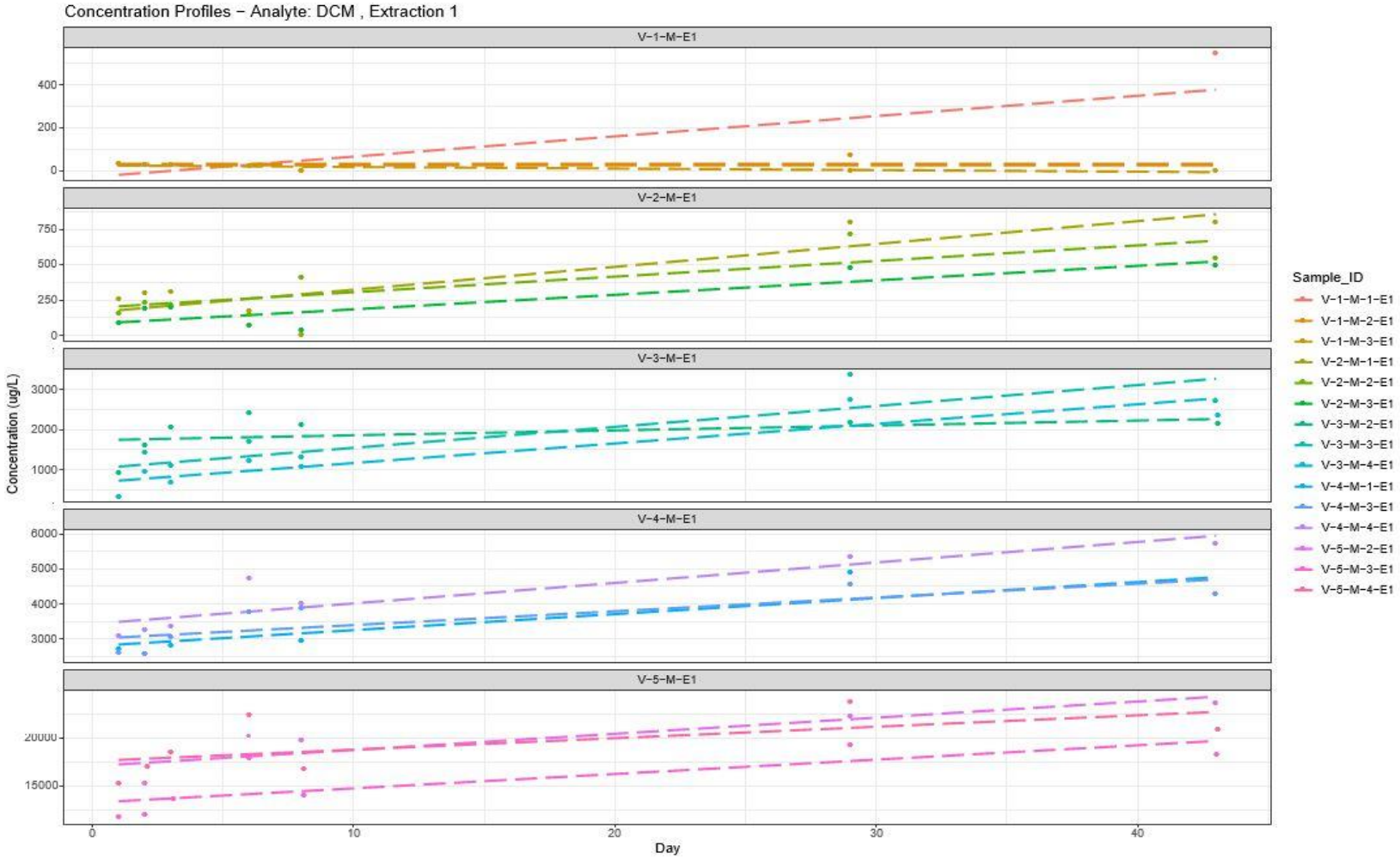
Concentration Profiles – Analyte: DCM , Extraction 1
V-1-M-E1
V-2-M-E1
V-3-M-E1
V-4-M-E1
V-5-M-E1
Concentration (ug/L)
Day
Sample_ID
V-1-M-1-E1
V-1-M-2-E1
V-1-M-3-E1
V-2-M-1-E1
V-2-M-2-E1
V-2-M-3-E1
V-3-M-2-E1
V-3-M-3-E1
V-3-M-4-E1
V-4-M-1-E1
V-4-M-3-E1
V-4-M-4-E1
V-5-M-2-E1
V-5-M-3-E1
V-5-M-4-E1

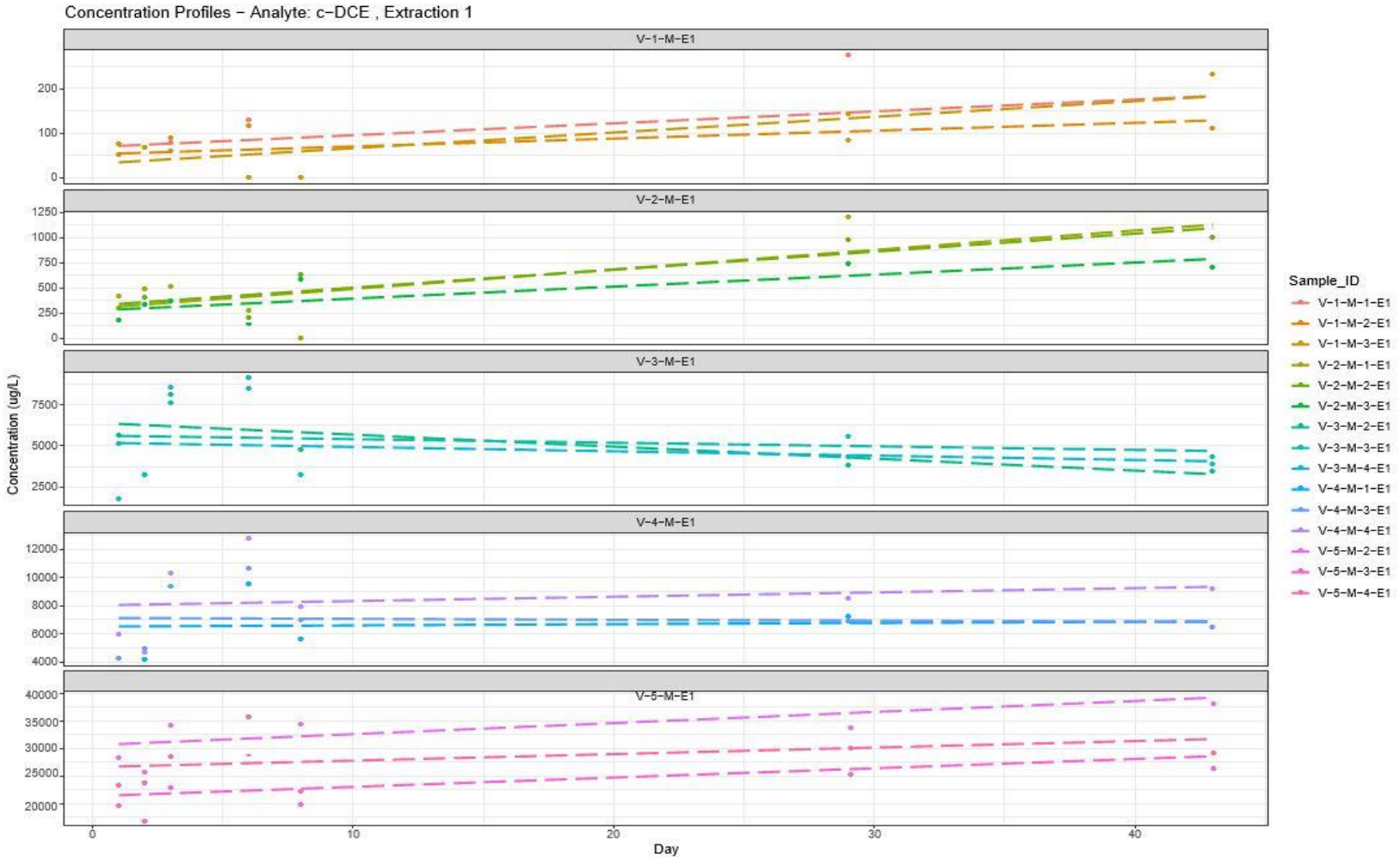
Concentration Profiles − Analyte: c−DCE , Extraction 1
V−1−M−E1
V−2−M−E1
V−3−M−E1
V−4−M−E1
V−5−M−E1
Concentration (ug/L)
Day
Sample_ID
V−1−M−1−E1
V−1−M−2−E1
V−1−M−3−E1
V−2−M−1−E1
V−2−M−2−E1
V−2−M−3−E1
V−3−M−2−E1
V−3−M−3−E1
V−3−M−4−E1
V−4−M−1−E1
V−4−M−3−E1
V−4−M−4−E1
V−5−M−2−E1
V−5−M−3−E1
V−5−M−4−E1

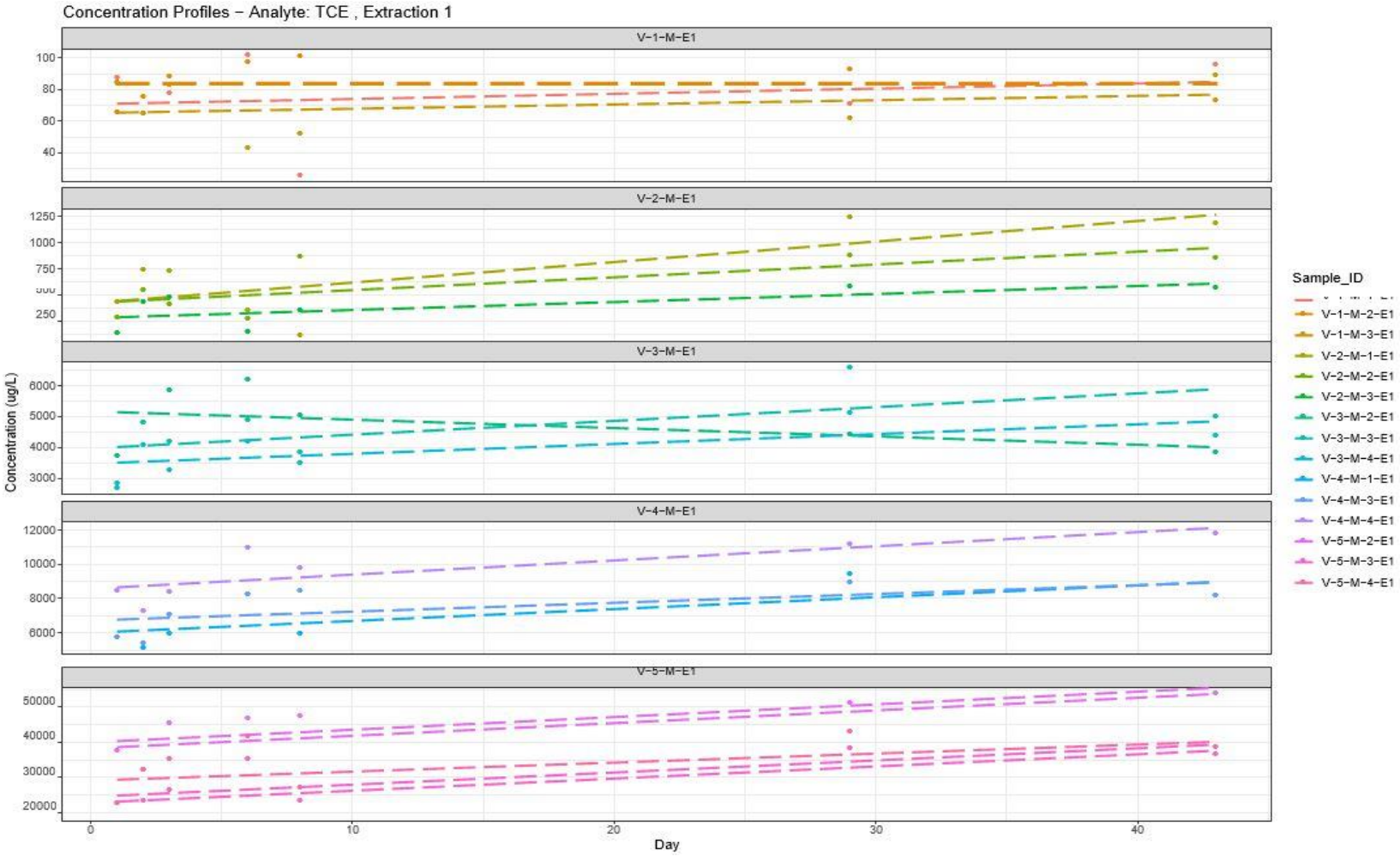
Concentration Profiles − Analyte: TCE , Extraction 1
V−1−M−E1
V−2−M−E1
V−3−M−E1
V−4−M−E1
V−5−M−E1
Concentration (ug/L)
Day
Sample_ID
V−1−M−2−E1
V−1−M−3−E1
V−2−M−1−E1
V−2−M−2−E1
V−2−M−3−E1
V−3−M−2−E1
V−3−M−3−E1
V−3−M−4−E1
V−4−M−1−E1
V−4−M−3−E1
V−4−M−4−E1
V−5−M−2−E1
V−5−M−3−E1
V−5−M−4−E1

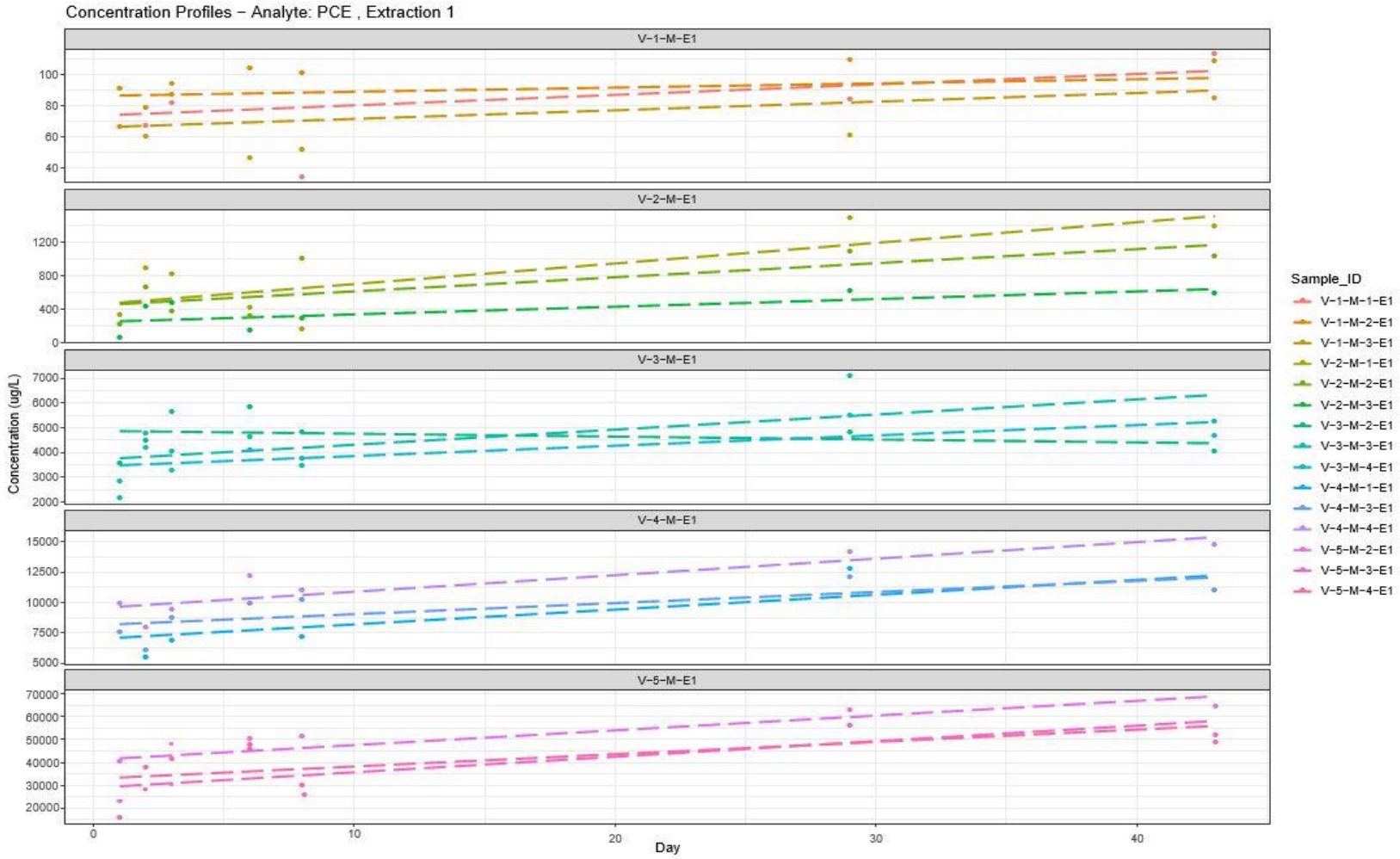
Concentration Profiles − Analyte: PCE , Extraction 1
V−1−M−E1
V−2−M−E1
V−3−M−E1
V−4−M−E1
V−5−M−E1
Concentration (ug/L)
Day
Sample_ID
V−1−M−1−E1
V−1−M−2−E1
V−1−M−3−E1
V−2−M−1−E1
V−2−M−2−E1
V−2−M−3−E1
V−3−M−2−E1
V−3−M−3−E1
V−3−M−4−E1
V−4−M−1−E1
V−4−M−3−E1
V−4−M−4−E1
V−5−M−2−E1
V−5−M−3−E1
V−5−M−4−E1

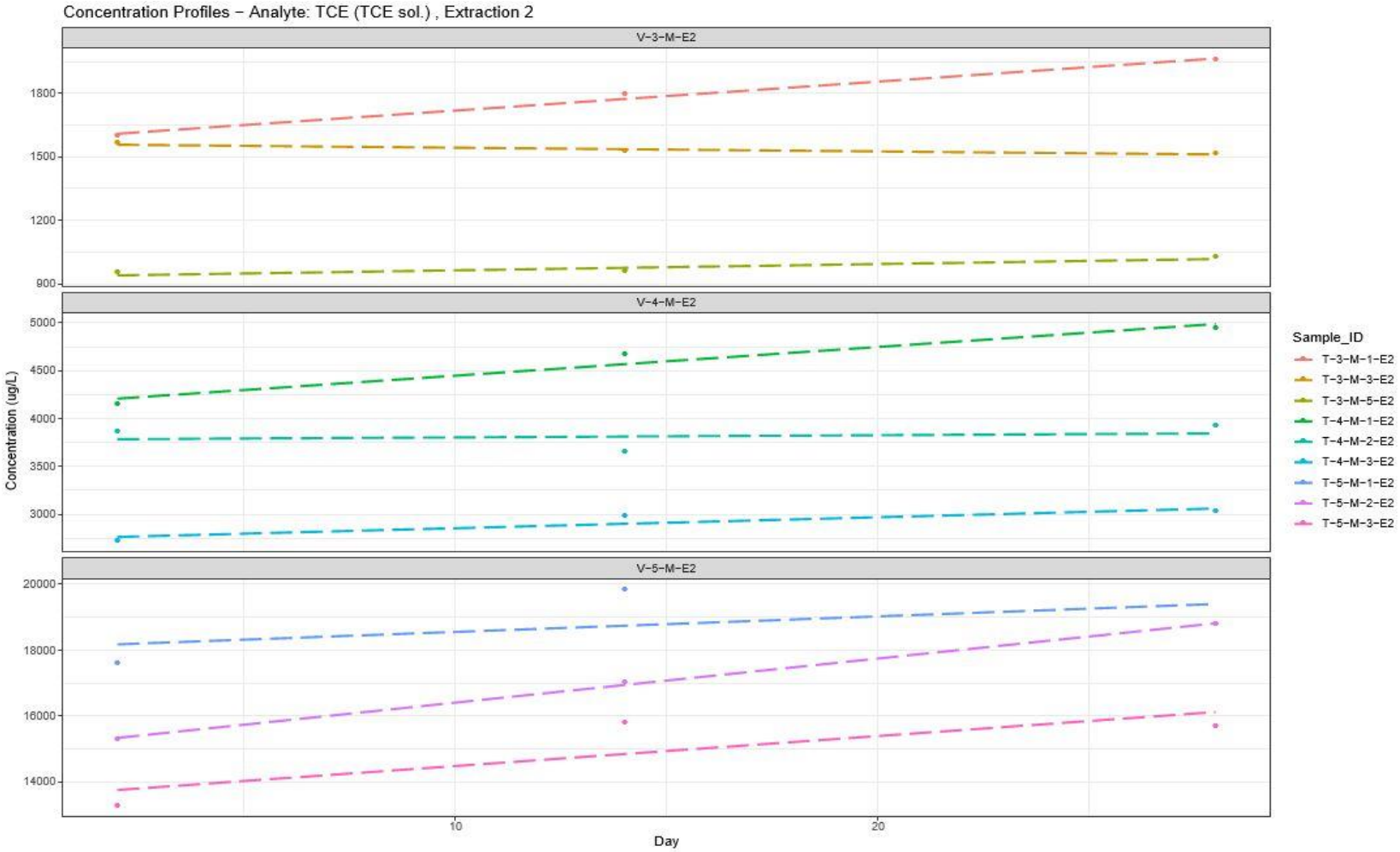
Concentration Profiles − Analyte: TCE (TCE sol.) , Extraction 2
V−3−M−E2
V−4−M−E2
V−5−M−E2
Concentration (ug/L)
Day
Sample_ID
T−3−M−1−E2
T−3−M−3−E2
T−3−M−5−E2
T−4−M−1−E2
T−4−M−2−E2
T−4−M−3−E2
T−5−M−1−E2
T−5−M−2−E2
T−5−M−3−E2

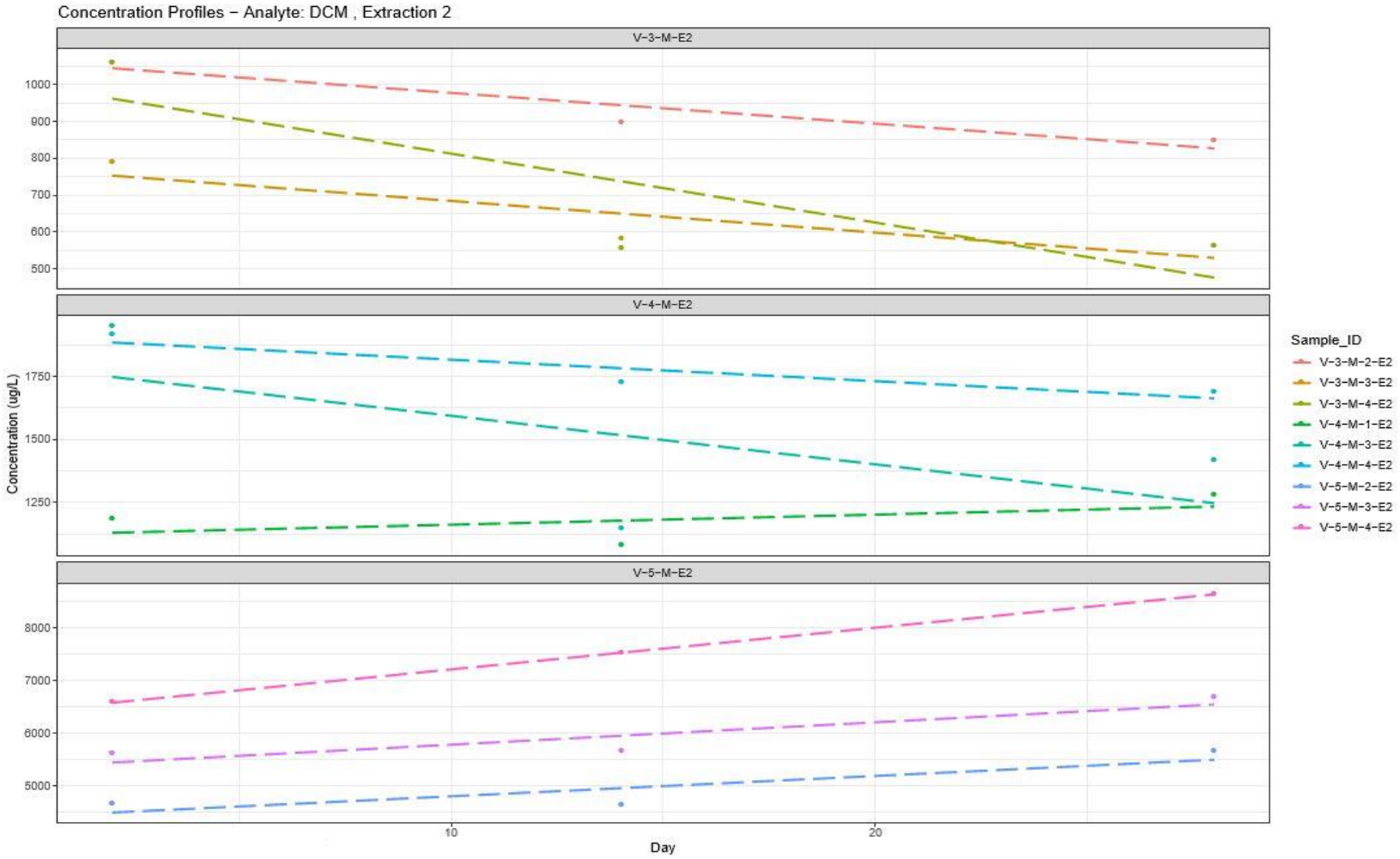
Concentration Profiles – Analyte: DCM , Extraction 2
V-3-M-E2
V-4-M-E2
V-5-M-E2
Concentration (ug/L)
Day
Sample_ID
V-3-M-2-E2
V-3-M-3-E2
V-3-M-4-E2
V-4-M-1-E2
V-4-M-3-E2
V-4-M-4-E2
V-5-M-2-E2
V-5-M-3-E2
V-5-M-4-E2

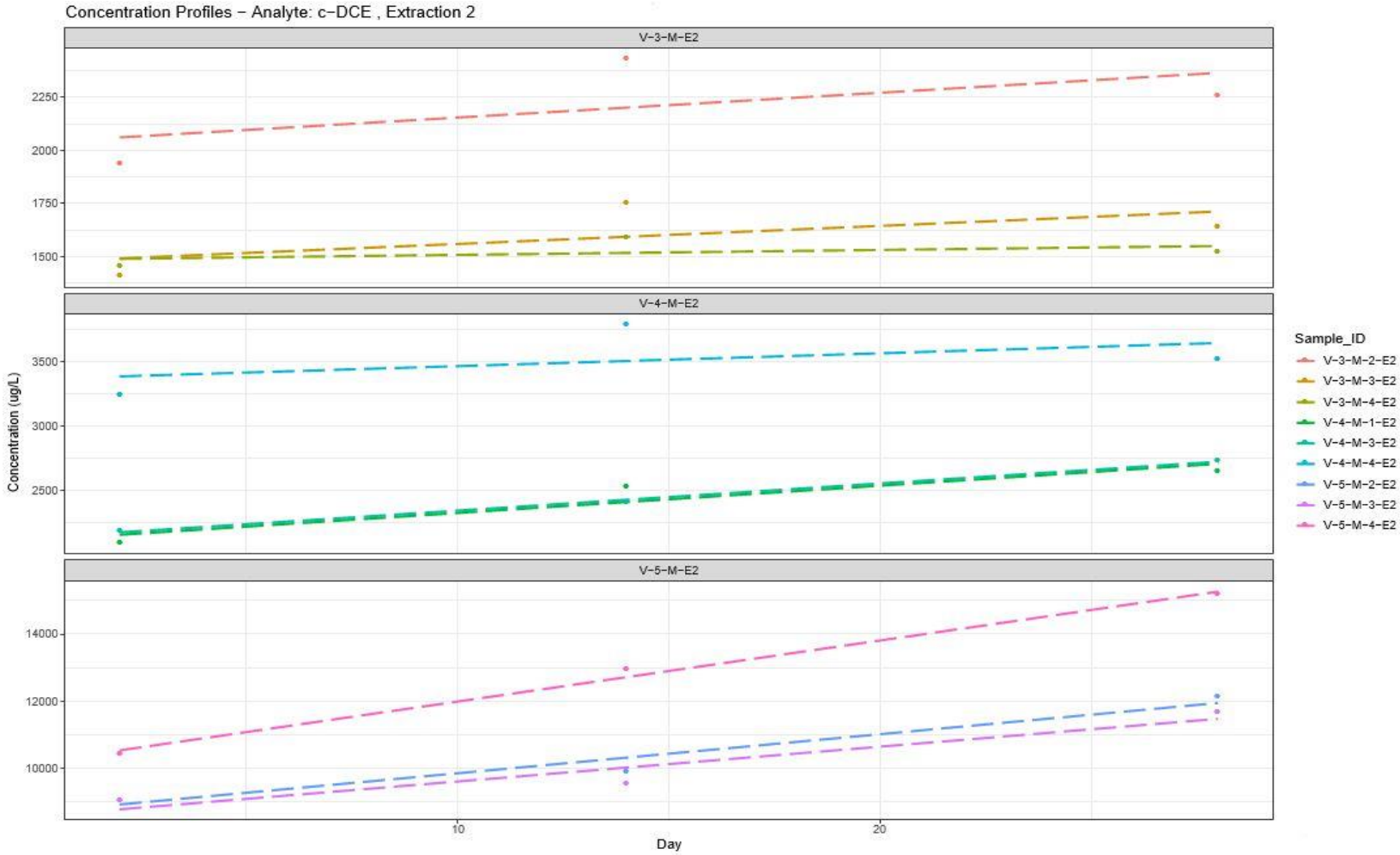
Concentration Profiles − Analyte: c−DCE , Extraction 2
V−3−M−E2
V−4−M−E2
V−5−M−E2
Concentration (ug/L)
Day
Sample_ID
V−3−M−2−E2
V−3−M−3−E2
V−3−M−4−E2
V−4−M−1−E2
V−4−M−3−E2
V−4−M−4−E2
V−5−M−2−E2
V−5−M−3−E2
V−5−M−4−E2

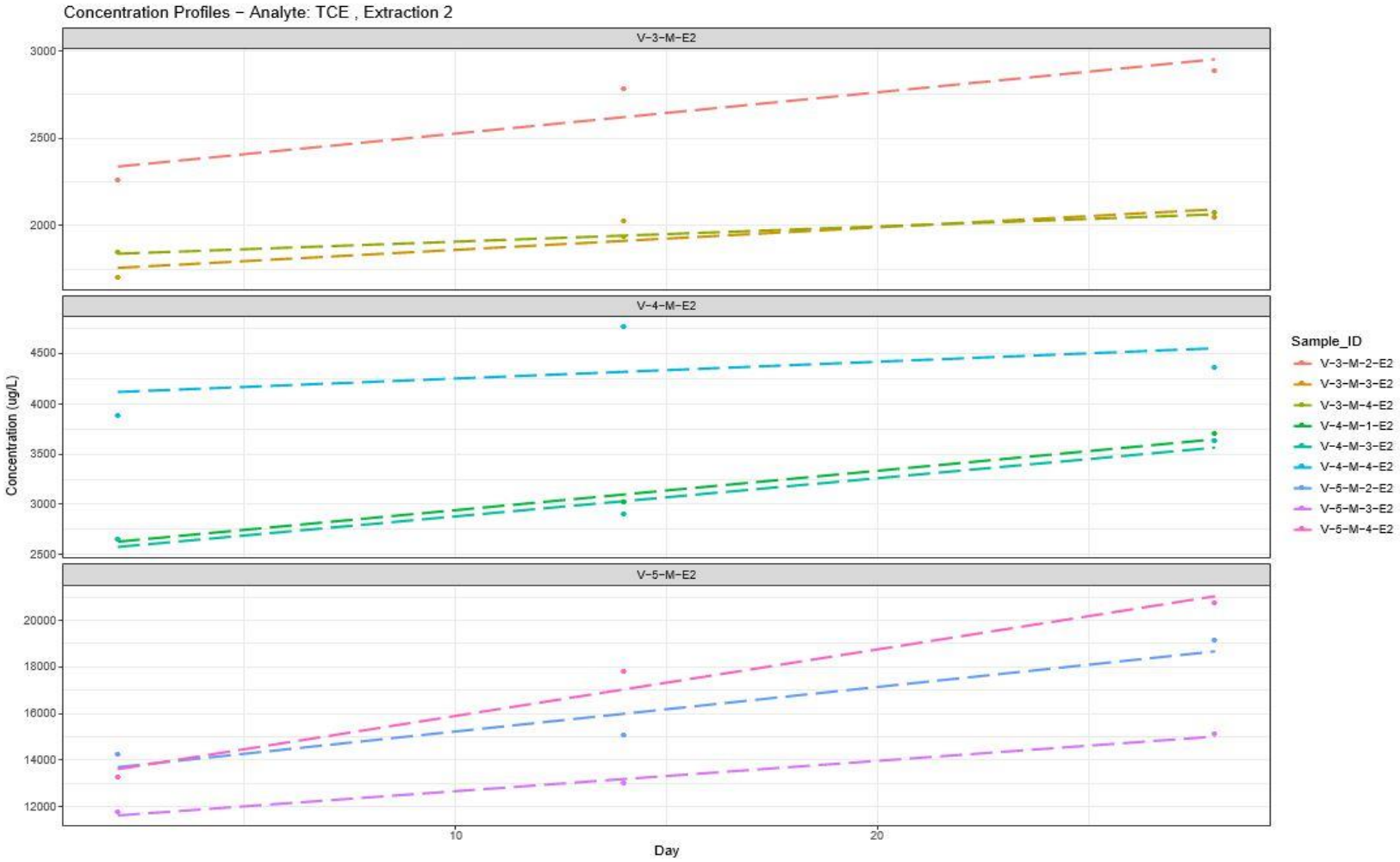
Concentration Profiles – Analyte: TCE , Extraction 2
V-3-M-E2
V-4-M-E2
V-5-M-E2
Concentration (ug/L)
Day
Sample_ID
V-3-M-2-E2
V-3-M-3-E2
V-3-M-4-E2
V-4-M-1-E2
V-4-M-3-E2
V-4-M-4-E2
V-5-M-2-E2
V-5-M-3-E2
V-5-M-4-E2

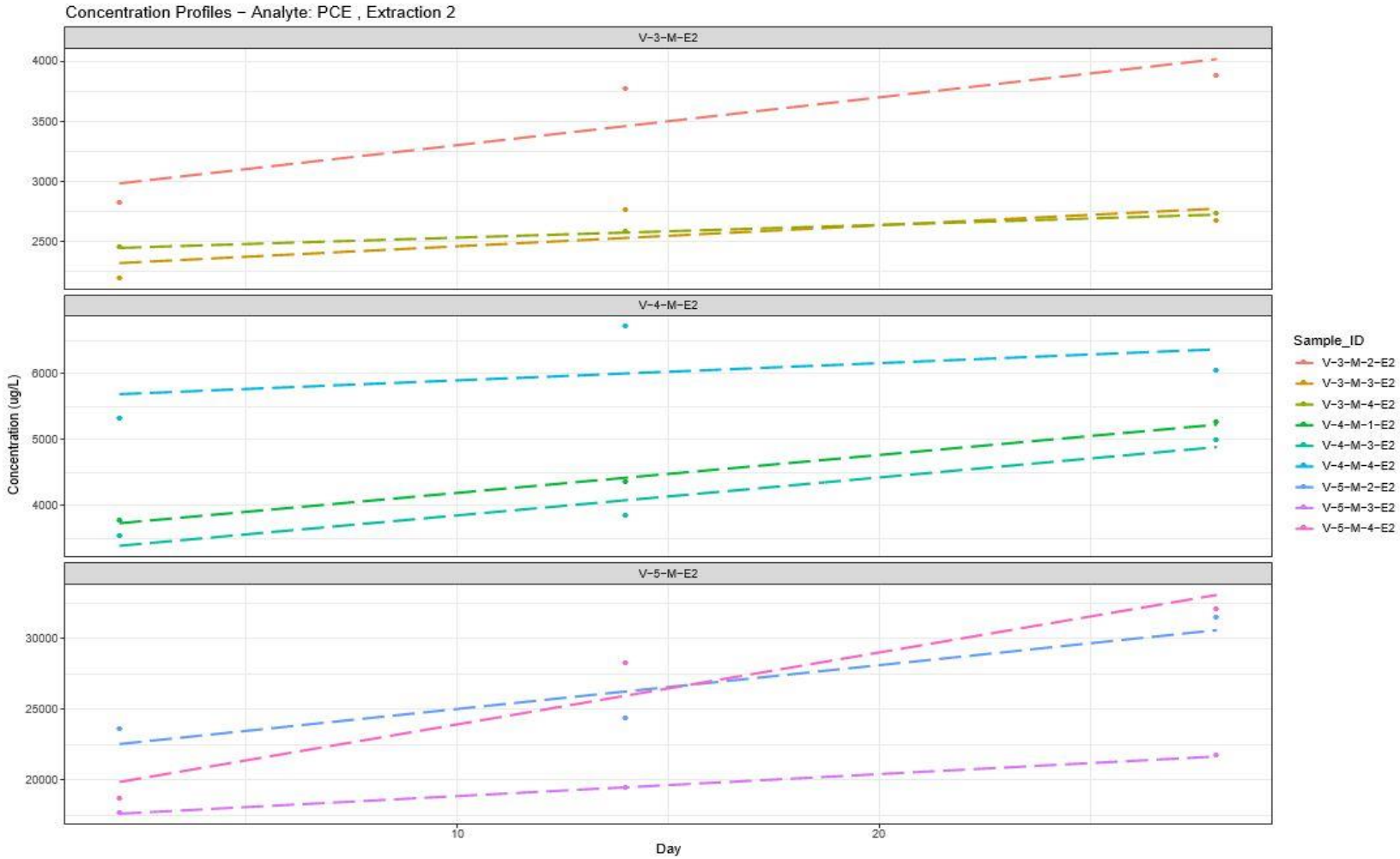
Concentration Profiles − Analyte: PCE , Extraction 2
V−3−M−E2
V−4−M−E2
V−5−M−E2
Concentration (ug/L)
Day
Sample_ID
V−3−M−2−E2
V−3−M−3−E2
V−3−M−4−E2
V−4−M−1−E2
V−4−M−3−E2
V−4−M−4−E2
V−5−M−2−E2
V−5−M−3−E2
V−5−M−4−E2

APPENDIX D: FACT MASS EXTRACTION TIME SERIES PLOTS-METHANOL WITH MICROWAVE ASSISTED EXTRACTION

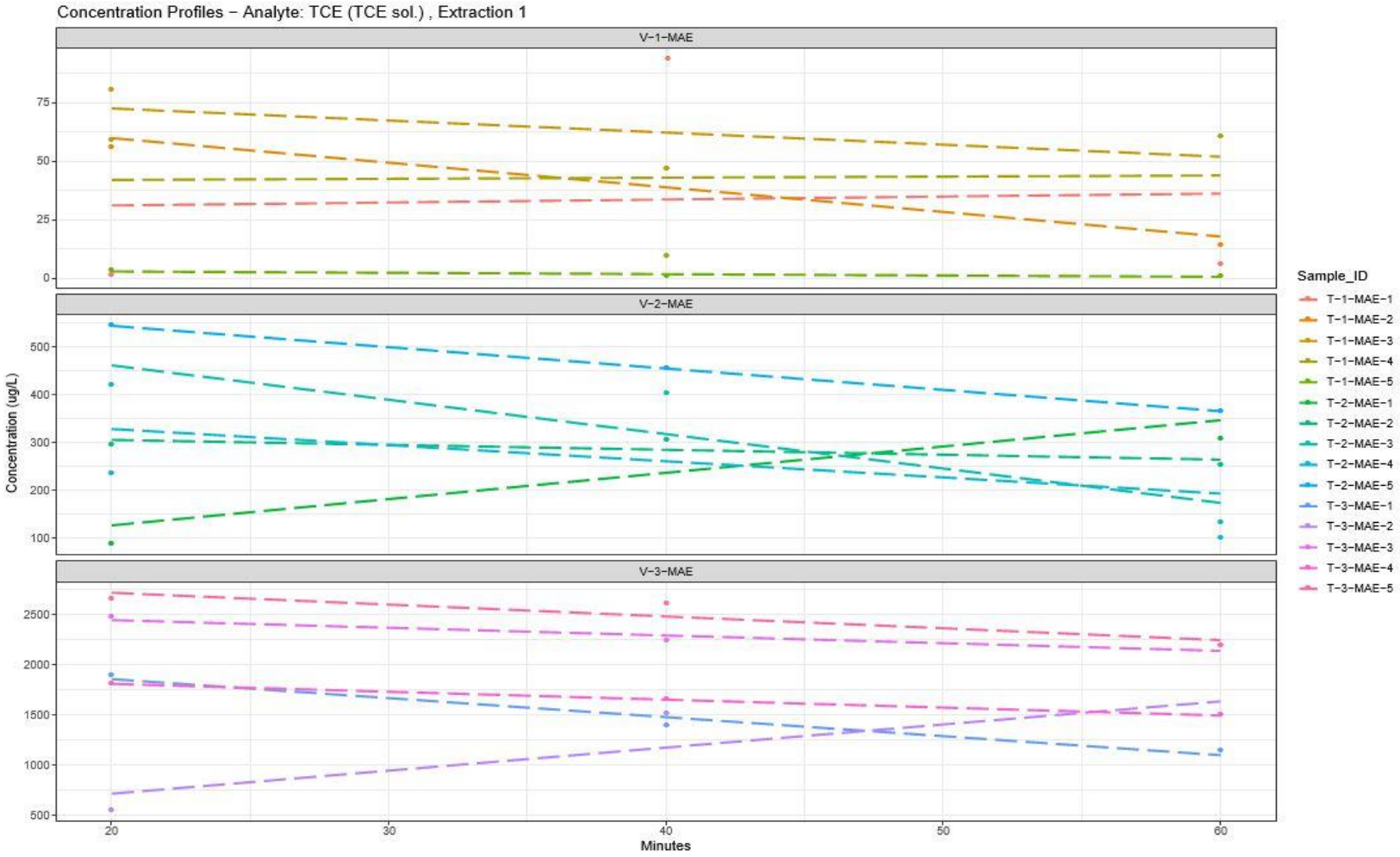
Concentration Profiles – Analyte: TCE (TCE sol.) , Extraction 1
V–1–MAE
V–2–MAE
V–3–MAE
Concentration (ug/L)
Minutes
Sample_ID
T–1–MAE–1
T–1–MAE–2
T–1–MAE–3
T–1–MAE–4
T–1–MAE–5
T–2–MAE–1
T–2–MAE–2
T–2–MAE–3
T–2–MAE–4
T–2–MAE–5
T–3–MAE–1
T–3–MAE–2
T–3–MAE–3
T–3–MAE–4
T–3–MAE–5

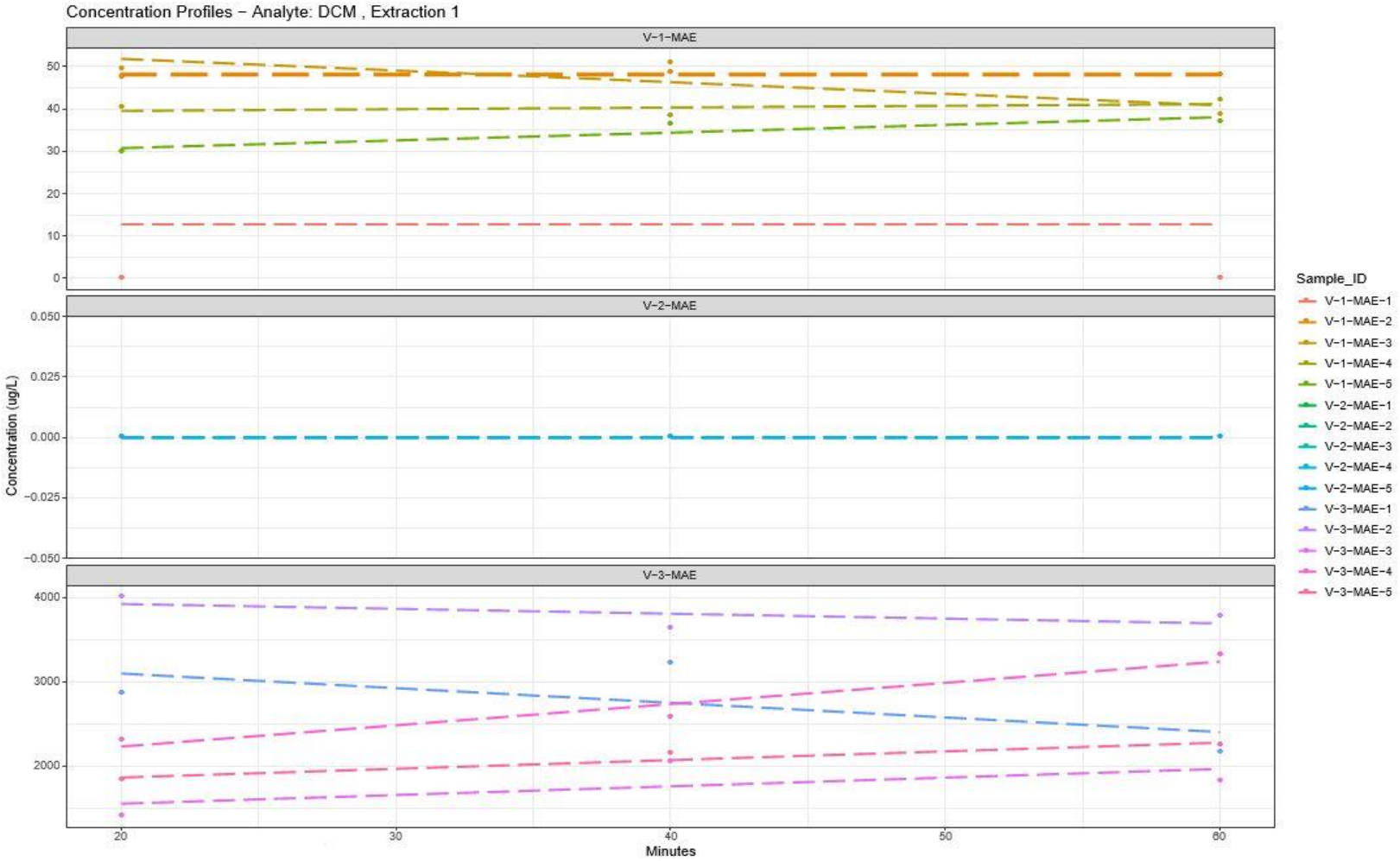
Concentration Profiles – Analyte: DCM , Extraction 1
V-1-MAE
V-2-MAE
V-3-MAE
Concentration (ug/L)
Minutes
Sample_ID
V-1-MAE-1
V-1-MAE-2
V-1-MAE-3
V-1-MAE-4
V-1-MAE-5
V-2-MAE-1
V-2-MAE-2
V-2-MAE-3
V-2-MAE-4
V-2-MAE-5
V-3-MAE-1
V-3-MAE-2
V-3-MAE-3
V-3-MAE-4
V-3-MAE-5

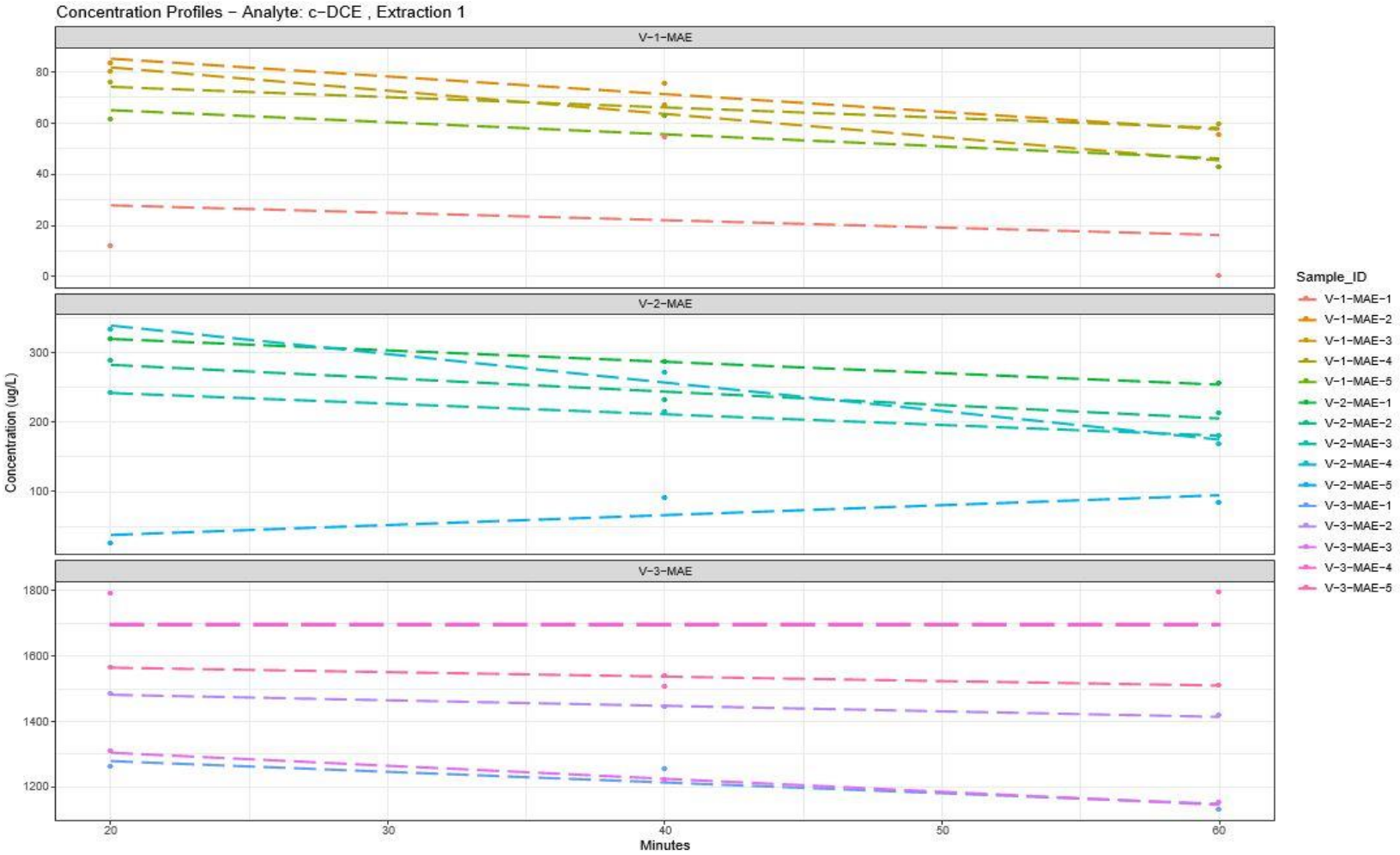
Concentration Profiles − Analyte: c−DCE , Extraction 1
V−1−MAE
V−2−MAE
V−3−MAE
Concentration (ug/L)
Minutes
Sample_ID
V−1−MAE−1
V−1−MAE−2
V−1−MAE−3
V−1−MAE−4
V−1−MAE−5
V−2−MAE−1
V−2−MAE−2
V−2−MAE−3
V−2−MAE−4
V−2−MAE−5
V−3−MAE−1
V−3−MAE−2
V−3−MAE−3
V−3−MAE−4
V−3−MAE−5

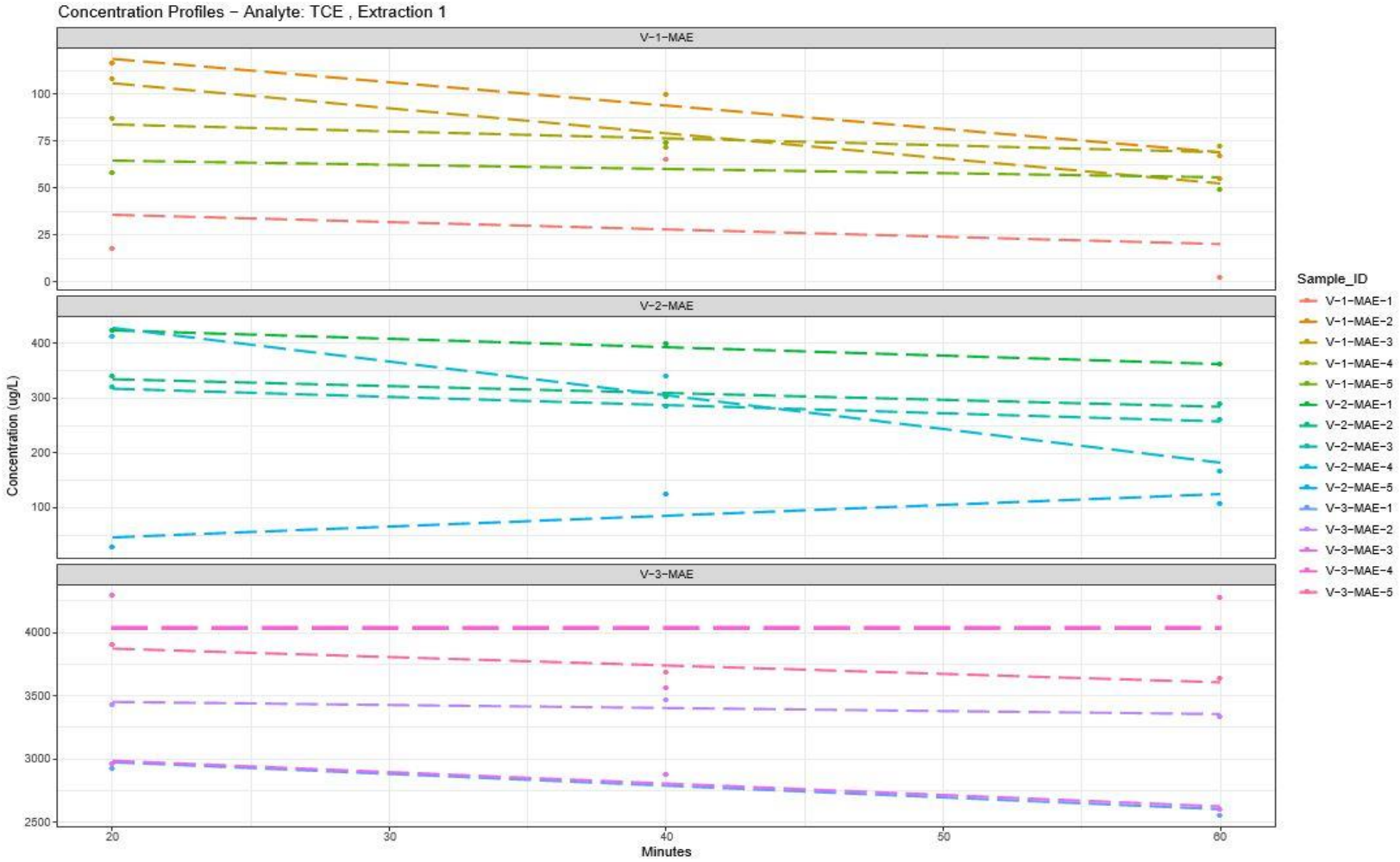
Concentration Profiles – Analyte: TCE , Extraction 1
V-1-MAE
V-2-MAE
V-3-MAE
Concentration (ug/L)
Minutes
Sample_ID
V-1-MAE-1
V-1-MAE-2
V-1-MAE-3
V-1-MAE-4
V-1-MAE-5
V-2-MAE-1
V-2-MAE-2
V-2-MAE-3
V-2-MAE-4
V-2-MAE-5
V-3-MAE-1
V-3-MAE-2
V-3-MAE-3
V-3-MAE-4
V-3-MAE-5

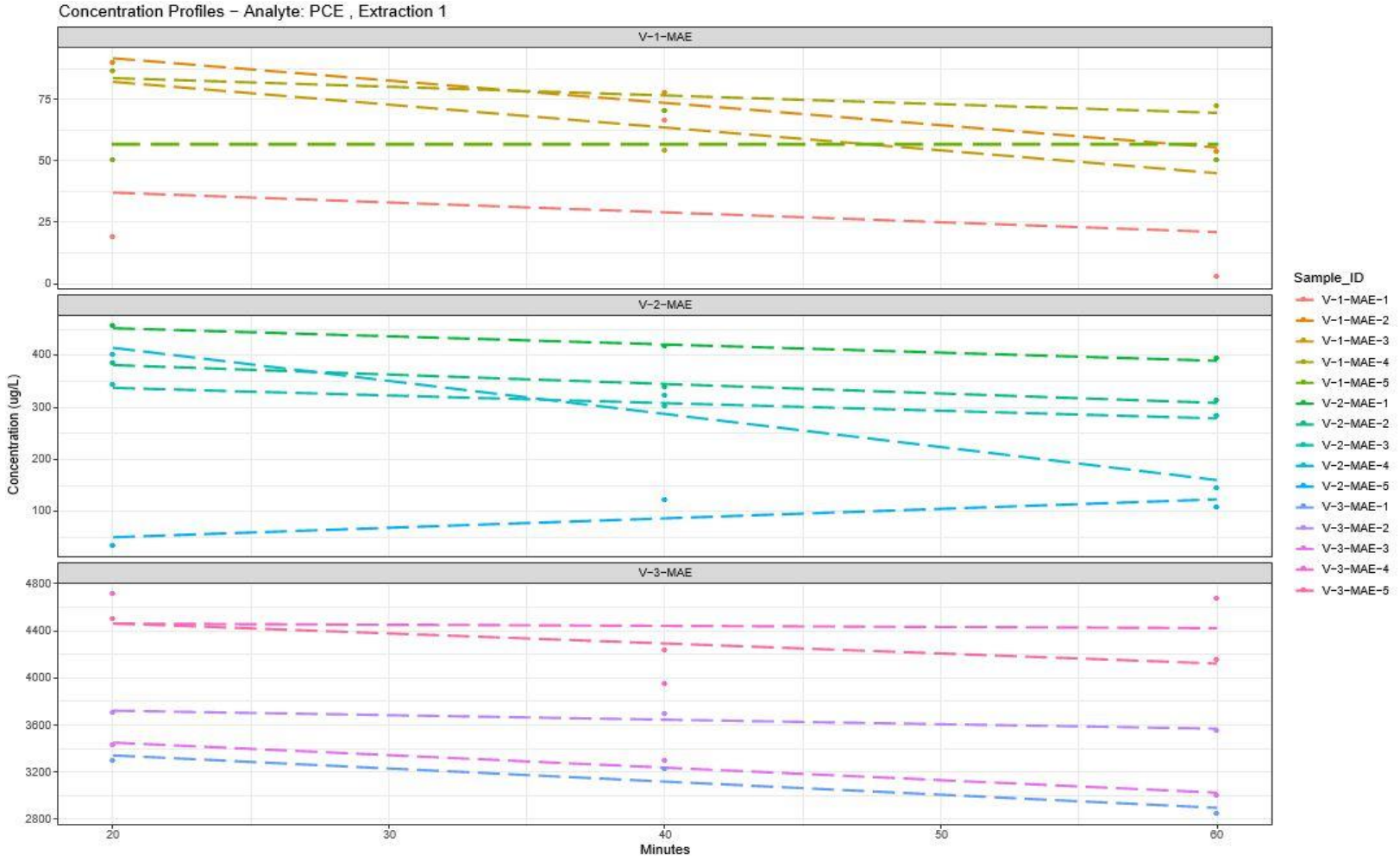
Concentration Profiles – Analyte: PCE , Extraction 1
V-1-MAE
V-2-MAE
V-3-MAE
Concentration (ug/L)
Minutes
Sample_ID
V-1-MAE-1
V-1-MAE-2
V-1-MAE-3
V-1-MAE-4
V-1-MAE-5
V-2-MAE-1
V-2-MAE-2
V-2-MAE-3
V-2-MAE-4
V-2-MAE-5
V-3-MAE-1
V-3-MAE-2
V-3-MAE-3
V-3-MAE-4
V-3-MAE-5

APPENDIX E: FACT MASS EXTRACTION TIME SERIES PLOTS-PENTANE/WATER MIXTURE SHAKE FLASK METHOD

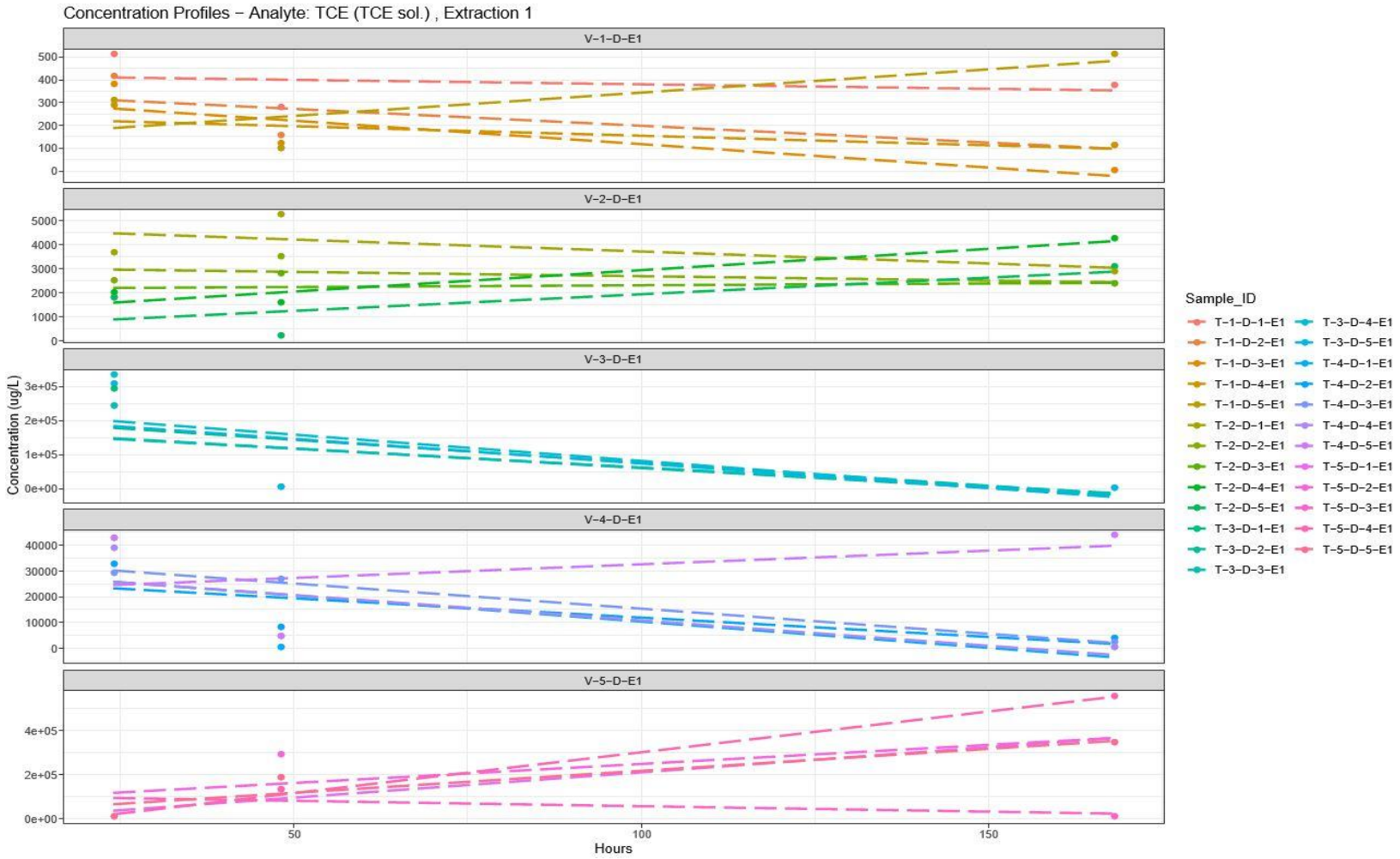
Concentration Profiles – Analyte: TCE (TCE sol.) , Extraction 1
V–1–D–E1
V–2–D–E1
V–3–D–E1
V–4–D–E1
V–5–D–E1
Concentration (ug/L)
Hours
Sample_ID
T–1–D–1–E1
T–1–D–2–E1
T–1–D–3–E1
T–1–D–4–E1
T–1–D–5–E1
T–2–D–1–E1
T–2–D–2–E1
T–2–D–3–E1
T–2–D–4–E1
T–2–D–5–E1
T–3–D–1–E1
T–3–D–2–E1
T–3–D–3–E1
T–3–D–4–E1
T–3–D–5–E1
T–4–D–1–E1
T–4–D–2–E1
T–4–D–3–E1
T–4–D–4–E1
T–4–D–5–E1
T–5–D–1–E1
T–5–D–2–E1
T–5–D–3–E1
T–5–D–4–E1
T–5–D–5–E1

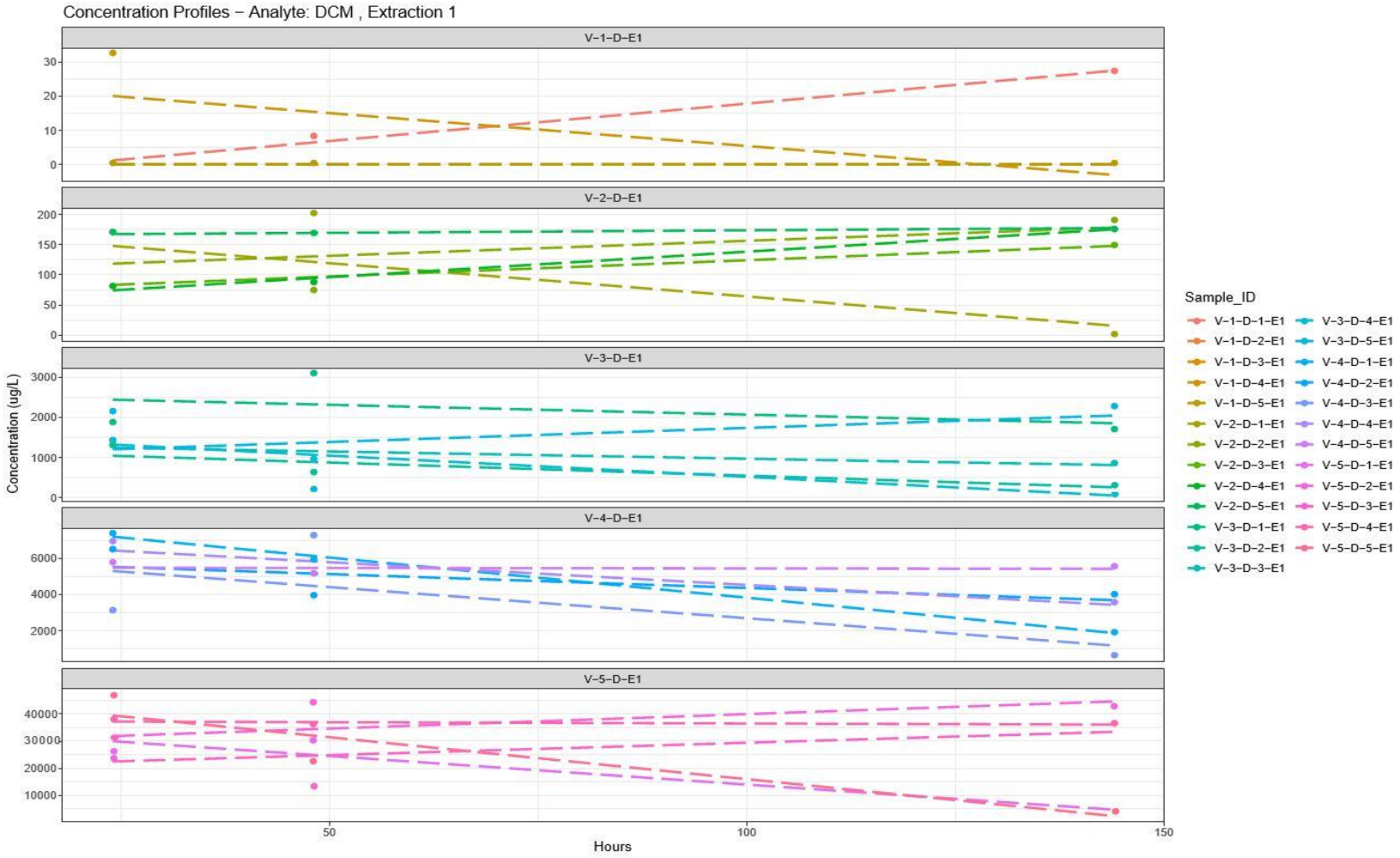
Concentration Profiles – Analyte: DCM , Extraction 1
V–1–D–E1
V–2–D–E1
V–3–D–E1
V–4–D–E1
V–5–D–E1
Concentration (ug/L)
Hours
Sample_ID
V–1–D–1–E1
V–1–D–2–E1
V–1–D–3–E1
V–1–D–4–E1
V–1–D–5–E1
V–2–D–1–E1
V–2–D–2–E1
V–2–D–3–E1
V–2–D–4–E1
V–2–D–5–E1
V–3–D–1–E1
V–3–D–2–E1
V–3–D–3–E1
V–3–D–4–E1
V–3–D–5–E1
V–4–D–1–E1
V–4–D–2–E1
V–4–D–3–E1
V–4–D–4–E1
V–4–D–5–E1
V–5–D–1–E1
V–5–D–2–E1
V–5–D–3–E1
V–5–D–4–E1
V–5–D–5–E1

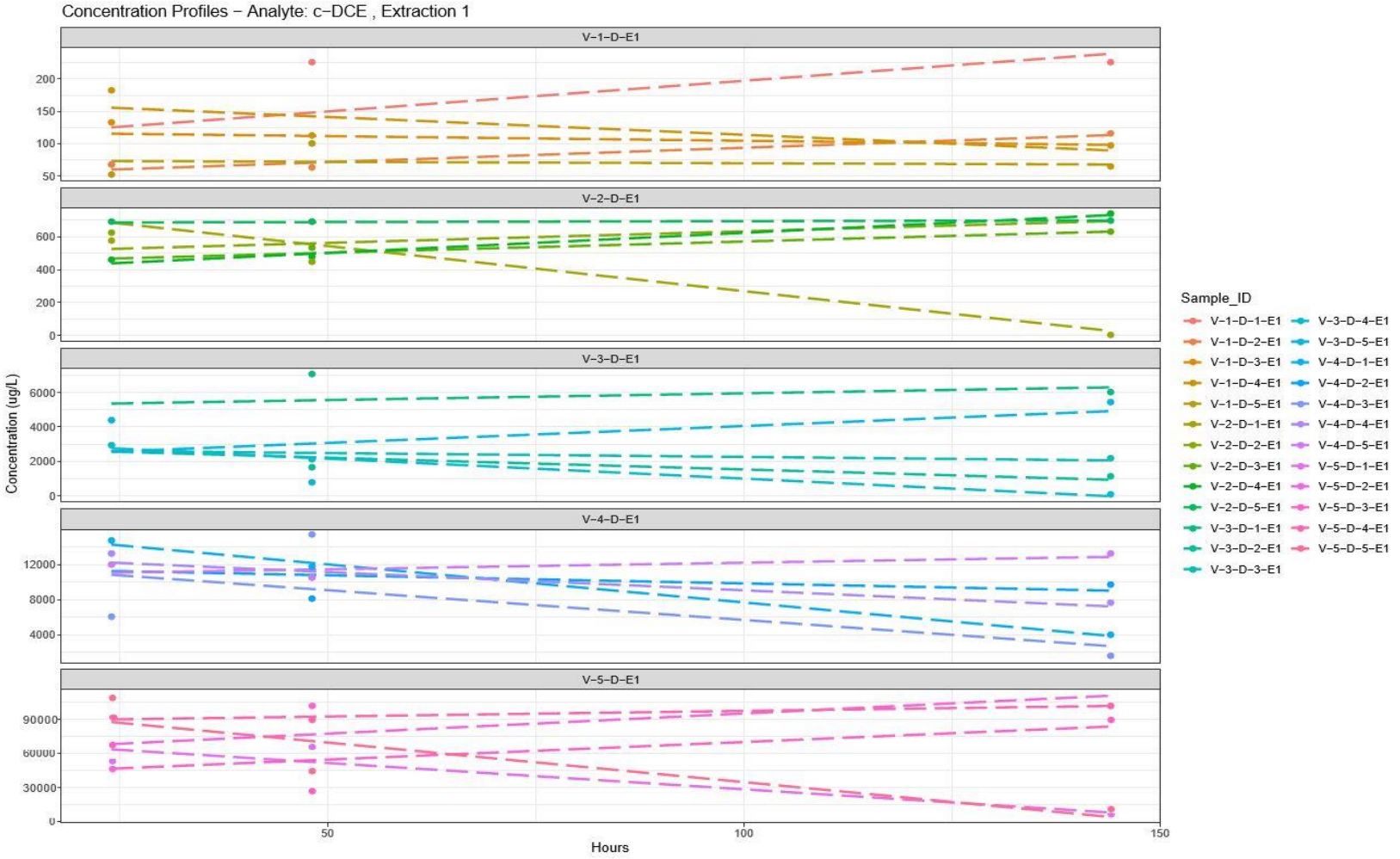
Concentration Profiles − Analyte: c−DCE , Extraction 1
V−1−D−E1
V−2−D−E1
V−3−D−E1
V−4−D−E1
V−5−D−E1
Concentration (ug/L)
Hours
Sample_ID
V−1−D−1−E1
V−1−D−2−E1
V−1−D−3−E1
V−1−D−4−E1
V−1−D−5−E1
V−2−D−1−E1
V−2−D−2−E1
V−2−D−3−E1
V−2−D−4−E1
V−2−D−5−E1
V−3−D−1−E1
V−3−D−2−E1
V−3−D−3−E1
V−3−D−4−E1
V−3−D−5−E1
V−4−D−1−E1
V−4−D−2−E1
V−4−D−3−E1
V−4−D−4−E1
V−4−D−5−E1
V−5−D−1−E1
V−5−D−2−E1
V−5−D−3−E1
V−5−D−4−E1
V−5−D−5−E1

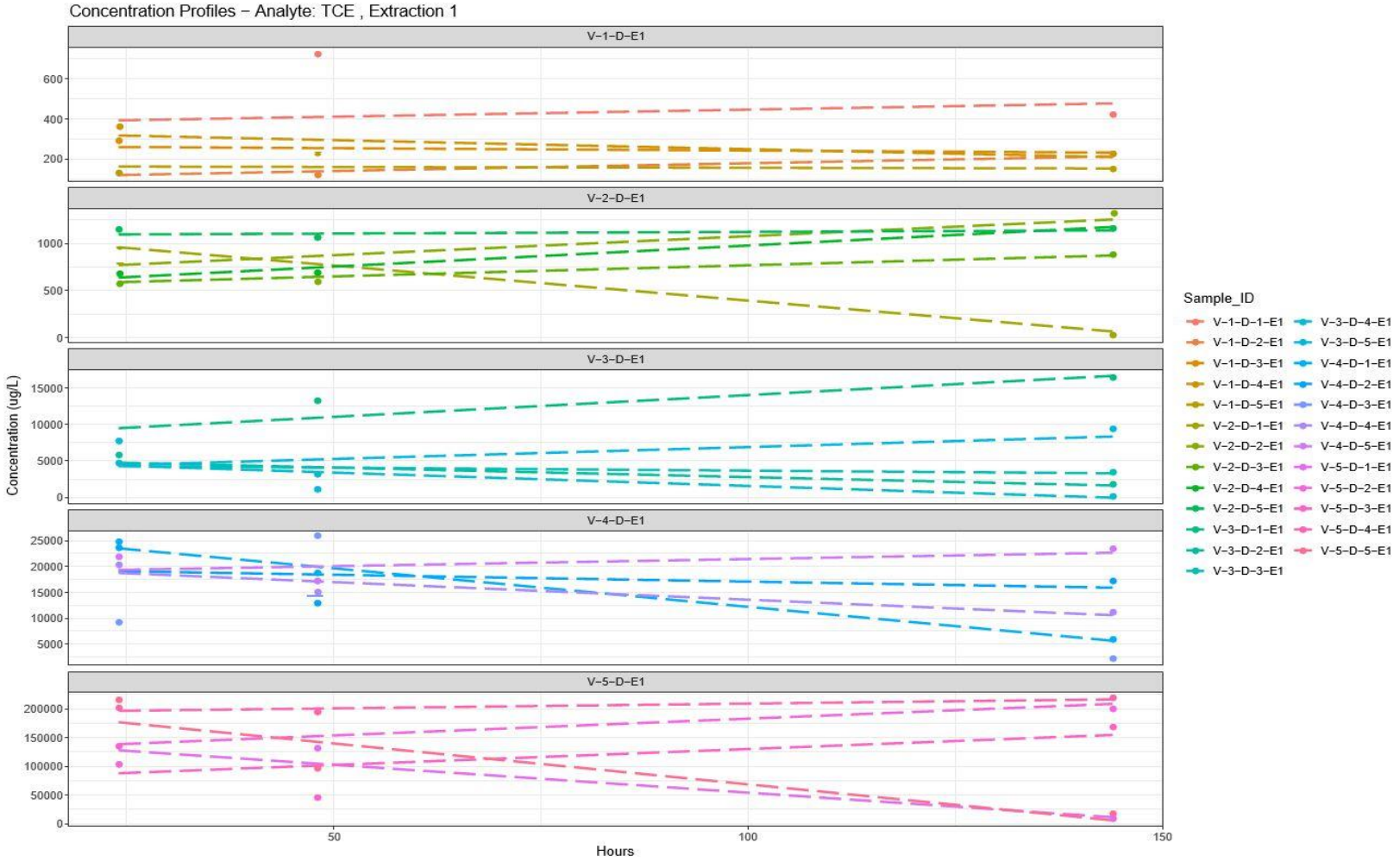
Concentration Profiles – Analyte: TCE , Extraction 1
V–1–D–E1
V–2–D–E1
V–3–D–E1
V–4–D–E1
V–5–D–E1
Concentration (ug/L)
Hours
Sample_ID
V–1–D–1–E1
V–1–D–2–E1
V–1–D–3–E1
V–1–D–4–E1
V–1–D–5–E1
V–2–D–1–E1
V–2–D–2–E1
V–2–D–3–E1
V–2–D–4–E1
V–2–D–5–E1
V–3–D–1–E1
V–3–D–2–E1
V–3–D–3–E1
V–3–D–4–E1
V–3–D–5–E1
V–4–D–1–E1
V–4–D–2–E1
V–4–D–3–E1
V–4–D–4–E1
V–4–D–5–E1
V–5–D–1–E1
V–5–D–2–E1
V–5–D–3–E1
V–5–D–4–E1
V–5–D–5–E1

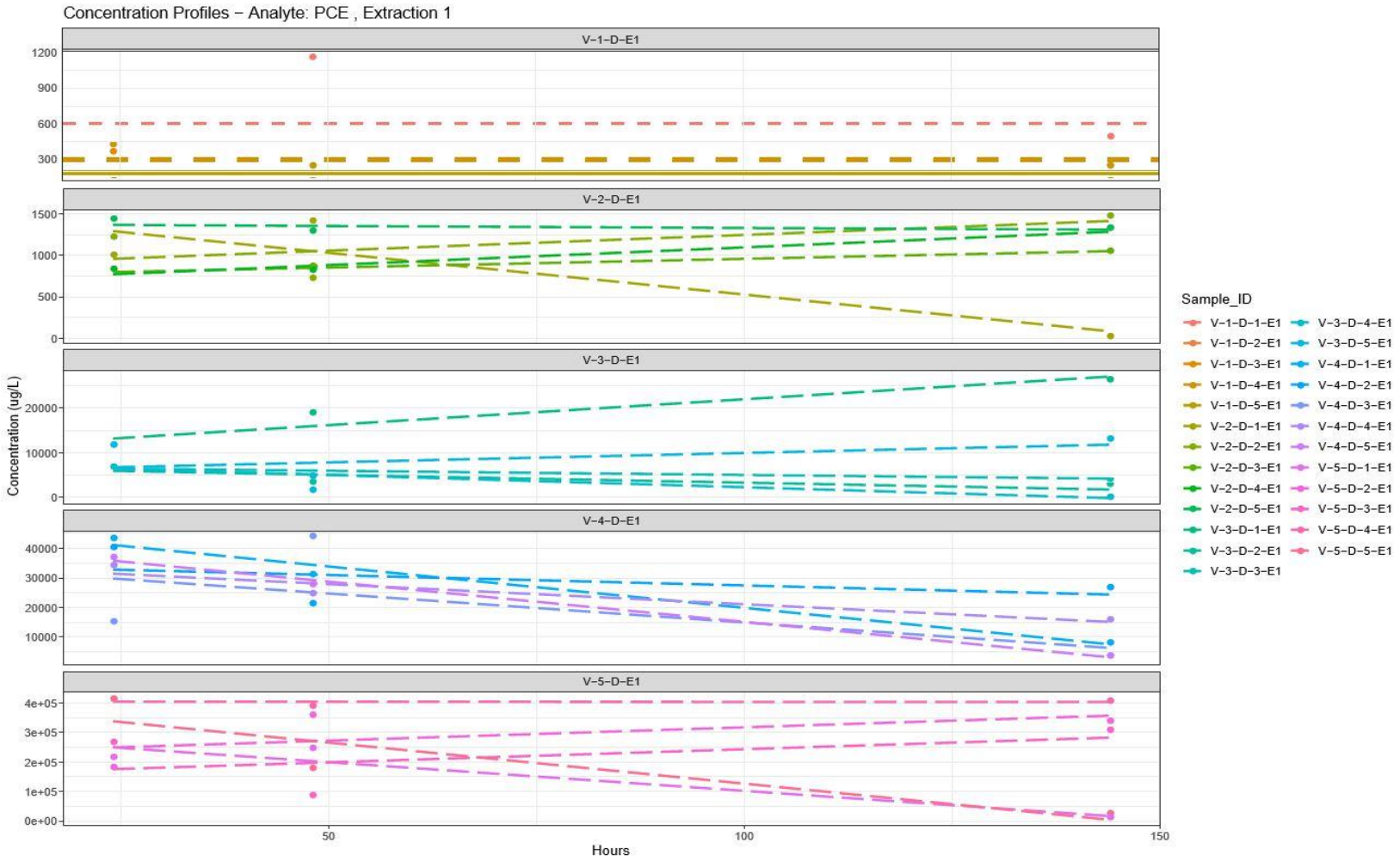
Concentration Profiles – Analyte: PCE , Extraction 1
V–1–D–E1
V–2–D–E1
V–3–D–E1
V–4–D–E1
V–5–D–E1
Concentration (ug/L)
Hours
Sample_ID
V–1–D–1–E1
V–1–D–2–E1
V–1–D–3–E1
V–1–D–4–E1
V–1–D–5–E1
V–2–D–1–E1
V–2–D–2–E1
V–2–D–3–E1
V–2–D–4–E1
V–2–D–5–E1
V–3–D–1–E1
V–3–D–2–E1
V–3–D–3–E1
V–3–D–4–E1
V–3–D–5–E1
V–4–D–1–E1
V–4–D–2–E1
V–4–D–3–E1
V–4–D–4–E1
V–4–D–5–E1
V–5–D–1–E1
V–5–D–2–E1
V–5–D–3–E1
V–5–D–4–E1
V–5–D–5–E1

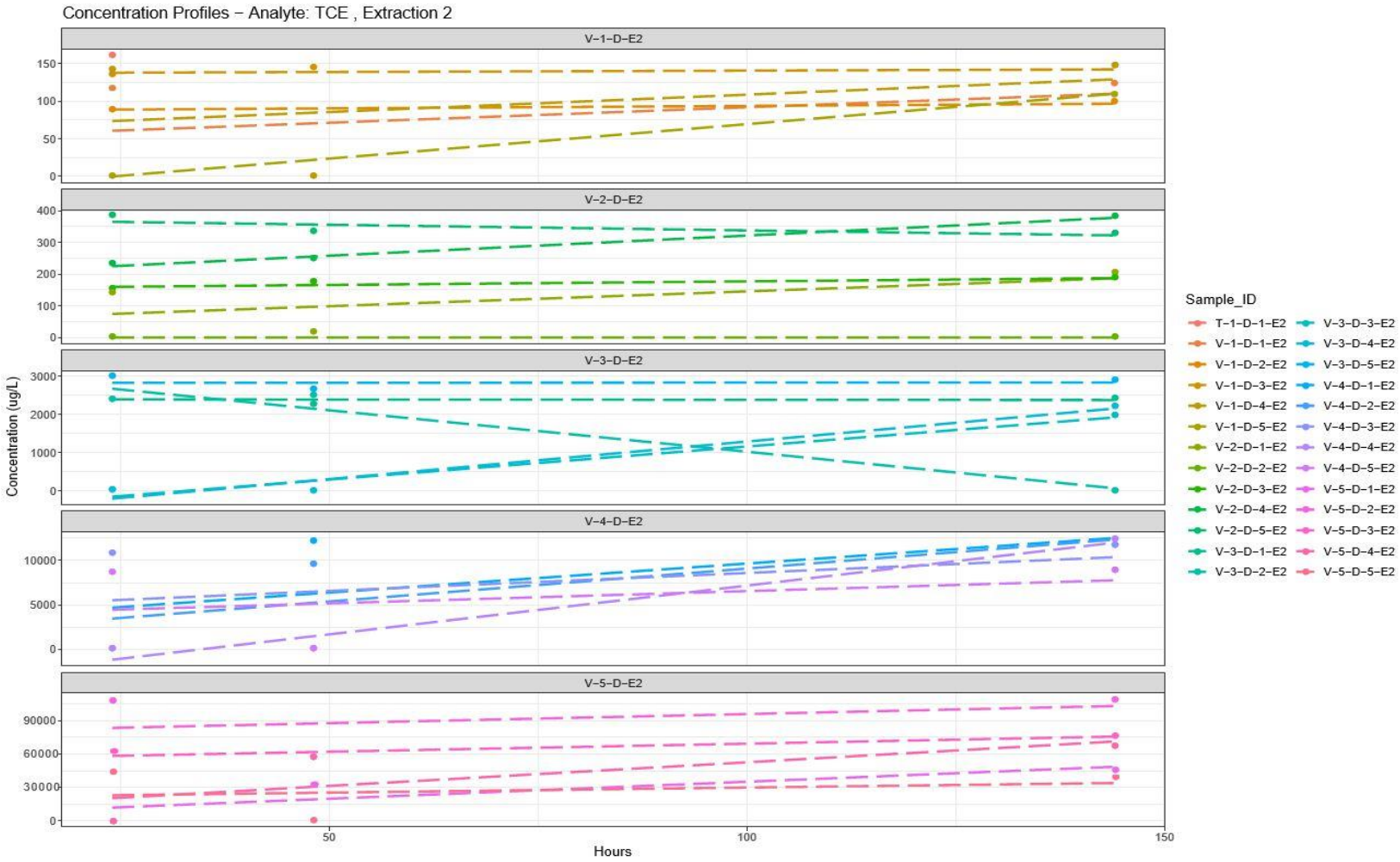
Concentration Profiles – Analyte: TCE , Extraction 2
V–1–D–E2
V–2–D–E2
V–3–D–E2
V–4–D–E2
V–5–D–E2
Concentration (ug/L)
Hours
Sample_ID
T–1–D–1–E2
V–1–D–1–E2
V–1–D–2–E2
V–1–D–3–E2
V–1–D–4–E2
V–1–D–5–E2
V–2–D–1–E2
V–2–D–2–E2
V–2–D–3–E2
V–2–D–4–E2
V–2–D–5–E2
V–3–D–1–E2
V–3–D–2–E2
V–3–D–3–E2
V–3–D–4–E2
V–3–D–5–E2
V–4–D–1–E2
V–4–D–2–E2
V–4–D–3–E2
V–4–D–4–E2
V–4–D–5–E2
V–5–D–1–E2
V–5–D–2–E2
V–5–D–3–E2
V–5–D–4–E2
V–5–D–5–E2

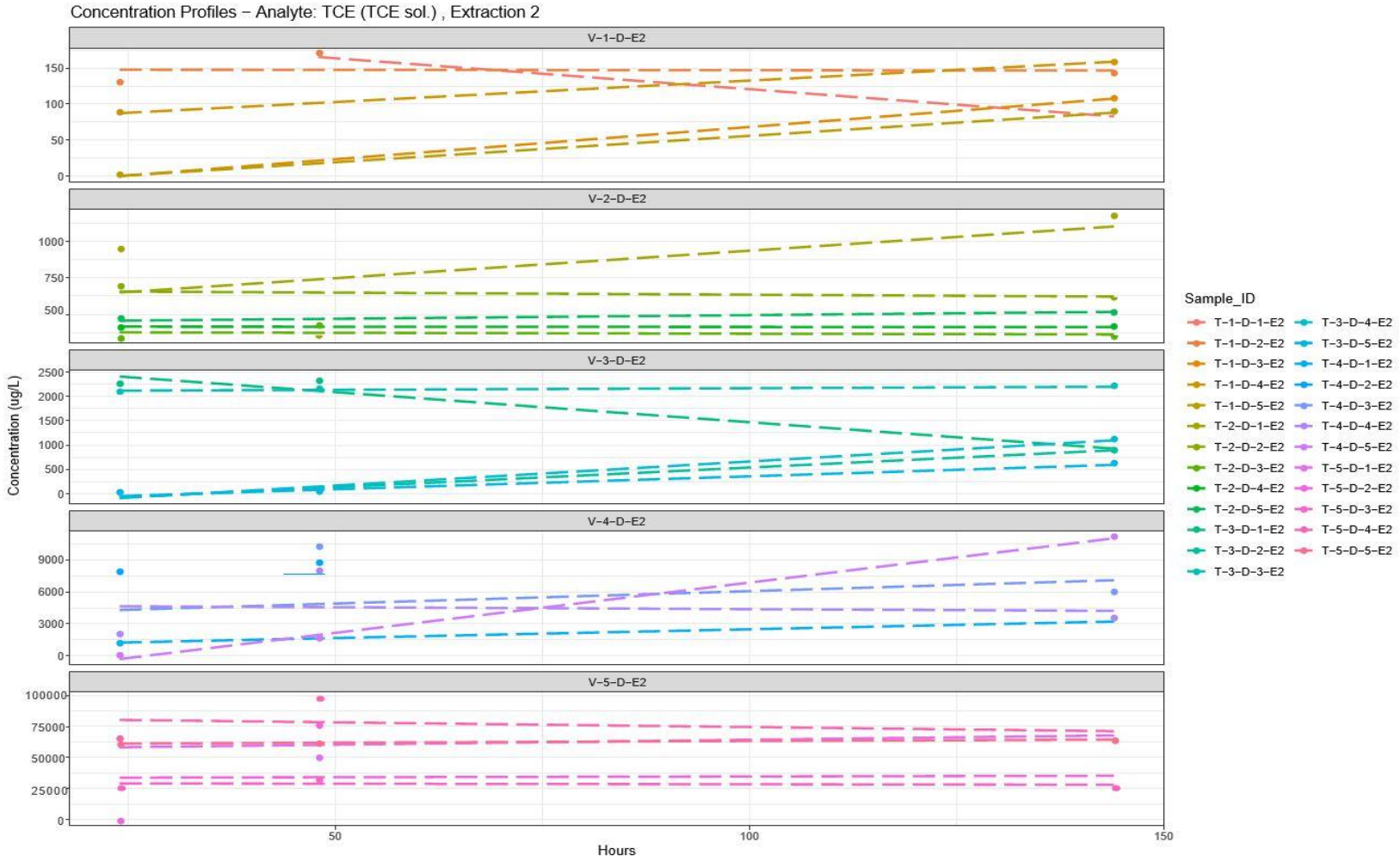
Concentration Profiles − Analyte: TCE (TCE sol.) , Extraction 2
V−1−D−E2
V−2−D−E2
V−3−D−E2
V−4−D−E2
V−5−D−E2
Concentration (ug/L)
Hours
Sample_ID
T−1−D−1−E2
T−1−D−2−E2
T−1−D−3−E2
T−1−D−4−E2
T−1−D−5−E2
T−2−D−1−E2
T−2−D−2−E2
T−2−D−3−E2
T−2−D−4−E2
T−2−D−5−E2
T−3−D−1−E2
T−3−D−2−E2
T−3−D−3−E2
T−3−D−4−E2
T−3−D−5−E2
T−4−D−1−E2
T−4−D−2−E2
T−4−D−3−E2
T−4−D−4−E2
T−4−D−5−E2
T−5−D−1−E2
T−5−D−2−E2
T−5−D−3−E2
T−5−D−4−E2
T−5−D−5−E2

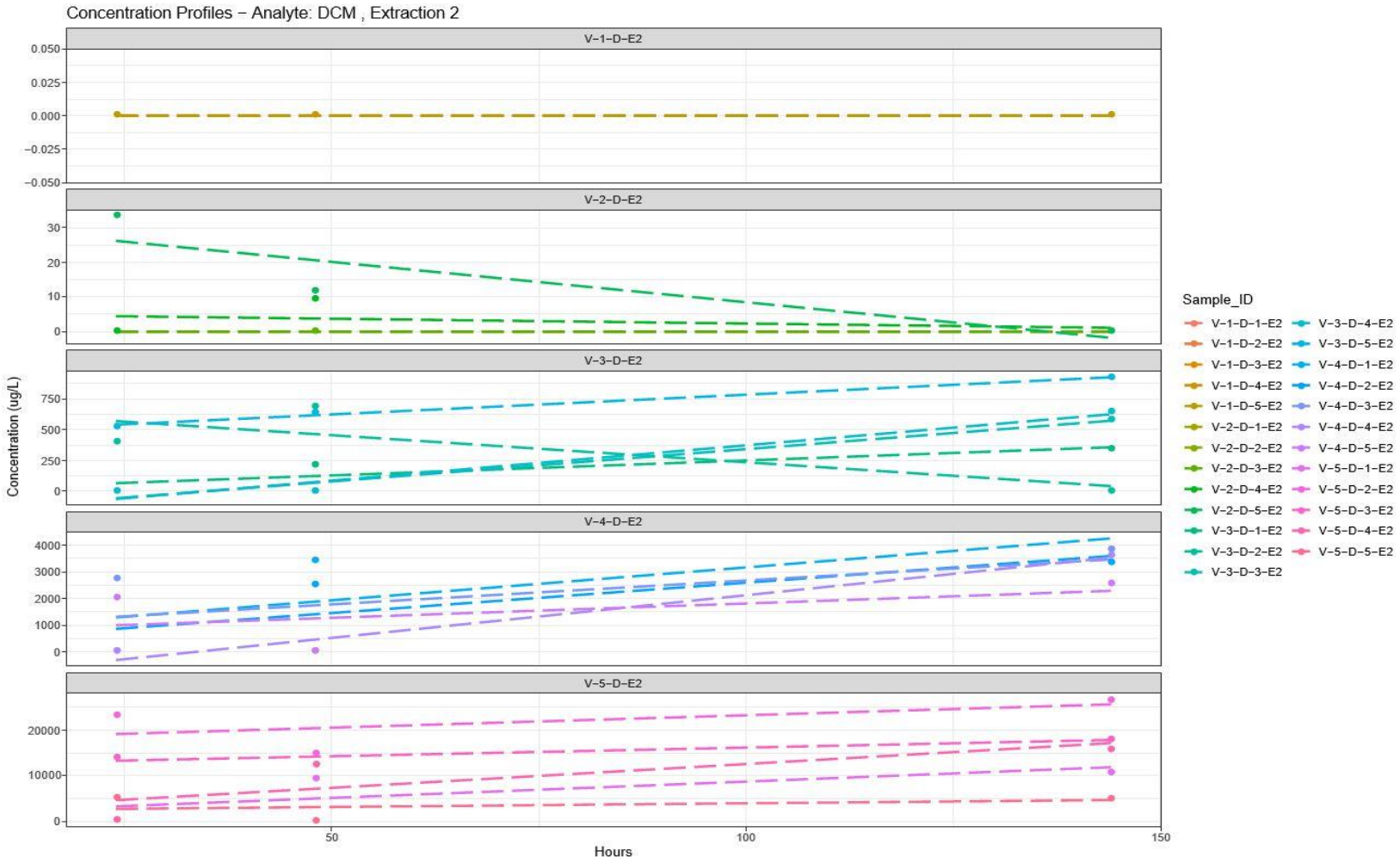
Concentration Profiles – Analyte: DCM , Extraction 2
V–1–D–E2
V–2–D–E2
V–3–D–E2
V–4–D–E2
V–5–D–E2
Concentration (ug/L)
Hours
Sample_ID
V–1–D–1–E2
V–1–D–2–E2
V–1–D–3–E2
V–1–D–4–E2
V–1–D–5–E2
V–2–D–1–E2
V–2–D–2–E2
V–2–D–3–E2
V–2–D–4–E2
V–2–D–5–E2
V–3–D–1–E2
V–3–D–2–E2
V–3–D–3–E2
V–3–D–4–E2
V–3–D–5–E2
V–4–D–1–E2
V–4–D–2–E2
V–4–D–3–E2
V–4–D–4–E2
V–4–D–5–E2
V–5–D–1–E2
V–5–D–2–E2
V–5–D–3–E2
V–5–D–4–E2
V–5–D–5–E2

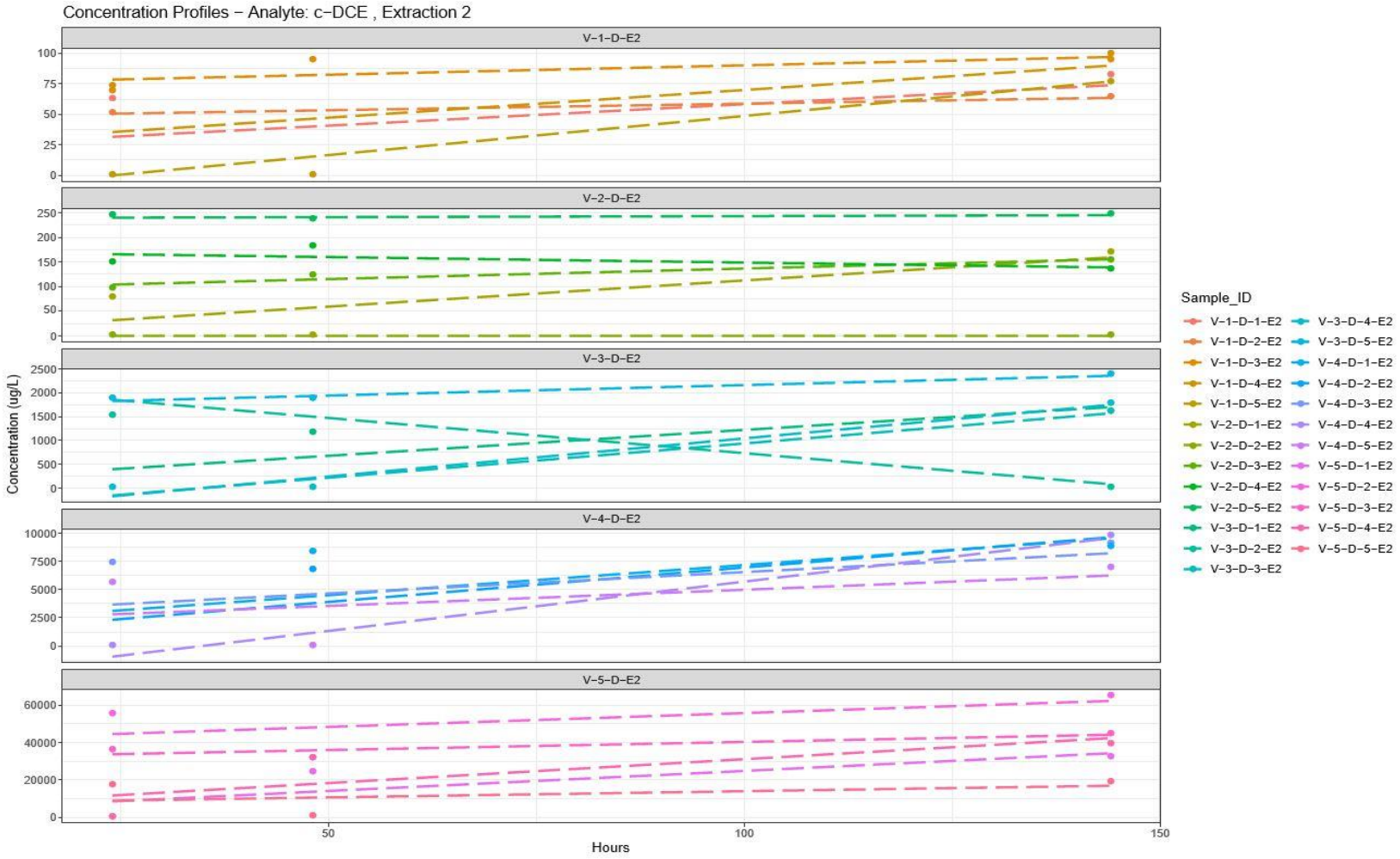
Concentration Profiles – Analyte: c–DCE , Extraction 2
V–1–D–E2
V–2–D–E2
V–3–D–E2
V–4–D–E2
V–5–D–E2
Concentration (ug/L)
Hours
Sample_ID
V–1–D–1–E2
V–1–D–2–E2
V–1–D–3–E2
V–1–D–4–E2
V–1–D–5–E2
V–2–D–1–E2
V–2–D–2–E2
V–2–D–3–E2
V–2–D–4–E2
V–2–D–5–E2
V–3–D–1–E2
V–3–D–2–E2
V–3–D–3–E2
V–3–D–4–E2
V–3–D–5–E2
V–4–D–1–E2
V–4–D–2–E2
V–4–D–3–E2
V–4–D–4–E2
V–4–D–5–E2
V–5–D–1–E2
V–5–D–2–E2
V–5–D–3–E2
V–5–D–4–E2
V–5–D–5–E2

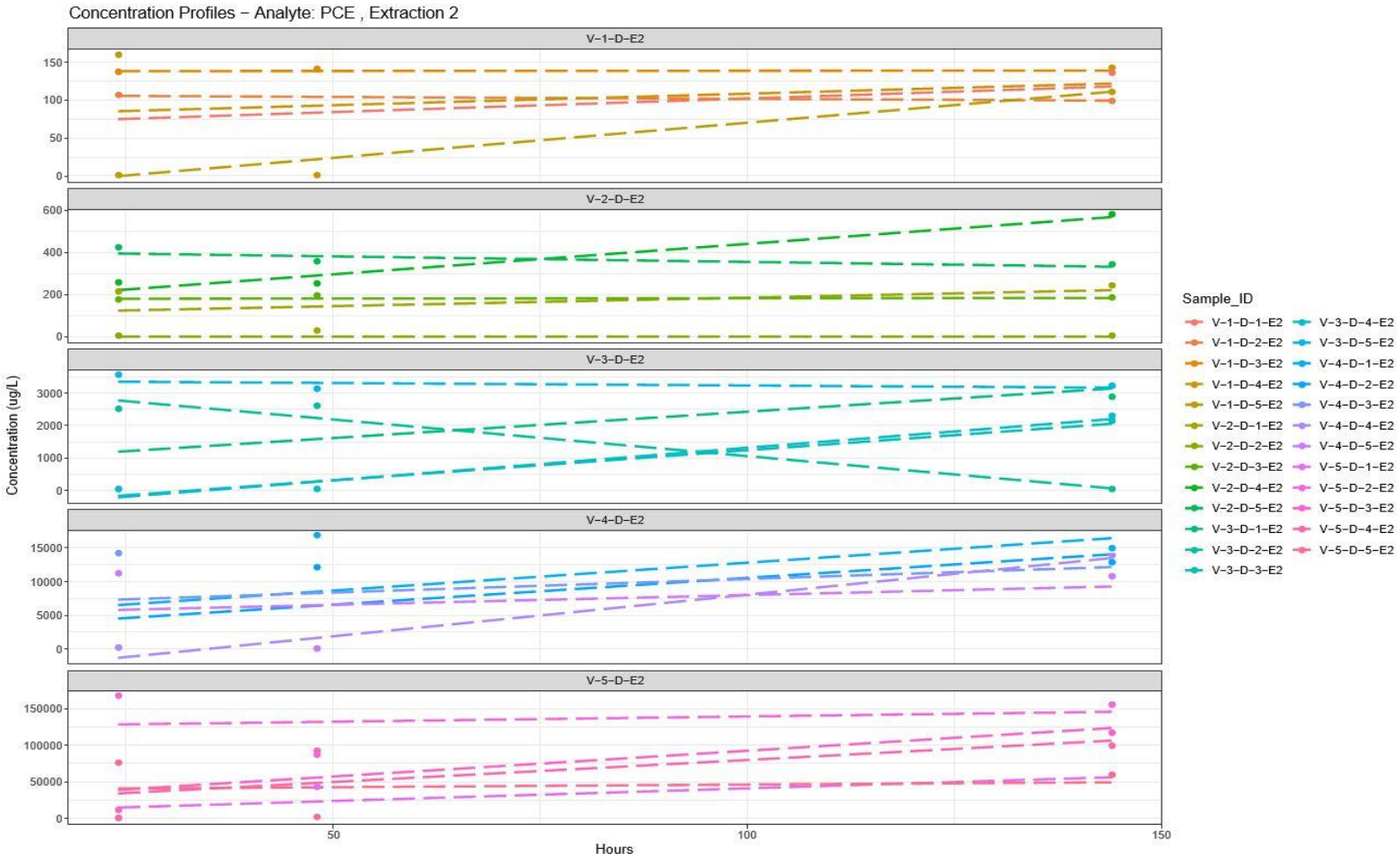
Concentration Profiles – Analyte: PCE , Extraction 2
V–1–D–E2
V–2–D–E2
V–3–D–E2
V–4–D–E2
V–5–D–E2
Concentration (ug/L)
Hours
Sample_ID
V–1–D–1–E2
V–1–D–2–E2
V–1–D–3–E2
V–1–D–4–E2
V–1–D–5–E2
V–2–D–1–E2
V–2–D–2–E2
V–2–D–3–E2
V–2–D–4–E2
V–2–D–5–E2
V–3–D–1–E2
V–3–D–2–E2
V–3–D–3–E2
V–3–D–4–E2
V–3–D–5–E2
V–4–D–1–E2
V–4–D–2–E2
V–4–D–3–E2
V–4–D–4–E2
V–4–D–5–E2
V–5–D–1–E2
V–5–D–2–E2
V–5–D–3–E2
V–5–D–4–E2
V–5–D–5–E2

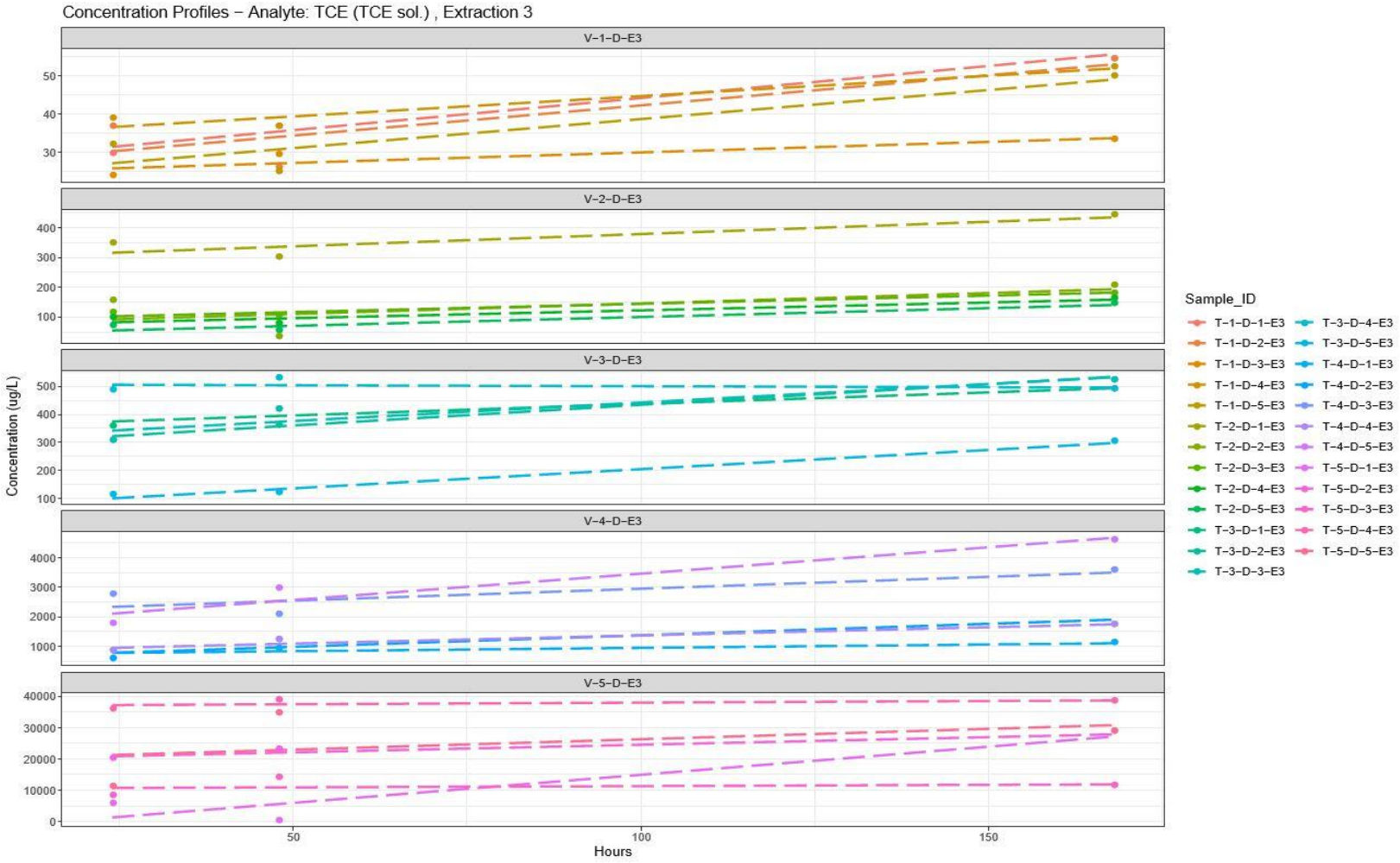
Concentration Profiles − Analyte: TCE (TCE sol.) , Extraction 3
V−1−D−E3
V−2−D−E3
V−3−D−E3
V−4−D−E3
V−5−D−E3
Concentration (ug/L)
Hours
Sample_ID
T−1−D−1−E3
T−1−D−2−E3
T−1−D−3−E3
T−1−D−4−E3
T−1−D−5−E3
T−2−D−1−E3
T−2−D−2−E3
T−2−D−3−E3
T−2−D−4−E3
T−2−D−5−E3
T−3−D−1−E3
T−3−D−2−E3
T−3−D−3−E3
T−3−D−4−E3
T−3−D−5−E3
T−4−D−1−E3
T−4−D−2−E3
T−4−D−3−E3
T−4−D−4−E3
T−4−D−5−E3
T−5−D−1−E3
T−5−D−2−E3
T−5−D−3−E3
T−5−D−4−E3
T−5−D−5−E3

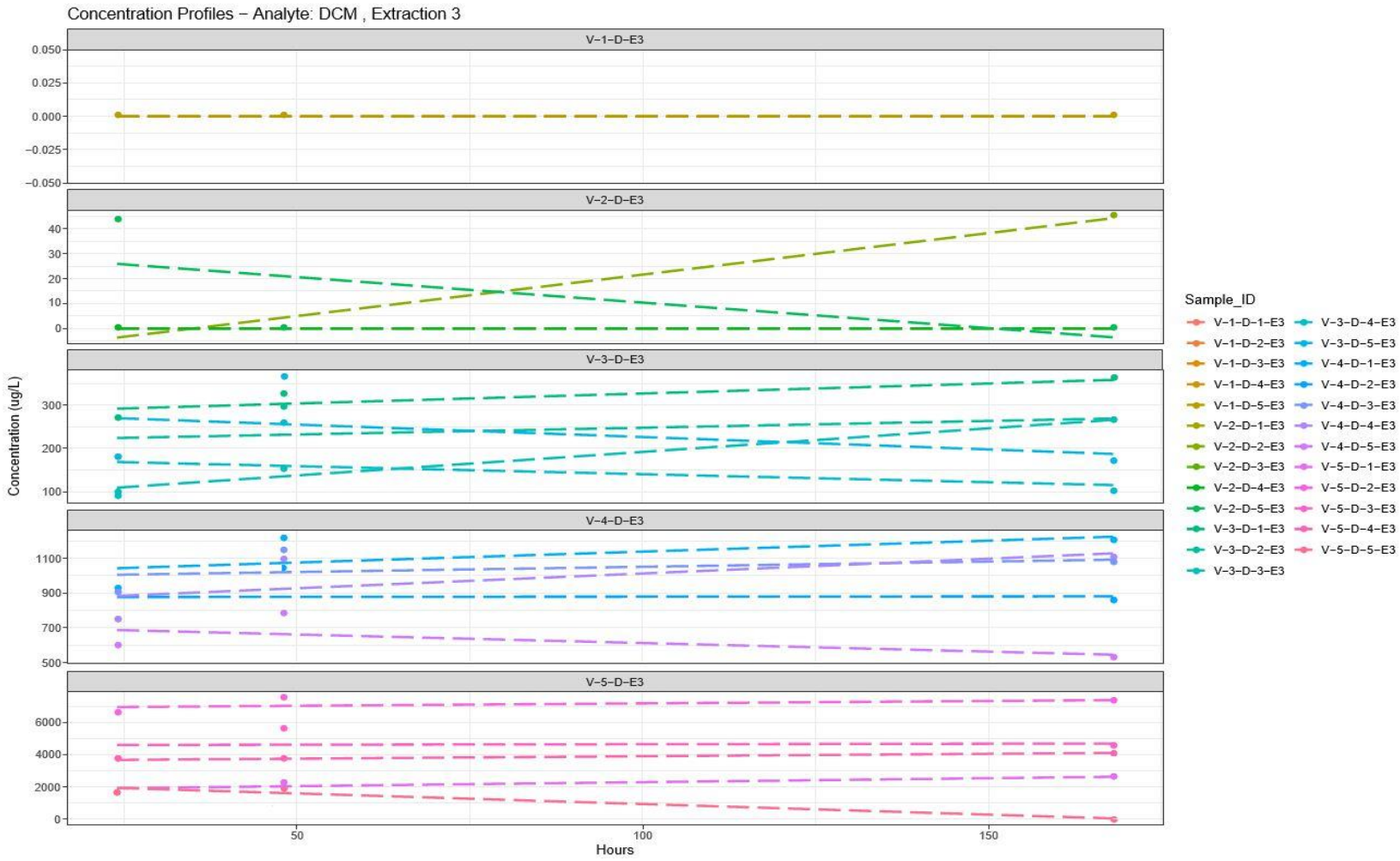
Concentration Profiles – Analyte: DCM , Extraction 3
V–1–D–E3
V–2–D–E3
V–3–D–E3
V–4–D–E3
V–5–D–E3
Concentration (ug/L)
Hours
Sample_ID
V–1–D–1–E3
V–1–D–2–E3
V–1–D–3–E3
V–1–D–4–E3
V–1–D–5–E3
V–2–D–1–E3
V–2–D–2–E3
V–2–D–3–E3
V–2–D–4–E3
V–2–D–5–E3
V–3–D–1–E3
V–3–D–2–E3
V–3–D–3–E3
V–3–D–4–E3
V–3–D–5–E3
V–4–D–1–E3
V–4–D–2–E3
V–4–D–3–E3
V–4–D–4–E3
V–4–D–5–E3
V–5–D–1–E3
V–5–D–2–E3
V–5–D–3–E3
V–5–D–4–E3
V–5–D–5–E3

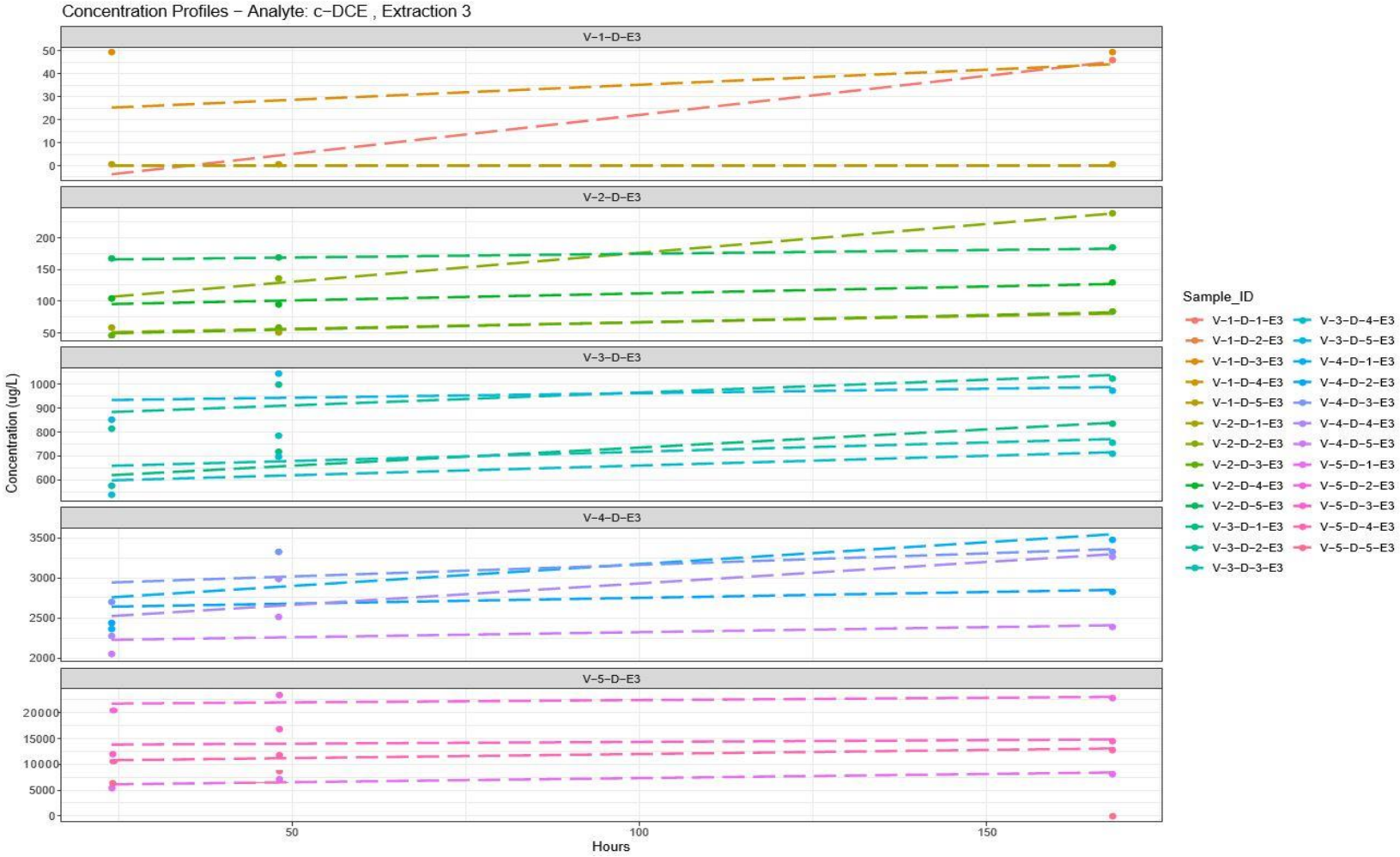
Concentration Profiles – Analyte: c–DCE , Extraction 3
V–1–D–E3
V–2–D–E3
V–3–D–E3
V–4–D–E3
V–5–D–E3
Concentration (ug/L)
Hours
Sample_ID
V–1–D–1–E3
V–1–D–2–E3
V–1–D–3–E3
V–1–D–4–E3
V–1–D–5–E3
V–2–D–1–E3
V–2–D–2–E3
V–2–D–3–E3
V–2–D–4–E3
V–2–D–5–E3
V–3–D–1–E3
V–3–D–2–E3
V–3–D–3–E3
V–3–D–4–E3
V–3–D–5–E3
V–4–D–1–E3
V–4–D–2–E3
V–4–D–3–E3
V–4–D–4–E3
V–4–D–5–E3
V–5–D–1–E3
V–5–D–2–E3
V–5–D–3–E3
V–5–D–4–E3
V–5–D–5–E3

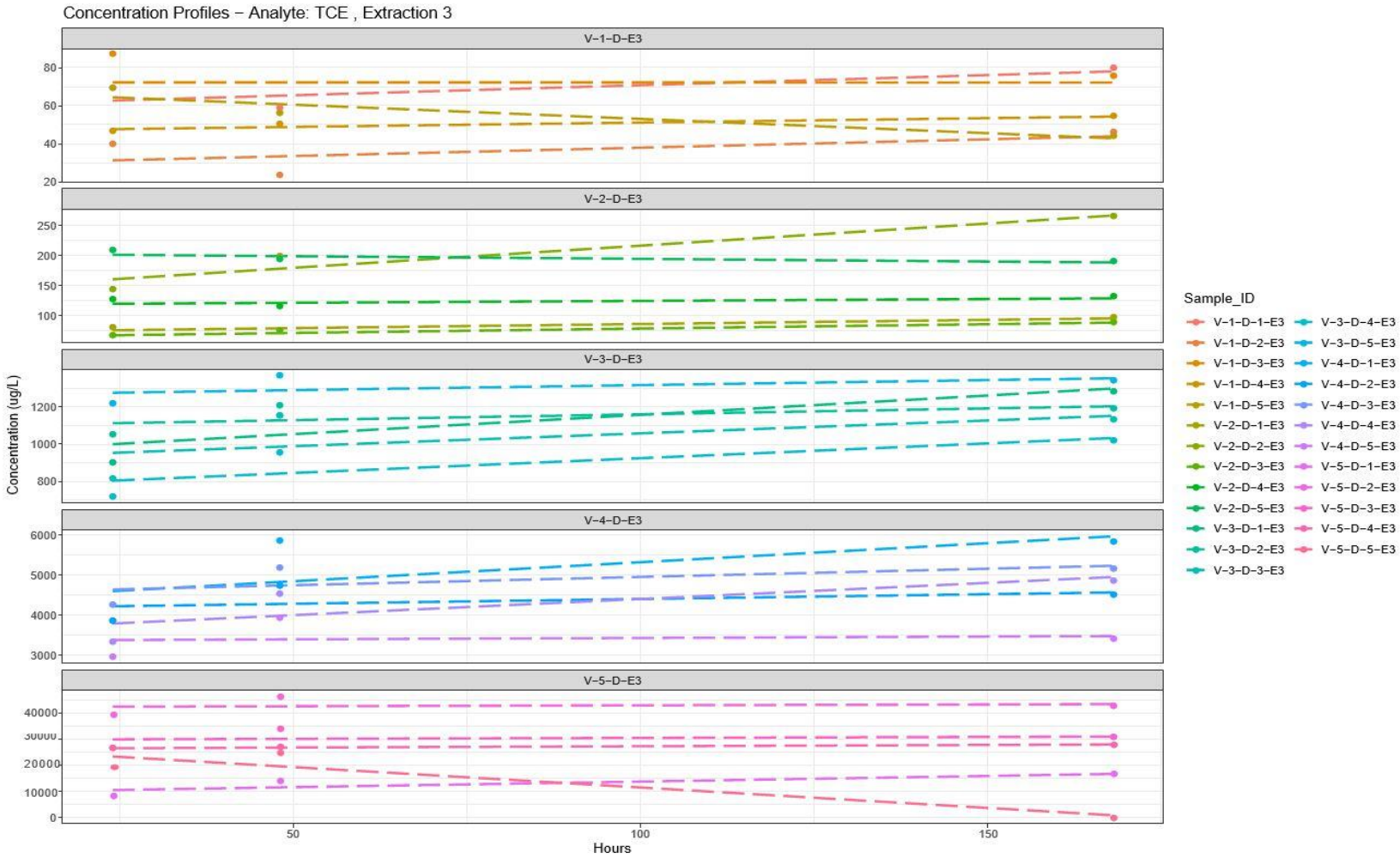
Concentration Profiles – Analyte: TCE , Extraction 3
V–1–D–E3
V–2–D–E3
V–3–D–E3
V–4–D–E3
V–5–D–E3
Concentration (ug/L)
Hours
Sample_ID
V–1–D–1–E3
V–1–D–2–E3
V–1–D–3–E3
V–1–D–4–E3
V–1–D–5–E3
V–2–D–1–E3
V–2–D–2–E3
V–2–D–3–E3
V–2–D–4–E3
V–2–D–5–E3
V–3–D–1–E3
V–3–D–2–E3
V–3–D–3–E3
V–3–D–4–E3
V–3–D–5–E3
V–4–D–1–E3
V–4–D–2–E3
V–4–D–3–E3
V–4–D–4–E3
V–4–D–5–E3
V–5–D–1–E3
V–5–D–2–E3
V–5–D–3–E3
V–5–D–4–E3
V–5–D–5–E3

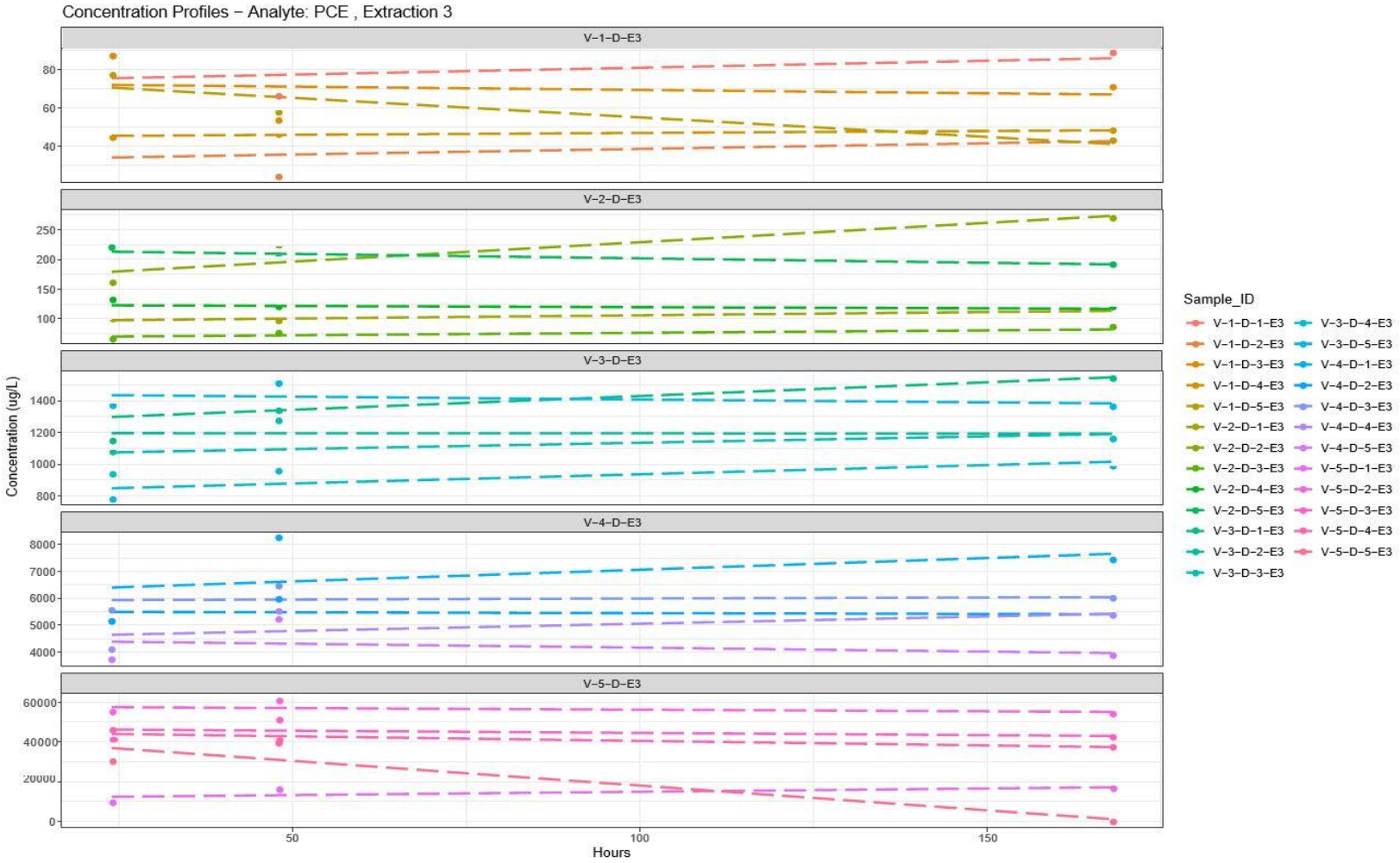
Concentration Profiles − Analyte: PCE , Extraction 3
V−1−D−E3
V−2−D−E3
V−3−D−E3
V−4−D−E3
V−5−D−E3
Concentration (ug/L)
Hours
Sample_ID
V−1−D−1−E3
V−1−D−2−E3
V−1−D−3−E3
V−1−D−4−E3
V−1−D−5−E3
V−2−D−1−E3
V−2−D−2−E3
V−2−D−3−E3
V−2−D−4−E3
V−2−D−5−E3
V−3−D−1−E3
V−3−D−2−E3
V−3−D−3−E3
V−3−D−4−E3
V−3−D−5−E3
V−4−D−1−E3
V−4−D−2−E3
V−4−D−3−E3
V−4−D−4−E3
V−4−D−5−E3
V−5−D−1−E3
V−5−D−2−E3
V−5−D−3−E3
V−5−D−4−E3
V−5−D−5−E3

APPENDIX F: BET SURFACE AREA ANALYSIS REPORTS

Report of Analysis

PTL Project 53054-73

Prepared for: Brent Redmond **P.O.#:** LV1422

Company: MORWICK G[360] GROUNDWATER RESEARCH INSTITUTE **Sample(s) Received:** 2021-10-21

BET SURFACE AREA SUMMARY

SAMPLE(S) SUBMITTED		
FACT 2017	**FACT 2019**	**FACT 2020**
F17-1	F19-1	F20-1
F17-2	F19-2	F20-2
F17-3	F19-3	F20-3
F17-4	F19-4	F20-4
F17-5	F19-5	F20-5

Analytical information, results, and any further commentary are detailed on the following page(s).

Project Director: Arielle Lopez, Particle Characterization Chemist II — 2021-11-10 Date

Technical Review: Cody Langellier, Laboratory Division Manager — 2021-11-10 Date

H:\Reports\53054-73.docx

BET SURFACE AREA SUMMARY

INSTRUMENT	NUMBER OF P/P_0 POINTS	TECHNIQUE
Micromeritics TriStar II 3020	3-Point	Static Pressure Gas Adsorption/Volumetric
REFERENCE(S)		
PTL Test Method: N/A		
Client Method: N/A		

BET SURFACE AREA DATA SUMMARY

SAMPLE ID	SPECIFIC SURFACE AREA (m^2/g)	DEGASSING CONDITIONS			ADSORBATE
		DURATION	TEMPERATURE	TECHNIQUE	
FACT 2017					
F17-1	1550.55	2 Hours	105°C	Vacuum	Nitrogen
F17-2	1441.42				
F17-3	1728.30				
F17-4	1969.45				
F17-5	3545.05				
FACT 2019					
F19-1	5.14	2 Hours	105°C	Vacuum	Nitrogen
F19-2	1.00				
F19-3	2.45				
F19-4	4.60				
F19-5	8.55				
FACT 2020					
F20-1	0.57	1 Hour	105°C	Vacuum	Nitrogen
F20-2	1.96				
F20-3	2.11				
F20-4	0.99				
F20-5	0.89				

Attachment(s):

- An explanation page titled *Interpreting Your BET Specific Surface Area by Gas Physisorption (Static Volumetric Method).*
- Original result page(s).

Comment(s):

Linearity of all collected data points in the relevant pressure range of samples F19-2, F20-1, and F20-3 do not meet the system suitability criteria. Additional samples would be required to improve the quality of the surface area measurement.

Particle Technology Labs

555 Rogers Street, Downers Grove, IL 60515
630-969-2703 ph 630-969-2745 fx
www.particletechlabs.com

THE PARTICLE EXPERTS

INTERPRETING YOUR BET SPECIFIC SURFACE AREA ANALYSIS BY GAS PHYSISORPTION (STATIC VOLUMETRIC METHOD)

INTRODUCTION

The surface area of your sample(s) has been measured via gas physisorption analysis, using the static volumetric method. For a typical multipoint determination, the amount of inert gas that adsorbs to the surface of a sample is measured at varying relative pressures. The surface area is calculated using the Brunauer–Emmett–Teller (BET) equation below:

$$\frac{1}{V_a\left(\left(\frac{P}{P_0}\right)-1\right)} = \frac{C-1}{V_m C} \; x \; \frac{P}{P_0} + \frac{1}{V_m C}$$

where $\frac{P}{P_0}$ = relative pressure,
V_a = volume of gas adsorbed,
V_m = volume of gas adsorbed to produce an apparent monolayer on the surface,
C = BET constant.

For the BET transform, the quantity $\frac{1}{V_a\left(\left(\frac{P}{P_0}\right)-1\right)}$ is plotted against the relative pressure (P/P_0). The BET plot should yield a straight line around the relative pressures where monolayer adsorption occurs, typically in the range of 0.05-0.3. The volume of gas needed to produce a monolayer on the sample surface (V_m) and the BET constant (C) are derived from the slope and y-intercept of the line from the BET plot. The specific surface area is determined using the calculated V_m, the cross sectional area of the adsorbate gas and the mass of the test powder.

The approximate BET surface area can also be determined at one single relative pressure only (commonly at $P/P_0 = 0.3$), either assuming the y-intercept of the BET plot is zero or using certain previously established parameters through multipoint determination for the sample type.

SAMPLE PREPARATION

As the amount of gas adsorbed onto the sample surface is critical to the analysis, moisture and other impurities must be removed from the sample surface prior to analysis. This process, called degassing, may involve pulling vacuum on, flowing inert gas over the sample, or both. Degassing can also be done at different temperatures depending on the thermal stability of the material. It is extremely important to choose a temperature and technique such that the sample is not altered physically or chemically since either could affect the surface area of the sample. The degassing conditions used in your analysis are included on the preliminary results summary page and the final report.

THE DATA

The header section contains various user-entered information specific to each project. It generally includes the client name, sample identification, and analysis notes. Each project is given its own unique seven digit code (PTL Project #) which can be found on these data pages. Please refer to this PTL Project # when contacting us with any questions regarding the analysis.

The data includes a BET tabular report and the BET plot. A table of the relative pressure and quantity of gas adsorbed at that relative pressure is provided in the tabular portion of the data. The last column on the right is the BET transform of the data, which can also be visualized in the BET plot.

Commonly reported values from your surface area data are explained below:

- **BET Specific Surface Area**: the surface area calculated based on the BET model normalized by the sample mass.
- **C Value (also called the BET constant)**: a value related to the affinity of the solid with the adsorbate gas. Since a negative C value has no physical meaning, the C value must be positive. A very low C value indicates the adsorbate gas did not interact well with the surface, suggesting the gas may not have formed a complete monolayer. On the other hand, a high C value may indicate a strong interaction between the surface and adsorbate gas, e.g. chemisorption sites or presence of micropores.
- **Correlation Coefficient**: a value that indicates the linear transform fit of the adsorption data. The BET surface area should only be evaluated over the linear region of the BET plot. At PTL, as per the current USP <846>, the correlation coefficient must be ≥ 0.9975 for data to be considered acceptable.

For additional questions specific to your sample results, please contact us directly.

Particle Technology Labs

MORWICK G360 GROUNDWATER RESEARCH INSTITUTE

Sample: 5305473A2
Operator: AL
Submitter: Particle Technology Labs
File: R:\Tristar II 3020\win3020\data\53054...\5305473A2.SMP

Started: 10/27/2021 9:36:19 AM
Completed: 10/27/2021 1:38:23 PM
Report Time: 11/3/2021 10:48:10 AM
Sample Mass: 0.1742 g
Cold Free Space: 72.5508 cm³
Low Pressure Dose: None
Automatic Degas: No

Analysis Adsorptive: N2
Analysis Bath Temp.: 77.350 K
Thermal Correction: No
Warm Free Space: 22.8511 cm³ Measured
Equilibration Interval: 20 s
Sample Density: 1.000 g/cm³

Comments: FACT 2017 F17-1 Project #53054-73 PTL ID: 492666-73

BET Report

BET Surface Area: 1550.5512 ± 3.1229 m²/g
Slope: 0.002803 ± 0.000006 g/cm³ STP
Y-Intercept: 0.000004 ± 0.000000 g/cm³ STP
C: 696.061895
Qm: 356.2374 cm³/g STP
Correlation Coefficient: 0.9999980
Molecular Cross-Sectional Area: 0.1620 nm²

Relative Pressure (P/Po)	Quantity Adsorbed (cm³/g STP)	1/[Q(Po/P - 1)]
0.012096406	322.2625	0.000038
0.048277020	364.4521	0.000139
0.065263793	373.1909	0.000187

R 2021-11-03

Particle Technology Labs

MORWICK G360 GROUNDWATER RESEARCH INSTITUTE

Sample: 5305473A2
Operator: AL
Submitter: Particle Technology Labs
File: R:\Tristar II 3020\win3020\data\53054...\5305473A2.SMP

Started:	10/27/2021 9:36:19 AM	Analysis Adsorptive:	N2
Completed:	10/27/2021 1:38:23 PM	Analysis Bath Temp.:	77.350 K
Report Time:	11/3/2021 10:48:10 AM	Thermal Correction:	No
Sample Mass:	0.1742 g	Warm Free Space:	22.8511 cm³ Measured
Cold Free Space:	72.5508 cm³	Equilibration Interval:	20 s
Low Pressure Dose:	None	Sample Density:	1.000 g/cm³
Automatic Degas:	No		

Comments: FACT 2017 F17-1 Project #53054-73 PTL ID: 492666-73

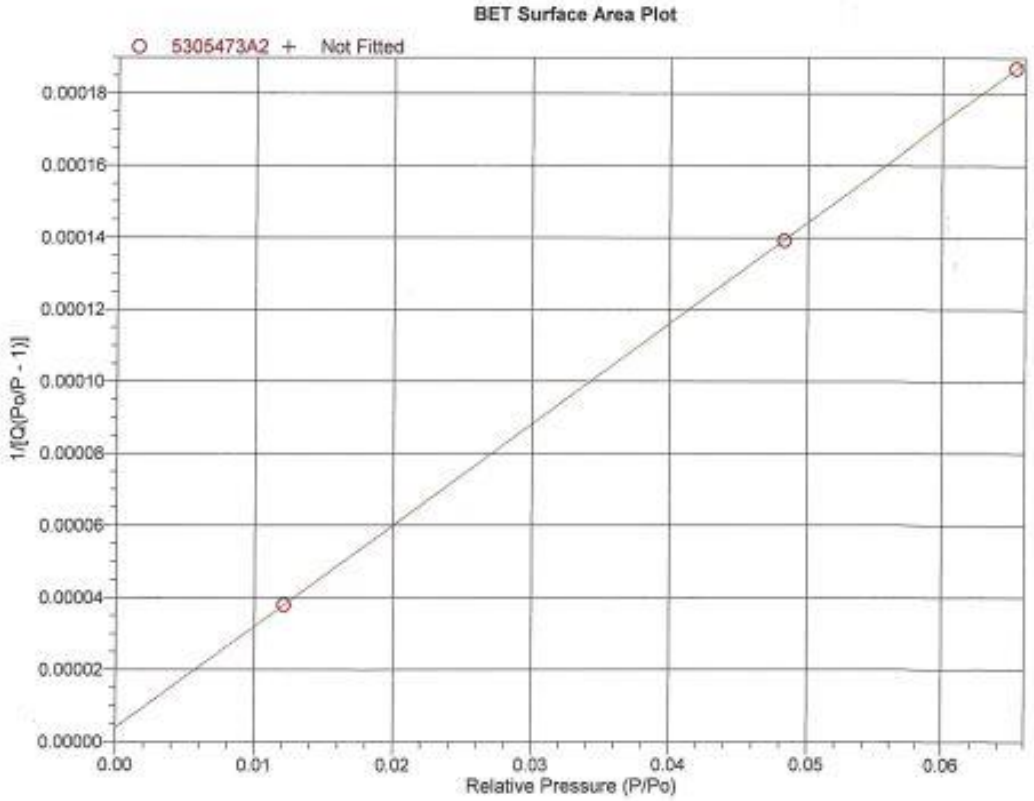

Particle Technology Labs

MORWICK G360 GROUNDWATER RESEARCH INSTITUTE

Sample: 5305473B
Operator: AL
Submitter: Particle Technology Labs
File: R:\Tristar II 3020\win3020\data\53054-73\5305473B.SMP

Started: 10/27/2021 1:56:20 PM
Completed: 10/27/2021 4:23:08 PM
Report Time: 11/3/2021 9:50:37 AM
Sample Mass: 0.1123 g
Cold Free Space: 71.0324 cm³
Low Pressure Dose: None
Automatic Degas: No

Analysis Adsorptive: N2
Analysis Bath Temp.: 77.350 K
Thermal Correction: No
Warm Free Space: 22.2680 cm³ Measured
Equilibration Interval: 20 s
Sample Density: 1.000 g/cm³

Comments: FACT 2017 F17-2 Project #53054-73 PTL ID: 492667-73

BET Report

BET Surface Area: 1441.4247 ± 1.3166 m²/g
Slope: 0.003015 ± 0.000003 g/cm³ STP
Y-Intercept: 0.000004 ± 0.000000 g/cm³ STP
C: 674.586533
Qm: 331.1657 cm³/g STP
Correlation Coefficient: 0.9999996
Molecular Cross-Sectional Area: 0.1620 nm²

Relative Pressure (P/Po)	Quantity Adsorbed (cm³/g STP)	1/[Q(Po/P - 1)]
0.012083540	299.2685	0.000041
0.035893855	330.1158	0.000113
0.060594946	344.6772	0.000187

AL 2021-11-05
CGL 2021-11-05

Particle Technology Labs

MORWICK G360 GROUNDWATER RESEARCH INSTITUTE

Sample: 5305473B
Operator: AL
Submitter: Particle Technology Labs
File: R:\Tristar II 3020\win3020\data\53054-73\5305473B.SMP

Started:	10/27/2021 1:56:20 PM	Analysis Adsorptive:	N2
Completed:	10/27/2021 4:23:08 PM	Analysis Bath Temp.:	77.350 K
Report Time:	11/3/2021 9:50:37 AM	Thermal Correction:	No
Sample Mass:	0.1123 g	Warm Free Space:	22.2880 cm³ Measured
Cold Free Space:	71.0324 cm³	Equilibration Interval:	20 s
Low Pressure Dose:	None	Sample Density:	1.000 g/cm³
Automatic Degas:	No		

Comments: FACT 2017 F17-2 Project #53054-73 PTL ID: 492667-73

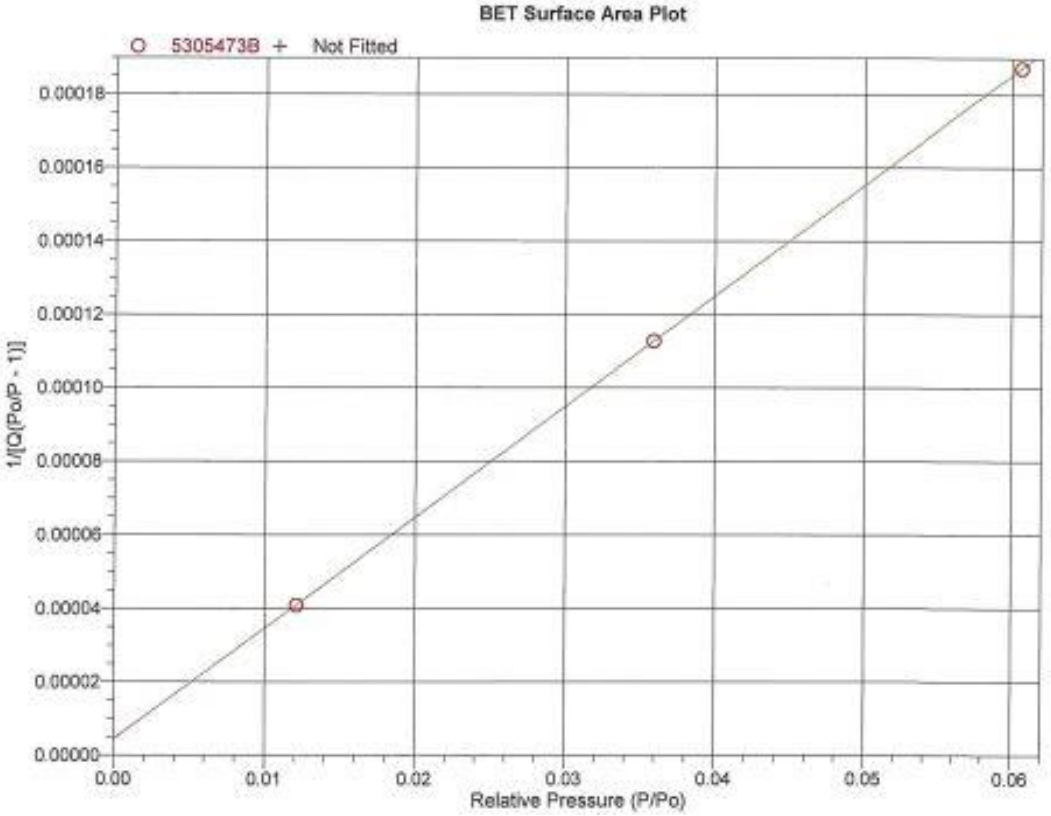

Particle Technology Labs

MORWICK G360 GROUNDWATER RESEARCH INSTITUTE

Sample: 5305473C
Operator: AL
Submitter: Particle Technology Labs
File: R:\Tristar II 3020\win3020\data\53054-73\5305473C.SMP

Started: 10/27/2021 1:56:20 PM
Completed: 10/27/2021 4:23:08 PM
Report Time: 11/3/2021 9:50:49 AM
Sample Mass: 0.0882 g
Cold Free Space: 72.2838 cm³
Low Pressure Dose: None
Automatic Degas: No

Analysis Adsorptive: N2
Analysis Bath Temp.: 77.350 K
Thermal Correction: No
Warm Free Space: 22.4499 cm³ Measured
Equilibration Interval: 20 s
Sample Density: 1.000 g/cm³

Comments: FACT 2017 F17-3 Project #53054-73 PTL ID: 492668-73

BET Report

BET Surface Area: 1728.3028 ± 1.5276 m²/g
Slope: 0.002515 ± 0.000002 g/cm³ STP
Y-Intercept: 0.000004 ± 0.000000 g/cm³ STP
C: 665.355746
Qm: 397.0756 cm³/g STP
Correlation Coefficient: 0.9999996
Molecular Cross-Sectional Area: 0.1620 nm²

Relative Pressure (P/Po)	Quantity Adsorbed (cm³/g STP)	1/[Q(Po/P - 1)]
0.012201402	358.6996	0.000034
0.036295107	395.9598	0.000095
0.060605141	413.1519	0.000156

AL 2021-11-05
CR 2021-11-08

Particle Technology Labs

MORWICK G360 GROUNDWATER RESEARCH INSTITUTE

Sample: 5305473C
Operator: AL
Submitter: Particle Technology Labs
File: R:\Tristar II 3020\win3020\data\53054-73\5305473C.SMP

Started:	10/27/2021 1:56:20 PM	Analysis Adsorptive:	N2
Completed:	10/27/2021 4:23:08 PM	Analysis Bath Temp.:	77.350 K
Report Time:	11/3/2021 9:50:49 AM	Thermal Correction:	No
Sample Mass:	0.0882 g	Warm Free Space:	22.4499 cm³ Measured
Cold Free Space:	72.2838 cm³	Equilibration Interval:	20 s
Low Pressure Dose:	None	Sample Density:	1.000 g/cm³
Automatic Degas:	No		

Comments: FACT 2017 F17-3 Project #53054-73 PTL ID: 492668-73

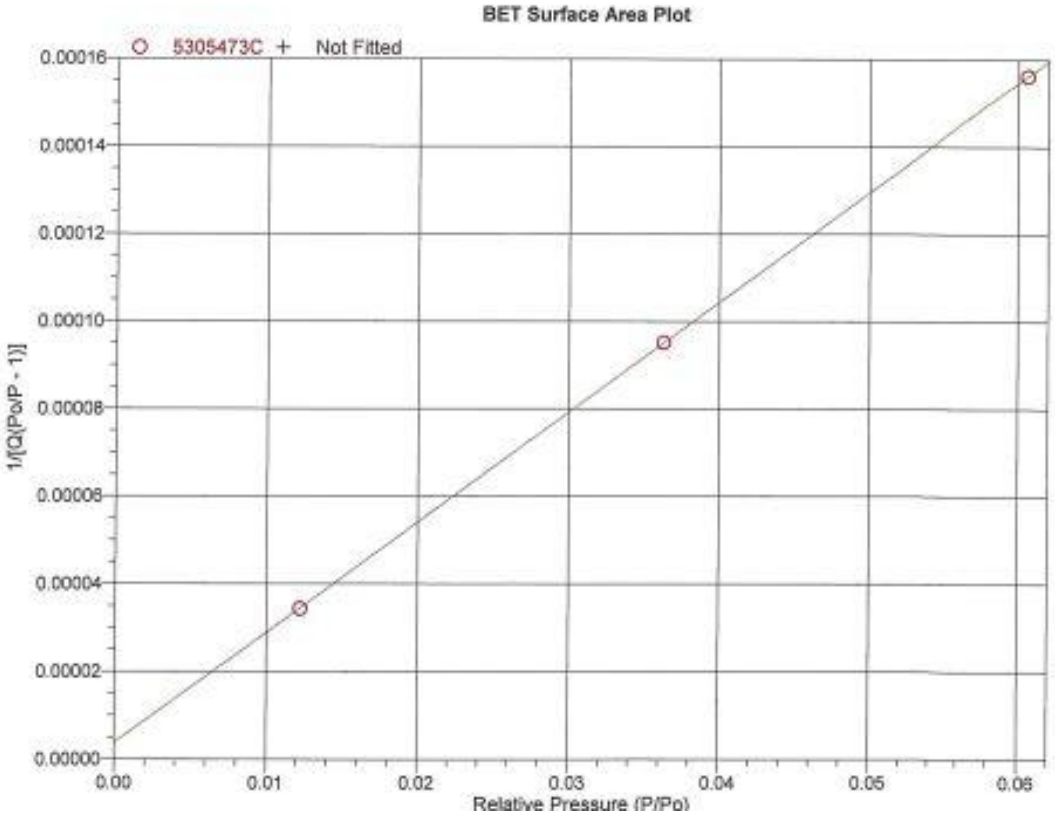

Particle Technology Labs

MORWICK G360 GROUNDWATER RESEARCH INSTITUTE

Sample: 5305473D
Operator: AL
Submitter: Particle Technology Labs
File: R:\Tristar II 3020\win3020\data\53054-73\5305473D.SMP

Started:	10/27/2021 5:02:29 PM	Analysis Adsorptive:	N2
Completed:	10/27/2021 7:44:51 PM	Analysis Bath Temp.:	77.350 K
Report Time:	11/3/2021 9:51:02 AM	Thermal Correction:	No
Sample Mass:	0.0810 g	Warm Free Space:	23.2173 cm³ Measured
Cold Free Space:	73.4388 cm³	Equilibration Interval:	20 s
Low Pressure Dose:	None	Sample Density:	1.000 g/cm³
Automatic Degas:	No		

Comments: FACT 2017 F17-4 Project #53054-73 PTL ID: 492669-73

BET Report

BET Surface Area: 1969.4462 ± 1.9053 m²/g
Slope: 0.002207 ± 0.000002 g/cm³ STP
Y-Intercept: 0.000003 ± 0.000000 g/cm³ STP
C: 669.074924
Qm: 452.4781 cm³/g STP
Correlation Coefficient: 0.9999995
Molecular Cross-Sectional Area: 0.1620 nm²

Relative Pressure (P/Po)	Quantity Adsorbed (cm³/g STP)	1/[Q(Po/P - 1)]
0.011901955	407.8002	0.000030
0.036140174	451.1208	0.000083
0.060840936	471.0283	0.000138

M 2021-11-03
COL 2021-11-03

Particle Technology Labs

MORWICK G360 GROUNDWATER RESEARCH INSTITUTE

Sample: 5305473D
Operator: AL
Submitter: Particle Technology Labs
File: R:\Tristar II 3020\win3020\data\53054-73\5305473D.SMP

Started: 10/27/2021 5:02:29 PM
Completed: 10/27/2021 7:44:51 PM
Report Time: 11/3/2021 9:51:02 AM
Sample Mass: 0.0810 g
Cold Free Space: 73.4388 cm³
Low Pressure Dose: None
Automatic Degas: No

Analysis Adsorptive: N2
Analysis Bath Temp.: 77.350 K
Thermal Correction: No
Warm Free Space: 23.2173 cm³ Measured
Equilibration Interval: 20 s
Sample Density: 1.000 g/cm³

Comments: FACT 2017 F17-4 Project #53054-73 PTL ID: 492669-73

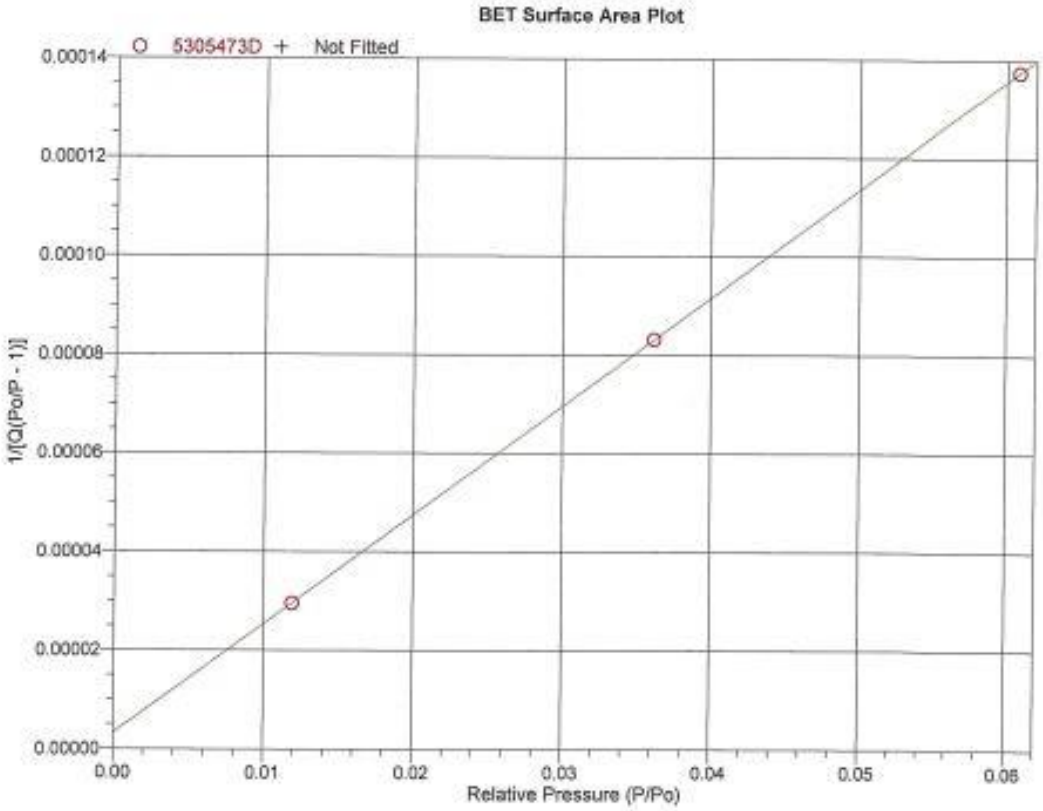

Particle Technology Labs

MORWICK G360 GROUNDWATER RESEARCH INSTITUTE

Sample: 5305473E
Operator: AL
Submitter: Particle Technology Labs
File: R:\Tristar II 3020\win3020\data\53054-73\5305473E.SMP

Started: 10/27/2021 5:02:29 PM
Completed: 10/27/2021 7:44:51 PM
Report Time: 11/3/2021 9:51:12 AM
Sample Mass: 0.0435 g
Cold Free Space: 71.1582 cm³
Low Pressure Dose: None
Automatic Degas: No

Analysis Adsorptive: N2
Analysis Bath Temp.: 77.350 K
Thermal Correction: No
Warm Free Space: 22.5363 cm³ Measured
Equilibration Interval: 20 s
Sample Density: 1.000 g/cm³

Comments: FACT 2017 F17-5 Project #53054-73 PTL ID: 492670-73

BET Report

BET Surface Area: 3645.0532 ± 4.4071 m²/g
Slope: 0.001192 ± 0.000001 g/cm³ STP
Y-Intercept: 0.000002 ± 0.000000 g/cm³ STP
C: 644.101602
Qm: 837.4469 cm³/g STP
Correlation Coefficient: 0.9999993
Molecular Cross-Sectional Area: 0.1620 nm²

Relative Pressure (P/Po)	Quantity Adsorbed (cm³/g STP)	1/[Q(Po/P - 1)]
0.012365680	755.3440	0.000017
0.035842708	833.0009	0.000045
0.081075330	871.3576	0.000075

2021-11-03
COL 2021-11-03

Particle Technology Labs

MORWICK G360 GROUNDWATER RESEARCH INSTITUTE

Sample: 5305473E
Operator: AL
Submitter: Particle Technology Labs
File: R:\Tristar II 3020\win3020\data\53054-73\5305473E.SMP

Started:	10/27/2021 5:02:29 PM	Analysis Adsorptive:	N2
Completed:	10/27/2021 7:44:51 PM	Analysis Bath Temp.:	77.350 K
Report Time:	11/3/2021 9:51:12 AM	Thermal Correction:	No
Sample Mass:	0.0435 g	Warm Free Space:	22.5363 cm³ Measured
Cold Free Space:	71.1562 cm³	Equilibration Interval:	20 s
Low Pressure Dose:	None	Sample Density:	1.000 g/cm³
Automatic Degas:	No		

Comments: FACT 2017 F17-5 Project #53054-73 PTL ID: 492670-73

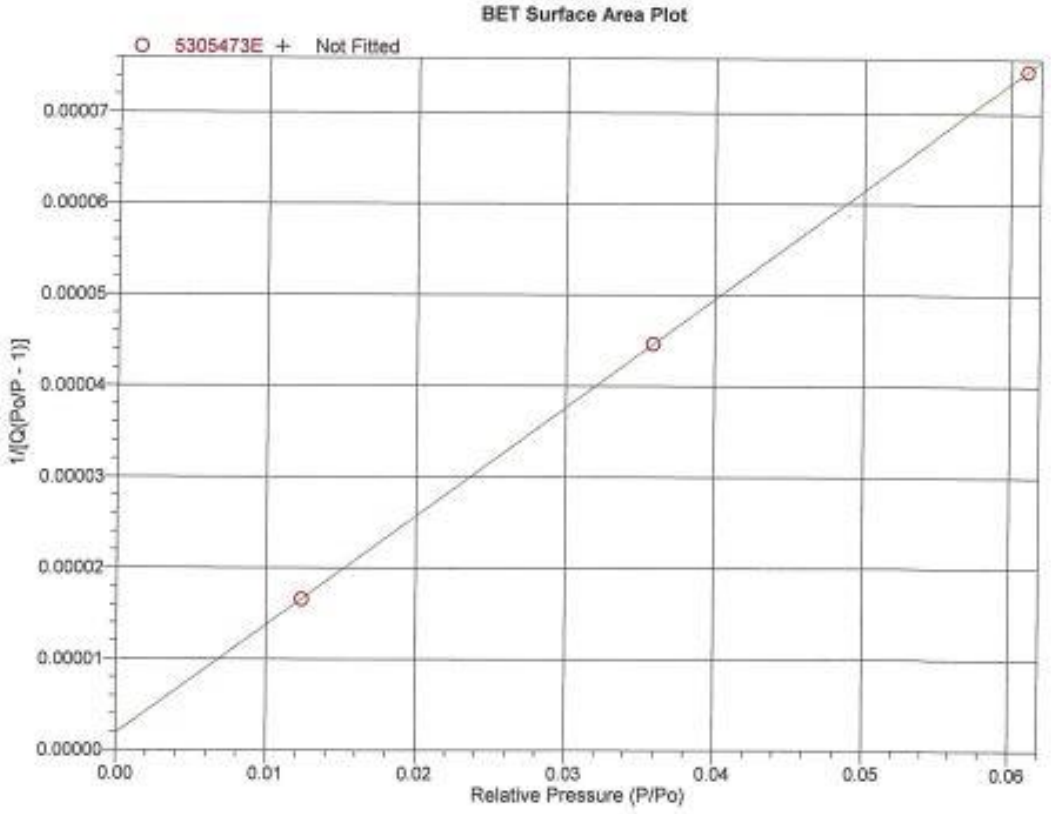

Particle Technology Labs

MORWICK G360 GROUNDWATER RESEARCH INSTITUTE

Sample: 5305473F
Operator: AL
Submitter: Particle Technology Labs
File: R:\Tristar II 3020\win3020\data\53054-73\5305473F.SMP

Started: 10/28/2021 12:55:19 PM
Completed: 10/28/2021 2:17:00 PM
Report Time: 11/3/2021 10:01:03 AM
Sample Mass: 0.1800 g
Cold Free Space: 65.9708 cm³
Low Pressure Dose: None
Automatic Degas: No

Analysis Adsorptive: N2
Analysis Bath Temp.: 77.350 K
Thermal Correction: No
Warm Free Space: 21.2949 cm³ Measured
Equilibration Interval: 20 s
Sample Density: 1.000 g/cm³

Comments: FACT 2019 F19-1 Project #53054-73 PTL ID: 492671-73

BET Report

BET Surface Area: 5.1423 ± 0.0195 m²/g
Slope: 0.841830 ± 0.003201 g/cm³ STP
Y-Intercept: 0.004591 ± 0.000208 g/cm³ STP
C: 184.372877
Qm: 1.1814 cm³/g STP
Correlation Coefficient: 0.9999928
Molecular Cross-Sectional Area: 0.1620 nm²

Relative Pressure (P/Po)	Quantity Adsorbed (cm³/g STP)	1/[Q(Po/P - 1)]
0.011900169	0.8297	0.014516
0.049908929	1.1232	0.046768
0.099940345	1.2525	0.088653

M 2021-11-03
CGL 2021-11-03

Particle Technology Labs

MORWICK G360 GROUNDWATER RESEARCH INSTITUTE

Sample: 5305473F
Operator: AL
Submitter: Particle Technology Labs
File: R:\Tristar II 3020\win3020\data\53054-73\5305473F.SMP

Started: 10/28/2021 12:55:19 PM
Completed: 10/28/2021 2:17:00 PM
Report Time: 11/3/2021 10:01:03 AM
Sample Mass: 0.1800 g
Cold Free Space: 55.9708 cm³
Low Pressure Dose: None
Automatic Degas: No

Analysis Adsorptive: N2
Analysis Bath Temp.: 77.350 K
Thermal Correction: No
Warm Free Space: 21.2949 cm³ Measured
Equilibration Interval: 20 s
Sample Density: 1.000 g/cm³

Comments: FACT 2019 F19-1 Project #53054-73 PTL ID: 492671-73

BET Surface Area Plot

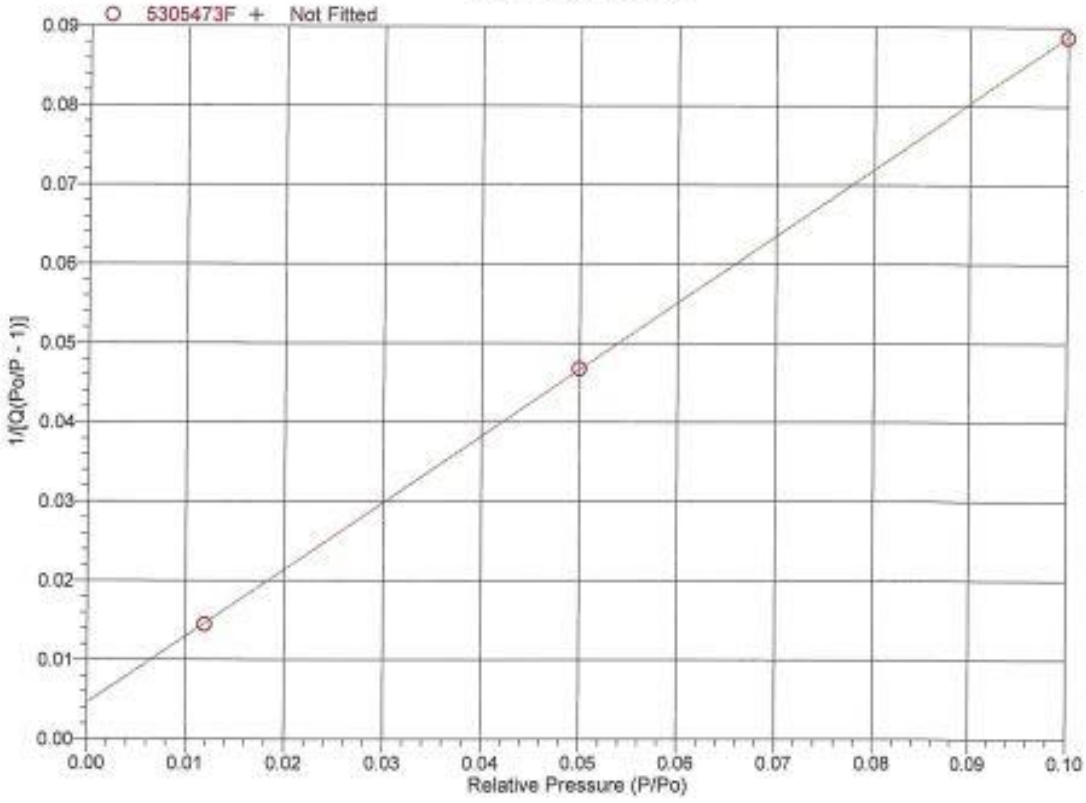

Particle Technology Labs

MORWICK G360 GROUNDWATER RESEARCH INSTITUTE

Sample: 5305473G
Operator: AL
Submitter: Particle Technology Labs
File: R:\Tristar II 3020\win3020\data\53054-73\5305473G.SMP

Started: 10/28/2021 12:55:19 PM
Completed: 10/28/2021 2:17:00 PM
Report Time: 11/3/2021 10:01:43 AM
Sample Mass: 0.2067 g
Cold Free Space: 67.5184 cm³
Low Pressure Dose: None
Automatic Degas: No

Analysis Adsorptive: N2
Analysis Bath Temp.: 77.350 K
Thermal Correction: No
Warm Free Space: 21.6576 cm³ Measured
Equilibration Interval: 20 s
Sample Density: 1.000 g/cm³

Comments: FACT 2019 F19-2 Project #53054-73 PTL ID: 492672-73

BET Report

BET Surface Area: 0.9964 ± 0.0323 m²/g
Slope: 4.351026 ± 0.141616 g/cm³ STP
Y-Intercept: 0.017418 ± 0.004375 g/cm³ STP
C: 250.802326
Qm: 0.2289 cm³/g STP
Correlation Coefficient: 0.9994707
Molecular Cross-Sectional Area: 0.1620 nm²

Relative Pressure (P/Po)	Quantity Adsorbed (cm³/g STP)	1/[Q(Po/P - 1)]
0.013732895	0.1832	0.075997
0.028684928	0.2042	0.144623
0.043035401	0.2210	0.203444

M 2021-11-03
CR 2021-11-03

Particle Technology Labs

MORWICK G360 GROUNDWATER RESEARCH INSTITUTE

Sample: 5305473G
Operator: AL
Submitter: Particle Technology Labs
File: R:\Tristar II 3020\win3020\data\53054-73\5305473G.SMP

Started:	10/28/2021 12:55:19 PM	Analysis Adsorptive:	N2
Completed:	10/28/2021 2:17:00 PM	Analysis Bath Temp.:	77.350 K
Report Time:	11/3/2021 10:01:43 AM	Thermal Correction:	No
Sample Mass:	0.2067 g	Warm Free Space:	21.6576 cm³ Measured
Cold Free Space:	67.5184 cm³	Equilibration Interval:	20 s
Low Pressure Dose:	None	Sample Density:	1.000 g/cm³
Automatic Degas:	No		

Comments: FACT 2019 F19-2 Project #53054-73 PTL ID: 492672-73

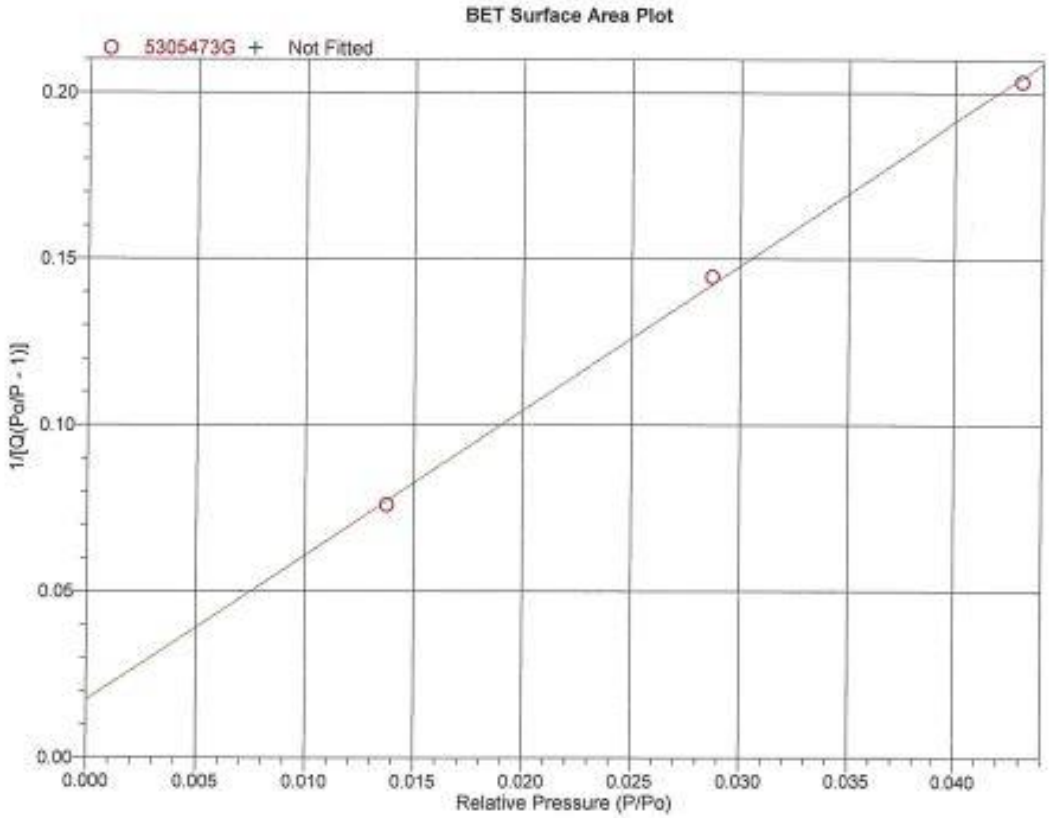

Particle Technology Labs

MORWICK G360 GROUNDWATER RESEARCH INSTITUTE

Sample: 5305473H
Operator: AL
Submitter: Particle Technology Labs
File: R:\Tristar II 3020\win3020\data\53054-73\5305473H.SMP

Started: 10/28/2021 3:50:04 PM
Completed: 10/28/2021 5:09:00 PM
Report Time: 11/3/2021 10:02:03 AM
Sample Mass: 0.1934 g
Cold Free Space: 71.2358 cm³
Low Pressure Dose: None
Automatic Degas: No

Analysis Adsorptive: N2
Analysis Bath Temp.: 77.350 K
Thermal Correction: No
Warm Free Space: 22.3824 cm³ Measured
Equilibration Interval: 20 s
Sample Density: 1.000 g/cm³

Comments: FACT 2019 F19-3 Project #53054-73 PTL ID: 492673-73

BET Report

BET Surface Area: 2.4532 ± 0.0018 m²/g
Slope: 1.764062 ± 0.001330 g/cm³ STP
Y-Intercept: 0.010150 ± 0.000086 g/cm³ STP
C: 174.796556
Qm: 0.5636 cm³/g STP
Correlation Coefficient: 0.9999997
Molecular Cross-Sectional Area: 0.1620 nm²

Relative Pressure (P/Po)	Quantity Adsorbed (cm³/g STP)	1/[Q(Po/P - 1)]
0.013189300	0.3995	0.033455
0.049913391	0.5353	0.098134
0.099843090	0.5953	0.186308

AL 2021-11-03
LA 2021-11-03

Particle Technology Labs

MORWICK G360 GROUNDWATER RESEARCH INSTITUTE

Sample: 5305473H
Operator: AL
Submitter: Particle Technology Labs
File: R:\Tristar II 3020\win3020\data\53054-73\5305473H.SMP

Started:	10/28/2021 3:50:04 PM	Analysis Adsorptive:	N2
Completed:	10/28/2021 5:09:00 PM	Analysis Bath Temp.:	77.350 K
Report Time:	11/3/2021 10:02:03 AM	Thermal Correction:	No
Sample Mass:	0.1934 g	Warm Free Space:	22.3824 cm³ Measured
Cold Free Space:	71.2358 cm³	Equilibration Interval:	20 s
Low Pressure Dose:	None	Sample Density:	1.000 g/cm³
Automatic Degas:	No		

Comments: FACT 2019 F19-3 Project #53054-73 PTL ID: 492673-73

BET Surface Area Plot

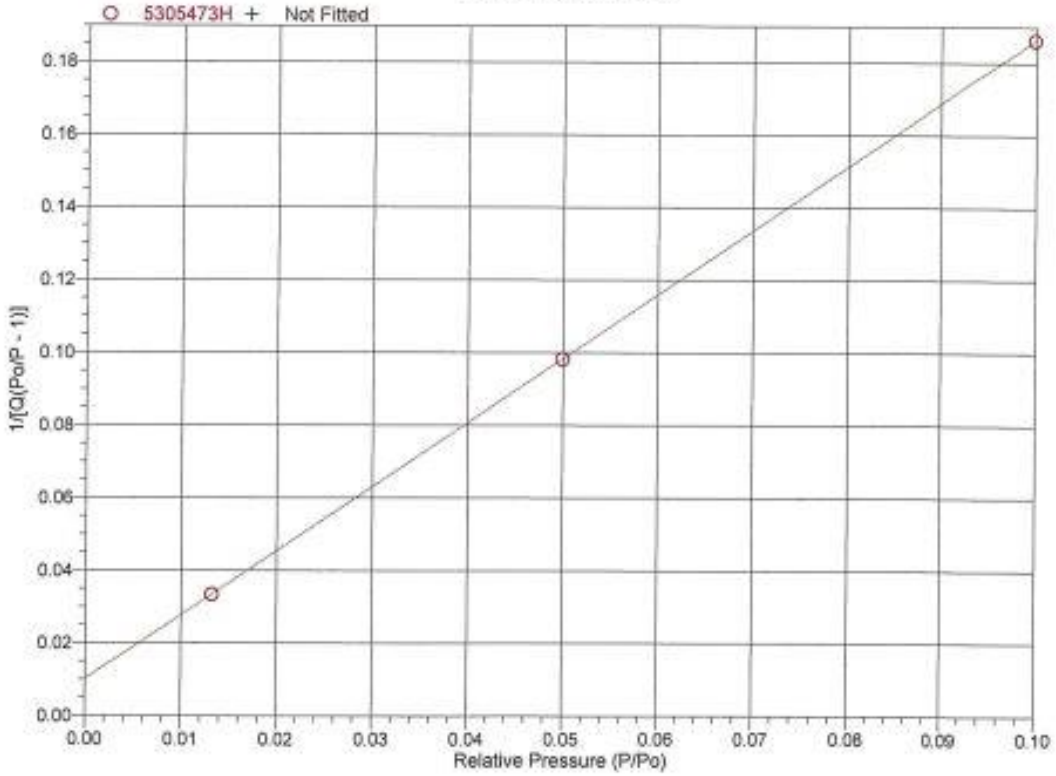

Particle Technology Labs

MORWICK G360 GROUNDWATER RESEARCH INSTITUTE

Sample: 5305473I
Operator: AL
Submitter: Particle Technology Labs
File: R:\Tristar II 3020\win3020\data\53054-73\5305473I.SMP

Started: 10/28/2021 3:50:05 PM
Completed: 10/28/2021 5:09:00 PM
Report Time: 11/3/2021 10:02:18 AM
Sample Mass: 0.1820 g
Cold Free Space: 71.4610 cm³
Low Pressure Dose: None
Automatic Degas: No

Analysis Adsorptive: N2
Analysis Bath Temp.: 77.350 K
Thermal Correction: No
Warm Free Space: 22.3760 cm³ Measured
Equilibration Interval: 20 s
Sample Density: 1.000 g/cm³

Comments: FACT 2019 F19-4 Project #53054-73 PTL ID: 492674-73

BET Report

BET Surface Area: 4.6042 ± 0.1681 m²/g
Slope: 0.936627 ± 0.034437 g/cm³ STP
Y-Intercept: 0.008724 ± 0.002235 g/cm³ STP
C: 108.356425
Qm: 1.0578 cm³/g STP
Correlation Coefficient: 0.9993248
Molecular Cross-Sectional Area: 0.1620 nm²

Relative Pressure (P/Po)	Quantity Adsorbed (cm³/g STP)	1/[Q(Po/P - 1)]
0.012712170	0.6556	0.019640
0.049996634	0.9187	0.057285
0.099851298	1.0928	0.101507

2021-11-03
2021-11-03

Particle Technology Labs

MORWICK G360 GROUNDWATER RESEARCH INSTITUTE

Sample: 5305473I
Operator: AL
Submitter: Particle Technology Labs
File: R:\Tristar II 3020\win3020\data\53054-73\5305473I.SMP

Started:	10/28/2021 3:50:05 PM	Analysis Adsorptive:	N2
Completed:	10/28/2021 5:09:00 PM	Analysis Bath Temp.:	77.350 K
Report Time:	11/3/2021 10:02:18 AM	Thermal Correction:	No
Sample Mass:	0.1820 g	Warm Free Space:	22.3760 cm³ Measured
Cold Free Space:	71.4610 cm³	Equilibration Interval:	20 s
Low Pressure Dose:	None	Sample Density:	1.000 g/cm³
Automatic Degas:	No		

Comments: FACT 2019 F19-4 Project #53054-73 PTL ID: 492674-73

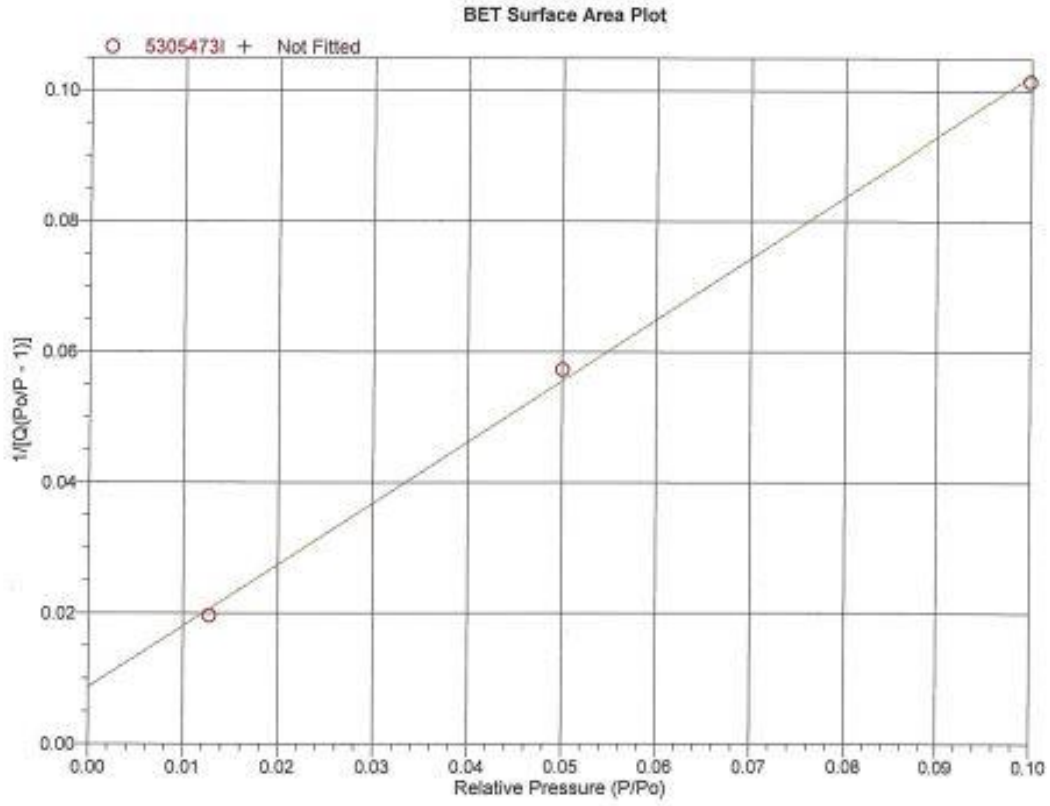

Particle Technology Labs

MORWICK G360 GROUNDWATER RESEARCH INSTITUTE

Sample: 5305473J
Operator: AL
Submitter: Particle Technology Labs
File: R:\Tristar II 3020\win3020\data\53054-73\5305473J.SMP

Started: 10/29/2021 3:23:40 PM
Completed: 10/29/2021 4:44:09 PM
Report Time: 11/3/2021 10:02:38 AM
Sample Mass: 0.1645 g
Cold Free Space: 70.8855 cm³
Low Pressure Dose: None
Automatic Degas: No

Analysis Adsorptive: N2
Analysis Bath Temp.: 77.350 K
Thermal Correction: No
Warm Free Space: 22.4162 cm³ Measured
Equilibration Interval: 20 s
Sample Density: 1.000 g/cm³

Comments: FACT 2019 F19-5 Project #53054-73 PTL ID: 492675-73

BET Report

BET Surface Area: 8.5476 ± 0.4925 m²/g
Slope: 0.500906 ± 0.029278 g/cm³ STP
Y-Intercept: 0.008309 ± 0.001921 g/cm³ STP
C: 61.288065
Qm: 1.9638 cm³/g STP
Correlation Coefficient: 0.9982962
Molecular Cross-Sectional Area: 0.1620 nm²

Relative Pressure (P/Po)	Quantity Adsorbed (cm³/g STP)	1/[Q(Po/P - 1)]
0.021190902	1.1975	0.018078
0.049911857	1.5166	0.034640
0.099886818	1.9180	0.057857

AE 2021-11-03
CQL 2021-11-03

Particle Technology Labs

MORWICK G360 GROUNDWATER RESEARCH INSTITUTE

Sample: 5305473J
Operator: AL
Submitter: Particle Technology Labs
File: R:\Tristar II 3020\win3020\data\53054-73\5305473J.SMP

Started: 10/29/2021 3:23:40 PM
Completed: 10/29/2021 4:44:09 PM
Report Time: 11/3/2021 10:02:38 AM
Sample Mass: 0.1645 g
Cold Free Space: 70.8855 cm³
Low Pressure Dose: None
Automatic Degas: No

Analysis Adsorptive: N2
Analysis Bath Temp.: 77.350 K
Thermal Correction: No
Warm Free Space: 22.4162 cm³ Measured
Equilibration Interval: 20 s
Sample Density: 1.000 g/cm³

Comments: FACT 2019 F19-5 Project #53054-73 PTL ID: 492675-73

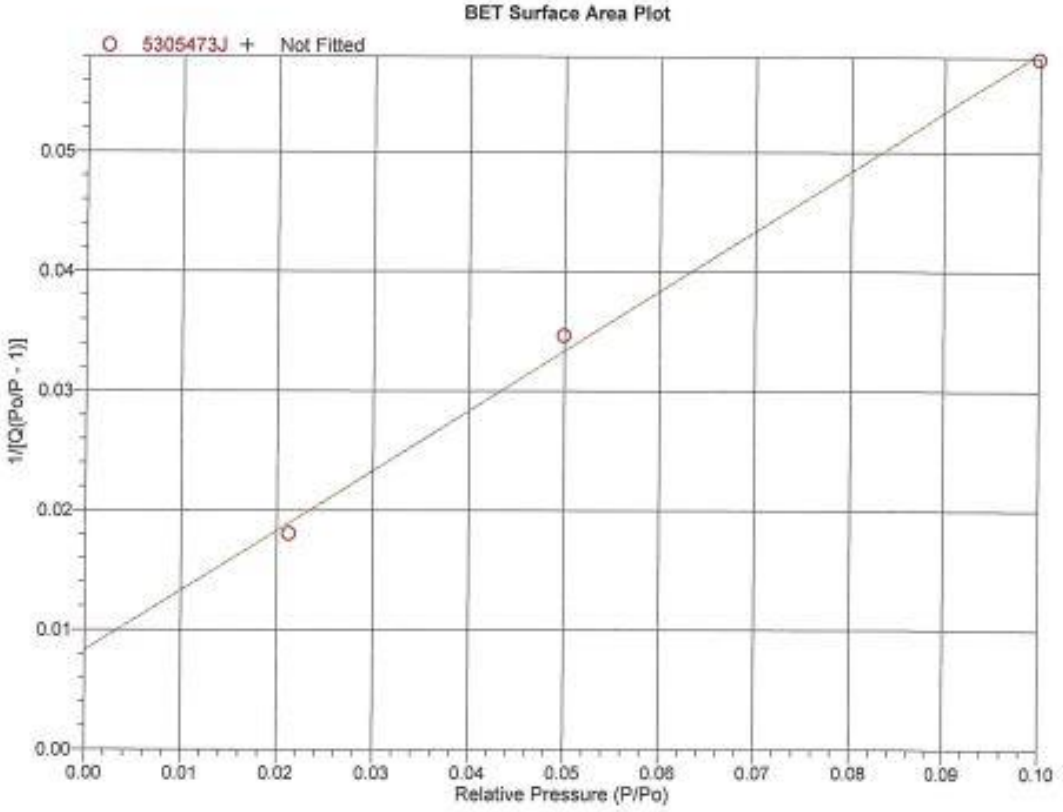

Particle Technology Labs

MORWICK G360 GROUNDWATER RESEARCH INSTITUTE

Sample: 5305473K2
Operator: AL
Submitter: Particle Technology Labs
File: R:\Tristar II 3020\win3020\data\53054...\5305473K2.SMP

Started: 11/2/2021 10:49:49 AM
Completed: 11/2/2021 12:12:50 PM
Report Time: 11/3/2021 10:11:57 AM
Sample Mass: 0.3234 g
Cold Free Space: 71.3371 cm³
Low Pressure Dose: None
Automatic Degas: No

Analysis Adsorptive: N2
Analysis Bath Temp.: 77.350 K
Thermal Correction: No
Warm Free Space: 22.4737 cm³ Measured
Equilibration Interval: 20 s
Sample Density: 1.000 g/cm³

Comments: FACT 2020 F20-1 Project #53054-73 PTL ID: 492676-73

BET Report

BET Surface Area: 0.5728 ± 0.0050 m²/g
Slope: 7.460754 ± 0.065660 g/cm³ STP
Y-Intercept: 0.138302 ± 0.008791 g/cm³ STP
C: 54.945486
Qm: 0.1316 cm³/g STP
Correlation Coefficient: 0.9999613
Molecular Cross-Sectional Area: 0.1620 nm²

Relative Pressure (P/Po)	Quantity Adsorbed (cm³/g STP)	1/[Q(Po/P - 1)]
0.062401581	0.1095	0.607653
0.099838807	0.1263	0.877967
0.199774064	0.1531	1.630186

AL 2021-11-03
CG 2021-11-05

Particle Technology Labs

MORWICK G360 GROUNDWATER RESEARCH INSTITUTE

Sample: 5305473K2
Operator: AL
Submitter: Particle Technology Labs
File: R:\Tristar II 3020\win3020\data\53054...\5305473K2.SMP

Started: 11/2/2021 10:49:49 AM
Completed: 11/2/2021 12:12:50 PM
Report Time: 11/3/2021 10:11:57 AM
Sample Mass: 0.3234 g
Cold Free Space: 71.3371 cm³
Low Pressure Dose: None
Automatic Degas: No

Analysis Adsorptive: N2
Analysis Bath Temp.: 77.350 K
Thermal Correction: No
Warm Free Space: 22.4737 cm³ Measured
Equilibration Interval: 20 s
Sample Density: 1.000 g/cm³

Comments: FACT 2020 F20-1 Project #53054-73 PTL ID: 492676-73

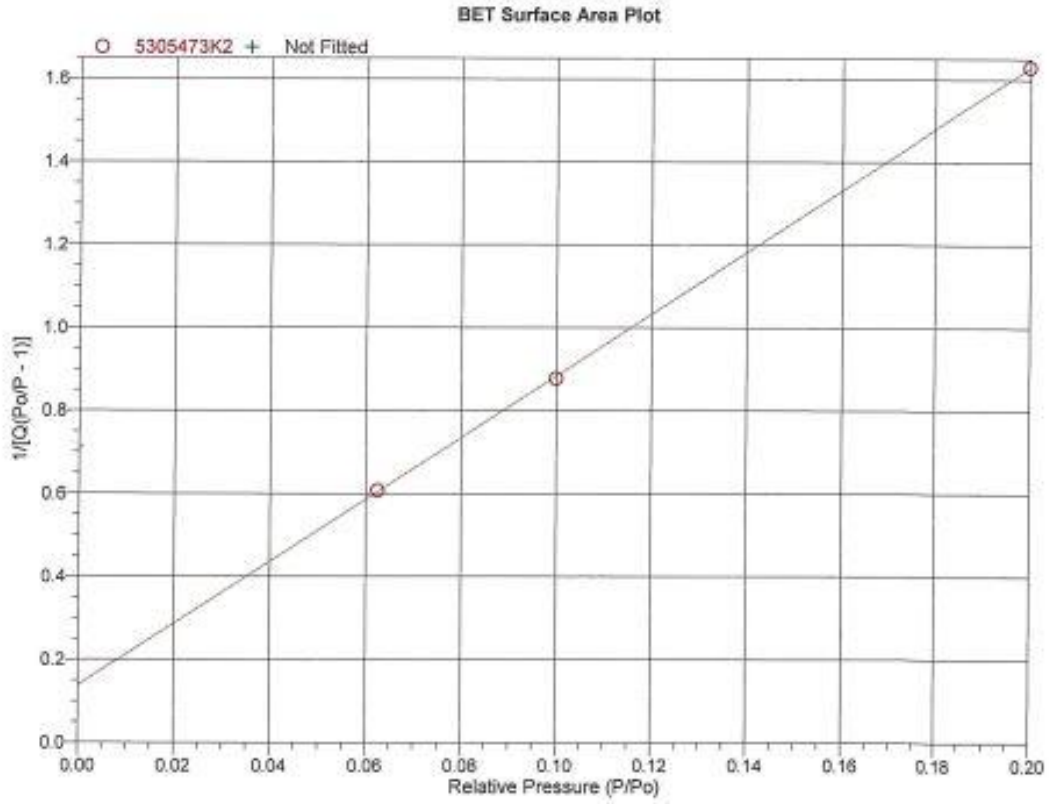

Particle Technology Labs

MORWICK G360 GROUNDWATER RESEARCH INSTITUTE

Sample: 5305473L3
Operator: AL
Submitter: Particle Technology Labs
File: R:\Tristar II 3020\win3020\data\53054...\5305473L3.SMP

Started: 11/2/2021 10:49:49 AM
Completed: 11/2/2021 12:12:50 PM
Report Time: 11/3/2021 10:21:50 AM
Sample Mass: 0.3736 g
Cold Free Space: 70.2815 cm³
Low Pressure Dose: None
Automatic Degas: No

Analysis Adsorptive: N2
Analysis Bath Temp.: 77.350 K
Thermal Correction: No
Warm Free Space: 22.2204 cm³ Measured
Equilibration Interval: 20 s
Sample Density: 1.000 g/cm³

Comments: FACT 2020 F20-2 Project #53054-73 PTL ID: 492677-73

BET Report

BET Surface Area: 1.9613 ± 0.0455 m²/g
Slope: 2.153034 ± 0.051076 g/cm³ STP
Y-Intercept: 0.066219 ± 0.006841 g/cm³ STP
C: 33.514050
Qm: 0.4506 cm³/g STP
Correlation Coefficient: 0.9997187
Molecular Cross-Sectional Area: 0.1620 nm²

Relative Pressure (P/Po)	Quantity Adsorbed (cm³/g STP)	1/[Q(Po/P - 1)]
0.062384418	0.3367	0.197586
0.099884127	0.3889	0.285326
0.199857502	0.5042	0.495413

AE 2021-11-03
CAL 2021-11-03

Particle Technology Labs

MORWICK G360 GROUNDWATER RESEARCH INSTITUTE

Sample: 5305473L3
Operator: AL
Submitter: Particle Technology Labs
File: R:\Tristar II 3020\win3020\data\53054...\5305473L3.SMP

Started:	11/2/2021 10:49:49 AM	Analysis Adsorptive:	N2
Completed:	11/2/2021 12:12:50 PM	Analysis Bath Temp.:	77.350 K
Report Time:	11/3/2021 10:21:50 AM	Thermal Correction:	No
Sample Mass:	0.3736 g	Warm Free Space:	22.2204 cm³ Measured
Cold Free Space:	70.2815 cm³	Equilibration Interval:	20 s
Low Pressure Dose:	None	Sample Density:	1.000 g/cm³
Automatic Degas:	No		

Comments: FACT 2020 F20-2 Project #53054-73 PTL ID: 492677-73

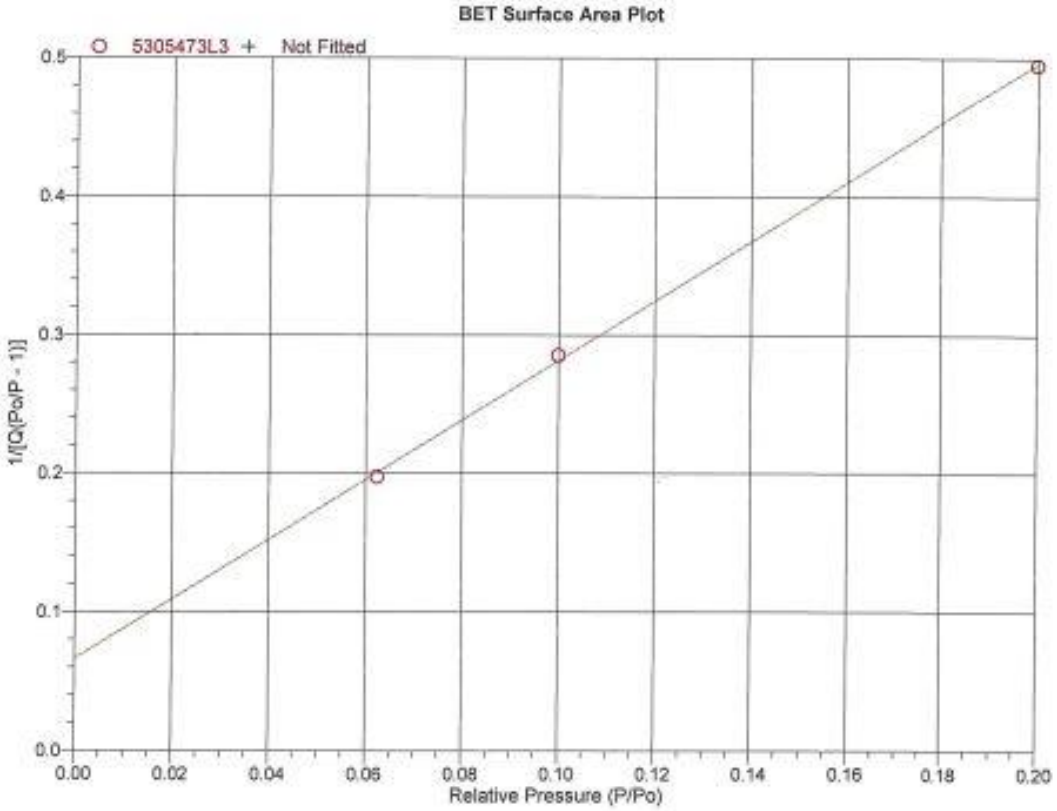

Particle Technology Labs

MORWICK G360 GROUNDWATER RESEARCH INSTITUTE

Sample: 5305473M
Operator: AL
Submitter: Particle Technology Labs
File: R:\Tristar II 3020\win3020\data\53054-73\5305473M.SMP

Started: 11/1/2021 1:50:21 PM
Completed: 11/1/2021 3:13:53 PM
Report Time: 11/3/2021 10:23:06 AM
Sample Mass: 0.1713 g
Cold Free Space: 71.0402 cm³
Low Pressure Dose: None
Automatic Degas: No

Analysis Adsorptive: N2
Analysis Bath Temp.: 77.350 K
Thermal Correction: No
Warm Free Space: 22.3593 cm³ Measured
Equilibration Interval: 20 s
Sample Density: 1.000 g/cm³

Comments: FACT 2020 F20-3 Project #53054-73 PTL ID: 492678-73

BET Report

BET Surface Area: 2.1135 ± 0.1210 m²/g
Slope: 1.840438 ± 0.117208 g/cm³ STP
Y-Intercept: 0.219016 ± 0.012482 g/cm³ STP
C: 9.403201
Qm: 0.4856 cm³/g STP
Correlation Coefficient: 0.9979783
Molecular Cross-Sectional Area: 0.1620 nm²

Relative Pressure (P/Po)	Quantity Adsorbed (cm³/g STP)	1/[Q(Po/P - 1)]
0.062437833	0.2020	0.329695
0.087392305	0.2482	0.385779
0.149964233	0.3576	0.493327

2021-11-03
DSL 2021-11-03

Sample: 5305473M
Operator: AL
Submitter: Particle Technology Labs
File: R:\Tristar II 3020\win3020\data\53054-73\5305473M.SMP

Started:	11/1/2021 1:50:21 PM	Analysis Adsorptive:	N2
Completed:	11/1/2021 3:13:53 PM	Analysis Bath Temp.:	77.350 K
Report Time:	11/3/2021 10:23:06 AM	Thermal Correction:	No
Sample Mass:	0.1713 g	Warm Free Space:	22.3593 cm³ Measured
Cold Free Space:	71.0402 cm³	Equilibration Interval:	20 s
Low Pressure Dose:	None	Sample Density:	1.000 g/cm³
Automatic Degas:	No		

Comments: FACT 2020 F20-3 Project #53054-73 PTL ID: 492678-73

BET Surface Area Plot

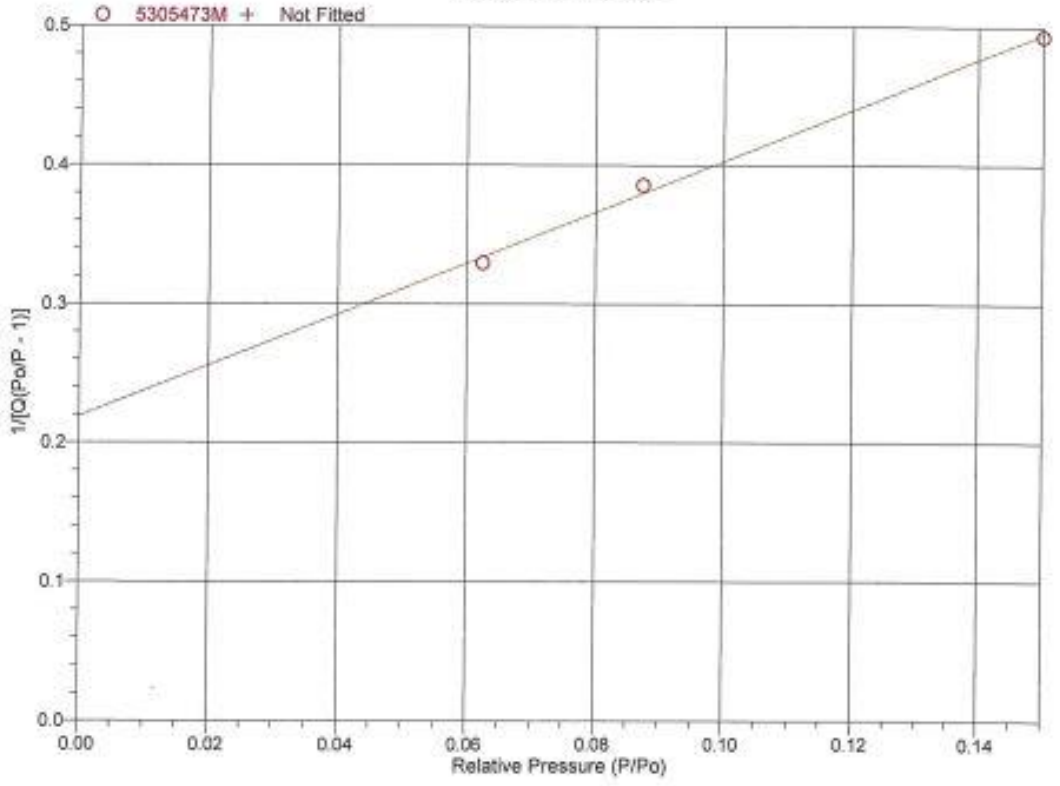

Particle Technology Labs

MORWICK G360 GROUNDWATER RESEARCH INSTITUTE

Sample: 5305473N
Operator: AL
Submitter: Particle Technology Labs
File: R:\Tristar II 3020\win3020\data\53054-73\5305473N.SMP

Started: 11/2/2021 1:14:18 PM
Completed: 11/2/2021 2:36:46 PM
Report Time: 11/3/2021 10:12:14 AM
Sample Mass: 0.3501 g
Cold Free Space: 72.1502 cm³
Low Pressure Dose: None
Automatic Degas: No

Analysis Adsorptive: N2
Analysis Bath Temp.: 77.350 K
Thermal Correction: No
Warm Free Space: 23.0012 cm³ Measured
Equilibration Interval: 20 s
Sample Density: 1.000 g/cm³

Comments: FACT 2020 F20-4 Project #53054-73 PTL ID: 492679-73

BET Report

BET Surface Area: 0.9898 ± 0.0173 m²/g
Slope: 4.366956 ± 0.076644 g/cm³ STP
Y-Intercept: 0.030314 ± 0.007301 g/cm³ STP
C: 145.059027
Qm: 0.2274 cm³/g STP
Correlation Coefficient: 0.9998460
Molecular Cross-Sectional Area: 0.1620 nm²

Relative Pressure (P/Po)	Quantity Adsorbed (cm³/g STP)	1/[Q(Po/P - 1)]
0.062413788	0.2186	0.304544
0.087427274	0.2341	0.409325
0.125220858	0.2475	0.578254

2021-11-03
2021-11-03

Particle Technology Labs

MORWICK G360 GROUNDWATER RESEARCH INSTITUTE

Sample: 5305473N
Operator: AL
Submitter: Particle Technology Labs
File: R:\Tristar II 3020\win3020\data\53054-73\5305473N.SMP

Started: 11/2/2021 1:14:18 PM
Completed: 11/2/2021 2:36:46 PM
Report Time: 11/3/2021 10:12:14 AM
Sample Mass: 0.3501 g
Cold Free Space: 72.1502 cm³
Low Pressure Dose: None
Automatic Degas: No

Analysis Adsorptive: N2
Analysis Bath Temp.: 77.350 K
Thermal Correction: No
Warm Free Space: 23.0012 cm³ Measured
Equilibration Interval: 20 s
Sample Density: 1.000 g/cm³

Comments: FACT 2020 F20-4 Project #53054-73 PTL ID: 492679-73

BET Surface Area Plot

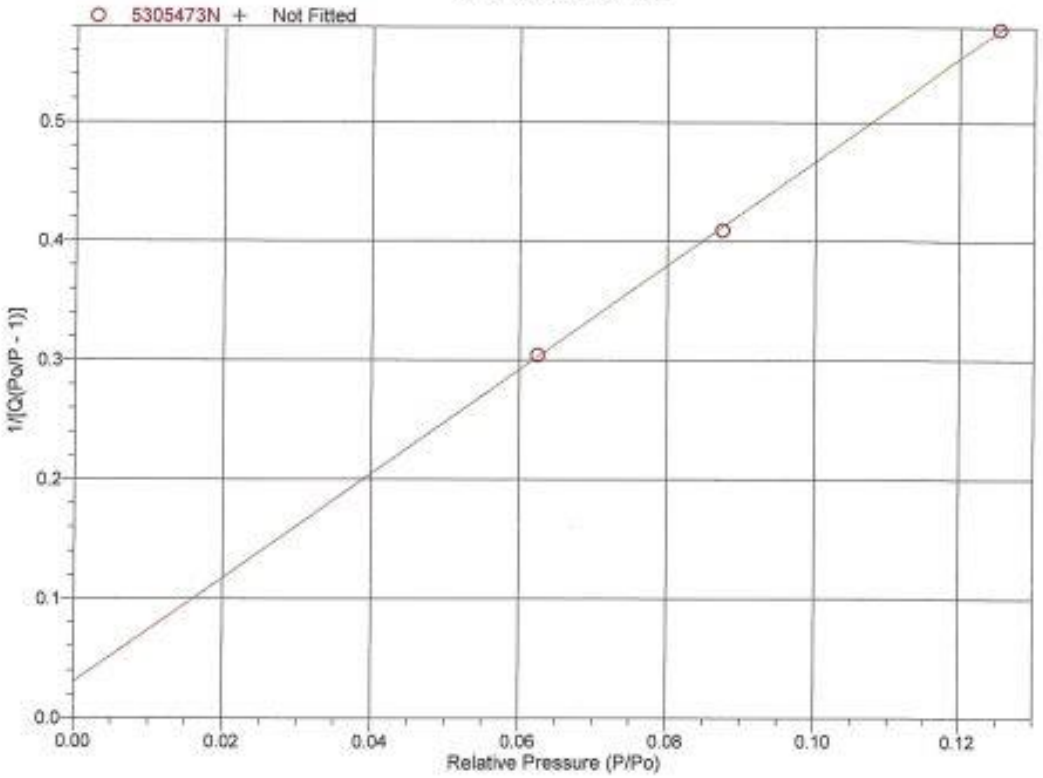

Particle Technology Labs

MORWICK G360 GROUNDWATER RESEARCH INSTITUTE

Sample: 5305473O
Operator: AL
Submitter: Particle Technology Labs
File: R:\Tristar II 3020\win3020\data\53054-73\5305473O.SMP

Started: 11/2/2021 3:41:59 PM
Completed: 11/2/2021 5:03:12 PM
Report Time: 11/3/2021 10:12:20 AM
Sample Mass: 0.3902 g
Cold Free Space: 67.8465 cm³
Low Pressure Dose: None
Automatic Degas: No

Analysis Adsorptive: N2
Analysis Bath Temp.: 77.350 K
Thermal Correction: No
Warm Free Space: 21.4756 cm³ Measured
Equilibration Interval: 20 s
Sample Density: 1.000 g/cm³

Comments: FACT 2020 F20-5 Project #53054-73 PTL ID: 492680-73

BET Report

BET Surface Area: 0.8906 ± 0.0302 m²/g
Slope: 4.796267 ± 0.165054 g/cm³ STP
Y-Intercept: 0.090895 ± 0.015699 g/cm³ STP
C: 53.767335
Qm: 0.2046 cm³/g STP
Correlation Coefficient: 0.9994084
Molecular Cross-Sectional Area: 0.1620 nm²

Relative Pressure (P/Po)	Quantity Adsorbed (cm³/g STP)	1/[Q(Po/P - 1)]
0.082394468	0.1690	0.393741
0.087347326	0.1899	0.503872
0.124973914	0.2062	0.692681

AL 2021-11-03
COL 2021-11-03

Particle Technology Labs

MORWICK G360 GROUNDWATER RESEARCH INSTITUTE

Sample: 5305473O
Operator: AL
Submitter: Particle Technology Labs
File: R:\Tristar II 3020\win3020\data\53054-73\5305473O.SMP

Started:	11/2/2021 3:41:59 PM	Analysis Adsorptive:	N2
Completed:	11/2/2021 5:03:12 PM	Analysis Bath Temp.:	77.350 K
Report Time:	11/3/2021 10:12:20 AM	Thermal Correction:	No
Sample Mass:	0.3902 g	Warm Free Space:	21.4756 cm³ Measured
Cold Free Space:	67.8465 cm³	Equilibration Interval:	20 s
Low Pressure Dose:	None	Sample Density:	1.000 g/cm³
Automatic Degas:	No		

Comments: FACT 2020 F20-5 Project #53054-73 PTL ID: 492880-73